

July 2021

Revisiting hydrogeology of a West Texas desert spring cluster: a data-rich geochemical and physical study of the Trans-Pecos Balmorhea-Area Springs



**Prepared for:
Apache Corporation, Houston, Texas
by**

**Jean-Philippe Nicot, Rebecca C. Smyth, Roxana Darvari,
Tara Bongiovanni, Jon Paul Pierre, S. Tyson McKinney,
Brad D. Wolaver, and Patrick J. Mickler**

**Bureau of Economic Geology
Jackson School of Geosciences
The University of Texas at Austin
Austin, Texas 78713-8924**

Cover photo: An arroyo in the southwestern Davis Mountains – June 2018. Flash flooding after significant rainfall events can transport large diameter rocks; rounded boulder to left of walking pole in foreground is ~3-ft diameter. Credit: R.C. Smyth.

Revisiting hydrogeology of a West Texas desert spring cluster: a data-rich geochemical and physical study of the Trans-Pecos Balmorhea-Area Springs

**Prepared for:
Apache Corporation, Houston, Texas
by**

**Jean-Philippe Nicot¹, Rebecca C. Smyth¹, Roxana Darvari¹,
Tara Bongiovanni¹, Jon Paul Pierre*, S. Tyson McKinney^{1,2},
Brad D. Wolaver*, and Patrick J. Mickler***

¹: Bureau of Economic Geology

²: Department of Geological Sciences

* formerly at the Bureau of Economic Geology

July 2021

Bureau of Economic Geology
Jackson School of Geosciences
The University of Texas at Austin
Austin, Texas 78713-8924

Abstract

Some Trans-Pecos perennial desert springs have dried up, some have seen a decrease in flow, others exhibit no change from the historical period. Six springs forming the Balmorhea Spring Complex (Phantom Lake, San Solomon, Giffin, East and West Sandia, and Saragosa) have received some attention in the past few years because of the multidecade-long decline in flow rate and because they are located at the edge of the tectonic Delaware Basin. The basin has experienced in the past decade an oil and gas exploration renewal thanks to the development of unconventional technology (long horizontal laterals and hydraulic fracturing). The amount of groundwater used for well stimulation in the general area when added to the large amount already used for irrigated agriculture may threaten the health of the springs. Apache Corp., with assets in the southern Delaware Basin, set out to investigate the potential impacts on the springs of water withdrawal from various aquifers in the vicinity of the Balmorhea Spring Complex. However, such a study cannot be performed in a vacuum, needs to be regional in nature, and requires extensive data collection complemented by a look back at historical and other recent work on the springs.

It has been known for almost a century that the springs have a distal-sourced regional baseflow component (total dissolved solids of ~2200 mg/L; temperature of ~25°C; mixed cation Na-Ca, mixed anion Cl-SO₄ water type) augmented multifold by irregular local stormflow after heavy rain events in the Davis Mountains, located southwest of the springs. When they occur, the springs experience a decrease in temperature and TDS as the baseflow mixes with the very low-TDS Ca-HCO₃ recharge water.

The springs emerge from fractures of the Cretaceous Edwards Group and associated formations (directly for Phantom Lake; through a thin veneer of alluvium for the other springs). If the stormflow component is easily observable and relatively well-known, many aspects of the baseflow source(s) and behavior are still unknown. The baseflow has been described as originating from the Salt Basin Bolsons to the west, where it receives its diagnostic high strontium isotope ratio. On its way to the springs along a well-known fault zone (>10,000 years travel time), the baseflow receives contributions from the Capitan, Rustler and Edwards Aquifers, but input from basinal brines was not detected.

The data collection part of the study included taking 84 geochemical samples from wells and springs (37 unique locations), drilling 13 monitoring wells, deploying data loggers in 6 springs, 10 stream locations and 14 wells as well as 8 acoustic sounders in wells. The monitoring period (data available from April 2018 at the earliest to Fall 2020) recorded only one major stormflow event (early Fall 2019) that fell short of the very large events observed in the past and that are further analyzed in this study. Many of the loggers are installed in the Balmorhea Spring Complex area (including very shallow wells) and upstream in the various watersheds believed to partly drain to the springs. Sounders were installed upgradient or slightly downgradient of the springs. Unfortunately, despite our best efforts, the team was not able to secure access to properties where the data were the most needed, along the presumptive flow lines between Van Horn in the Salt Basin and the springs in southeastern Culberson County.

Examination of historical data and of data collected during this study led us to conclude that: (1) the most likely distal origin of a significant fraction of baseflow is in the northern section of the Salt Flats (Salt Basin); then the flow interacts with the Castile Fm. in the vicinity of the Apache Mountains where it acquires its geochemical signature before reaching the springs; and (2) each

regional precipitation event of relatively high intensity (>1-2" per day for a few days) results in storing large water volumes upflow from the springs which are slowly released in the following months. Less well-understood aspects of the spring complex with operational significance include possible cross formational flow between aquifers.

Table of Contents

Abstract	i
Table of Contents	iii
List of Figures	vi
List of Tables	viii
Acknowledgments	ix
Acronyms	xi
Executive Summary	xiii
1 Introduction	1
1.1 Motivation and outline	1
1.2 Administrative matters	1
1.3 Spring description and quick overview of the accepted conceptual model	2
1.4 Objectives of the study	3
2 Geographic and geological settings	5
2.1 Topography and land use	5
2.1.1 Balmorhea area	5
2.1.2 Broader area	6
2.2 Geological Formations	6
2.2.1 Balmorhea Area	6
2.2.2 Western edge of the Delaware Basin, Capitan Reef, and Salt Basin	9
2.3 Structural Features	10
2.4 Regional Hydrogeology	11
2.5 Anthropogenic actions	15
2.5.1 Phantom Lake Spring	16
2.5.2 San Solomon Spring	16
2.5.3 Giffin Spring	17
2.5.4 East and West Sandia Springs	17
2.5.5 Saragosa Spring	17
3 Previous work – Literature Review	17
3.1 Succinct overview of past field studies	17
3.2 Dynamic hydrogeology	19
4 Data sources	22
4.1 Collaborations	23
4.2 Well drilling	23
4.3 Geological data	25
4.4 Geochemical sampling and analysis	25
4.4.1 This study	25
4.4.2 Historical data	26
4.5 Physical sampling	27
4.5.1 This study	27
4.5.2 Historical data	31
4.6 Precipitation data	31
5 Methodology	32
6 Geochemical Results	33
6.1 General geochemistry	33
6.1.1 Spring and shallow well samples	36

6.1.2	Produced waters	37
6.1.3	San Solomon time series	37
6.1.4	Sulfate as a tracer	38
6.1.5	Nitrate as a tracer	39
6.1.6	Silica and B/Cl ratio as tracers	40
6.1.7	Results from other geochemical databases	42
6.2	Water isotopes	42
6.2.1	Rain water	42
6.2.2	Igneous springs	43
6.2.3	Balmorhea area springs	43
6.2.4	Groundwater	44
6.2.5	Produced water	44
6.3	Strontium isotopes	44
6.3.1	Background	44
6.3.2	Igneous springs	45
6.3.3	Balmorhea area springs	46
6.3.4	Groundwater	46
6.3.5	Produced water	46
6.4	Carbon isotopes and bicarbonate and methane	47
6.4.1	Bicarbonate	47
6.4.2	Light hydrocarbons	47
6.5	Chloride-bromide ratio	48
6.5.1	Balmorhea area springs	48
6.5.2	Igneous springs and related groundwater	49
6.5.3	Produced water	49
6.6	Chlorine isotopes	49
6.6.1	Background	49
6.6.2	Analysis	49
6.7	Sulfate isotopes	50
6.7.1	Background	50
6.7.2	Analysis	50
7	Physical hydrogeological results	51
7.1	Groundwater levels and potentiometric surfaces	51
7.2	Spring response: Analysis of historical records of recharge events	55
7.3	Spring response: Analysis of logger data	58
7.3.1	Logger examination	59
7.3.2	Early Fall 2019 event	60
7.4	Spring Response: Analysis of watershed precipitation	63
8	Discussion	65
8.1	Discussion of geochemical results	65
8.2	Discussion of physical results	67
9	Conclusions and future work	71
	Supplementary Information	72
	References	72
	Tables	84
	Figures	88

Appendix A: Well diagrams	183
Appendix B: Logger outputs.....	197
Appendix C: Sounder outputs.....	213
Appendix D: Methods for Chemical Analyses	219
Appendix E: Field photos	223

List of Figures

Figure 1. Balmorhea spring location.....	88
Figure 2. Major Springs of Trans-Pecos Texas	89
Figure 3. Mean gridded annual precipitation.....	90
Figure 4. Historical spring flow	91
Figure 5. Map of watersheds.....	92
Figure 6. Stratigraphic column of various components of the Permian Basin.	93
Figure 7. Generalized E-W cross-section of the Delaware Basin.....	94
Figure 8. BEG-drilled monitoring well locations	95
Figure 9. Sorted histogram of BEG-drilled well depths	96
Figure 10. Location map of BEG and other geochemical samples.....	97
Figure 11. Spring sampling time distribution	98
Figure 12. Well loggers (a) and Wellntel [®] (b) generalized locations.	100
Figure 13. Locations of InSitu [®] loggers	101
Figure 14. Time line of logger data.	102
Figure 15. Time line of Wellntel [®] data.....	103
Figure 16. Locations of all wells with useable water level elevations.....	104
Figure 17. Official rain gauge locations	105
Figure 18. Piper plot of samples collected in this study	106
Figure 19. Map of generalized hydrochemical water types with Stiff diagrams.....	107
Figure 20. Distribution of saturation indices	108
Figure 21. Ca/Mg vs. Ca/SO ₄	109
Figure 22. Na/Cl vs. Ca/SO ₄	110
Figure 23. Spring temperature	111
Figure 24. TDS of San Solomon spring samples taken during the study	112
Figure 25. Elements and anions as a function of the time of the year	114
Figure 26. This study sample sulfate distribution.....	115
Figure 27. Nitrate concentration in water samples	116
Figure 28. Nitrate concentration vs. month of the year	117
Figure 29. San Solomon Spring nitrate concentration	118
Figure 30. Silica concentrations normalized by TDS	119
Figure 31. Boron concentrations normalized by Cl	120
Figure 32. Silica vs. boron	121
Figure 33. Historical data Piper plots of aquifers.	122
Figure 34. Seasonal variations of rainwater isotopes.....	124
Figure 35. Water isotope cross-plot.....	125
Figure 36. Stable water isotopes as a function of the time of the year	127
Figure 37. Strontium ratio.....	128
Figure 38. Strontium isotope ratio vs. water oxygen isotope	129
Figure 39. Field alkalinity bicarbonate as a function of the DIC $\delta^{13}\text{C}$	130
Figure 40. Cl/Br ratio as a function of Na/Cl ratio	131
Figure 41. Chlorine isotopes	132
Figure 42. Cross-plot of sulfur and oxygen isotopes of aqueous sulfate	133
Figure 43. MATLAB [®] -processed logger plots of Davis Mountains springs.....	134
Figure 44. MATLAB [®] -processed logger plots of Davis Mountains stream.....	135
Figure 45. MATLAB [®] -processed logger plots of water wells	136

Figure 46. Unprocessed WellIntel® measurements.....	137
Figure 47. Well locations with groundwater potentiometric contours	138
Figure 48. Elevated water levels in Pecos Valley wells	139
Figure 49. Differences in water level elevations	140
Figure 50. Spring flow measurement temporal density	141
Figure 51. Historical San Solomon spring flow rates	142
Figure 52. Historical Phantom Lake spring flow rates	143
Figure 53. Historical Giffin flow rates.....	144
Figure 54. San Solomon above-baseflow historical flow rates.....	145
Figure 55. Phantom Lake and Giffin above-baseflow historical flow rates	146
Figure 56. San Solomon and Phantom Lake extreme event spring flow (1932-33).....	148
Figure 57. San Solomon extreme event spring flow (1941-42).....	150
Figure 58. San Solomon minor extreme events (1933 and 1942-1946).	155
Figure 59. TDS of Balmorhea springs historical water samples.	156
Figure 60. San Solomon daily flow rate and daily precipitation at nearby weather stations.....	157
Figure 61. San Solomon daily flow rate and daily precipitation (Fall 2019 event).....	158
Figure 62. Contemporaneous plots of data from regional rainfall gauges.....	159
Figure 63. Logger response to Early Fall 2019 event.	160
Figure 64. Logger data from June 25 to December 22, 2019	165
Figure 65. Logger data from Spring to December 2019	168
Figure 66. Precipitation (NOAA MRMS) for selected months of 2019.....	177
Figure 67. Daily rainfall as recorded in several weather stations	178
Figure 68. San Solomon Spring flow rate at the USGS gauge	179
Figure 69. Oil and Gas exploratory wells in Jeff Davis County	180
Figure 70. Time interval between successive precipitation events.....	182

List of Tables

Table 1. BEG monitoring well characteristics.....	84
Table 2. Location and simplified characteristics of the InSitu [®] loggers.....	85
Table 3. BEG WellIntel [®] installations.	86
Table 4. Well data (2010-2020) for water table/potentiometric surfaces	87

Acknowledgments

This project was funded from November 2017 through December 2020 by Apache Corporation. Data interpretation and report preparation extended into 2021. This 2021 work has been made possible through use of BEG general funds, and with support from The University of Texas at Austin (UT) Jackson School of Geosciences and the state-funded STARR program (State of Texas Advanced Resource Recovery). Brian Bohm of Apache Corporation spearheaded the research effort and encouraged continued financial and logistical support; we are grateful to Brian and the Apache land department for helping with land access. In addition, Justin Mondrik, Apache summer intern, and Mark Dowell, also with Apache, greatly supported field activities.

Many BEG researchers and State entities have contributed to the study.

Dr. Brad D. Wolaver initiated the project at BEG. Other BEG researchers who contributed to field, laboratory, data interpretation, and reporting efforts are, in alphabetical order: Tara Bongiovanni, Caroline Breton, Dr. Todd Caldwell, Lucie Costard, Amanda Covington, Roxana Darvari, Ramon Gil, Shawna Graves, Kelly Hattori, Linda McCall, Tyson McKinney, Parker Medford, Dr. Patrick Mickler, Dr. Jean-Philippe Nicot, Dr. Jeffrey Paine, Jon Paul Pierre, Rebecca C. Smyth, Dr. Alex Sun, and Dr. Michael Young. Other support came from BEG departments of Contracts (especially Amelia Bridges and Julie Duiker), Graphics (esp. Jana Robinson), Purchasing (esp. Jan Braboy), and Travel (esp. Jessica Rowling). Thank you to Alexandros Savvaidis and his team for use of the Balmorhea State Park TexNet station and help with data downloads. We also appreciate the general administrative support received from Jay Kipper and Mark Blount. Pr. Bayani Cardenas (UT Department of Geological Sciences) graciously offered to use his diving expertise to help download loggers at the orifice of the San Solomon Spring.

We received outside technical and logistical support from numerous State and private entities. Dr. John M. “Jack” Sharp, professor emeritus, UT Department of Geological Sciences served as Senior Technical Advisor. Previous work completed by Jack and many of his former graduate students provided the scientific foundations for this study. Groundwater conservation district personnel in Jeff Davis and Reeves counties, esp. Janet Adams (General Manager, Jeff Davis Underground Water Conservation District) and Greg Perrin (General Manager, Reeves County GCD), assisted greatly. We appreciate the field support provided by Texas Parks and Wildlife personnel from Austin (esp. Chad Norris), Balmorhea State Park (esp. Carolyn Rose), and Davis Mountains State Park (esp. Wanda Olszewski).

Private groups who assisted with field work and/or provided land access include: Boy Scouts of America (esp. David Chapman and Keith Morrison), Caldwell Ranch (Will and Pam Harte), Fort Davis Water Supply Corporation (esp. Scott Adams), Hamilton Ranches (esp. Chris Wilson), King Land & Water (esp. James King), Leoncita Cattle Company (Val and Tom Beard), Madera Valley Water Supply Corporation (esp. Terry Gilcrest and Craig Huelster), McCoy-Remme Ranches (esp. Kaare Remme and Tommy Vines), McDonald Observatory, McKnight Ranches (Bob McKnight), Reeves County Water Improvement District #1 (esp. Abel Baeza), Scripps Family, Shield Cherry Canyon Ranch (esp. Tres McElroy, Blake Murden, and Terry Gilcrest), The Nature Conservancy (esp. Tara Polosky and Ryan Smith), and Don Weinacht, as well as the U.S. Bureau of Reclamation (Dustin Armstrong), and the U.S. Fish and Wildlife Service. Private contractors who worked on the project included Andy Prude Well Service in Ft. Davis, TX, Arrowhead Drilling and Well Service LLC, Bullock, Bennett & Associates (Chris Winkler), Matthew Uliana (independent hydrogeologist), SD Services, Skinner’s Drilling and Well Service LLC, and WellIntel[®] Inc.

Acronyms

AF	Acre-foot
AT	AquaTroll (logger)
amsl	above mean sea level
BEG	Bureau of Economic Geology (The University of Texas at Austin)
BOR	Bureau of Reclamation
BSP	Balmorhea State Park
cfs	cubic feet / second (second-feet)
DIC	Dissolved inorganic carbon
DMG	Delaware Mountain Group
DO	Dissolved oxygen
ES-WS	East Sandia and West Sandia springs.
Fm.; Fms.	Formation; Formations
GAM	Groundwater Availability Model
GCD	Groundwater Conservation District
GMA	Groundwater Management Area
gpm	Gallon per minute
HUC	Hydrological unit codes
kAF	Thousand acre-feet
Ma	Millions years
MAP	Mean average precipitation
MAV	Mean average volume
MW	Monitoring well
NOAA	National Oceanic and Atmospheric Administration
NCKRI	National Cave and Karst Research Institute
n.d.	no data
ORP	Oxydation-reduction potential (redox)
PL	Phantom Lake
PVA	Pecos Valley Aquifer
RT	RuggedTroll (logger)
SDR	Submitted driller's records
SI	Saturation index
SpC	Specific conductivity
SSS	San Salomon Spring
SS-PL-G	San Salomon, Phantom Lake and Giffin springs
SWN	State well number
SWRI	Southwest Research Institute
TDLR	Texas Department of Licensing and Regulations
TDS	Total dissolved solids
TNC	The Nature Conservancy
TPWD	Texas Parks & Wildlife Department
TWDB	Texas Water Development Board
USFWS	U.S. Fish and Wildlife Service
UWCD	Underground Water Conservation District
VOA	Volatile organic acid
WQ	Water quality

Executive Summary

The study (~2018-2020) was commissioned by Apache Corp. as they were developing their unconventional assets in the southern tectonic Delaware Basin in close proximity to the Balmorhea spring complex in Reeves County. The spring complex is one, and possibly the most well-known, of many desert spring clusters in west Texas. The study's stated overarching goal was to assess the vulnerability of the springs to additional pumping load. The proximal objectives were to determine how much each geographic source contributes to the flow rate of the springs and to assess potential cross-formational flow between aquifers. The spring locations at the faulted boundary of the tectonic Delaware Basin where no less than 7 aquifers intersect still render any study challenging despite the number of high-level hydrogeological investigations of the area.

The springs are located at the transition between the mountain front of the Davis Mountains to the southwest and the onset of the physiographic Toyah Basin to the north. They emerge from Cretaceous limestones, which are sometimes covered by a thin veneer of recent deposits. The springs exhibit a so-called baseflow that is fairly constant throughout the year and year to year in rate and in geochemical characteristics but is punctuated by pulses of dilute storm flow related to heavy precipitation in the Davis Mountains. Flow rate monitoring that started almost a century ago shows a slow but steady decline in baseflow from >35cfs to ~25cfs at the main spring (San Solomon). The decrease in baseflow has been attributed to regional irrigation pumping, mostly on circumstantial evidence based on a more clear-cut example (Fort Stockton Comanche Springs), and on the timing of water withdrawals.

The geology of the area is complex. The tectonic Delaware Basin consists of a thick Paleozoic fill of mostly marine siliciclastic basinal sediments but is capped by evaporites (anhydrite and halite from the Castile Formation) and the overlying Rustler Formation (Fm.), characterized by the presence of clastics, dolomite, and some evaporites. The Rustler Fm. hosts a regional brackish aquifer (Ca-SO₄ water type). Ringing the margins of the Basin, the Capitan Reef and associated facies, hosts another brackish aquifer that plays an important role in transmitting the spring baseflow. Moving one more step away from the tectonic Basin edge, a large section of the shelf deposits (Diablo Platform), also of Permian age, have been down-dropped thousands of feet following the creation of the Salt Basin (graben), which is the easternmost manifestation of the Basin and Range tectonic event (Neogene, 23-2.5 Ma). The same event lifted old Precambrian rocks (horst), some of which crop out at the western edge of the Salt Basin; this turns out to be an important clue to delineate the drainage area of the springs. The Salt Basin is filled with recent sediments that form several Bolson aquifers. Before this tectonic event, at the end of the Mesozoic, Cretaceous limestones were deposited on top of the Paleozoic layers; they form an important regional aquifer, the Edwards-Trinity Aquifer; the springs emerge from a Cretaceous stratum, the Buda Limestone. Cenozoic-age rhyolitic volcanism laid massive amounts of silicic lava flows and ignimbrites whose remains form the Davis Mountains. Another important aspect of the Neogene tectonic episode was the uplift and tilting of the entirety of west Texas towards the east. It controls the current regional hydrogeological flow to the east, and led to the dissolution of evaporites by meteoric waters and the deposition of the Pecos Valley Alluvium (PVA) in the subsiding areas. The PVA forms an important aquifer of the Toyah Basin. Oil and gas operators use supply wells in the PVA, Edwards-Trinity, and Rustler Aquifers to perform hydraulic fracturing stimulations in the southern Delaware Basin.

Three of the springs (Phantom Lake, San Solomon, and Giffin) are typically described as artesian, that is, sourced from a confined aquifer, whereas East and West Sandia and Saragosa are typically described as gravity springs originating from the shallow water-table unconfined aquifer. Phantom Lake ceased to flow for the most part in 1999; flow at San Solomon spring has been altered by construction of a large pool and irrigation canals, starting more than a century ago. The natural environment of the other springs has been less altered but their cumulative flow is low. Previous studies have determined that a significant fraction of the spring baseflow originates in the salt flats, 50+ miles to the west as suggested by geochemical evidence (high strontium isotope ratio; stable water isotopes). Flow lines leading to the spring complex start in some of the Salt Basin Bolson Aquifers and, likely, in the Permian strata underlying the recent bolson sediments. The groundwater then acquires its mixed anion Cl-SO₄ mixed cation Na-Ca signature as it enters the Toyah Basin / Delaware Basin from the west.

Thanks to the collaboration of many individuals, landowners, and organizations, two types of data were collected for this study: geochemical (84 samples from 37 unique locations -springs, streams, water wells, and an additional 7 oil producing wells) and physical (14 loggers in springs and surface water bodies and 14 loggers in water wells; all high-frequency sampling); 13 new monitoring wells, mostly shallow, were drilled in the vicinity of the springs. Acoustic sounders were installed on 8 additional wells. We also processed NEXRAD weather radar data. Geochemical analyses included major, minor, and trace elements as well as stable isotopes of water, strontium, sulfate, and bicarbonate. Loggers measured water stage (derived from actual pressure measurements, which were corrected with data from dedicated barometers), temperature, and specific conductivity (proxy for TDS). Rain samples were also systematically collected to analyze for stable water isotopes. In addition, a total of ~2250 historical geochemical analyses were assembled from various sources. Thorough daily streamflow data collection by the USGS from the 1930's to the 1960's (estimated flow rate) complemented the current high-frequency data recording. Geochemical analyses were used to discriminate between endmember sources, detect the ultimate origin of the water samples, and assess groundwater mixing. Physical data were used to relate precipitation and stream flow in the relevant watersheds to spring flow.

Geochemical analyses confirmed the already observed three end-members and refined their geochemical characteristics: (1) the low-TDS Ca-HCO₃ so-called igneous category (recent water originating from the Davis Mountains); (2) the variable TDS Ca-SO₄ category from the Rustler Aquifer (north and northwest of the spring cluster); and (3) the mixed anion (Cl-SO₄) and mixed cation (Na-Ca) Balmorhea Spring category with a mildly elevated TDS (2000-3000 mg/L). The Edwards-Trinity Aquifer, an important aquifer in the Balmorhea area, shows mixtures of these three end-members and denotes the existence of crossformational flow. Geochemical analyses that had not been performed in the past confirm that the Balmorhea Spring category is itself a mixture of mostly Bolson aquifer water dissolving Castile evaporites. However, there is no observed contribution of basinal brines (their Cl/Br ratio is too low). The sulfate and Ca present in the spring water originate from anhydrite dissolution as indicated by sulfate stable isotopes, and the spring Cl and Na come from halite dissolution as indicated by the high Cl/Br ratio; the respective corresponding molar ratios are close to 1 but slightly altered by ion exchange of Na for Ca. Spring water strontium isotope ratio confirms previous observations, that elevated values cannot be explained by local sources and denote contributions from Precambrian rocks present in the Salt Basin.

Spring water stable isotopes confirm the distal nature of the baseflow and long travel time. Simple averaging of 66 ~weekly San Solomon samples between March 2018 and September 2019 yielded $\delta^{18}\text{O} = -9.04 \pm 0.25\text{‰}$ and $\delta\text{D} = -62.24 \pm 1.06\text{‰}$ (1 standard deviation) with a fairly constant TDS at 2244 ± 36 mg/L and a weak correlation between water isotopes and TDS; these values are lower than that of the local rain water. Dedicated rain collectors at the McDonald Observatory and Bamorhea State Park show clear seasonal variations but yields an average of $\delta^{18}\text{O} = -7.0\text{‰}$ and $\delta\text{D} = -45.0\text{‰}$ overall. The so-called gravity springs show a higher TDS, more nitrate, a lower and more variable temperature, lower strontium isotope ratio, higher stable water isotope values, and lighter DIC carbon isotope; all characteristics denoting recent meteoric influence but not negating the possibility of artesian contributions.

An examination of detailed historical spring flow and precipitation data (1930's and 1940's) combined with data from this study suggests that 80% or more of the multi-decadal long-term spring flow is provided by the distally-sourced baseflow. However, this contribution can temporarily drop to 10-20% during strong storm events. Effects of strong events are long lasting with an elevated spring flow being observed for months after the event ("local baseflow"). The karstic nature of the recharge allows for the system to capture a significant fraction on the precipitation on the various watersheds of the Davis Mountains; a fraction of it is stored in Cretaceous formations and possibly alluvium on the plain below or Davis Mountains permeable units and released over time. The multiple loggers installed during this study and the high frequency recording (5 min) allow for a fine understanding of the contributions of each watershed and inform on the relationship between precipitation and spring flow. We examined in details an early Fall 2019 composite event from which we can infer travel time as short as 3 to 4 days. Potentiometric maps of major aquifers (Pecos Valley, West Texas Bolson, Igneous, Edwards-Trinity, and Permian) were redrawn using recent data (2010-2020 period). They suggest that both upward and downward cross-formational flow are possible, which is confirmed by examining pairs of neighboring wells drilled in different formations.

Potential future work includes well monitoring and sampling of areas that were not accessed during this study (west of the springs to Van Horn) and, in the medium term, building a regional flow model centered on the springs, and a higher-resolution local model handling the periodic recharge mounding.

1 Introduction

1.1 Motivation and outline

Apache Corporation based in Houston, TX (Apache) announced in 2016 the discovery of the ~1,400-km² (352,000-acre) Alpine High, a resource play in the otherwise undeveloped southwest tectonic Delaware Basin. The Delaware Basin is the westernmost sub-basin of the Permian Basin bounded to the southwest by the Davis Mountains from which it is separated by a fault zone. A historically and environmentally important string of desert springs emerge from the fault zone and there is concern that water withdrawal from local and distant fresh and brackish water aquifers impact flow rates of the springs and their endangered species. Such concerns have been realized elsewhere in the past as shown by the drying up of Comanche Springs, a large desert spring in the Fort Stockton area, because of irrigation pumping, possibly exacerbated by increased pumping during the drought of the 1950's (Small and Ozuna, 1993; Sharp et al., 2003; Mace et al., 2020). A secondary concern is potential contamination of the springs either directly through oil and gas activities (oil/gas wells, salt water disposal wells) or indirectly through a redirection of the groundwater flow lines. The present hydrogeological study was conducted to assess these risks and refine the conceptual flow model for the springs and related groundwater flow system. The study domain encompasses a small area of Trans-Pecos Texas along I-10 (between El Paso and Fort Stockton) and includes a portion of eastern Culberson, northern Jeff Davis, and southern Reeves Counties (Figure 1). The overarching goal of this and future studies is to advance the science in order to develop mitigating approaches to ensure the long-term survival of the springs.

This first section of the document presents the study background from an administrative standpoint as well as a quick overview of previous hydrogeological work in the Balmorhea area. It also provides details on the objectives of the study. Section 2 gives a broad brush overview of the regional geographic, geological, and hydrogeological features. Section 3 details previous work put in the context of the information given in Section 2. Data sources and methods are given in Sections 4 and 5. Geochemical and hydrological results follow in Sections 6 and 7, respectively. A discussion is presented in Section 8, followed by conclusions and future work suggestions in Section 9. The subsequent section lists electronic files and other data supporting this report. Appendix A presents the diagrams of BEG monitoring wells; logger and sounder raw data are plotted in Appendix B and Appendix C. Laboratory procedures are detailed in Appendix D. Field photos of some sampling and logger locations are shown in Appendix E.

1.2 Administrative matters

The official start date of the project was November 1, 2017 with an initial end date of October 31, 2019 (a two-year project). The effective start date of February 2018 pushed the end date to December 31, 2019 (Amendment 1). The end date was further postponed to December 31, 2020 because of delays in implementing the field monitoring tasks, an important component of the “Year2” phase. The total budget was not impacted by the delays. In the course of the project, BEG collaborated with various entities: U.S. Bureau of Reclamation (BOR), U.S. Geological Survey (USGS), The Nature Conservancy (TNC), Texas Parks and Wildlife Department (TPWD) (Balmorhea State Park and Davis Mountains State Park), the McDonald Observatory, Jeff Davis Underground Water Conservation District, Reeves County Groundwater Conservation District, Reeves County Water Improvement District 1, and many land owners. The original Principal Investigator (PI), Dr. Brad Wolaver, left the BEG in June 2020 and was replaced by Dr. J.-P. Nicot.

This final report is complemented by Year1 report (Wolaver et al., 2019) submitted to the sponsor in April 2019. Year1 tasks were completed with minimal monitoring data, which were implemented and collected mostly in Year 2. Several tasks or subtasks of the Year1 report are not revisited in this Final Report, they have not been further investigated or discussed and their findings stand.

1.3 Spring description and quick overview of the accepted conceptual model

Desert springs represent important historical and environmental features in many arid environments and settings around the world thanks to their perennial flow. West Texas is no exception, where tens of such springs have been observed and data compiled (Heitmuller and Reece, 2003; Brune, 1975) (Figure 2). Many of the springs have dried up in the 20th century without formal investigation but several have been the subject of detailed studies and long-term flow measurements. For example, Comanche Springs in Fort Stockton, TX, with historical rates of ~40-50 cubic feet per second (cfs) and higher, currently only flows intermittently. Its decline has been attributed to irrigation pumping, and increased withdrawal volumes during drought periods, and the springs mostly dried up in 1962, ~10 years after high-capacity groundwater-fed irrigation started ~16km (10mi) to the west along the presumed flowpath (Leon-Belding area). Diamond Y springs 7 miles north of Fort Stockton is still flowing at a few cfs. Desert springs are understood to have, as a major component, a long, deep flowpath that makes them perennial. Such is the case of the well-known Balmorhea area desert springs. They have been investigated for decades. Earlier authors proposed that recharge to the Balmorhea area springs occurred through the Davis Mountains to the southwest. But the low TDS of Davis Mountains groundwater did not match the sulfate-rich slightly brackish water of the springs. Subsequent authors suggested a regional component from the Apache Mountains to the west (e.g., White et al., 1941; Harden, 1972; LaFave and Sharp, 1987). Further studies concluded that discharge from the Salt Basin farther to the west must also contribute to the regional flow (Uliana, 2000; Chowdhury et al., 2004).

This conceptual model of spring flow for the Balmorhea area springs is now generally accepted; it entails a two-component system: (a) a deep, steady, relatively brackish component flowing from the west along a regional structural feature (base flow); and (b) a short-term shallow component responding to recharge events in the Davis Mountains to the southwest (episodic stormflow) as implied by flow rate increases after some storm events on the mountains with annual rainfall almost twice as high as in the basin (Figure 3), along with turbidity increases, and TDS decrease. Typical TDS values are slightly brackish in the 2,000-3,000 mg/L range but can decrease to <1000 mg/L after a heavy rain event in the Davis Mountains. The Balmorhea spring complex include six springs: Phantom Lake, San Solomon, Giffin, East and West Sandia, and Saragosa. These spatially distinct springs could be composed of closely associated individual springs and seeps. Sometimes a seventh group of springs is added: Toyah Creek springs located not far from Saragosa Spring (White et al., 1938, 1941). All springs are located in Reeves County except Phantom Lake which is in northernmost Jeff Davis County. Other springs sampled and monitored in this study also exist in the Davis Mountains but are unrelated to the Balmorhea area spring complex.

All Balmorhea area springs except Phantom Lake discharges at the ground surface through alluviums or other recent deposits. Phantom Lake Spring, which has seen a quick decline in rate, discharges directly from a Buda Limestone bluff. It is the surface expression of a large flooded network of caves and passage ways that have been explored by speleologists and National Cave

and Karst Research Institute (NCKRI) researchers. Although the Phantom Lake Spring has ceased to flow perennially, a quasi-constant water level pond is maintained artificially at the entrance of the cave to conserve endangered species. San Solomon Spring (SSS) is the largest spring of the complex and the best documented. It has experienced a slow decline in discharge in the past few decades (currently 20-30 cfs). In its natural state, SSS used to emerge from fissures in the limestone basement covered by a few tens of feet of alluvium; spring flow used to cover extensive shallow wetlands (“*ciénagas*”) draining into Toyah Creek. Some of the alluvium was excavated in the 1930’s and the largest of the SSS springs currently discharges at the bottom of a large, man-made pool open to the public in Balmorhea State Park (BSP). TWDB (2005) located 6 individual springs at the bottom of the SSS pool. Neither Phantom Lake or SSS springs are in their natural state. Like Phantom Lake spring, SSS is heavily altered by pool operations, lowering the technical value of physical monitoring in the pool. Giffin Spring is located close to the SSS in a similar environment but with a much smaller, relatively constant discharge rate (3-5 cfs).

San Solomon, Phantom Lake, and Giffin springs (SS-PL-G) have consistently been described as artesian, that is, their piezometer head at emergence is higher than the local water table. On the other hand, East and West Sandia (ES-WS) and Saragosa springs have been presented by some authors as gravity or water-table springs whose emergence is a topographic accident where the local water table intersects the ground surface. They might also represent a reemergence of flow by the other springs (see Discussion below) (White et al., 1938, 1941; Knowles and Lang, 1947; Ogilbee and Wesselman, 1962; Ashworth et al., 1997). Similarly to SSS and Giffin springs, ES-WS and Saragosa springs emerge from alluvium. Ashworth et al. (1997) suggest several contributions to their flow: local rainfall, seepage from the canal system, irrigation return flow, and runoff from the Davis Mountains. Their flow is low and has been measured at a few cfs or less. TDS in East and West Sandia is typically higher than that of the clearly artesian springs, which could be an argument against a local source. However, Ashworth et al. (1997) suggest that the concentration could be elevated thanks to evaporation. White (1941), after water table mapping efforts, reasoned that the spring emergence elevation is consistent with the water table and therefore, they must be gravity springs. Other authors have described them as artesian (Brune, 1975; TWDB-TPWD, 2005). Brune (1975) asserts all the area springs are likely artesian but provides no evidence. TWDB-TPWD (2005) presented a model in which all the springs are artesian but are located in different fault compartments.

Flow at Balmorhea area springs has been declining for decades and perennial flow at some springs has ceased (Figure 4). Authors have hypothesized that the decline may be due to climatic changes since the end of the Pleistocene or to the more proximal drought of record of the 1950’s (Ashworth et al., 1987). Arguing against this later scenario, Brune (1981) noted the declines had started earlier. It is true that regional flow systems are slow to adapt to climatic changes and their response time to new forcing is delayed compared to the forcing variations. It follows that regional systems are rarely at steady state but rather reacting to the latest change in forcing, such as a decrease in recharge compared to when climate was cooler (as indicated by the lighter water isotopes) more than 10,000 years ago. However, anthropogenic effects owing to far-field or near-field pumping (irrigation) has been the generally accepted origin of the decline.

1.4 Objectives of the study

The overall goal of the study was to assess the vulnerability of the springs to development, both in terms of alteration of spring discharge and degradation of water quality. A key aspect of this

investigative study was to assess and complement the groundwater flow conceptual models of past decades. Previous investigations relied mostly on geochemical data and relatively little on physical measurements. This study was set to provide a close examination of water levels from different aquifers to elucidate key aspects of the regional and local flow systems. An essential part of the study was then to install data loggers at relevant locations to operate over the longest possible time frame.

In order to achieve this goal, the study proposed to address a few objectives:

- (1) Refine the regional, conceptual flow model that supplies water to the springs including relationships with associated aquifers (Alluvium / Pecos Valley, Igneous, Edwards-Trinity, Rustler, West Texas Bolsons, and Capitan aquifers). The research focus was to be on the Capitan of the Apache Mountains and neighboring area, which are thought to make an important contribution to spring baseflow (recharge zone).
- (2) Determine the local vertical flow gradient and potential exchange between aquifers in the Balmorhea area with the help of recently drilled wells and historical data using both water levels and geochemistry, paying attention to dual completion wells; this includes investigating potential contribution from so-called deep or basinal brines from the Permian Delaware Mountain Group (DMG).
- (3) Better understand the various flow contributions, regional versus locally-derived sources, at each of the Balmorhea-area springs.

These objectives follow from the official scope of work agreed on that includes:

- 1) Develop a refined hydrogeologic conceptual model / improve the hydrogeologic conceptual model of the regional groundwater-flow system that supplies water to the springs based on existing data and limited data collection (Task1);
- 2) Conduct a preliminary local aquifer recharge area delineation and groundwater flow assessment of aquifer vulnerability at the springs by developing a framework using the pre-existing regional groundwater flow system conceptual model (Task1);
- 3) Identify potential fluid migrations pathways through fault networks (Task3);
- 4) Evaluate and quantify the component of local recharge to the springs associated with nearby storms using continuous monitoring data and event-based, water sampling (Task4);
- 5) Develop an aquifer vulnerability assessment using results from previous tasks to identify a plausible recharge area (based upon hydrogeologic data), including assessment of high-consequence actions and estimates of timelines for any response actions and mitigation activities (Task2 and Task5);

Tasks 2 and 5 (bullet point #5 above) were addressed in a preliminary study documented in the Year1 progress report (Wolaver et al., 2019) and will not be revisited in this final report. Task 3 (bullet point #3 above) was to rely heavily on an analysis by BEG researchers of a proprietary 3D-seismic survey completed over the Alpine High Apache assets, including in the Balmorhea area. Because of unforeseen circumstances, this analysis did not take place and the task could not move forward. The budget was reallocated to monitoring well drilling efforts. The remaining Tasks (Task1 and Task4) correspond to bullet points #1, 2, and 4 above, and match the three objectives proceeding the original scope of work.

Year1 work, as defined by the content of Year1 progress report (February 2018 to April 2019), included mostly desktop tasks and preparation for the extensive field work that occurred during Year2 (May 2019 to December 2020). The initial plan called for installation of data loggers on springs, wells, and streams early on but, due to delays in securing permissions from land owners,

many of them were installed more than a year, and sometimes two years, after the effective start of the project (which was February 2018). Ad hoc geochemical monitoring of the springs took place throughout the study but sampling of wells and other features occurred mostly during Year2.

2 Geographic and geological settings

The study area lies within over 6,000 square miles covering southern Culberson, southwestern Reeves, most of Jeff Davis and small portions of Ward, Brewster, and Presidio counties. The area is bisected west to east by IH-10, centered on the intersection of IH-10 and IH-20 near Kent, TX. Van Horn, TX is on the western edge, with the city of Pecos, TX at the northeastern corner. Our study focuses on Balmorhea-area springs and the related groundwater flow systems. However, we consider a larger area to place the study within the regional hydrogeologic context of Trans-Pecos Texas. The larger study area includes the Alpine High play, the southwest portion of the Delaware Basin, the northeast side of the Davis Mountains located to the south of the Balmorhea area, and the Apache Mountains and the Bolson Aquifers to the west.

2.1 Topography and land use

2.1.1 Balmorhea area

The Balmorhea spring complex is located at the southern edge of a basin fill (physiographic Toyah Basin) extending to the north with little elevation changes to the center of the broad depression approximately 30 miles to the north. The Toyah Basin is a topographic feature that is also a hydrogeologic discharge zone for shallow flow. The Toyah Basin boundaries coincide with those of the southern section of the tectonic Delaware Basin (e.g., Brand and DeFord, 1962). The SSS elevation is 3306 ft (~1000 m), nearby Giffin Spring is approximately at the same elevation 750 ft to the west of SSS (LaFave and Sharp, 1987). Phantom Lake Spring cave opening, located ~3.5 miles to the west of SSS, occurs at the slightly higher elevation of 3475 ft (~1050 m) whereas East Sandia (3187 ft), West Sandia (3205 ft), and Saragosa (3250 ft) springs are located 3.5-4 miles to the northeast of SSS at lower elevations. Approximately 10 miles to the SW the basin fill transitions to the Davis Mountains whose highest peak (Mount Livermore) reaches 8,378 ft (2,492 m), 31 miles (50 km) to the SW of SSS (Figure 1). A small mountain range, the Barilla Mountains, aligned with a fault block, is individualized between Balmorhea and the Davis Mountains northeast of the main massif. Other geographic features of interest include the man-made Balmorhea Lake, 4 miles to the east of SSS, that collects spring flow and episodic stormflow, and the McDonald Observatory near the summit of Mount Locke (~6800 ft, ~2070m).

A topographic feature of great importance to this study, the Davis Mountains, consisting mostly of subhorizontal lava and ash layers and associated igneous bodies, can be more aptly described as a higher-elevation plateau abruptly connecting to the plain below (larger Toyah Basin to the northeast) and dissected by streams in narrow V-shaped valleys or canyons (White et al., 1941). These ephemeral streams and their watersheds are, from northwest to southeast: Cherry Creek, Madera Canyon, Little and Big Aguja Canyons and Limpia Creek (Figure 5). All, but one, watersheds merge shortly downstream of the mountain front, in the alluvial plain, to form Toyah Creek, a tributary of the Pecos River, ~40 miles to the northeast. Limpia Creek flows to the east toward the Leon-Belding irrigation area and Fort Stockton.

We use the following terminology to label the various zones: the “upper” mountain zone, high in the Davis Mountains; the “lower” mountain zone, at lower elevation in the Davis Mountains

where intermittent spring and stream flows are not uncommon; mountain front and piedmont, where the Cretaceous substratum is sometimes visible; the hills area, where faults along the Davis Mountains front have raised or dropped rocks of various resistance to erosion, and helped create linear small landforms such as the Barilla Mountains; and, finally, the flat Toyah Basin. The Balmorhea-area springs occur in between the latter two zones.

The local climate is semi-arid with no perennial streams, except those downstream of the springs, with large flashy summertime (monsoonal) storms and wintertime regional storms (Larkin and Bomar 1983). Rainfall events have two origins: summer convective thunderstorms (May to September) and cyclonic frontal stratiform storms, typically of a larger extent; both compounded by orographic effects. Total rainfall increases with elevation. Mean annual precipitation (1981–2010) is 678 mm (26.7 in) in the highest elevations in the Davis Mountains to 344 mm (13.6 in) in the basin floor at Balmorhea State Park (Figure 3). The maximum annual temperature is 36°–39°C (96.8°–102.2°F) during summer and 18°–24°C (64.4°–75.2°F) in winter (PRISM, 2018) at Balmorhea. The mean annual temperature is 11 C (51.8 F) in the Davis Mountains and 17.7 C (63.9 F) at Balmorhea.

Land use in the study area comprises mostly shrub/scrub (~88%), grasslands/herbaceous (~5%), evergreen forest (~5%), barren land (~0.9%), developed land (medium intensity, low intensity, and open space) (~0.8%), cultivated crops (~0.5%), wetlands (emergent herbaceous and woody; ~0.2%), deciduous forest (0.1%), and open developed land (MRLC, 2018) (T. Caldwell, pers. comm.). The major activity is ranching with some agricultural activities. A particular point of interest relates to the relative position of springs and irrigated land. There is no cultivated or irrigated land upslope and upstream of SS-PL-G springs but there is agricultural activities upslope of ES-WS and Saragosa springs, as well as the presence of Balmorhea Lake.

2.1.2 Broader area

Several features of interest exist west and upstream of the Balmorhea area: the Apache Mountains (Capitan Reef and associated formation outcrop), the Rustler Hills (Rustler Formation outcrop), the Delaware Mountains (late Permian deposits), Patterson Hills (Capitan Reef outcrop), and the salt flats (Figure 1). The Salt Basin includes, from north to south, the Salt Flat, bounded to the east by the Delaware Mountains, Wildhorse Flat, just west of the Apache Mountains, and Lobo Flat, bordering the Davis Mountains to their west. The Edwards Plateau stretches east of the Balmorhea area towards Fort Stockton.

Towns and communities in decreasing population size in the study area are: Van Horn located in the Salt Basin to the west, Fort Davis, located southwest of the Davis Mountains, Balmorhea, and Kent, a small community south of the Apache Mountains. These four locales, in addition to Mt Locke, each house an official weather station. The weather stations are used throughout this document as proxies to understand rain events.

2.2 **Geological Formations**

2.2.1 Balmorhea Area

The study area is located at the far southern edge of the tectonic Delaware Basin, a mostly Paleozoic sedimentary fill, developed as a foreland basin ahead of the Ouachita Thrust Front (Pennsylvanian) on top of earlier mostly passive shelf deposits, and resting on a Proterozoic basement. The Delaware Basin is characterized by a very thick Permian section at its center (Ruppel, 2019, 2020; Ewing, 2016). The Permian section consists of an accumulation of mostly siliciclastic basinal sediments with detrital carbonate rocks at the basin margins. Toward the

margins (where the study area is located), the basin fill, especially Permian formations, is much thinner, allowing organic-rich fine-grained formations of various ages (Devonian Woodford, Mississippian Barnett, and Permian Wolfcamp shales) to somehow coalesce into an interval targeted by oil and gas operators (Alpine High).

The youngest Permian formations, representing the final step of basin filling, consist of an evaporitic series with thick halite and anhydrite (older Castile and younger Salado Fms. of Ochoan age). The Salado Fm. does not exist in the study area but is present to the northeast (Anderson, 1981). The Castile Fm. is present in the study area but its interactions with the Stocks Fault zone and other faults NW of the Davis Mountains are complex and not fully deciphered in the context of this study. Castile and Salado Fms. are capped by the Rustler Fm. also of Ochoan age, and mostly of non-marine origin (Ewing, 2016). In its extent of interest, the Rustler Fm. consists of halite/anhydrite, karstified dolomite, and siltstones and is considered more clastic in its lower portion (Ewing et al., 2012). It is approximately 400 to 500 ft thick in the Balmorhea area and not known to contain halite in that same area. Water bearing Rustler units in the Balmorhea area are the ~80 ft-thick Culebra Dolomite and the underlying limestones of the Los Medanos Member (cumulative ~50 ft) (Lupton et al., 2016). The Dewey Lake Fm., comprising red beds, traditionally caps the Permian, particularly in the Midland Basin (alternative name Pierce Canyon Fm. in the northern Delaware Basin); however, it has not been observed in the study area.

Although of Permian age, from an hydrogeologic operational standpoint, the Rustler Fm. belongs to the same system as more recent formations of Triassic, Cretaceous, and Cenozoic age because it is separated from the other water-bearing Permian formations by the thick Castille-Salado aquitard. The Rustler Fm. crops out in the western margins of the Delaware basin in the Rustler Hills. The lacustrine Triassic Dockum Fm. made of red bed siltstones and mudstones with some more sandy intervals such as the Santa Rosa Sandstone, is well represented in the Permian Basin but does not exist in the study area and was likely never deposited there (Brown, 2019). Meyer et al. (2012) map its closest occurrence to the study area at 1000+ft in the subsurface approximately at the mouth of Limpia Creek into the Toyah Basin.

Overall, late Lower Cretaceous strata (mostly of Albian age) rest unconformably on Permian formations, and Triassic when present, and consist of cycles of transgressive-regressive stages of marine sediments (Barker and Ardis, 1992; Barker et al., 1994). The Cretaceous strata are coeval and sometimes similar to well-known formations to the east that have been described in Central Texas, such as the lithostatigraphic groups of the Trinity (Antlers Sands and Glenrose Limestone), Fredericksburg (lower section of the Edwards Limestone), and Lower Washita (including upper section of the Edwards Limestone) stages. North of the Davis Mountains Front and of the Reeves-Jeff Davis county line, Trinity sediments are absent and Edwards Limestone equivalents rest directly on Permian Rocks. They consist of the Finlay Limestone (Fredericksburg), an open shelf massive limestone, and, after a short sedimentation gap, of the Boracho Limestone (Washita), deposited in a shallow basin with clayey input resulting in some marl intervals (Ewing, 2016). They represent facies different from those of the Edwards platform (whose western edge does not go passed Fort Stockton) deposited in shallow environments, and characterized, in particular, by the lack of dolomite (i.e., groundwater with geochemical dolomitic markers could indicate a Permian source). An older Lower Cretaceous Trinity facies is possibly present underneath the Davis Mountains, a Glen Rose equivalent, the Bluff Mesa Formation, a cyclic shelf limestone. To the west, south of the Apache Mountains, and to the NE,

in the footprint of the Salt Basin, the Trinity-age shoal-like limestone Yearwood Formation and the slightly younger deltaic Cox Sandstone (with some carbonates), respectively, crop out or underlie Edwards Group equivalent rocks. The iconic Glen Rose Limestone, which shows many cycles including very shallow deposits, and the fluvial Antlers Sandstone, well-known markers of Central Texas Cretaceous deposits are not present in West Texas (Ewing, 2016).

The Lower Cretaceous ended with a general flooding of the Washita-stage platform and other basins in Texas depositing the Del Rio Clay and coeval formations followed by the extensive open-marine Buda Limestone. Del Rio Clay and Buda Limestone are formally of Cenomanian age and thus belong to the Upper Cretaceous. However, they are still part of the Washita stage and mark the end of the Comanchean series, which includes the Trinity, Fredericksburg, and Washita stages. The Gulfian series starts with the first formation overlying the Buda Limestone. Note that the Del Rio Clay, which typically underlies the Buda Limestone in most of its footprint and disconnects it from the Edwards limestones, is replaced by the San Marine argillaceous limestone in the study area. Comanchean carbonate sediments were subaerially exposed and karstified prior to deposition of the Gulfian sediments. The early Upper Cretaceous Boquillas Fm. (organic-rich marl and clay Eagle Ford and Austin Chalk equivalent) rests unconformably on top of the Buda Limestone and marks the first episode of the (anoxic) Cretaceous Western Interior Seaway (~95 Ma). Younger Upper Cretaceous sediments of the Gulfian series (older literature mentions marl of the Taylor Group, stratigraphically above the Austin Chalk) were eroded when not protected by the Cenozoic volcanic rocks; for example, they can be observed on the periphery of the Barilla Mountains (Ewing, 2016).

Thick volcanic deposits that were laid down on an eroded surface cap the Cretaceous formations (Cretaceous period ended at ~66 Ma) and their remnants are currently observable in the Davis Mountains. They initially covered the southern half of Reeves County (Brown, 2019). Volcanic activity started ~48 Ma, peaked during late Eocene–early Oligocene (~38–36 Ma), and ended ~17 Ma ago. The volcanites were impacted by normal faulting and have been heavily eroded. They were part of a vast volcanic field composed of rhyolitic and trachytic pyroclastic flows (ignimbrites) and lava flows and occasional volcanoclastic material, including conglomerates (Barker, 1977, 1979, 1987; Gibbon, 1969; Henry et al., 1988; Parker, 1988; Parker et al., 2017). The Gomez Tuff is the most extensive ignimbrite of the Davis Mountains while the Star Mountain Rhyolite marked the onset of flood rhyolite magmatism (Parker et al., 2017). The basal formation, the Huelster Formation, consists mostly of volcanic tuff but with thin layers of sandstone and conglomerate, lenses of non-marine limestones and mafic lava (Fort Stockton GAT sheet). Multiple authors (e.g., Pearson, 1985) note that the Huelster Formation crops out mainly as a slump or thick landslide deposit (Q1 of the GAT sheet). The landslide rocks are somewhat chaotic but moved as a coherent unit (so-called Toreva style) on top of the incompetent clayey and marly Upper Cretaceous. When intact, the basal unit of the Huelster Formation, the Jeff conglomerate, is a few tens of feet-thick high permeability unit that fills up the valleys of the Upper Cretaceous landscape (Pearson, 1985).

A relatively thin mostly siliciclastic cover of recent deposits and alluvium completes the stratigraphic succession. Land et al. (2020)'s resistivity profiles in the vicinity of San Solomon and Giffin springs suggest an irregular thickness of ~50 ft for these deposits. The TWDB report on the Pecos Valley Aquifer (Meyer et al., 2012) combines the Balmorhea area alluvial deposits together with those along the Davis Mountains front. Quaternary deposits at the mountain front are likely in the unsaturated zone but they ultimately recharge the major aquifer of the Toyah

Basin (Pecos Valley Aquifer). Although operationally, the aquifer begins north of I-10 where its thickness increases sharply to >600 ft.

2.2.2 Western edge of the Delaware Basin, Capitan Reef, and Salt Basin.

There are other rock units of potential interest to this study (Urbanczyk et al., 2001). One category of such rocks are Paleozoic formations underlying the Balmorhea area that form the regional basement, and, in particular, rocks of pre-Ochoan Permian age, which are notably thick and common in West Texas (Figure 6 and Figure 7). These rocks are well-known thanks to abundant hydrocarbon accumulations. Oil and gas operators target the Wolfcamp and Bone Spring Fms., of Wolfcampian and Leonardian age, respectively. They consist mostly of fine-grained rocks (mudrocks and siltstones), some of them organic-rich sources of the oil being produced. The Bone Spring is overlain by the Delaware Mountain Group (DMG) (Guadalupian age), a thick interval composed of three formations (Brushy Canyon, Cherry Canyon, and Bell Canyon in ascending stratigraphic order) and made of siltstones and sandstones with some carbonates (Smye et al., 2021). The DMG crops out in the Delaware Mountains, just west of the Rustler Hills. The importance of the DMG formations resides in the fact that they have a recharge zone at higher elevation (that is, potentially higher downgradient heads) than that of the Rustler, can potentially contain highly saline brines, and might directly underlie the Rustler (except when the Castile is present) or even Cretaceous rocks (e.g., Finch, 2017) in areas of structural complexity, such as in the Stocks Fault zone, and in the Balmorhea area.

The Delaware Basin is ringed by an important reefal system, the Capitan Reef complex (Figure 1), whose core is made of massive carbonates, particularly dolomites, and which is of Guadalupian age, coeval with the DMG, but systematically positioned at higher elevation, then and now (Hiss, 1976; Uliana, 2001). The western arm of the Capitan is exposed in the Guadalupe Mountains, close to the New Mexico state line, but is down-dropped south of the Guadalupe Mountains by a major N-S fault (Border Fault Zone), which also marks the eastern boundary of the northern section of the Salt Basin. Proceeding south, the western arm of the Capitan crops out in a small area just south of the Guadalupe Mountains and west of the Border Fault Zone (Patterson Hills outcrop), is buried under the Salt Flat fill, and reemerges to the south in the Apache Mountains, south of the Stocks Fault. The buried western arm of the Capitan, the Apache Mountains, and the Stocks Fault all play an important role in the hydrogeology of the Balmorhea springs. The Capitan has a third major exposure in the Glass Mountains, southeast of the study area along the eastern arm of the reef complex. The gap between the Capitan of the Glass Mountains and the southern end of the western arm was created by the Hovey Channel, which put the Permian Basin in communication with the open ocean in Permian time (Standen et al., 2009).

Also, in Permian time, approximately landward of the Capitan footprint, the Delaware Basin was surrounded by shelves that were episodically exposed to the atmosphere, counterclockwise from south, the Southern Shelf, the Central Basin Platform, the Northern Shelf, the Northwest Shelf, and the Diablo Platform. The backreef and lagoonal area behind the core of the Capitan and farther away to the Permian shore is composed of siltstones/ fine sandstones and fractured carbonates of the Artesia Group such as the Yates Formation (alternating very fine-grained sandstone and dolomite) that crops out south of the Apache Mountains. The bottom of the Artesia aquifer is assumed to be the Cutoff Shale at the top of the Leonardian Bone Spring and coeval formations such as the Victorio Peak Limestone.

The Diablo Platform was later disconnected from what is now the Permian Basin by the easternmost manifestation of Basin and Range tectonics (Neogene), creating the multiple bolsons (or deep narrow basins) of the Salt Basin. They include from north to south: the Salt Flat, which is an endorheic basin with evaporitic salt deposits at its center, the Wildhorse and Michigan Flats, the Lobo Flat, and the Ryan Flat. The later four, unlike the Salt Flat, have been described as having a single outlet to the east for the water recharged from the surrounding mountains, just south where the Salt Flat starts. All the bolsons have at least locally a thick Cenozoic fill overlying Permian and Cretaceous rocks and in some cases directly on top of the Precambrian basement. The Precambrian basement crops out in the vicinity of Van Horn. The sediment fill of the Salt Basin bolsons can be as thick as 1600 ft (Beach et al., 2004).

2.3 Structural Features

Two major tectonic events directed the current topographic features of the Delaware Basin and nearby areas: Laramide Orogeny (Paleocene) and Neogene uplift and tilting. The Salt Basin denotes the easternmost expression of the post-Laramide Basin-and-Range tectonics and represents a drop-down section of the Diablo Platform bounded to the east by a series of normal faults (~N-S Border Fault Zone). Some of these faults can have throws exceeding 1000 feet. In the Neogene period (10-20 Ma), the entire Texas craton (including Trans-Pecos area) was uplifted and tilted toward the Gulf of Mexico. The uplift, along with faulting, exposed features of the western section of the Delaware Basin such as the Capitan Reef in the Guadalupe and Apache Mountains, the DMG in the Delaware Mountains, and the Rustler in the Rustler Hills. It also promoted the erosion of the volcanic rocks currently exposed in the Davis Mountains. Overall, layers, including Permian layers, have a small variable dip and are mostly undisturbed except in the vicinity of faults.

The structural feature of utmost importance remains the WNW Stocks Fault north of the Apache Mountains and associated features. The Stocks and related faults play two roles: they increase the permeability in the direction of the faults and they put into contact two permeable formations: the Capitan Reef and the Cretaceous limestones. The Stocks Fault is a normal fault system with throws varying from 500 to 1100+ ft (LaFave and Sharp, 1987) that predates the Laramide Orogeny and may be a reactivation of Paleozoic features. The biggest throw of the Stocks fault (>1100ft) is expressed in the Apache Mountains scarp, with the throw attenuating to the ESE to ~500 ft at the northern tip of the Davis Mountains (Brand and DeFord, 1962). Geological maps stop the trace of the Stocks Fault 10-15 miles to the west/northwest of the Balmorea spring area. A structural feature aligned with the Stocks Fault to the west is the NW-SE NNW-SSE Victorio Flexure across the Salt Basin and Diablo Platform where it is best expressed. The flexure might be the surface expression of an Ouachita-related deep-rooted fault (Pearson, 1985).

The Basin and Range faulting impacts the Stocks Fault in the western third of the Apache Mountains. Gentle folding after the volcanic episode created a marked anticline at the mountain front exposing Lower Cretaceous rocks south of the main branch of the Stocks Fault. The Stocks Fault is well-developed on the northern flank of the Apache Mountains, but its expression is less obvious along the Jeff Davis-Reeves county line. The folding there is unusual in an area dominated by normal faulting but may represent an extension of the Stocks Fault expressed as broad folds thanks to the presence of the thick Upper Cretaceous marly sediments (Pearson, 1985). Pearson also proposed that the folding deformation style on the NE flank of the Davis Mountains (as opposed to faulting) is due to the presence of incompetent Upper Cretaceous rocks

as well as the presence of thick Castile rocks at the connection of the Diablo Platform with the Delaware Basin proper.

Deformation along the northeastern Davis Mountains is expressed by an ample SE-plunging syncline with Cretaceous formations on its flanks and Cenozoic volcanic rocks along its axis: the Rounsaville Syncline (true syncline, not tilted fault blocks). Note that the southwest flank along the mountain front is masked by the Huelster formation-derived landslide material (“QI” of GAT maps). The syncline is noticeable at the western end of the Apache Mountains north of the Stocks Fault then changes direction from WNW-ESE to NW-SE to be parallel to the northern front of the Davis Mountains southeast to the mouth of Limpia Creek into the Toyah Basin at the SE end of the Barilla Mountains. Progressively younger formations are observed to crop out on each side of the syncline axis, underlining its southeastern plunge: from (1) Trinity-stage Yearwood and Cox Formations, north of the Apache Mountains and of the Stocks Fault, (2) to mostly Fredericksburg- and Washita-stage limestone with volcanic rock remnants along the syncline axis, SW of the Balmorhea spring area, (3) to Washita-stage and Upper Cretaceous rocks into Pecos County (Pearson, 1985). The north flank of the Rounsaville Syncline can also be described as the south flank of the Barilla Mountains Anticline, which is well-expressed by the erosion-resistant volcanic rocks of the Barilla Mountains, then transitions to the NE to a subdued feature that can be called the Balmorhea Syncline. In the same fashion, the south flank of the Rounsaville Syncline is sometimes described as the northern flank of the Star Mountain Anticline. Phantom Lake Spring emerges from one of the numerous NW-SE faults impacting the Rounsaville Syncline (on its northeastern flank at a topographic low). Note that there is a series of exposed NW-SE to NNW-SSE normal faults mostly downthrow to the NE towards the Toyah Basin. A few are downthrow to the Davis Mountains, creating small grabens. The Fort Stockton GAT sheet shows a dense population of these faults when not covered by quaternary deposits. Undoubtedly many more exists underneath the recent cover. The Brogada Hills, a Huelster Formation outcrop, 1 mile east of the town of Balmorhea, is an expression of this fault system. Recent work by the BEG on deep faults attenuating in the early Permian (Horne et al., 2021) and shallow faults impacting the DMG (work in progress), including in the Balmorhea area, has not been including in this study.

2.4 Regional Hydrogeology

The regional hydrogeology is simple in its main features but complicated in the Balmorhea area because of faulting and because the confines of several aquifers overlap there. No current regional hydrogeological flow model includes the Balmorhea springs as a feature centrally positioned in the model and therefore all models show edge effects. TWDB-recognized aquifers present in the study area, sorted by increasing age of the host formation, are: the Pecos Valley Aquifer, the Igneous Aquifer, the Edwards-Trinity Aquifer, and the Rustler Aquifer, to which the DMG aquifer can be added. There might be other unnamed aquifers of importance. Away from the Balmorhea spring complex to the west but of importance are the TWDB-sanctioned Capitan Reef Aquifer and the Bolson Aquifers. Alluvium deposits exist in the area that can be considered the southernmost extension and feathered edge of the Pecos Valley Aquifer, whose main body is to the north. The Dockum Aquifer (Bradley and Kalaswad, 2003; Ewing et al., 2008) is not present in the study area or upstream/updip/upflow/upslope of the study area and is no further discussed.

The Davis Mountains contain the Igneous Aquifer (Beach et al., 2004). The pyroclastic tuffs and lava flows are fractured and porous and can accept abundant recharge on a short flow path

(White, 1941; Beach et al., 2004). The regional model of the Igneous Aquifer by Beach et al. (2004) assumed that recharge is a function of annual rainfall, that is, a function of elevation, initially estimating recharge values from 1.8% of precipitation at 14 in/yr (~Balmorhea) to 7% of precipitation at 20 in/yr (upper areas of the Davis Mountains); additional intermediate values are provided in their report. Their calibrated model suggests annual average recharge is lower at ~half of this initial guess. The volcanic rocks are porous and generally assumed to rest on top of the clayey Upper Cretaceous, a flow barrier, and are drained by several high permeability intervals, including the basal conglomerate of the Huelster Fm. The aquifer is typically recharged by monsoonal summer precipitation and discharges through evapotranspiration and seeps and springs (some sampled by BEG). If the valleys or canyons are incised deep enough into the igneous deposits to reach one of these draining layers, in particular, the Huelster conglomerate in the northern section of the Davis Mountains, semi-perennial flow can ensue. The regional picture is that of an aquifer with centrally positioned recharge (higher elevation), centrifugal subsurface flow into valleys, and possibly recharging the underlying Cretaceous when the low-permeability Upper Cretaceous is absent, providing a low-level baseflow. However, it seems that the likelihood that the volcanic rocks could directly overlie the Lower Cretaceous and recharge it is low. An examination of the GAT sheets suggests that it would be uncommon if it exists at all as the Boquillas Fm. is often present on the periphery of the volcanic rock outcrops. On the other hand, when water reaches the impervious upper Cretaceous, it forms springs where the contact is exposed in stream valleys. In the details, the aquifer is fragmented by the deep and steep incised valleys. Overall, the composite aquifer discharges downslope into the alluvial aquifers of the West Texas Bolsons to the west, to the Pecos Valley Aquifer to the north and also the Edwards-Trinity Aquifer to the north and east (Limpia Creek). The geochemistry of the aquifer is as expected from silicic rocks with silica-rich and very low TDS groundwater, a Ca-HCO₃ water type.

Some of the Cretaceous formations form the Edwards-Trinity (Plateau) Aquifer, whose far southwestern edge corresponds to the study area. Note that the TWDB use the term Edwards-Trinity (Plateau) Aquifer to differentiate it from other sections of the aquifer in Central Texas and west of the Dallas Fort Worth area. Here, we use Edwards-Trinity Aquifer as short for Edwards-Trinity (Plateau) Aquifer. The aquifer has a large areal extent on par with the extent of the Cretaceous layers extending all the way from West Texas to the Balcones Fault zone where Austin and San Antonio are located ~350 miles to the east. In actuality, the Edwards-Trinity Aquifer comprises several individual aquifers in vertical communication (Anaya and Jones, 2009). One of the aquifers, the basal aquifer, typically occurs in the mostly clastic Trinity formations. However, the Trinity stage is not expressed in the Balmorhea spring area; it is represented by the Cox Sandstone that crops out east of the Apache Mountains in Culberson County where its thickness is ~170 ft (Ogilbee and Wesselman, 1962) and provides some water for agricultural activities (Brand and DeFord, 1962). The Cox Sandstone is also present at the base of the Salt Flat fill in the northwestern part of the study area. It seems that the absence of the Cox Sandstone in the Balmorhea area is not erosional but rather due to a lack sediment deposition there. The Maxon Sandstone in Pecos and Brewster Counties is the next small deltaic sandy accumulation corresponding to another small river (Ewing, 2016). The Edwards Group proper is represented by the massive Finlay Limestone (40 ft, Ogilbee and Wesselman, 1962) and the thicker but clayey Boracho Limestone (400 ft, Ogilbee and Wesselman, 1962), including the San Marine Fm., a Del Rio Clay equivalent. The Buda Limestone (160 ft, Ogilbee and Wesselman, 1962), which overlies the Edwards Group, is a tight carbonate and generally

considered an aquitard and not formally part of the Edwards-Trinity Aquifer. It turns out that the Buda Limestone is often above the water table –south of the Stocks Fault / Rounsaville Syncline structural trend (Ogilbee and Wesselman, 1962). The Edwards-Trinity aquifer is a fresh water aquifer but it has a variable chemistry depending on the recharge area (Permian carbonates, Davis Mountains, Glass Mountains) (Thomas et al., 2013). A common water type is mixed cation (Na-Ca)-mixed anion (Cl-SO₄) (influence of the Rustler and Pecos Valley Alluvium aquifers) whereas some autogenous water samples (recharged through an outcropping Edwards Fm.) show a Ca-HCO₃ water type (Piper plot from our extended database – 313 samples). The Edwards-Trinity Aquifer historically discharges to the Pecos River to the NNE and the regional potentiometric contour lines are oriented WNW (Bush et al., 1993, measurements 1915-1969, mostly in the 1930's). Regional TDS is moderately fresh except in northern Reeves County (impact of the Pecos Valley Aquifer and, maybe, Rustler) and in Central Pecos County (Rustler upflow) (Bush et al., 1993). Kreitler et al. (2013) did a thorough and sophisticated analysis of geochemical data collected in the Edwards-Trinity Aquifer footprint, in particular focusing on isotopes in their interpretation.

The Rustler Aquifer is a brackish water aquifer underlying the Cretaceous on most of its extent (Boghici and Van Broekhoven, 2001; Ewing et al., 2012; Lupton et al., 2016). In its outcrop and shallow downdip, in the Rustler Hills, the aquifer is composed mostly of siltstone and dolomitic limestone (both towards the base of the Rustler Fm.) with anhydrite (towards the top of the Rustler Fm., confining the more permeable water-bearing intervals) yielding waters of calcium-sulfate (Ca-SO₄) with high magnesium composition, and of moderate to high salinity from the interaction with anhydrite and dolomitic intervals. It seems that clastics are more abundant toward the northern section of the Rustler in New Mexico. There, numerous studies have been associated with the WIPP facility where the Culebra Dolomite is the most significant water-bearing formation; in the southern section, including the Balmorhea area, the Rustler contains more carbonate at the base of the section (Los Medaños of Lupton et al., 2016). A second recharge zone may exist east of the Davis Mountains, in the Glass Mountains, through a formation coeval with the Rustler and Salado, the Tessey Limestone, that would force the flowlines to align north toward the Pecos River, the natural discharge area of the Rustler. The southern Rustler boundary along the Davis Mountains is not clear because of the structural complexities of faulting and pre-Cretaceous events. However it seems that the southern limit is erosional and dictated by faulting; it is unknown whether the Rustler is present below the Cretaceous formations of the Davis Mountains region although a data point in Pearson (1985) suggests it is not. The Rustler is not hydraulically connected to Permian aquifers because of the thick Castile Fm. except maybe at the south boundary where it meets the structural complexity along the mountain front; there the Castile is thin and might have been removed by erosion. Based on geochemical arguments, it is accepted that Rustler waters migrate upward into Cretaceous and Pecos Valley Aquifers (Bush et al., 1994; Ewing et al., 2012; Bumgarner et al., 2012); for example, at the Diamond Y spring near Fort Stockton (Boghici, 1997). It is not clear if that is true in the Balmorhea area where Ewing et al. (2012) hypothesized that the Rustler might be recharged, possibly through the regional flow supporting the springs.

The Rustler has relatively low TDS along its southern border up to 2000 mg/L (that is, lower than that of the Balmorhea area springs) increasing to >10,000 mg/L towards the NE to Winkler County (Lupton et al., 2016). Lupton et al. (2016) describes two populations that cannot be ascribed a spatial subarea: a dominant group with the expected high Ca-SO₄ with minor Na, Mg, and Cl and a minor population still Ca- and SO₄-rich but trending towards higher Na and Cl.

However, the water type is still Ca-SO₄ (Piper plot of our extended database – 56 samples) but with some Mg. No halite is known to occur in the Rustler in the Balmorhea area to provide Cl; it can only provide Ca and SO₄.

Although far from being a fresh-water aquifer except maybe in its outcrop area, the DMG is coeval with the Permian Capitan and might directly underlie Rustler or even Cretaceous formations. The DMG is the recipient of waste water produced during oil and gas operations and could potentially perturb the local hydrogeology given the large volumes injected (Ge et al., 2021).

Other aquifers of importance to this study are the Capitan Reef Aquifer and the West Texas Bolson Aquifers to the west of the study area. The Capitan Reef and associated reef complex is a heavily karsted formation of Permian age that rings the Delaware Basin (Figure 1) (Hiss, 1976; Standen et al., 2009; Jones, 2016a,b). The Capitan Reef, because of deeply incised valleys and faulting, does not make a single well-connected aquifer, its northern section in New Mexico is the best studied whereas the western arm south of the Border Fault Zone and of the Guadalupe Mountains (and including the Apache Mountains and the Balmorhea area) is the least studied. There, the Capitan Aquifer is in lateral contact with the Trinity-Edwards Aquifer across the Stocks Fault. The Capitan Fm. crops out at several locations, including in the Apache Mountains just south of the Stocks Fault (WNW portion of the study area). Its western arm is considered an aquifer when present in the Salt Basin but the section SE of the Apache Mountains underlies the foothills of the Davis Mountains along the Reeves-Jeff Davis County line and can be deeper than 1000 ft. Standen et al. (2009) shows a sharp reduction in thickness of the Capitan core in the downfaulted block north of the Apache Mountains, likely corresponding to one of the many incised valleys that fed the DMG deep basin deposits. This fill may direct the flow towards the Toyah Basin and away from the flow lines along the Stocks Fault zone. Because of the paucity of data, there are likely more of these incised valleys that have not been detected or mapped in the western arm of the Capitan Reef.

Capitan Aquifer geochemistry is very variable from fresh in the exposed sections of the reef (e.g., Carlsbad area where it is a municipal water source) to saline in the deepest sections of the water-bearing formation (middle of the eastern arm in Ward County). The section south of the Guadalupe Mountains underlying the Salt Basin is likely to have a TDS between 1000 and 3000 mg/L. Farther south, water quality sampling by Finch (2017) shows evidence of recharge in the Apache Mountains with low TDS, relatively high bicarbonate, and heavier water isotopes, analogous to processes in the Davis Mountains (recent recharge); precipitation events there could also send a signal to the Balmorhea springs. The deeper Capitan section in Jeff Davis County which completes the western arm, is buried relatively deep and not well known but TDS is expected to be in the 5,000 to 10,000 mg/L range. The 91 samples of our extended database show variable water types but all with higher Mg.

The Salt Basin fills are mostly alluvium of variable thickness but that could be >1500 ft at several locations (Beach et al., 2004). Recharge is through the adjacent mountain ranges, some of them of Precambrian age. In addition, Michigan Flat and Ryan Flat are bordered on their eastern side by the Davis Mountains. Water is mostly discharged through evaporation and evapotranspiration with some water egress on the eastern side of the Wild Horse Flat through Permian deposits south of the Apache Mountains as demonstrated by Sharp (1989) based on predevelopment heads. However, by the 1950's, contoured potentiometric maps show that predevelopment discharge was captured by cones of depression of local irrigation wells (Beach et

al., 2004). A groundwater divide exists along the Victorio Flexure. The northern basin (“Salt Flat”) has been described as closed hydraulically as recharge is lost through evaporative discharge in playas. The Victorio Flexure, creating a basement high on the north side of Wild Horse Flat, represents a groundwater flow divide isolating the endorheic Salt Flat to the north (Beach et al., 2004). It prevents groundwater in Wild Horse Flat from discharging to the playa lakes of the Salt Flat to the north, although the flow would be favored by the topographic slope. Surfaces of the playas show deposits of halite and gypsum and was occupied by a lake in a recent past (Wilkins and Currey, 1997). Groundwater composition also marks the divide; groundwater is mostly fresh to brackish south of the divide whereas it is mostly saline north of the divide. The groundwater quality is good in the Lobo and Ryan Flats but degrades locally in the Wild Horse and Michigan Flats where it can reach 3000 mg/L (Beach et al, 2004). The divide funnels Bolson discharge east to the Apache Mountains. The waters are of the Na- HCO₃ to Na-mixed Cl- HCO₃ with some SO₄ types (Piper plot of our extended database – 366 samples).

The Pecos Valley Aquifer (PVA) is an important regional aquifer to the north of the Balmorhea area (Meyer et al., 2012; Anaya, and Jones, 2009) but, in the study area, the southernmost continuation of deposits making up the aquifer are thin. Some publications consider that the PVA begins at the Davis Mountains mountain front where the deposits (mostly alluvium) are <100 ft-thick south of I-10. However, the PVA operational boundary is north of I-10 where the thickness increases sharply to >600 ft (maximum >1500 ft in northern Reeves County). The chemistry of the alluvium in the Balmorhea area is strongly impacted by the underlying material. Geochemistry of the main PVA body is described in detail in Meyer et al. (2012). The TDS is typically in the 1000-3000 mg/L range north of the Balmorhea area and increase to >5000 mg/L when approaching the Pecos River. The groundwater typically has similar Cl and SO₄ concentrations and shows a mixed cation (Na-Ca)-mixed anion (Cl-SO₄) water type (Piper plot of our extended database – 303 samples).

2.5 Anthropogenic actions

Springs of Trans-Pecos Texas have undergone documented decade-long reduction of flows or even drying following various settlements in the late 1880s (Brune, 1975; Simonds, 1996; Sharp et al., 2003; FWS 2004; Unmack and Minckley, 2008; Lewis et al 2013; Tyler, 2020). The exact cause(s) for most springflow decline are poorly understood, including for the Balmorhea spring complex. An exception is the Comanche Springs in Fort Stockton, which dried in 1961 following the advent of groundwater pumping of the Edwards-Trinity Aquifer for irrigated agriculture. Although it is clear that native tribes and Spanish travelers visited and used the Balmorhea springs in earlier times (Boren, 2012), the first documented extensive use of the spring water by white settlers dates back to 1853 (Knowles and Lang, 1947). Natural characteristics of the springs started to be profoundly modified in the late 1890’s with the construction of canals and the draining of the natural wetlands (“*ciénegas*”) for irrigation. Water wells in support of ranching and irrigated agriculture were also drilled at that time. The dam holding Lake Balmorhea was built in 1917 in order to store water. Dowell and Breeding (1967) state: “*Principal source of water for Lake Balmorhea is flow from San Solomon Springs. This flow is supplemented by water delivered to the lake from Toyah Creek by the Madera Diversion Dam and canals. Surplus water from Phantom Lake Canal (fed by Phantom Lake Spring) is also stored in the lake until needed for irrigation.*” The large swimming pool around San Solomon spring was built in 1936 by excavating the alluvium to a depth of ~25 ft. After the Phantom Lake Spring went dry in 1999, a pumping system was installed in the early 2000’s to maintain a quasi-constant water level to protect the endemic aquatic species living there.

Human actions have modified the natural environment in several ways: (1) the natural *ciénagas* associated with the springs have disappeared or have been reduced in size with digging of canals and construction of dams and pools. These elements have modified the local hydrogeology of the springs, in particular, they have limited the usefulness of continuous monitoring at the springs given the numerous human interferences; (2) pumping for domestic use or irrigation have created local cones of depression; pumping from more recent, larger and more numerous water supply wells to cover the oil and gas industry water needs may have created regional cones of depression (unobserved so far given lack of data). Note that this study did not compile groundwater pumping rates and volumes; and (3) multilevel completion of wells has created pathways for aquifers to communicate vertically. The latter is likely negligible at the regional scale but could matter at the local scale, such as next to a spring, and could blur scientific understanding of the system.

2.5.1 Phantom Lake Spring

Phantom Lake Spring, approximately 5.5 km (~3.5 mi) west of San Solomon Springs (and the highest elevation of the Balmorhea-area springs group), shows a monotonic decline in spring discharge that started in 1950's, which may correspond to regional-scale increases in groundwater extraction for irrigated agriculture. Spring discharge used to flow into canals, built by Bureau of Reclamation following WWII, but springflow ceased in 1999. A nearby smaller satellite spring dried up in 1993 (Hershler et al., 1993). However, the main Phantom Lake Spring still experiences discharge following elevated precipitation in Davis Mountains. The U.S. Bureau of Reclamation currently oversees management of pumps that lift water from the spring to an artificial wetland providing habitat for endangered species of conservation interest to the U.S. Fish and Wildlife Service. Because of the pumping and recirculation of water for the constructed wetlands at this spring, the water near the cave opening, where there is a pump intake, might not be representative of formation water quality. The temperature-conductivity-stage logger likely only provides representative data when the spring flows naturally following heavy precipitation. The spring is morphologically different from the other springs as it flows (flowed) directly from a cave opening in upper Cretaceous Buda limestone. It has been observed (TWDB-TPWD, 2005) that the spring egress is the highest-elevation point of the flooded cave network and that a small variation in the local head can severely impact the spring flow rate without necessarily impacting the much larger volume flowing through the cave network system.

2.5.2 San Solomon Spring

San Solomon Spring, at Balmorhea State Park (BSP), is the spring with the largest flow rate of the Balmorhea spring complex. It used to flow out into a large, shallow wetland (*ciénega*) which provided aquatic habitats. Currently, following agricultural development that started in the 1880's, all spring flows are conveyed to Lake Balmorhea or immediately used for crop irrigation. The spring initially discharges in a man-made pool constructed into gravel deposited by the ancestral Toyah Creek. The underlying local bedrock is understood to be the Buda Limestone. San Solomon Spring is the easiest spring to access and also the most monitored of the complex. USGS has installed a discharge gauge and TCEQ has installed a temperature and specific conductance logger at the spring outflow canal but their data are sometimes hard to interpret because of operations at the pool. In addition, during periods in which the pool was drained, it was observed that some of the water leaks into surrounding sands and gravels, maybe suggesting that the USGS gauge does not capture the entire spring flow. Outflows are through the main discharge canal where USGS gauge is located (south side pool) and through the Reeves County Water Improvement District irrigation canal (north side of pool) used during the spring and

summer irrigation season. A pool drain is located below the main diving board on the east side of pool.

Dye tracing by Veni (2013) (injection at Phantom Lake Spring and monitoring at San Solomon Spring) confirmed the presence of fast-flow paths in the local karstified carbonate rocks. However, the tracer was not observed at the nearby Giffin Spring or more distant East and West Sandia and Saragosa Springs, highlighting the complexity of discrete flow in a faulted karstic environment. It took 6 days for the dye to travel between the springs in base flow conditions (~1 km/day; 6 days to travel the 6 km, in a straight line, between the 2 springs). But note the difference between solute transport and pressure diffusion. Couch (1978) noted that it takes ~24 hours after a large rain event for the signal to be seen at Phantom Lake Spring and an additional ~24 hours before it reaches San Solomon Spring (and TDS change travels with the pulse). Observing that the recharge zone is higher up along the mountain front during storm events (strongly losing streams) but that the average head gradient is not much increased, it can be concluded that the porosity of the system must decline between Phantom Lake and San Solomon to stay consistent with the much smaller travel time during storm events.

2.5.3 Giffin Spring

Giffin Spring is very close to San Solomon Spring and they share similar geochemistry, but the springs behave differently. The Giffin flow rate has held relatively steady (no decline) albeit at a much lower rate than that of San Solomon over the 100-year period of record. TWDB-TPWD (2005) performed a careful elevation survey and determined that Giffin pool water level was ~1 feet higher than SSS pool (natural conditions?). The USGS maintains a discharge gauge there.

2.5.4 East and West Sandia Springs

East and West Sandia springs are often discussed together although they are separated by ~1 km. They are located downstream of Balmorhea Lake (which is at higher elevation than the springs) and they are within an area of irrigated agriculture.

2.5.5 Saragosa Spring

Saragosa Spring is not always discussed in the context of the Balmorhea spring complex, although it clearly belongs to it. It is located on the northern bank of Toyah Creek, NW of San Solomon and Giffin. The spring was recently sampled (2019-2020) by us but also by NCKRI (2020 interim report) and by SWRI (Nunu et al., 2020). It is unclear if the three research groups sampled the same location, large differences in chemistry would tend to suggest not. White et al. (1941) describe what they called “Toya Creek” springs that they saw as different from Saragosa Spring but in close proximity. After further consideration, we concluded that all three groups did sample the same spring but it shows more variability and stand apart chemically from the Sandia springs on one side and the SS-PL-G on the other side.

3 Previous work – Literature Review

3.1 Succinct overview of past field studies

Authors recognized early the two components of flow at the Balmorhea area springs: a steady baseflow component and an occasional transient stormflow increasing spring flow and originating from the Davis Mountains. The first comprehensive study on Balmorhea area springs was performed by USGS in collaboration with the TWDB (White et al., 1938, 1941), in which the authors analyzed one of the largest ever recorded rainfall event on the Davis Mountains (1932) and related these events and others to the local geology. In particular, they delimited an “intake area” at the mountain front where stream stormwater disappears through karsted Buda

Limestone to recharge the underlying Edwards-Trinity Aquifer. The authors did not investigate the source of the spring baseflow although they hypothesized it comes from the west along the Stocks Fault and related features. The origin of the baseflow was elucidated later and attributed to the Apache Mountains to the west (Couch, 1978) and then to water recharged in the Salt Basin west of the Apache Mountains. In the intervening years, USGS has shown an intermittent interest in recording data related to the springs but their published studies are spatially broader and deal with the western half of the Edwards-Trinity and Pecos Valley Aquifer (Kunianski and Holligan, 1994; Bush et al., 1994; Bumgarner et al., 2012; Clark et al., 2013; Thomas et al., 2013).

Maybe prompted by the abrupt flow decrease and eventual drying up of several desert springs of the Fort Stockton area in the 1950's (Comanche Spring), a strong interest developed in maintaining the environmental health of the so-called "Crown Jewel of West Texas." In the 1980's and 1990's, Dr. J.M. Sharp, Jr., from The University of Texas at Austin, and co-workers and students focused on investigating the regional spring base flow (Neilson and Sharp, 1985; LaFave and Sharp 1987; Sharp, 1989; Sharp, 1990; Hart, 1992; Boghici, 1997; Schuster, 1997; Uliana, 2000; Uliana and Sharp, 2001; Sharp et al., 2003; Uliana et al., 2007) and put it in the larger context of desert springs of West Texas. The studies confirmed that the source of the springs baseflow lies in the Salt Basin to the west), and they concluded more specifically that the Wild Horse Flat is a major contributor the spring baseflow.

The State of Texas through the TWDB also performed several studies (Couch, 1978; Chowdhury et al., 2004; TWDB-TPWD, 2005) in addition to their regular geochemical and water level monitoring. Although not focused on the springs, the TWDB published several historical reports dealing with flow and water resources in the broader area (Knowles and Lang, 1947; Ogilbee and Wesselman, 1962; Harden, 1972; Ashworth, 1990; Ashworth et al., 1997; Boghici and van Broekhoven, 2001) as well as the more recent Groundwater Availability Models (GAM) making use of the historical and more recent data: Ewing et al. (2012) on the Rustler Aquifer, Anaya and Jones (2009) and Meyer et al. (2012) on the Pecos Valley Aquifer, Rees and Buckner (1980), Anaya and Jones (2009) and Hutchinson et al. (2011) on the Edwards-Trinity Aquifer, Beach et al. (2004) on the Igneous and Bolsons aquifers, Standen et al. (2009) and Jones (2016a, b) on the Capitan Reef Aquifer. Although many TWDB reports and studies discuss Balmorhea Springs, there has never been a comprehensive model of the springs because Balmorhea is located at the intersection of several geographic, geological, and hydrogeological domains. Potentiometric map examination has been used in several studies of the Balmorhea Springs, but there is no groundwater model centered on them.

The National Cave and Karst Research Institute (NCKRI) has also invested significant, still ongoing, research efforts (Veni, 2013; Land and Veni, 2018) by physically exploring the Phantom Lake cave system, performing dye tests, and undergoing a study parallel to this one. More generally, the development of unconvensionals in the Delaware Basin initiated a new round of research either to understand the dynamics of the spring system (this study, NCKRI's study, SWRI's Nunu and Green, 2020; Nunu, 2020) or better understand the water resources potentially hydrologically connected to the springs (Finch, 2017)

Other stakeholders, state and federal agencies, quasi-governmental entities, and non-profit organizations, have been active in other fields related to the Balmorhea springs. The Nature Conservancy (TNC), Texas Parks & Wildlife Department (TPWD), and U.S. Fish and Wildlife Service (USFWS) are involved in aquatic animal species conservation. Studies peripheral to this study include work by the University of Texas at Arlington (CLEAR group) interested in the

organic chemistry of shallow and deep groundwater and by the Bureau of Reclamation (BOR) focused on surface water and irrigation.

3.2 Dynamic hydrogeology

The generalized flow system of West Texas follows the overall topographic slope to the east and south toward the Gulf of Mexico and the Rio Grande. The Bolson aquifers discharge to the Rio Grande or to outlets feeding aquifers hosted by Permian and Cretaceous formations. The structural dip of the formations also favor such a general flow direction with recharging outcrops located west of the main aquifer bodies. The pre-development regional-scale discharge is upward and NE flow discharging to the Pecos River. Diamond Y Spring (from the Rustler) and Comanche Spring (from the Edwards-Trinity), both located in the Fort Stockton area, are discharge points of such a system. The Balmorhea spring system represents another discharge cluster but upgradient from those springs (baseflow), and is supplemented by surficial recharge from the Davis Mountains (stormflow).

In the Balmorhea area, the baseflow vs. stormwater recharge model has been largely accepted by the hydrogeology community and considerable efforts has gone into refining it. There are many potential contributors to the long-term spring component with distal sources (Salt Basin), proximal sources, such as upward flow from the underlying Rustler and possibly basinal brines migrating into the Edwards-Trinity limestones, and medium / intermediate in-between potential contributions from the Capitan Reef and associated formations. Uliana and Sharp (2001) and Uliana et al. (2007), using PHREEQC modeling and following Uliana (2000), proposed that three flow components contribute to spring flow: (1) Wild Horse Flat characterized by a high Sr isotope ratio also present in the spring water, (2) Rustler Aquifer with high Ca and SO₄ (anhydrite dissolution), and (3) occasional input from the Davis Mountains and other upstream recharge areas such as the Wylie Mountains, just SE of Van Horn, in the Salt Basin.

Examining the distal contribution to the springs, several authors have attempted to model the geochemical path from the various source contributions to the Springs. A key element of the Balmorhea area spring water is high Sr isotope ratio indicative of prolonged contact with Proterozoic rocks such as those found in the Wild Horse and Lobo Flats and more generally in the Salt Basin in varied proportions. Proterozoic rocks crop out in Salt Basin Bolson area but, maybe more importantly, the Bolson fill consists, at least in part, of Proterozoic rock fragments along with Permian-age rock fragments. Beach et al. (2004) stated that Lobo Flat and Ryan Flat received sediments mostly from igneous-rock terrains, whereas Wild Horse Flat and Michigan Flat received them from areas with Permian Formations.

However, multiple authors have stated that excess flow from the Wild Horse Flat in the Salt Basin cannot account for the flow at the springs and that there must be another western source (Finch, 2017; Chowdhury et al, 2014; TWDB-TPWD, 2005). Natural egress of discharge from the Salt Basin to the east is shallow and narrow and pumping for irrigation may have captured most of the outflow in past decades. Pumping for irrigation in the salt flat bolsons (especially near Van Horn) has captured discharge that used to flow to the east as the drop in groundwater levels has created a groundwater divide at the natural egress of the basin. Beach et al.(2004) confirmed that large water level declines and cones of depressions due to agricultural pumping in the bolsons have realigned some flowpaths, which now converge toward the pumping centers rather than the natural outlet of the Bolson Aquifers toward the Apache Mountains; potentially cutting some of the recharge to the Balmorhea springs. Modeling by Beach et al. (2004) suggests

that, by the 1970's, eastward flow through the surficial alluvium and deeper parts of the Bolsons had stopped and that flow through the underlying Cretaceous substrate was reduced.

These authors have pointed out that numerical flow models of the salt flats suggests that no more than 10% of the average Balmorhea spring baseflow can originate from the Wild Horse Flat. Neilson and Sharp (1985) and Beach et al. (2004) suggested an annual egress rate of 2-3 kAF, much lower than the cumulative ~30 kAF/year (or, equivalently, 40 cfs) measured at the springs (Neilson and Sharp, 1985). Ashworth et al. (1997) computed 50 kAF/yr spring discharge. They also suggested that pumping in the Salt Basin over the past decades may have captured this historical Wild Horse Flat discharge. A caveat of such observation is that the 2-3 kAF is the estimated flow through the Neogene fill, but neglects any flow through the underlying Permian. Indeed, Neilson and Sharp (1985) suggested that the main flowpath out of the Salt Basin is through the underlying Permian carbonates. Such a conceptual regional flow model is not rare and is commonly described in closed basins that are nevertheless drained (e.g., Hibbs, 2020).

Chowdhury et al. (2004) suggested that the Salt Flat in the northern section of the Salt Basin contributes to the flow that ultimately reaches the springs. Similarly, Uliana et al. (2007) updated the Uliana et al. (2001) model by adding potential contribution from the northwest ("C" on their Fig.2). Conclusions from Chowdhury et al. (2004) are supported by NETPATH geochemical modeling along a presumed flow path from the northwest. They argue that the heavily fractured transition with an overall N-S orientation between the Salt Basin and the Delaware Mountains (Border Fault Zone) is conducive to flow and is hydraulically connected to the Apache Mountains and the ESE-WNW Stocks Fault system. Flow path geochemical modeling indeed favors additional flow from the northwest (Salt Flat). This flow path would follow the heavily faulted eastern border of the Salt Basin and merge in the Apache Mountains with the flow component coming from the Wildhorse Flat and other bolsons to the south. Some authors have noted that the Salt Flat is hydrogeologically closed with no perennial streams (LaFave and Sharp 1987); others that the closed basin in the Bolson fill does not necessarily mean that there is no outlet via deeper formations, such as the Permian substrate, or formations on the margins of the Salt Flat (Angle, 2001; Finch and Bennett, 2002; Standen et al., 2009; Jones, 2016a; Boyd and Kreitler, 1986; Davis and Leggat, 1965).

Chowdhury et al. (2004) hypothesized that deeper formations do contribute to the eastward flow through the Apache Mountains using volumetric (flow from the southern bolsons cannot account for spring baseflow) and geochemical arguments. A good candidate is the Capitan and associated shelf deposits, such as the Victorio Peak Limestone. The western arm of the Capitan underlies the Salt Flat and crops out in the Patterson Hills, SW of the Guadalupe Mountains and of the Border Fault zone from where it is connected in the subsurface to the Apache Mountains area. A few fresh water wells have been drilled in the Patterson Hills. Finch (2017) also revealed head measurements from two well pairs in the Salt Basin, one well completed in the Bolson and the other in the Capitan. Both well pairs show a downward gradient toward the Capitan. Other wells show a similar trend in water level decline suggesting potential hydraulic communication between the Capitan and the Salt Flat Bolson, at least at these two locations. Hydraulic conductivity of the Salt Flat fill is lower than that of the Capitan.

Considering now the flowpath through the Apache Mountains, the flow is likely to follow the backreef facies rather than the core of the reef, which is at higher elevation and unsaturated, although it can provide recharge to lower elevation formations. The Artesia Group (Yates Fm.) crops out south of the Apache Mountains but groundwater flow is through the lower half of the

Artesia Group (Grayburg, Queen, and Seven Rivers Fms.), most of which are carbonates (limestones). It is also likely to provide additional flow contribution to the springs as attested by the similar geochemistry of the Apache Mountains backreef and the Balmorhea artesian springs.

In the early interpretations, stormwater runoff was believed to be the main flow component of the springs. This belief was quickly dispelled but the concept remained that stormwater was an important contributor to the overall flow and is still recognized as significant. Many observers noticed that following heavy rains in the Davis Mountains, spring discharge and turbidity increase, while salinity and temperature decrease (San Solomon and Phantom Lake springs). An increase in turbidity suggests the presence of large conduits. Interestingly and anecdotally, a more turbid slug out of the main SSS vent was observed by a geologist diver when exchanging loggers at the bottom of the pool (end of December 2020). The event was recorded on camera and lasted about 1 min.

The basic concept is that discharge from the igneous aquifer and stream flow that follows the topographic slope to the northeast would infiltrate, at the mountain front, into the karstic system of the Washita-stage limestones through elongated “windows” (along the structural anticline where the impervious upper Cretaceous layers are missing). The water is thought to re-emerge along branches of the mountain front fault system. Such a model was put forward by Pearson (1985). The arrival of storm water is denoted by an increase in turbidity and a decrease in temperature. However, given that large precipitation events can impact spring flow for many months after the event, it is reasonable to state that the springs receive a storm baseflow from the Davis Mountains, which is possibly stored upgradient of the spring complex.

Sampling during baseflow periods, LaFave and Sharp (1987) age-dated the spring water at $8,954 \pm 235$ years before present using carbon-14. TWDB-TPWD (2005)'s proposed a 10,000-15,000 year age-range depending on the method used to process the raw data. Uliana (2000) determined that the water age-dating constraint can be met only if low recharge and high conductivity are realized because of the low head gradient. Additional age-dating was performed in two studies: (1) Chowdhury et al. (2005) who analyzed well water along the flowpath from the West Texas Bolsons plus a sample from Phantom Lake (0.06 TU) and from San Solomon (0.17 TU), putting them both in the clear category of old waters (prior to 1950); and (2) 2019-2020 tritium data Nunu (2020) show similar results with a low tritium count in the SS-PL-G springs and E-W Sandia springs but relatively higher tritium levels (1.31 and 2.66) in Saragosa spring, implying mixed recharge and input of modern water there.

Turning to the exact causes of the decline in the spring flow rates, it is fair to say that they are poorly understood but with advantage to irrigation pumping. The actual start of the decline is also unknown, dense measurements started with the White et al. (1941) study with only rare, sporadic earlier measurements. Many have postulated that flow decrease is related to reduced flow through the Apache Mountains because of either local pumping or lower recharge. There is strong circumstantial evidence that groundwater withdrawals plays a role but it is unclear at which point or points along the flowpath it would happen. Authors have variously suggested withdrawals from the Salt Basin bolsons (Sharp et al., 2009), the Apache Mountains, the Rustler and Edwards-Trinity Aquifers. However, the fact that the seasonality of pumping is not apparent in spring flow variation (as seen at Comanche Springs, Mace et al., 2020) suggests a distal origin. Others have noted that a secular decrease in recharge and general lowering of groundwater levels since cooler, wetter Pleistocene climate (Corbet, 2000; Wong et al., 2015; Darling, 2017) with a higher recharge rate and a greater hydraulic gradient having contributed to

the decline. Paleolake deposits of that period have been described in what is now the Salt Flat (Wilkins and Currey, 1997). Deposits were dated from 23,000 to 16,000 years ago in 4 cycles. However, the sharp flow rate decline in the past century casts doubt on this hypothesis. Ashworth et al. (1997) suggested a decrease in average recharge because of changes in decadal weather patterns. TWDB-TPWD (2005) noted that multiple causes may be at play and also relayed more exotic hypotheses such as negative impacts of the August 16, 1931 Valentine earthquake (which is described in Doser, 1987) (Note: the drying up of Comanche Springs was also attributed wrongly to earthquake activity, Mace et al., 2020), or excessive development of phreatophytes, increasing ET (salt cedar encroachment).

Robertson et al. (2019) is the first paper focusing on a better understanding of the meteoric recharge component of the springs. They used NEXRAD datasets combined with high-frequency measurements (15 min or less) at the San Solomon Spring for one year (April 2011 to March 2012) (spring data apparently unavailable). They relied mostly on spring water conductivity for their interpretative work after concluding that pH, temperature, pressure (water level), and turbidity were too impacted by external factors to be consistently useful. They noted that conductivity and temperature distributions are not normal, which is to be expected because deviations from the long-term average (or mode) are one-sided and guided by pulses of colder dilute waters. They correlated these changes with NEXRAD rainfall events in Cherry Creek, Upper Madera Canyon, Herds Pass and Adobe draws, and Limpia Creek. Unfortunately, of all the “large” events (2 in July 2011-Fig.2e-f, 1 in August 2011-Fig.2h, and 1 in September 2011-Fig.2k, their figures), only the subdued one of September 2011 corresponds to a variance of San Solomon flow parameters. Overall, the large postulated time lag of 30-45 days is difficult to reconcile with data from the USGS and this study. The lack of spring data during the strongest rain events might bias high the lag results by mistakenly linking large events to consequences of subsequent minor events. An alternative explanation is that the Robertson et al. study detected recharge input from the Apache Mountains.

4 Data sources

The specific subtasks called for interpreting groundwater geochemistry of historical datasets and of those collected specifically for this study, and for creating maps of historic and modern potentiometric surfaces and inferred groundwater flow. In addition to those collected by BEG during the study, geochemical samples include historical data by TWDB, by academic researchers, and more recent samples by Apache and their consultants. Other parameters such as discharge rates, water levels, temperature, and specific conductivity were monitored continuously through at least part of the study. An important objective of the study was to correlate spring and water well geochemistry with rain events and surface flow in the Davis Mountains. Some notable rain events did occur during the study period but they were far from reaching the level of extreme events observed in the first half of the 20th century (White et al., 1938, 1941).

The study relied on two types of data: (1) historical and pre-study data, they are both geochemical (ionic make up and other characteristics of the water) and physical (some or all of the following parameters: water level, discharge rate, temperature, specific conductivity); and (2) newly collected data. New data consist of the same geochemical and physical properties acquired at streams, springs, and wells. Some of the latter were specifically drilled for the purpose of this study. The pre-field work ideal monitoring network was planned to help meet the multiple goals of the study. However, we were not successful at securing monitoring locations to the northwest

of the Balmorhea area towards the Apache Mountains, which is believed to be along the regional flow path to the springs.

4.1 Collaborations

Governmental or pseudo-governmental entities present in a broad area centered on Balmorhea and whose policies have a potential impact on the springs include three Groundwater Management Areas (GMAs) and four Groundwater Conservation Districts (GCDs), all with different allowable pumping limits and no spring flow triggers. GMAs were created by the State to conserve and protect groundwater resources from waste. Sixteen GMAs cover the state including GMA 3 (matching essentially the footprint of the Pecos Valley Aquifer), GMA 7 (matching essentially the footprint of the Edwards-Trinity (plateau) Aquifer), and GMA 4 (essentially Far-West Texas beyond the Delaware Basin, minus El Paso area, including the Igneous Aquifer and the West Texas Bolsons). No GMA was contacted during the study.

State and local residents grant GCDs the charge of managing the groundwater resource according to agreed-upon goals. GCDs are typically about the size of a county, but can be larger and include multiple counties, or smaller and include only a fraction of a county or of several counties. There is no requirement for a constituency to belong to a GCD and many Texas counties do not belong to one. GCDs typically track water well drilling, estimate water use, and sometimes impose limits on pumping rates and annual withdrawal. We worked closely with the Reeves County GCD and the Jeff Davis UWCD (Underground Water Conservation District), both of whom assisted greatly. The Culberson County GCD is incorporated only in the western half of the county, which includes a section of the western arm of the Capitan and a section of the West Texas Bolsons; the Middle Pecos GCD is mostly east of our study area. Neither of these GCDs were involved in the study.

The Nature Conservancy (TNC) provided access to the 246-acre Sandia Springs Preserve (<https://www.nature.org/en-us/get-involved/how-to-help/places-we-protect/sandia-springs-preserve/>), which includes East and West Sandia Springs, and the 33,075-acre Davis Mountains Preserve (<https://www.nature.org/en-us/get-involved/how-to-help/places-we-protect/davis-mountains-preserve/>). Texas Parks and Wildlife (TPWD) allowed access to the Balmorhea State Park (<https://tpwd.texas.gov/state-parks/balmorhea>) and Davis Mountains State Park (<https://tpwd.texas.gov/state-parks/davis-mountains>). Both TNC and TPWD allowed drilling of BEG monitoring wells on their properties. Reeves County Water Improvement District 1 allowed access and escorted BEG staff to springs, canals, and other local features of the Balmorhea spring complex. We installed rain collectors at the McDonald Observatory, next to Mount Locke up in the Davis Mountains. We also collaborated with several landowners who were kind enough to give us permission to sample their wells and occasionally to drill monitoring wells or install monitoring devices.

4.2 Well drilling

Arrowhead Well Services and Construction LLC drilled 14 boreholes on six properties, which are from west to east (Table 1, Figure 8, Figure 9) (MW = monitoring well):

- Cherry Canyon Ranch [5 boreholes, 3 wells completed (2 producing, 1 dry)]
 - BEG Cherry Shallow MW (dry) – There is no data logger in this well and it was not developed after completion or sampled. There is currently no data logger in this well.

- BEG Cherry Deep MW – This well is located at the main ranch entrance; it produces from upper Cretaceous strata, but has different chemistry from ANY other Cretaceous wells in the area. The BEG water quality (WQ) sample ID is WTX-SRMWD. There is a data logger in this well.
- BEG Cherry Ultra Deep boring – Drilling advanced to 780 ft without hitting water; the adjacent (30 ft to north) Cherry Deep MW must be completed in a fracture that was not encountered in this boring. This borehole was plugged and abandoned by Skinner Drilling.
- BEG Lodge MW – There were several attempts to complete this well in two separate borings, resulting in one producing well. The BEG WQ ID is WTX-SRMWL. There is a data logger in this well.
- 4JMadera Ranch (1 dry well; 1 possibly producing well)
 - BEG 4J Shallow MW (dry) – This well was not developed after completion or sampled, but contains a data logger to track possible future pulses of stormwater runoff in alluvium of the immediately adjacent Madera Creek.
 - BEG 4J Deep MW – This well has a 100+ foot water column; it was not developed after completion or sampled; bailed liquid appears to be residual drilling fluid. The well contains a data logger to track possible future pulses of stormwater runoff in either the immediately adjacent Madera Creek, or Cretaceous strata in which it is completed. A cavernous interval was encountered during drilling at this location.
- McCoy-Remme Ranch along Big Aguja (Big A) (1 dry well, 1 low-volume production well)
 - BEG BigA Shallow MW (dry) – This well was not developed after completion or sampled. It contains a data logger to track possible future pulses of stormwater runoff in immediately adjacent Big Aguja.
 - BEG BigA Deep MW – This well was not completely developed after completion or sampled because it could only be produced at about one gallon per minute. However, in July 2020 the well had a 250+ foot water column. Recent data from the installed data logger show responses to rainfall events. A complication with this well is that it is screened in both shallow and deep intervals; water can be heard cascading from the shallower to deeper intervals.
- Balmorhea State Park (1 producing well – BEG BSP MW); The BEG WQ ID is WTX-BSPMWS. There was a data logger in this well through December 2020.
- TNC Sandia Preserve (1 well, 1 incomplete borehole)
 - BEG Sandia Shallow MW – The BEG WQ ID for this well is WTX-SPMWS. There is a data logger in this well.
 - BEG Sandia Deep MW – Drilling at this borehole ceased due to TNC Covid-19 protocol; hence the borehole only contains surface casing to a depth of 60 ft; it is an open borehole from 60 to ~350 ft depth with a 300+ foot water column. There was no BEG WQ sample collected from this location; there is a BEG data logger installed that appears to have responded to recent rainfall events.
- Leoncita Cattle Company, Limpia Creek (2 wells)
 - BEG Limpia Shallow MW – The BEG WQ ID for this well is WTX-LLMWS. There is a data logger in this well.

- BEG Limpia Deep MW – This well was not developed after completion or sampled because the estimated production rate of two gallons per minute was not enough to sufficiently purge the well. However, in July 2020 the well had a 40+ foot water column. Recent data from the installed data logger show responses to rainfall events. A complication with this well is that the borehole collapsed during well completion; water can be heard cascading from the shallower to deeper intervals.

Well completion diagrams are shown in Appendix A and state-required driller logs are in the Supplementary Information folder.

4.3 Geological data

Surface geology was provided by the following 1:250,000 geological maps (Geological Atlas of Texas -GAT- sheets) developed by the Bureau of Economic Geology at The University of Texas at Austin: Pecos (1976), Marfa (1979), Fort Stockton (1982), and Van Horn-El Paso (1983) sheets, observable at <https://txpub.usgs.gov/txgeology/>. In addition, Brand and DeFord (1962) developed a 1:63,360 map of the eastern Apache Mountains almost to the Balmorhea area. All geological maps made at various scales in the study area are available for inspection at https://ngmdb.usgs.gov/ngmdb/ngmdb_home.html.

4.4 Geochemical sampling and analysis

4.4.1 This study

In the course of the study, we hand-sampled springs, creeks, surface waters, monitoring wells, domestic wells, public water supply wells, and rig water supply wells, a total of 84 samples and 37 unique locations. The groundwater samples were taken from surficial alluvium and Igneous, Cretaceous, and Rustler aquifers. Many locations were sampled at least twice. Repeat samples were taken at the six Balmorhea area springs. The samples were analyzed internally for major, minor and trace elements, water stable isotopes, and strontium (Sr) isotope ratio (some analyses were done externally). Several samples were also internally analyzed for dissolved inorganic carbon (DIC) and DIC carbon isotopes (^{13}C). Details about methods of chemical analysis and laboratories that performed the analyses are given in Appendix D. Some samples were sent to external laboratories for analyses of sulfate isotopes (^{34}S and ^{18}O), chlorine isotope of chloride (^{37}Cl), dissolved methane, and dissolved methane isotopes (^{13}C and ^2H) when appropriate. We also examine and discuss very recent geochemical results published in Nunu (2020) and NCKRI file (Jones, 2020) as the sampling in these two external studies overlaps our study. A total of 7 produced water samples from Apache oil and gas production wells have also been analyzed for major, minor, and trace elements as well as for water and strontium isotopes.

Wells were sampled using pre-installed groundwater pumps. The wells were continuously pumped until the temperature, pH, and conductivity (sometimes also DO or ORP) stabilized to insure a representative aquifer sample was obtained, approximately 30-45 minutes. A portion of the outflow was diverted through a Waterra FMT, 0.45 micron cartridge filter or a 0.45 micrometer syringe filter. Water samples were taken at the outflow of the filter. pH and temperature were determined using an Orion 3-star pH meter and gel filled pH/ATC Triode. For most samples, alkalinities were determined by titrating 50 mL of water with 1.600 N H_2SO_4 in the field using a Hach digital titrator. Final alkalinity values were calculated using the inflection point method on the USGS alkalinity calculator (<http://or.water.usgs.gov/alk/>). Note that, when it was not possible to follow field sampling procedure, for example, because of well owner or time constraints, a sample was simply taken after stabilization of the environmental parameters. Water

samples for major ion analyses were filtered (0.45 μ m) and collected in 30-mL high density polyethylene (HDPE) bottles. Water samples for trace element analysis were collected in the acid-cleaned HDPE bottles and acidified with 2% HNO₃ immediately after collection. Samples for DIC analyses were collected in 20 ml amber VOA vials. Samples for water isotopes were filtered (0.45 μ m) and collected in 30-ml HDPE bottles. Samples for Sr isotope ratio analysis are stored in a 60 ml acid cleaned HDPE bottles. Samples for sulfate isotopes analysis were collected in 1-L bottle to be shipped to the external laboratory. Samples for chlorine isotopes were collected in HDPE bottles. Dissolved gas samples were collected by two methods: the isoflask® designed by Isotech and a custom made sampling process in which the water sample is held in a serum vial with a crimped cap. Trip and field blanks as well as duplicates were also taken as reasonable.

We also performed regular sampling of the San Solomon spring. Samples were analyzed for water isotopes and major elements. A total of ~90 samples were taken at least once a week between January 2019 and July 2020 (but with some gaps). A few samples were taken before (3 samples) and after (1) as well as within (3) this time interval for full analyses. The sampling was done regularly but not necessarily at exactly the same locations depending on accessibility; samples from January 2019 to August 2019 (24 samples) were taken from a small boat lowering the special sampling device as close as possible to the spring orifice or using a peristaltic pump with the tubing secured close to the spring orifice. A few samples were taken by divers right at the orifice or from the pool edge at the surface. Several samples were also taken from a canal. Pool operations and construction made it difficult to consistently sample from the vicinity of the spring orifice. From September 2019 on, samples (66) were systematically taken from the canal draining the pool.

Other springs were sampled as closely as possible to the orifice but the exact method ultimately depended on the sampling operator and external constraints. When possible, a 60 ml luer-lock syringe close to the orifice when visible, sometimes aided by a short wire to sample closer to the orifice was used (for example, East Sandia). Giffin spring was not sampled at the spring orifice but by scooping from the exiting canal away from the spring and Saragosa spring was sampled directly from the water pooling above the hidden orifice.

We installed rain collectors at two sites (June 2018): McDonald observatory, high in elevation, and Balmorhea State Park, at low elevation. Two collectors were installed at each location (for a total of four rain collectors) in areas away from trees and bushes (Photo 1). The purpose of these simple samplers (1-L amber glass bottles protected in large buckets with a funnel mounted on top and vinyl tube to convey water directly below an ~1-cm layer of mineral oil to stop evaporation) was not to measure precipitation volume but to capture some of the rain water throughout the year to analyze for water isotopes. Bottles were collected irregularly but at an approximate 2/3-month interval with efforts to reduce the collecting interval during the monsoon seasons. In the laboratory, sample volume is noted, water is extracted and centrifuged to separate water from remaining oil before analysis.

4.4.2 Historical data

In addition to the samples taken in the course of the study, geochemical data used in this study belong to three datasets: (1) academic investigations dating back 50+ years, including data from researchers such as J.M. Sharp, M. Uliana, L. Land and G. Veni, A. Chowdhuri, and others; some of the sampling campaigns in this category overlap with the next category; (2) regular monitoring by state agencies (mostly TWDB), data from 1930 to 2018 (1871 samples); and (3)

Apache baseline sampling from 2016 to 2018 (304 samples). All the data were organized in a single spreadsheet (Supporting Information).

Most of the data collected during academic work were integrated in the public-domain TWDB database. Water samples have been analyzed for major and, very often, trace elements. Some samples lack field parameters that are typically taken during sample collection. On occasion, TWDB database also report water isotopes, DIC isotopes, strontium isotopes, and more exotic parameters, such as, sulfate isotopes, tritium content, and ^{14}C content. The chosen geographic extent of the samples we considered is much larger than the Balmorhea spring area and in addition to Alluvium (Pecos Valley), Igneous, Cretaceous, and Rustler Aquifers, we also included analyses of water from Permian (Capitan) and Salt Flat Aquifers. Notable sources of the data are: (1) Ogilbee and Wesselman (1962; Table 11 in Bulletin #6214) with extensive analyses of major ions of all aquifers in Reeves County (~140 data points from 1939 to 1959); (2) relevant samples from Kreitler et al. (2013), a study performed by LBG-Guyton (now part of WSP, since 2017) for the TWDB, provided ~75 additional unique samples whose collection dates are spread irregularly from the 1930's to the 2000's; (3) TWDB BRACS (Brackish Resources Aquifer Characterization System) database (Meyer, 2020) with ~140 samples from 1930 to the 2000's; and (4) the regular TWDB Groundwater database with ~1500 samples collected more or less regularly from the 1930's to present with a peak at ~180 samples in 1970. There is some overlap between the TWDB BRACS and Groundwater databases, one focuses on brackish water, the other on fresh water, but they mostly provide data from different wells. We also added a single-digit number of analyses by USGS. In addition, Apache shared with the BEG their third-party baseline monitoring database assembled by CH2M-Hill (now part of Jacobs Engineering Group, since 2017) (Behl et al., 2018), a total of approximately 375 samples taken in 2016, 2017, and 2018.

The historical dataset contains ~2250 unique samples (duplicates deleted) of which ~680 are post-2000 (Figure 10). Some wells and locations in the Balmorhea area have been sampled multiple times, for example, SSS has been sampled 46 times in addition to the samples taken in this study. Samples from the other 5 Balmorhea area springs comprise 117 samples. The majority of the Balmorhea spring samples were taken recently but all springs have been periodically, if haphazardly, sampled since the 1930's (Figure 11). The samples, of various value to this project, include ~25% of Pecos Valley Aquifer, ~22% of West Texas Bolson Aquifer, ~23% Cretaceous Aquifer (Edwards Trinity), and ~13% Igneous Aquifer samples as well as samples from the Rustler and Capitan Aquifers.

4.5 Physical sampling

4.5.1 This study

Many previous studies focused on a geochemical investigation of the springs. Few studies performed a thorough analysis relying on physical and flow parameters. A notable exception is the USGS/ TWDB study by White et al. (1938, 1941). They recorded flow and other parameters at Phantom Lake and San Solomon in a manner similar to this study for 2 years (1931-33), a time interval that happens to fortuitously include a very large rain event in September 1932. They also tracked water levels in 13 shallow wells.

BEG installed loggers on selected streams, springs, and wells (Figure 12) in Jeff Davis and Reeves counties. They fall into two broad categories:

- (1) loggers in direct contact with water. We rely on equipment purchased from the InSitu[®] company (<https://in-situ.com/us/>). BEG installed three types of loggers recording different parameters:
 - a. Aqua TROLL 200 (AT) loggers that measure pressure (psi), temperature (°C), and specific conductivity (SpC). (SpC is measured in microsiemens per centimeter (μS/cm). ATs are installed in 11 wells, 6 springs, and 1 stream;
 - b. Rugged TROLL 100 (RT) loggers that measure pressure (psi) and temperature (°C). These are mostly installed in streams (7 loggers); 3 RTs are installed in monitoring wells where the goal is to document changes in water level rather than specific conductivity.
 - c. Rugged BaroTROLL loggers measure barometric pressure and temperature, which are used to correct for atmospheric changes in the AT and RT datasets. We have two of these at high (5896 ft, TNC Davis Mountains Preserve, 4 miles WNW from the McDonald Observatory) and low (3310 ft, Balmorhea State Park) elevations. Elevations of loggers range from 3159 to 5945 ft above sea level.
- (2) WellIntel[®] acoustic sounders, which indirectly measure depth to water in wells.

Logger specifics are shown in Table 2 and Appendix B. There are a total of 29 loggers (+ two barometric loggers) in the field, including 12 at the new BEG-drilled monitoring wells. A total of 14 loggers monitor springs and surface water bodies whereas 15 loggers monitor water wells, only three of which were installed early in the study in 2018 (Figure 12a and Figure 13). Time line of some of the loggers is shown on Figure 14. A total of nine wells with lack of access to the wellbore casing to install a logger (pumping well) or for some other reason have a WellIntel[®] system installed (Table 3, Figure 12b, and Appendix C). Timeline of some of the WellIntel[®] wells is shown on Figure 15. Although some loggers were installed before April 2019, most of the data recording occurred in this second reporting period.

InSitu[®] loggers deployed in springs and streams are encased in protective housings of PVC and/or galvanized pipe. RTs are inserted directly into galvanized pipe segments that have been affixed with welded cross-bars, and bolted to bedrock in stream beds. The intent is to protect the loggers from cobbles or boulders being transported during peak stormwater runoff events. ATs installed in springs and streams are also inserted into galvanized pipe housings, but have PVC liners to reduce corrosion potential. Both RTs and ATs in wells are suspended on stainless steel wire crimped with galvanized ferrules. Since encountering issues with corrosion of ferrules used to crimp the stainless-steel wire, we also wrap all connections with electrical tape.

Data from loggers (recording at a 5-minute interval) were downloaded relatively regularly and sometimes loggers were switched at some locations for repairs or ease of download. All of our InSitu[®] loggers must be downloaded by manually connecting to a field laptop running WinSitu[®] software. Downloaded and exported files are then imported into custom MATLAB[®] software to stitch together datasets downloaded at different times, and time-series plotting. The loggers were installed unvented and pressure measurements need to be corrected for atmospheric pressure variations. We also generated MATLAB[®] scripts to pressure-correct logger data and calculate relative stage (i.e. height of water over pressure sensor). The non-vented pressure sensors measure absolute pressure; hence all pressure data needed to be corrected to eliminate barometric pressure fluctuations. For that purpose, we installed barometers (BaroTroll) at two locations: up in the mountain in the TNC Davis Mountains Preserve (4 miles WNW from the McDonald Observatory) and at low elevation on the basin floor at the Balmorhea State Park (Photo 2).

Stream and spring stages were corrected for barometric pressure fluctuations assuming 100% barometric efficiency. For convenience, groundwater wells were also corrected assuming 100% barometric efficiency.

Stream loggers in the Davis Mountains to the south of the Balmorhea spring complex were installed in several watersheds in a relatively dense network of probes. They typically organized in pairs, one logger located in the headwaters area and the other one towards the base of the mountains, to capture information about ephemeral flow episodes and their impact on the Balmorhea springs. Some Davis Mountains springs were also instrumented. All spring InSitu[®] AquaTroll 200 (Davis Mountains and Balmorhea area) use the same housing as used in ephemeral stream locations, with the exception of Phantom Lake Spring, which was zip-tied to the housing of a pump providing water for the Bureau of Reclamation-maintained artificial wetland at the site.

Groundwater level in wells was measured using three techniques: down-hole loggers, wellhead-mounted loggers, and electric wireline sounder. Down-hole loggers were installed in existing wells and recorded groundwater level, temperature, and conductivity. Pumping wells in the alluvial plains were equipped with acoustic sounders because of the physical difficulty of installing loggers in wells actively pumping and the obstruction of the pump system. The technology comes from WelIntel (<https://wellintel.com/>). The WelIntel sensors were installed late in the study (late 2019). We installed a WelIntel[®] acoustic sounder to existing 1 ¼-inch NPT vents and cellular data transmission permitted remote logger diagnostics and data visualization without removing a pump or risking tangling a logger on pump wiring. These wells are also equipped with a telemetry system that allows for inspection real time of the data from the office. Some water levels were measured using the traditional electric wireline sounder, either to collect data unavailable otherwise or to calibrate down-hole loggers and WelIntel[®] sounders.

In coordination with Texas Parks & Wildlife Department (TPWD), the Nature Conservancy (TNC), the Bureau of Reclamation (BOR), and Fish and Wildlife Service (USFWS), we were able to install loggers in all of the primary Balmorhea-area springs and two nearby wells (Balmorhea State Park and Sandia Preserve). A total of five loggers were installed at the Balmorhea spring complex: Phantom Lake, San Solomon orifice, San Solomon pool canal, Giffin and East Sandia. Phantom Lake AquaTroll 200 logger was installed inside the cave beyond the steel gate. San Solomon logger was installed at the bottom of the pool near the main spring orifice (Photo 3). A licensed diver helped on several occasions to switch loggers. One logger was installed in the canal used to drain Balmorhea State Park pool during maintenance to evaluate leakage from a poorly repaired gate valve, which occasionally caused the USGS gauge for San Solomon Springs to report erroneous discharge values. Repairs at Balmorhea State Park from May through the end of 2019 impacted the record. As of July 2021, most of the downhole loggers are still active but with a longer recording interval (15-min interval). Most of the acoustic sounders are transmitting data as well.

Of the 32 InSitu[®] data loggers installed within the study area, 7 are in springs, 9 are in streams, and 14 are in wells. Two loggers are installed at high and low elevations for barometric corrections of data collected in the other 30 loggers. Spring monitoring has been mainly focused in the lower elevation Balmorhea area:

- Phantom Lake spring (1 AT logger at 3491 ft amsl) (Photo 4)
- San Solomon springs (2 AT loggers at 3320 ft amsl) (Photo 3)
- Giffin spring (1 AT logger at 3327 ft amsl) (Photo 5)

- East Sandia (1 AT logger at 3159 ft amsl) (Photo 6)

Two AT data loggers are installed in springs in igneous-type waters at higher elevations in the Davis Mountains (Seven Springs, 3806 ft amsl and Willow spring, 4744 ft amsl) (Photo 7 and Photo 8).

Eight loggers are installed in streams flowing along igneous terrain at higher elevations in the Davis Mountains (from higher to lower elevations):

- Madera Upper Stream (1 RT logger at 5945 ft amsl) (Photo 9)
- Cherry Upper Stream (1 RT logger at 5719 ft amsl) (Photo 11a)
- Limpia Upper Stream (1 RT logger at 4921 ft amsl) (Photo 13)
- Cherry Lower Stream (1 RT logger at 4577 ft amsl) (Photo 11b)
- Little Aguja Stream (1 RT logger at 4386 ft amsl) (Photo 12a)
- Madera Lower Stream (1 RT logger at 4324 ft amsl) (Photo 10)
- Limpia Lower Stream (1 RT logger at 4154 ft amsl) (Photo 14)
- Big Aguja Stream (1 AT logger at 4085 ft amsl) – This location is along a stream channel fed by multiple perennial springs issuing from igneous rocks (Photo 12b). Because of the potential for “freshening” of spring flow after rainfall events, we also wanted to measure specific conductivity there.

An additional RT logger was installed along a canal downstream from San Solomon springs (BSP Drain Canal) as an auxiliary check for changes in spring discharge, but has since been lost.

Late in the study period (July 2020) we installed RT and AT loggers in 11 of the BEG monitoring wells; hence there are limited data available for analysis from these locations:

- BEG BSP MW at Balmorhea State Park (Photo 20a)
- BEG Sandia Shallow MW on the south edge of Balmorhea, TX (Photo 19)
- BEG Sandia Deep MW on the south edge of Balmorhea, TX (Photo 19)
- BEG Lodge MW along Cherry Canyon in the Davis Mtns.
- BEG Cherry Deep MW along Cherry Canyon in the Davis Mtns. (Photo 15)
- BEG 4J Shallow MW along Madera Creek in the Davis Mtns. (Photo 17)
- BEG 4J Deep MW along Madera Creek in the Davis Mtns. (Photo 17)
- BEG BigA Shallow MW along Big Aguja Canyon in the Davis Mtns. (Photo 20b)
- BEG BigA Deep MW along Big Aguja Canyon in the Davis Mtns. (Photo 20b)
- BEG Limpia Shallow MW along Limpia Creek between the Davis and Barilla Mtns. (Photo 21)
- BEG Limpia Deep MW along Limpia Creek between the Davis and Barilla Mtns. (Photo 21)

An objective of completing closely spaced monitoring wells at multiple depths was to further document potential for cross-formational groundwater flow, especially for pulses of rainfall runoff in the Davis Mtns. Limitations with this approach to date include dry wells at some locations such as the BEG Cherry Shallow MW; the logger from this well has been removed for use in another BEG MW location.

InSitu[®] data from 3 wells in which we have had loggers installed for longer duration do support interpretations of spring flow responses to rainfall events:

- Huelster #3 Well (1 AT logger at 3507 ft asl) (Photo 18a)

- Hamilton WM Well (1 AT logger at 3550 ft asl) (Photo 18b)
- Cherry Lower Well (1 AT logger at 4455 ft asl) (Photo 16)

We also made use of the USGS (https://waterdata.usgs.gov/tx/nwis/uv?site_no=08427500) “08427500 San Solomon Spgs at Toyahvale, TX” and TCEQ “C808 Balmorhea Pool Discharge Canal” (https://www.tceq.texas.gov/cgi-bin/compliance/monops/water_yearly_summary.pl) gauges. Examples of Wellntel[®] acoustic sounders are shown on Photo 22.

San Solomon valid data points the time interval used to be 5 min then was changed to 15 min during the data download of July 2020:

Number of useful data points	2018	2019	2020	Last processed download
San Solomon	72,933	105,136	73,867	July 2020
Phantom Lake	58,267	105,120	87,118	October 2020
Giffin	34,232	54,791	47,660	October 2020

4.5.2 Historical data

We downloaded all groundwater well water level data in the study area from the TWDB and Submitted Driller Record databases (TWDB), which assigns an aquifer to each well using best available data. We describe our approach to verify aquifer classification in the Methodology Section with the Alluvial, Igneous, Cretaceous, Permian categories and their subcategories (Figure 16).

4.6 Precipitation data

We gathered and used two types of precipitation data: (1) traditional local gauges from official weather stations and (2) precipitation estimated from radar data. Precipitation data were downloaded from <https://www.ncdc.noaa.gov/cdo-web/search?datasetid=GHCND>, a NOAA website, for the following locations: Van Horn, Kent, Balmorhea, Fort Davis, Alpine, and Mount Locke (Figure 17). In addition, we extracted 800-m gridded rainfall data (PRISM, 2019) for each hydrological unit (HUC) including its normal (annual cumulative precipitation over the most recent three decades: 1981 to 2010), annual maximum, and minimum. Mean annual precipitation (MAP) and mean annual (precipitation) volume (MAV) was summed for each watershed, and an initial estimate of a 5% recharge rate (see Beach et al., 2004) was applied to estimate annual flux. We also evaluated daily 1 km²-gridded rainfall totals for each watershed from Multi-Radar/Multi-Sensor System (MRMS; Zhang et al., 2016). While lower resolution than PRISM, MRMS gridded precipitation is available on a daily time step. Precipitation in each watershed was summed and peak rainfall events identified. We visually inspected spatially distributed precipitation for the study area for three to four weeks prior to the rain event.

The total study is nearly 2 million acres of which ephemeral drainages cover 676,000 acres or 34%. We also suspected that the largest drainage in the Davis Mountains, Limpia Creek, may also have some contribution to the springs, despite its trajectory away from Balmorhea. First, we assessed drainage size based on hydrological unit codes (HUC) and extracted the gridded rainfall data (PRISM, 2019) for each HUC including its normal (annual cumulative precipitation over the most recent three decades: 1981 to 2010), annual maximum and minimum. PRISM normals are a long-term average data set modeled at 800 m resolution using the Parameter-elevation Regressions on Independent Slopes Model (PRISM) which uses a digital elevation model, rain gauge data, and other spatially explicit data sets to develop a geo-statistically based rainfall product on 4 km grid over the continental United States (Daly et al., 2008).

5 Methodology

Geochemical analytical results are evaluated using traditional tools of (1) ternary diagrams (Piper plots), which map the relative concentrations of the various ions but not the absolute concentrations, (2) Stiff diagrams, a representation of the major ions that accounts for the absolute concentrations, and (3) various binary cross-plots of relevant dissolved ions and of their ratios. Some samples can be considered end-members characterizing their aquifers and help establish the mixing relationship visible in many samples, and are more representative of the aquifer as a whole. Several parameters can be used as natural tracers such as temperature and conductivity/TDS, both can be measured at a high frequency, and pH, water isotopes, and conservative ions.

During this multi-year study, we have used water level data measured in multiple types of water wells to construct water table (unconfined) and potentiometric surface (confined aquifers) maps. Such data can be used to assess directions and velocity of groundwater flow, and evaluate potential for vertical or cross-formational flow between stacked hydrogeologic units via faulting or via wells constructed across multiple subsurface water-bearing units.

Sources of water level data used here include:

- TWDB Groundwater Database; these are identified with a 7-digit State Well Number (SWN); <https://www.twdb.texas.gov/groundwater/data/gwdbbrpt.asp>
- Texas Department of Licensing and Regulations (TDRL), Submitted Driller's Records (SDR), <https://www.twdb.texas.gov/groundwater/data/drillersdb.asp>. These are identified with a 4- to 6-digit well identifier and are only available for wells drilled since 2002.
- BEG InSitu[®] and WellIntel[®] data loggers in select wells (some pre-existing and some newly drilled by BEG) and springs.

Ideally a water table or potentiometric surface map should be constructed using water level data measured in wells (1) across a wide geographic area within a short time-frame (i.e., within a single season, a few weeks or even days), (2) of known construction (total depth, screened-interval, filter pack-interval, placement of annular seals), and (3) within a single water-bearing or aquifer unit. But these ideal conditions can rarely be met using pre-existing water wells as sources of monitoring data. While serving as a valuable resource, the TWDB water level database has limitations. Many of the water wells in the TWDB database are of unknown construction and/or are completed across more than one water-bearing or aquifer unit. Water wells in adjacent counties are often measured by TWDB personnel in different years, generally with fewer numbers of wells being accessed over time. To overcome sparse water level data, we, like authors of TWDB Groundwater Availability Model (GAM) and other groundwater studies, have had to include water level data from wells completed in multiple aquifers, and measured over large time intervals (e.g., Beach et al., 2004; Chowdhury et al., 2004). Similarly, we have grouped water level data by (1) alluvial aquifers; temporally by Pre-1960, 1960–1979, and Post-2000 intervals, (2) Igneous aquifers; temporally by Pre-1980 and Post-2000 intervals, and (3) Cretaceous and Permian aquifers; temporally by Pre-1980 and Post-2000.

Since 2015, interest in protection of water resources in the southern Delaware Basin has peaked as many new water wells have been drilled to support oil and gas development. Consequently, we have been able to compile enough water level data from years 2010 through 2020 to show meaningful results. More sparse water level data available for the YR1 report necessitated compiling all post-2000 data. By using non-irrigation season, or “winter”, groundwater levels

(i.e., November through April, following Bumgarner et al., 2012), we also avoid year-to-year changes in timing and magnitude of monsoonal-type rain events that typically occur between June and September in the Davis Mountain/Balmorhea region.

The region of interest is hydrogeologically complex in that it is underlain by two major and four minor aquifer units, as formally defined by TWDB. Two major aquifers are Cretaceous-age Edwards-Trinity Plateau (K) and recent Pecos Valley (QPVA). Four minor aquifers are Permian-age Capitan Reef; Permian-Age Rustler [lumped here as Permian (P)]; Cenozoic-age Igneous (TIg); and recent West Texas Bolson (QWTB). Our initial review of TWDB-defined aquifer classifications of wells with useable water level data noted several inaccurate aquifer picks. This effort by TWDB is admittedly complicated by water wells with completions in mixed aquifers and inaccurate aquifer depth mapping or lithologic logging by the well driller. In addition, wells are sometimes classified according to individual hydrostratigraphic units, of which there are about a dozen (Table 4); this makes regional mapping of groundwater levels difficult without considerable efforts.

Current objectives are to complement past and current hydrogeochemical studies of spring water recharge by compiling and evaluating more recent water level data from wells completed in known stratigraphic intervals. To gain confidence in aquifer designations of wells with water level data, we cross-checked the TWDB-defined aquifer for each well in the study area (1) against structure-contour-surfaces generated for key stratigraphic intervals compiled in ArcGIS software using point data (where possible) and (2) from multiple sources including, BRACS database, GAM models, TWDB/SDR lithologic logs and well completion reports, and sponsor-provided formation picks (e.g. Lupton et al., 2016; Meyer et al., 2012; TWDB online databases in bulleted list above). Data compiled to evaluate groundwater surfaces and sets of closely spaced wells completed in different water-bearing zones are summarized in Table 4.

6 Geochemical Results

In this section, we present results of BEG recent geochemical sampling and put it in the context of our previous geochemical knowledge. After presenting general results from major element chemistry, we provide interpretations from isotopes and other chemical tracers.

6.1 General geochemistry

As has been observed by earlier authors, most water samples fall neatly into one of three geochemical categories (regardless of the actual formation well drilling data suggest they come from) (Figure 18 and Figure 19): the Igneous category, characterized by a low TDS (<400 mg/L) and a Ca- HCO₃ water type, the Rustler category, characterized by variable TDS but consistently high sulfate and a Ca- SO₄ water type, and the Balmorhea Spring category, characterized by a mildly elevated TDS (2000-3000 mg/L) and a mixed anion (Cl-SO₄) and mixed cation (Na-Ca) water type. Several wells, sometimes described as alluvial, fall into one of these categories. Wells whose screened interval is assigned to Cretaceous formations have a more variable ionic distribution and fall in-between the three geochemical categories denoting multiple influences.

The Igneous category (16 locations, 28 samples) is clearly geographically constrained and includes samples from wells, 4J Madera Pole Pen well (275 ft, n=2), MVWSC Huelster Well 1 (354 ft, n=3), Cherry Canyon Ranch HQ well (100 ft, n=2), BEG Cherry Canyon Ranch Lodge MW well (600 ft, n=1), Cherry Canyon Ranch NW well (605 ft, n=1), Buffalo Trail Scout cAMP well (428 ft, n=2), McCoy Remme Pump Jack well (270 ft, n=1), BEG Leoncita Limpia Shallow MW well (83 ft, n=1); from springs, Big Aguja Side Spring (n=1), Cherry Canyon Ranch

Willow Spring (n=2), McCoy-Remme Seven Springs (n=2), and surface water, Davis Mountains State Park Limpia Creek (n=2) and Madera Creek (n=1). Davis Mountains State Park WS well (400 ft, n=2), Fort Davis WSC wells #2 (306 ft, n=4) and #3 (unknown, n=1) are somewhat removed from the area of interest. We can also distinguish a subcategory that includes Willow Spring and Seven Springs as well as Pole Pen, Huelster #1, and BEG Limpia Shallow wells.

The Rustler category (4 locations, 9 samples) comprises Apache Bennett #2 (860 ft, n=2), Apache Cedar (1805 ft, n=2), and Apache 2 SW (Rustler 2) (1950 ft, n=2), and Gobble Hole (2407 ft, n=3) wells. These four Apache water supply wells represent the expected composition of Rustler groundwater with relatively high TDS (3000-4000 mg/L). The Hidalgo Rustler well (1416 ft, n=2) also belongs to the same Piper plot cluster but exhibits a much lower TDS (900-1000 mg/L), due to the open borehole completion of the well and downward flow from the Cretaceous.

The Balmorhea Spring category (11 locations, 32 samples) includes samples from springs Phantom Lake (n=4), San Solomon (n=7), Giffin (n=4), East Sandia (n=5), West Sandia (n=2), Saragosa (n=2), as well as samples from 3 wells, Hamilton Windmill (83 ft, n=3), which taps water in Phantom Lake Cave, BEG Sandia Shallow MW well (80 ft, n=1), and BEG BSP Shallow MW well (40 ft, n=1), and surface water samples (canals, Lake Balmorhea) (n=3). The Balmorhea Spring group is sometimes described as included in a larger Cretaceous groundwater group as discussed later. Recent NCKRI (Jones, 2020) and Nunu (2020) data show a total agreement with our own results, except for the Saragosa Spring.

Well samples discussed below do not belong to any of the three previously relatively narrowly defined categories; these narrowly defined categories can be described as end-members. The following wells, often denoted as “Cretaceous” may represent a simple binary mixture of two of the end-members if their position on a piper plot falls on the line joining the two end-members (Piper, 1944) given that the constraint of an intermediate TDS value is met. Or they may represent a ternary mixture if the position falls in the triangle delimited by the three end-members. However, such a case may also represent a binary mixture with mineral precipitation or dissolution. Finally, they may represent one or more endmembers not captured previously. Here we present a preliminary interpretation based on major ion geochemistry that will be adjusted when minor element and isotope results are considered.

- Apache Artesian 1 WSW well (700 ft, n=3) appears to be a mix of the Rustler and Balmorhea Spring water categories. This Apache water supply well is in Cretaceous rocks ~15-20 miles east of the Apache Mountains on the presumed flow path to the springs. Apache Bennett #2, Apache Cedar, and Apache 2 WSW (Rustler 2) wells are located ~10 miles north to northwest of this well and do not show any Cretaceous influence. The Apache Artesian 1 WSW TDS is moderate at ~2100 mg/L, lower than the other three Apache wells, but similar to that of the Balmorhea springs.
- MVWSC McIntire well 1 (450 ft, n=3) shows a water composition close to that of the Balmorhea Spring category but with a lower TDS (1100-1200 mg/L). The Piper plot suggest some input from the Igneous category but the well location on the plot also suggests input of fresher water than typical Igneous groundwater, possibly direct dilution input from Cherry Creek. This well appears to be located upgradient of the Hamilton well and Phantom Lake spring.
- McCoy Remme Duncan Camp well (762 ft, n=2) located in Big Aguja drainage near confluence with Little Aguja and the 4J Wildcat well (1025 ft, n=1). These two wells

share similar characteristics (with a TDS ~500 mg/L) with a mostly igneous flavor and are both located in the Rounsaville Syncline. They clearly show a strong Igneous signal but the anion ternary plot suggests mixing with the Balmorhea Spring category whereas the cation ternary plot suggests some input from the Rustler category

- Hidalgo WSW3 well (700 ft, n=1) is located at the mouth of Limpia Creek as it enters the Toyah Basin whereas the geochemically similar BOR Windmill well (750 ft?, n=1) is at the mouth of Cherry Creek. These two Apache water supply wells show a relatively low TDS of ~800 and 1250 mg/L, respectively. Both wells fall close to the Balmorhea Spring category on the Piper plot and share similarities with the McIntire well.

The BEG Cherry Canyon Ranch Deep MW well (420 ft, n=2) is a singular case as it was drilled into the Upper Cretaceous clays, which suggests that the water there is little mobile. It shows a Na-HCO₃ water (TDS of ~1000 mg/L) with very little Ca and Mg and low Cl and ~no SO₄.

The field-measured pH (data for 67 out of 81 samples) is circumneutral. pH of Balmorhea springs, Rustler and Cretaceous wells varies between 6.8 and 7.4 with a rough trend of decreasing pH with increasing TDS. Igneous wells display a larger pH range from 6.4 to 7.9. Dissolved oxygen (DO, 48 acceptable measurements) and redox potential (ORP, 53 acceptable measurements) are consistent across the dataset with a wide range of values: from ~0 to 9 mg/L and from -400 to +400+ mV. Average Eh and DO for the Igneous category are +150 mV and ~5 mg/L. Measurements from the Balmorhea Spring category are variable, relatively high if the samples are taken at the surface of a body of water (diffusion of atmospheric oxygen) but low (<100 mV) in other cases. Samples from the Rustler category indicate reducing conditions with low to no DO and Eh=~-330 mV on average. Eh measurements can help in identifying the source of a sample. Temperatures were also recorded during geochemical sampling but we rely more on the data from the InSitu[®] loggers to interpret their variations. We observed small variations related to seasons with a slight temperature drop in the wintertime for the artesian springs.

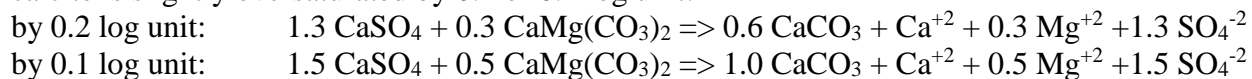
Simple calculations of saturation indices (SI's) of relevant minerals (PHREEQC) are consistent with geological observations and geochemical results (Figure 20). The Spring category as well as the Rustler category (less true for dolomite) are mostly saturated relative to both calcite and dolomite whereas the Igneous category is close to saturation relative to calcite but not to dolomite. This is particularly true for the artesian springs (San Solomon, Phantom Lake, and Giffin) whose Ca/Mg molar ratio hovers around the theoretical dolomitization / dedolomitization ratio of ~1.35 at these temperatures (Figure 21). The calcite and dolomite equilibrium constraints force the Ca/Mg ratio to be a constant value at a given temperature, pressure, and ionic strength. The other Balmorhea springs (East and West Sandia and Saragosa) have a slightly higher Ca/Mg ratio at 1.73 on average and a relatively higher Ca concentration. This is potentially due to calcite dissolution related to a higher P_{CO2} in the water (PHREEQC results). Artesian spring averages of logP_{CO2} range from -1.85 to -1.78 (1.41% to 1.66% partial pressure) whereas the average values for the other springs range from - 1.70 to -1.41 (2.0% to 3.9%). Uliana (2000) justly noted that mixing two solutions saturated relative to calcite but of different TDS (Igneous and Spring categories) will result in an undersaturated mixture that may enhance cave forming.

Geochemical characteristics of the Cretaceous samples are between that of the Igneous and Rustler endmembers (Figure 20a). Rustler samples (minus one diluted one) are saturated relative to gypsum and anhydrite (Figure 20b). However, most of the other samples, in particular from the Igneous category, are undersaturated relative to the two types of calcium sulfate. All samples

are oversaturated with quartz but typically groundwater is in equilibrium with amorphous silica not quartz (Hem, 1985). The Igneous category is the closest to amorphous silica saturation (Figure 20c), these samples do have a high silica content but they remain very dilute. Minor minerals controlling the concentration of F and Sr are for the most part unsaturated (Figure 20d) except for the Rustler samples where anhydrite dissolution controls the amount of F (precipitation of low-solubility CaF_2) and Sr (precipitation of low-solubility SrSO_4). A corollary of these observations is that F and, to a lesser extent, Sr can be used as tracers except in Rustler wells. In addition, given their very diluted nature, all samples are far from being saturated with halite but all, except the igneous samples, are close to barite saturation, which an expected outcome given the typically high sulfate concentrations in these samples.

Crossplots of the ratios of common major ions Na/Cl and Ca/SO_4 , both molar, reveals the partition between the various samples and provide clues to the origin of the waters (Figure 22). Equimolar samples would clearly suggest halite and anhydrite/gypsum dissolution. Both ratios in samples originating from the Igneous category show high values because of the lack of sulfate and dominance of bicarbonate, both common features in recent meteoric water (Figure 22a). Produced water also show a relatively low sulfate content but an almost stoichiometric dissolved halite. Figure 22c, at the other end of the spectrum, shows that Balmorhea area samples (springs and wells) and Rustler samples have close to equimolar ratios for halite and gypsum/anhydrite. The Ca/SO_4 ratio slightly <1 and the Na/Cl ratio slightly >1 is likely due in part to ion exchange with calcite precipitation. Some Rustler wells (BOR windmill, Gobble Hole) seem to have undergone more intense ion exchange (middle panel, Figure 22b). The location of the McIntire well at the (1,1) center of the molar plot seems to be a coincidence. The other Cretaceous wells show affinities with the Balmorhea category but with a reduced sulfate content.

The combined occurrence of anhydrite/gypsum and dolomite typically suggests dedolomitization where the excess Ca due to sulfate dissolution would tend to integrate the carbonate mineral network and force out Mg (reaction generalized as $\text{CaSO}_4 + \text{CaMg}(\text{CO}_3)_2 \Rightarrow 2 \text{CaCO}_3 + \text{Mg}^{+2} + \text{SO}_4^{-2}$) (e.g., Appelo and Postma, 2005). The Rustler geochemical signature is very similar to that of a well-known and well-described dedolomitization case (Plummer et al., 1990). The case is summarized in Appelo and Postma (2005) who proposed the following reaction assuming that calcite is slightly oversaturated by 0.2 or 0.1 log unit:



From which reactions we can extract the Ca/Mg molar ratio (3.3 and 2) and the Ca/SO₄ molar ratio (0.77 and 0.67). These are the ranges of ratio observed in Figure 21.

6.1.1 Spring and shallow well samples

The baseline TDS of Phantom Lake spring (average 2280 mg/L) is slightly larger than that of San Solomon (average 2250 mg/L) and Giffin (average 2210 mg/L) as confirmed by the continuous conductivity measurements. However, the TDS of these artesian springs is consistently lower than that of the other Balmorhea springs which average 2700-2800 mg/L at the East and West Sandia springs and almost 3000 mg/L at Saragosa spring. TWDB-TPWD (2005) describes an increase in sulfate from Phantom Lake to San Solomon to East Sandia (based on only 1 sample per spring location); we observed the increase to East Sandia but not from Phantom Lake to San Solomon. All the spring samples make a tight cluster on the Piper plot (Figure 18) and the geochemical variance between the springs is subtle. Higher TDS values of the water table springs could be due to rock-water interactions and long residence time, a

typical explanation for deep groundwater, but unlikely in this case. Likely explanations are evaporation from Lake Balmorhea and, possibly, irrigation return flow flushing out the secular evapotranspiration-related solute accumulation bulge common in arid areas (as described in Scanlon et al., 2010a,b). Both mechanisms would be induced by human activities and recent.

According to their geochemical properties, the 6 springs can be sorted in 2 categories, artesian springs (SS-PL-G) and the other springs, the latter subdivided into two subcategories, East and West Sandia springs, and Saragosa spring. During baseflow periods with little storm disturbances, SS-PL-G have a consistent conductivity. E-W Sandia do too but with a higher value whereas Saragosa's conductivity has been variable from high in this study to similar to the artesian springs in Nunu (2020), to low to very low in the NKRI studies. Temperatures, relatively elevated for the artesian springs, and their variations, small in the case of the three artesian springs, are lower with bigger swings for the other springs (Figure 23). This is another suggestion of long pathways for the artesian springs and shorter and shallower pathways for the other springs.

The 15-year average temperature at Balmorhea (2006-2020), around which shallow groundwater temperature should oscillate, is 64.3°F (17.9°C) (<https://www.ncei.noaa.gov/access/us-climate-normals/>). The Balmorhea weather station is the warmest of those considered in this study whose average temperature is between 17 and 18°C (the Mount Locke value is 15.3°C). Conversely, if we assume a geothermal gradient of 1.25°F/100ft (22.75°C/km), artesian water corresponds to an approximate circulation depth of $(22.75 - 17.9)/22.75 = \sim 210$ m (700 ft) or deeper if we assume heat losses along the way. Such a depth is not inconsistent with water circulation in the Castile Fm. (see cross-sections in Finch, 2017).

Actual temperature measurements at the non-artesian springs are slightly warmer than expected, both using temperature collected during sampling (Figure 23b) and examination of data loggers (~20°C average temperature, 18-22°C range), notwithstanding artifacts introduced when sampling in the pool associated with the spring, not the spring orifice itself. Data presented by TWDB-TPWD (2005) on East Sandia Spring with a temperature drop to 18°C in the winter 2002-2003 flanked by higher temperatures in the preceding and following summers (21-22°C) is fully consistent with our observations.

6.1.2 Produced waters

We also sampled the water of seven wells producing from the Alpine High play. Their TDS ranges from ~40,000 ppm to ~90,000 ppm in agreement with overall salinity distribution in the low-permeability intervals of the Delaware Basin (Nicot et al., 2020). They are mostly Na-Cl waters with no sulfate and little Ca and Mg. Some of their characteristics (stable water isotopes, Sr isotope ratio) can be used as tracers to detect mixing with or contributions to shallower waters.

6.1.3 San Solomon time series

A total of 134 samples were taken from the San Solomon Spring (spring orifice, pool surface, canals) (Figure 24). Although the general composition of the samples stays the same overall (Figure 25) with a TDS slightly above 2000 mg/L, operational issues at the pool prevented us from sampling the spring consistently. It follows that it is difficult to decipher impact from different sampling procedures from actual concentration variations in historical events, unless the event is out of the ordinary, such as captured on 9/13/1932, 11/1/1990, and 8/18/2010 when the TDS went down to 974, 827, and 1560 mg/L, respectively (but it is unclear where the samples

were taken, they could have been diluted by runoff and local rain). Figure 25 displays concentration as a function of the time of the year with the aim of capturing slight seasonal variations in composition. No such variation is apparent.

A Principal Component Analysis (PCA) of 43 pre-study San Solomon samples (including the low-TDS samples mentioned above) shows that the variability in the sample composition is mostly related to the changes in major ion concentration (Na, Ca, Mg, Cl, SO₄), which explains more than half of the variability (first component at 56%). The major ion concentrations are strongly correlated (Spearman's rank correlation) and all have similar loadings. The second principal component (20% of variability) is essentially field alkalinity that is not correlated to any major ion. These PCA results are not surprising because of the baseflow with steady composition. To more finely understand the relationship between the ions and eliminate the impact of varying TDS, we ran a PCA with TDS-normalized samples. Cl and SO₄ are strongly correlated and they also explain the variability in the samples (first principal component at 45% with high loadings for Cl and SO₄ and minor loadings for Na and Mg). The second principal component (29% of the variability) includes Ca and bicarbonate with Na and Mg. These results are consistent with periodic inputs of Ca-HCO₃ "Igneous" waters.

A similar PCA was performed on San Solomon samples from this study (112 samples to 3/18/2020) and also includes water stable isotopes and some minor elements (Li, NH₄, NO₃, F, Br) but no field alkalinity or bicarbonate. Similarly to the previous dataset, the first principal component includes most ions but is dominated by Cl and SO₄, but here explains less of the variability (38%). NH₄ and NO₃ have intermediate loadings but they are negatively correlated with other ions (that is, when concentrations in one group go up, concentrations in the other group go down). The second principal component (~16% of variability) is dominated by water stable isotopes. Water isotopes are not strongly correlated to any other parameter (Spearman's rank correlation), maybe suggesting that their variability is mostly random noise. Examination of the TDS-normalized PCA results still assigns the second principal component to water isotopes (which cannot and are not TDS-normalized) but to which Ca and K can be added (21% of the variability). This is consistent with PCA results of the pre-study samples as K is common in the Davis Mountain rocks, which tend to the rhyolitic pole. The first principal component explains 31% of the variability and consists of normalized Cl and SO₄ negatively correlated with normalized Na and Li. Na and Li were already correlated when non-normalized hinting that ion exchange from clay is important. Both Na and Li cations are single-charged and mostly interact with clays in typical groundwater. Li is also associated with acidic igneous rocks but they do not seem to be its source for groundwater sampled in this study.

6.1.4 Sulfate as a tracer

Sulfate can be used as a tracer because of the contrast between two water type endmembers: the Igneous category with no sulfate and the Rustler category with dominant sulfate. Balmorhea Springs and Cretaceous categories fall in between these two endmembers (Figure 26). Sulfate increases with increasing TDS but the relative proportion of sulfate stays approximately constant. The shape of the Balmorhea Springs Piper plot show that the fraction of sulfate in the sample is approximately constant despite variations in TDS. East and West Sandia have a slightly higher Ca/SO₄ but a similar Na/Cl ratios than SS-PH-G, maybe denoting a clearer influence of the Rustler.

6.1.5 Nitrate as a tracer

Background concentrations of nitrate in shallow groundwater have been estimated at 1.0 mg/L (Dubrovsky et al., 2010). The most common cause of deviation from background values and source of distributed elevated nitrate in surface water and groundwater (>50 mg/L N-nitrate) is fertilizer. Another common source, often more local, is also anthropogenic: septic tanks or septic fields and farm animals. Natural nitrate results from the fixation of nitrogen in soils and abiological nitrate is due to lightning followed by recharge. Whichever the source, presence of nitrate in groundwater suggests recent connection to the very shallow subsurface. Nitrate is typically quickly removed from groundwater in anoxic, confined environments by anaerobic denitrifying bacteria using nitrate as an electron acceptor.

The highest NO₃ values are found in the Madera Creek and McCoy-Remme Seven springs samples (14.2 and 9.2 mg/L, respectively), both samples were taken mid-June 2019. Nitrate concentration is essentially zero in Apache water supply wells (Rustler and others), small in samples from SS-PL-G and Hamilton WM well with an average of 1.0 mg/L (0.5-1.4 mg/L range). ES-WS have higher values with an average of 4.1 mg/L. Nunu (2020) also observed higher nitrate in E-W Sandia springs than in SS-PL-G and Saragosa. Saragosa Spring does not show nitrate, possibly all consumed at the exact sampling location because of the observed amount of decaying organic material in the small puddle formed by the spring. The Saragosa values reported by NCKRI (Jones, 2020) are also lower than SS-PL-G, ranging from 0.1 to 0.2 mg/L. Lake Balmorhea (0.3 mg/L), the BEG BSP shallow well (1.7 mg/L) and BEG Sandia Shallow MW well (3.8 mg/L) fit the pattern (Figure 25g,h and Figure 27). Water supply wells operated by Apache withdraw water from confined aquifers (Rustler and Cretaceous) and show no nitrate. Davis Mountains groundwater wells, springs, and creeks show variable nitrate concentrations. There is no obvious nitrate seasonality in the Balmorhea area spring samples (Figure 28), although the sampling frequency is on the low side to have full confidence in this conclusion. More numerous samples taken at the San Solomon Spring tend to confirm this conclusion, but with periodic peaks tentatively related to rain events (Figure 29). The early March 2020 nitrate spike (6.3 mg/L on 03/07/2020 preceded by 3.6 and 5.9 mg/L two days prior, 03/05 and 03/06, respectively) corresponds to a large Balmorhea rain event on 03/03/2020 at 1.82"; this event was not seen on Mount Locke but a minor event on 03/04 at 0.51" was recorded). The USGS San Solomon gauge did not capture a flow rate increase during this period but anthropogenic actions (not documented and unknown) may be the reason. The TDS does not seem to have varied much during the events. There is, however, a relationship between nitrate and TDS (increasing nitrate with decreasing TDS, Figure 29d) although this might be related to the change in sampling location. Ammonium, when present, was detected at low values between 0.1 to 1-2 mg/L, typically in samples at low or undetected nitrate and is understood to be a byproduct of microbial nitrate reduction. It is observed in 16 wells, mostly deep wells, several tapping the Rustler Aquifer, but also in one of the Lake Balmorhea samples (0.2 mg/L) and in the well (BEG Cherry Canyon Deep MW) drilled into the Boquillas Formation (1.8 mg/L).

The 8/3-4/2004 rain event for which we have data (low TDS) shows an increase in NO₃ as the spring water TDS decreases (PL and G). The increase in nitrate is likely related to the storm water capturing organics and related nitrate, as cattle and wildlife are abundant on the lower slopes of the Davis Mountains. Note that SSS shows a small TDS decrease with NO₃ concentration higher than the average. It is unclear if the SSS TDS was lower before or after that single geochemical sampling event. Interestingly, NO₃ of the Sandia springs slightly increases with TDS; a behavior opposite to that of the SS-PL-G springs. It could denote evaporative

enrichment (which should also be seen in the water isotopes). Consistently different nitrate concentrations in the SS-PL-G and ES-WS groups suggests that their respective source diverge far away from the springs or that the addition of nitrate is very close to the ES-WS system. It should also be noted that proper sampling at the Sandia and Saragosa springs is difficult to achieve and that the sampling is often not done at the spring vents/orifice as it could be done at SS-PL-G.

Robertson and Sharp (2013) conducted a study focused on nitrate as a means to estimate recharge in the salt flats of far west Texas (including Wild Horse Flat). Approximately half of the 80 samples fall between 6 and 9 mg/L, range is <1 mg/L to >18 mg/L (with irrigated areas tending to the higher values of the range). They show an overall increase in nitrate concentration since sampling started more than 50 years ago. However, the natural egress of some of the Salt Basin recharge goes through the Apache Mountains where nitrate values are mostly <1 mg/L (Finch, 2017) suggesting that any nitrate is consumed by reduction reactions under the confined conditions of the aquifers. The non-zero nitrate level in the Balmorhea area springs, mostly fed through a long regional flow path acting as baseflow, suggests some local baseflow component. Nitrate can enter the flowpath from the Davis Mountains recharge and also upgradient of the springs along the Stocks Fault.

6.1.6 Silica and B/Cl ratio as tracers

Silica:

Silica is typically an uncharged colloidal species present at low concentrations in most groundwaters. The Igneous water samples are very high in silica despite their low TDS and low pH (Figure 30) owing to the acidic nature of the predominantly rhyolitic volcanic rocks of the Davis Mountains. We use the SiO₂/TDS mass ratio to properly compare samples of various origins. Other samples with high silica would suggest exposure to Davis Mountains recharge or at least to igneous rock clasts (in alluvium).

The produced water samples are not particularly high in SiO₂, on par with non-alkaline formation waters (50 mg/L Si or 107 mg/L SiO₂). They are oversaturated relative to quartz but undersaturated relative to amorphous silica. Their SiO₂/TDS mass ratio averages 1.6×10^{-3} . The SiO₂/TDS mass ratio for the Balmorhea Springs and associated samples (shallow wells and surface waters) ranges from 6.7 to 16.0×10^{-3} (average 10.2×10^{-3}), their average SiO₂ concentration is 26 mg/L. As a result of being exposed to volcanic rocks trending to the rhyolitic pole, dissolved SiO₂ of samples from the Igneous group is relatively high at an average of 46 mg/L. Their SiO₂/TDS mass ratio is also high ranging from 108 to 381×10^{-3} (average 180×10^{-3}). Three of the Rustler samples show an average ratio of 5.1×10^{-3} and an average concentration of ~15 mg/L but the Hidalgo Rustler shows a higher ratio at $\sim 16 \times 10^{-3}$ because of a lower TDS with similar SiO₂ content. This suggests that the dilution of this sample by low-TDS high-SiO₂ Igneous water is unlikely (local recharge or input from the overlying Cretaceous?). The Cretaceous groundwater shows a wide range of concentrations and mass ratios with two subgroups by TDS: (1) low TDS (Duncan Camp, 4J Wildcat, and Hidalgo WSW3 wells) with high SiO₂ (36 mg/L) and ratio (63×10^{-3}) and (2) higher TDS (Apache Artesian 1 WSW, WVWSC McIntire, and BOR Windmill wells) with low SiO₂ (17 mg/L) and ratio (12×10^{-3}). The low TDS Cretaceous water are clearly mixing with Igneous waters.

Boron:

Boron is a common minor element typically dissolved as uncharged oxyanion borate at circumneutral pH's (as B(OH)₃ also written H₃BO₃). Boron behaves conservatively in clay-poor

environments and thus could act as a good tracer as chloride does. Both concentrations are combined in a B/Cl molar ratio.

Balmorhea springs and associated samples show a narrow range of B concentrations (0.32 to 0.48 mg/L) and B/Cl molar ratio values (1.6 to 2.5×10^{-3}) for a TDS ranging from ~ 2000 to ~ 3000 mg/L (Figure 31). Boron concentrations in Igneous samples is lower (0.017 to 0.057 mg/L) but higher relative to Cl. Their B/Cl molar ratio is the highest of all groups and ranges from 7 to 40×10^{-3} . Igneous springs have the lowest B/Cl ratio within this group. Three of the 4 Rustler wells show a ratio ranging from 3.4 to 5.3×10^{-3} , the Gobbler Hole well has a higher ratio at ~ 15 due to its low Cl content. These wells have a ~ 0.4 mg/L B on average. The miscellaneous Cretaceous groundwaters show a relatively small range of molar ratios (1.7 to 4.3×10^{-3}) and concentrations (0.05 to 2.8 mg/L) of B.

Isotopes of boron are unusual in the sense that the heavier isotope is the most common (^{11}B $\sim 80\%$ - ^{10}B $\sim 20\%$). It is a light element and isotope fractionation effects are pronounced, although, once in solution, boron typically remains dissolved and can be used as a tracer to determine the origin of the groundwater. Boron isotope systematics show that seawater is very heavy ($\sim 40\%$) and that crustal rocks are typically depleted ($< 0\%$). Groundwater would show influence from rock-water interaction (which would tend to decrease the ratio) and from salt deposition (which would tend to increase the ratio). Note that marine carbonates and evaporites also show a relatively high ratio ($> 0\%$) as they are sourced from seawater. Seawater is a boron reservoir but its concentration is not very high at ~ 4.6 mg/L ($\sim 0.8 \times 10^{-3}$ B/Cl molar ratio)

The B/Cl ratio is not very discriminatory relative to the artesian springs and the other non-Igneous samples but the $\delta^{11}\text{B}$ is (data extracted from Nunu, 2020). Out of 12 spring samples taken in 2019-2020, artesian springs (6 samples) $\delta^{11}\text{B}$ is between $+8\%$ and $+12\%$ whereas that of the other springs (6 samples) ranges from $+12\%$ to $+18\%$. The lack of $\delta^{11}\text{B}$ values of groundwater away from the spring area limits the opportunity of narrowing down potential explanations but two can be proposed. Seawater and marine deposits tend to have high values ($\delta^{11}\text{B} > +20\%$) whereas continental crust (igneous) tend to have low values ($\delta^{11}\text{B} < 0\%$). Given that samples were taken outside of large rain event episodes, the igneous signal acquired in the West Texas bolsons is strong enough to lower the signal given by the carbonates. Another explanation for the higher $\delta^{11}\text{B}$ in some springs would involve anthropogenic activities and be correlated with the higher nitrate, but such a correlation is not manifest at this point.

Although their B concentrations are much higher (37 to 63 mg/L), produced water B/Cl ratios (7 samples) are also low (average 4.3×10^{-3} ; range 2.5 - 8.3×10^{-3}). However, although no $\delta^{11}\text{B}$ analyses have been done on the Alpine High produced water, published articles suggest it is high. Engle et al. (2016) in the Permian formations of the Midland Basin, observed $\delta^{11}\text{B} > +30\%$; Warner et al. (2014) in the Appalachian Basin describe $\delta^{11}\text{B} > 35\%$ in conventional formations and $\delta^{11}\text{B} > +25\%$ in unconventional formations (Marcellus Shale). This is another element suggesting there is no contribution from the deep Guadalupian (Permian) aquifer (DMG) because the springs have the lowest $\delta^{11}\text{B}$ of all sampled water.

The Igneous group is characterized by a high B/Cl molar ratio but its samples can already be easily identified with their low TDS. On the other hand, Balmorhea Spring samples are characterized by a low B/Cl molar ratio. The Cretaceous samples with low B/Cl ratio are also the ones close to the Balmorhea Spring category on the Piper plot, which suggest that a crossplot of the ratios could be informative.

B-SiO₂ Crossplot:

Because silica and boron are somewhat discriminatory and behave more or less conservatively, plotting one against the other should provide useful information (Figure 32). Three wells (4J Wildcat, Duncan Camp, and Hidalgo WSW3) trend toward the Igneous cluster both in absolute concentrations (Figure 32a) and normalized concentrations (Figure 32b). The absolute concentration plot does not discriminate well between Rustler and Balmorhea Spring samples, but the normalized concentrations show the McIntire 1 and Apache Artesian 1 wells to be close to the Balmorhea Spring cluster. The BOR Windmill well, in an uncertain position on the Piper plot, shows here affinities the Rustler cluster.

6.1.7 Results from other geochemical databases

One of the early goals of the study was to sample groundwater broadly upgradient of the springs. This effort remains unsuccessful. However, several historical data sets are available. Although often missing the diagnostic isotopes and other elements, they are useful to provide the geochemical context of the study. Piper plots of samples taken from these large aquifers show multiple influences (Figure 33). Bolson Aquifers samples show water types varying from Na-HCO₃ to Na-mixed anion Cl-SO₄ (Figure 33a). There is a limited number of data points from the Capitan Reef Aquifer (Figure 33b) because the study area is located away from the main productive groundwater supply area in New Mexico. There is no clearly discernable Capitan trend except maybe the relatively high Mg in many samples, which is related to the dolomitic nature of the formation, but may also denote the influence of dolomites in the Rustler as suggested by some high sulfate samples. The Rustler is the most clearly defined aquifer with a Ca-SO₄ water type (Figure 33c). The Pecos Valley Alluvium (Figure 33e) shows the influence of evaporites, anhydrite and halite, with mixed cation Na-Ca and mixed anion Cl-SO₄ water type whereas Igneous Aquifer samples (Figure 33f) show a clear Ca-HCO₃ water type. The Edwards-Trinity Aquifer (Figure 33d) is the most geochemically complex. It shows influence of Rustler water with a Ca-SO₄ pole at the top of the diamond and a mixed cation Na-Ca and mixed anion Cl-SO₄ water type reminiscent of both the Balmorhea Springs water and of the Pecos Valley Alluvium Aquifer. Such similarities underscore exchange between aquifers. The Edwards-Trinity also shows a Ca-HCO₃ pole as would be expected in a limestone.

6.2 Water isotopes

In the course of this study, we sampled potential contributors to the water isotope signature of the Balmorhea area springs including rainwater.

6.2.1 Rain water

Water isotopes of groundwater depends on the location of the recharging water(s) (elevation, latitude, temperature, climate, continentality), which might have occurred under different climatic conditions, and potential mixing of groundwater from different origins. Isotope exchange and equilibration with rock minerals is not relevant for shallow groundwaters unlike deeper formation, such as basinal brines which are typically isotopically heavier. In the small geographic area, variance in stable water isotopes is due to elevation difference and to seasons (and type of precipitation events). In our dataset, the seasonal variation is larger than that due to the elevation difference (~3000 ft, 940 m). The data set is consistent through the two years of record (Figure 34). The noise in the data is due to individual events but also due to the fact that the rain sampler (Photo 1) was emptied relatively frequently but irregularly every few weeks to every couple of months. According to global averages, McDonald Observatory samples, collected from rain fallen at higher elevation, have slightly lighter stable water isotopes than

Balmorhea State Park samples, collected at lower elevation (maybe by one $\delta^{18}\text{O}$ unit and 5-10 δD units), which is consistent with the Global Meteoric Water Line (GMWL) and its slope $\delta\text{D}/\delta^{18}\text{O}$ of ~ 8 . This effect, due to decreased average temperature, is well documented and seems to be weaker than the average elevation effect collated from world-wide data (Clark and Fritz, 1997). Clark and Fritz (1997) stated that depletion with altitude varies from 0.15 to 0.5‰ and from 1 to 4‰ for $\delta^{18}\text{O}$ and δD , respectively. The elevation difference between McDonald and Balmorhea rain collectors ($\sim 1000\text{m}$) generates a low gradient of $\sim 0.1\text{‰}$ $\delta^{18}\text{O}/100\text{m}$ and $\sim 1\text{‰}$ $\delta\text{D}/100\text{m}$.

A large seasonal effect is not unexpected because it typically increases with the continentality of the sites. However it is also typically less marked at lower latitudes (about 31°N here). The seasonal difference is ~ 6 units for $\delta^{18}\text{O}$ and ~ 50 units for δD , again consistent with the GMWL slope, demonstrating that no evaporation is involved (that is, summer months are not heavier because of evaporation but because of higher temperatures). This difference should be large enough to be observed in short-path local springs and streams.

Weighted average of water isotopes by rainfall is -6.8‰ ($\delta^{18}\text{O}$) and -45.0‰ (δD) for BSP and -7.1‰ and -44.7‰ for McDonald, that is, essentially the same given the data uncertainty (-7.0‰ and -45.0‰ overall). The seasonal variations are markedly stronger than the elevation differences and are likely related to the type of precipitation (Sun et al., 2019). $\delta^{18}\text{O}$ of rainwaters from summer convective storms is typically lighter than that of cyclonic events and, apparently, rain type exerts a stronger control than the temperature on the stable water isotopes (Sun et al., 2019).

6.2.2 Igneous springs

The two spring samples (Willow Spring and Seven Spring) and two upper Limpia Creek samples (sampled at an elevation of 1580 m) were taken in May-June. They are complemented by two older samples from Big Aguja Spring. All the samples were taken in the spring / early summer. They show values $\sim -48\text{‰}$ (range -44 to -51‰) for δD and $\sim -6.9\text{‰}$ (range -7.4 to -6.5‰) for $\delta^{18}\text{O}$ consistent with the rainwater of these months which suggests that travel time is small and that igneous springs and stream baseflow are very local. Overall the Davis Mountains (“igneous”) ground water and surface water (base flow) are slightly lighter than the observed rainwater weighted average suggesting that recharge occurred when rain water is lighter, second half to last third of the year, when precipitation is more abundant.

6.2.3 Balmorhea area springs

This study period of record does not show large variations in specific conductivity or TDS as was observed in 1932 or 1990. It follows that the sampled water represents the spring baseflow. Simple averaging of the 66 SSS samples between March 2018 and September 2019 yields $\delta\text{D} = -62.24 \pm 1.06\text{‰}$ and $\delta^{18}\text{O} = -9.04 \pm 0.25\text{‰}$ (1 standard deviation) with a fairly constant TDS at 2244 ± 36 mg/L and a weak correlation between water isotopes and TDS. Phantom Lake and Giffin springs have each a couple of samples but TDS and water isotopes are very similar to SSS (Figure 35b). On the other hand the Sandia springs display a higher TDS but show slightly heavier water isotopes. Older samples from previous campaigns (mostly TWDB) do fall within the general range of samples from this study but with more scatter making their interpretation more difficult because the sampling details are not known. Saragosa Spring samples at $\delta\text{D} = -46.6\text{‰}$ and $\delta^{18}\text{O} = -5.9\text{‰}$ are heavier than the other springs and within the general field of recently-recharged meteoric water. It is possible that this sample was contaminated by the nearby

Toya Creek surface water. Plotting San Solomon water isotope time series as a function of the month of the year (Figure 36a,c) and of TDS (Figure 36b,d) shows consistency between sampling campaigns and no obvious trend. The impact of using different sampling locations at San Solomon is shown in Figure 36e,f, and g.

6.2.4 Groundwater

Deeper formations (Cretaceous and Rustler) tend to have lighter water isotopes, maybe related to older recharge when the climate was cooler or to higher elevation recharge. Data by Jasechko (2019) show that groundwater is commonly heavier than its recharge water as most subsurface processes would pull average water isotopes toward heavier values. Most groundwater samples are heavier than Balmorhea area spring waters, in particular, the samples from the Davis Mountains and Alluvium. They also tend to be lighter than the precipitation volume-weighted average water isotopes suggesting that recharge occurred preferentially when the temperature is lower in the Fall and Winter seasons. Such behavior has been observed in West Texas and in many other arid places where spring and summer rains are quickly evapo-transpired because of active plant growth or intense heat (Scanlon et al., 1991; Walvoord and Phillips, 2004).

6.2.5 Produced water

A total of seven oil and gas wells producing from the Alpine High field north of the Balmorhea area were sampled for produced water. Two of the samples are on a mixing line with local freshwater (Figure 35a), likely a side effect of residual hydraulic fracturing fluid. The five remaining samples are geochemically clustered with a TDS ranging from 77 kppm to 88 kppm (average 83 kppm) and water isotopes with oxygen (range 3.5 / 4.43.8‰ and average 3.8‰) much heavier than that of fresh water and hydrogen (range -22.9 / -17.9‰ and average -20.9‰) heavier than Balmorhea area spring water but overlapping with the extreme upper range of the rainwater samples. Such results are consistent with waters observed in formations targeted by oil and gas operators in the Delaware Basin (Nicot et al., 2020). Comparing the various sources of the water samples (Figure 35), there is no obvious impact of deeper formation water on the shallow subsurface and surface waters. The two data points trending to the PW are samples taken from Balmorhea Lake that show some impact of evaporation (Figure 35b).

6.3 **Strontium isotopes**

6.3.1 Background

Strontium isotope ratio ($^{87}\text{Sr}/^{86}\text{Sr}$) is a robust conservative tracer useful to decipher mixing relationships (Figure 37 and Figure 38). Sr readily substitutes for Ca and, consequently, is mobilized during carbonate, plagioclase, and sulfate dissolution with the caveat of the reduced solubility of strontianite (SrCO_3) and, particularly, celestine (SrSO_4) relative to calcite and gypsum/anhydrite. The interest of the Sr isotopic ratio is that it is barely impacted by dissolution and precipitation reactions (no or very little fractionation) given the very similar molecular weight of the two relatively common isotopes, and that the ratio is the same in a single solid phase and corresponding equilibrated aqueous phase. The Sr ratio of sea water, which marine carbonates are in equilibrium with during deposition, has fluctuated through time but the origin of the fluctuations is well understood; they have been explicitly and consistently described in several papers (e.g., Veizer, 1989; Halverson and Théou-Hubert, 2015). A common assumption is that the solid phase will imprint the aqueous phase, however the reverse can happen if the rock/water ratio is favorable, for example, in fracture fillings.

Marine sediments relevant to this study are of Permian and Cretaceous age (Burke et al., 1982; Veizer et al., 1999; Korte et al., 2003; Korte et al., 2006). The Permian Sr ratio shows a quick decrease from ~0.7084 to ~0.7067 with a fast rebound to 0.7074 at the very end of the period during deposition of the Ochoan evaporites. Samples from the Castile Formation (anhydrite and gypsum) yielded an average value of 0.70692 (Denison et al., 1998; Kirkland et al., 2000; -225 in their metric of the Δ between sample and seawater Sr ratio times 10^5). Carbonates and evaporite samples from the WIPP site in New Mexico yielded Sr ratio between 0.7068 and 0.7084 (Siegel et al., 1991). Register and Brookins (1980) present similar results for the Salado Fm. but show the large impact of K-bearing mineral when abundant (sylvite, polyhalite) when a Sr ratio often >0.720 and sometimes >0.800. The Salado Fm. is not believed to be present in southwest Delaware Basin. One Sr ratio measurement in the eastern arm of the Capitan Reef in Loving County yielded a value of 0.7076 (Saller and Stueber, 2018). Cretaceous marine carbonates show a regular increase during the period from 0.7068 to 0.7077. It follows that the Sr ratio cannot fully discriminate between Cretaceous and Permian sources. The current sea water Sr ratio of 0.7091 is as high as it has ever been since the early Paleozoic.

Sr ratio is often higher in igneous rocks because of the presence of K and Rb commonly substituting for it and of the negative correlation between Ca and K at the continental scale. ^{87}Rb decays into the radiogenic ^{87}Sr , slowly increasing the Sr ratio in these rocks. K is typically a minor dissolved element but can be abundant in some sedimentary clastic rocks such as illite-rich mudstone, arkosic sandstones with K-feldspar, or evaporitic K-rich salt. Permian rocks and rocks from older formations in the study area contain K minerals and sylvite is common in the late Permian Salado Formation as well. The Sr ratio of many Davis Mountains volcanics ranges from 0.7037 to 0.7077 (18 samples) (Cameron et al., 1996; Uliana, 2000); the lower values of the range corresponds to more mafic units, which are volumetrically minor. These values are relatively low with the notable exception of a sample at 0.7113 south of the Davis Mountains (Paradise Mountain) and of the Star Mountain rhyolite (0.7117 and 0.7274), observed in the northeast quadrant of the Davis Mountains close to the base of the volcanic section (Cameron et al., 1996). Such high values could possibly impact the Limpia, Big Aguja, and Little Aguja watersheds but have not been observed in the water samples taken there.

In order to better assess subtle differences in ratio, we introduce the commonly used epsilon coefficient notation that measures the distance to the current sea water Sr ratio, similarly to relative abundance of an isotope compared to a standard:

$\epsilon_{\text{Sr}} = ([^{87}\text{Sr}/^{86}\text{Sr}]_{\text{sample}} - [^{87}\text{Sr}/^{86}\text{Sr}]_{\text{sea water}}) / [^{87}\text{Sr}/^{86}\text{Sr}]_{\text{sea water}}$ where $\epsilon = 0$ for Sr = 0.70917 (current sea water) and a ratio of 0.7100 corresponds to $\epsilon = +11.76$ and 0.7070 corresponds to $\epsilon = -30.5$.

6.3.2 Igneous springs

Low TDS samples representative of the Davis Mountains meteoric water and of the mountain front alluvium exhibit a Sr concentration <1 ppm and clustered around 0.3 ppm. Their Sr ratio is consistently low at approximately 0.7077 ($\epsilon_{\text{Sr}} = -20.7$) and is consistent with that of the igneous rocks of the Davis Mountains. The high Sr ratio value observed in the Star Mountain rhyolite is not observed in the wells seemingly downstream of it (Leoncita Limpia shallow well, which, at 0.7078 ($\epsilon_{\text{Sr}} = -19.3$), is not particularly high).

6.3.3 Balmorhea area springs

The samples taken from Balmorhea area springs SS-PL-G as well as from the Hamilton well have a consistent isotope signature with an average Sr ratio of 0.7100 ($\epsilon_{\text{Sr}} = +11.8$) (value also reported in Uliana et al., 2007; note that analytical work was done in the same UT Austin lab) as opposed to a slightly lower value in the Sandia springs, 0.7097 ($\epsilon_{\text{Sr}} = +7.53$) (value also reported in Uliana et al., 2007). Value from Saragosa Spring, extracted from Nunu (2020) is slightly lower still (0.7095; $\epsilon_{\text{Sr}} = +4.71$) but higher than the rest of the dataset. Balmorhea area springs show the highest Sr ratio of all water sampled in this study (deep produced water excluded). Samples from the BEG BSP Shallow MW well and BEG Sandia Shallow well, both of which are shallow and close to the springs, share similar Sr ratio: 0.7099 ($\epsilon_{\text{Sr}} = +10.3$) and 0.7097 ($\epsilon_{\text{Sr}} = +7.53$), respectively. The fact that the springs and related wells have a higher Sr ratio than local wells away from the springs (tapping alluvial/igneous, Cretaceous, or Rustler aquifers) confirms that the origin of the spring water is not local. Uliana et al. (2007) and others hypothesized that a sizable fraction of spring baseflow originates in the Salt flats. For example, a well from the city of Van Horn shows a Sr ratio of 0.7127; that of another nearby well is 0.7148 (Uliana et al., 2007). Their main initial hypothesis was that the high Sr ratio is brought in by the Salt Flat component whereas the high TDS is due to the Rustler component (6-12 ppm Sr). This model, however, only works if the Salt Flat component is modified when flowing through the Apache Mountains to reach an ionic composition comparable to that of the Balmorhea springs with similar Cl and SO₄ mass concentrations (samples 5, 6, 7, and 9 of Uliana et al., 2007). A disappointment of this current project was not to be able to access wells in the Apache Mountains and vicinity in order to test / better support this hypothesis with more spatial details. Uliana et al. (2007) further hypothesized that anhydrite dissolution provided the additional Sr needed to make the model work but the hypothesis relies more on geochemical modeling than on actual field observations.

6.3.4 Groundwater

The McIntire well, already noticeable by the similarity of its geochemical characteristics with the Balmorhea spring water, is confirmed to be closely related to them because of its high Sr ratio. The BOR Windmill and McCoy-Remme Duncan Camp wells also show a relatively elevated Sr ratio that places them in a group different from the other local wells. .

The BEG Cherry Canyon Deep MW well, from which the low permeability Boquillas Formation was sampled at depth (as recognized by the high dissolved biogenic methane content), shows the lowest Sr ratio of the study (0.7073; $\epsilon_{\text{Sr}} = -26.3$) and is representative of an aqueous phase in equilibrium with upper Cretaceous carbonates. All other Cretaceous water wells have a higher Sr ratio.

A total of four water supply wells operated by Apache tap the Rustler Aquifer (variable TDS but dominant sulfate) show values (0.7079; $\epsilon_{\text{Sr}} = -17.8$) consistent with the single sample discussed by Kreitler et al. (2013) from the Rustler outcrop at 0.7080. Kreitler et al. (2013) also present four Rustler samples from Pecos County, have a Sr ratio of 0.7074-0.7076, more in line with the seawater Sr ratio at sediment deposition time.

6.3.5 Produced water

Five of the seven produced water samples show a high Sr ratio >0.712 ($\epsilon_{\text{Sr}} >40$) (max 0.7135; $\epsilon_{\text{Sr}} = 61.1$) including the two samples residing on a mixing line with fresh water (Sr concentrations

are low in fresh water and the Sr ratio signal is overwhelmingly given by the produced water even if somewhat diluted). The Sr ratio of the first outlier sample is relatively high (0.7099; $\epsilon_{\text{Sr}} = +10.3$), the second outlier has a lower TDS and a ratio on 0.7087 ($\epsilon_{\text{Sr}} = -6.6$) about the same as those of the Balmorhea artesian springs, but with clear formation water characteristics (TDS of ~77,000 ppm, in par with the other PW samples, and heavy water isotopes). A reasonable explanation for the outlier is a lack of a source of radiogenic Sr rather than input of shallow fresh water with a low Sr ratio.

The Alpine High PW dataset does not share the same Sr ratio signature as produced waters from the Wolfcamp (early Permian) observed in samples taken at the center of the Delaware Basin. There, a total of 36 samples have an average of 0.7090 (min: 0.7087, max: 0.7097) (ϵ_{Sr} ranging from -6.6 to +7.5; average of -2.3) (Nicot et al., 2020), and are somewhat in agreement with early Permian expected Sr ratio. The authors have no knowledge of Sr ratio analyses of formations older than Permian in the Delaware Basin. Engle et al. (2014) described samples with ratio <0.710 for Permian and Pennsylvanian formation water in the Midland Basin. Silurian and Devonian samples consistent with the late Devonian Woodford Shale, main target of the Alpine High play, and with the general increase of the Sr ratio with increasing Paleozoic age. However it is difficult to envision brines migrating up from the depths of the Delaware Basin without them impacting intermediate intervals such as Permian formations.

6.4 Carbon isotopes and bicarbonate and methane

6.4.1 Bicarbonate

Field alkalinity measurements were performed for most samples throughout the study as well as analyses C isotopes of dissolved inorganic carbon (DIC, i.e., ~bicarbonate). The DIC carbon isotopes are indicative of the source of the sample (Figure 39). Samples from the Rustler Aquifer exhibits a relatively heavy and slightly negative signature close to that of marine limestones (e.g., Clark and Fritz, 1997), itself close to that of ocean DIC, which is, by definition, 0‰ VPDB. Samples from the well-studied (WIPP site) Culebra Dolomite Member of the Rustler Fm. show a $\delta^{13}\text{C}$ of 6‰ (Siegel et al., 1991). These values denote a long residence time with DIC equilibrated with the aquifer host rock. Samples from the Davis Mountains, Igneous Aquifer and related samples, show a DIC carbon isotope in the -15 to -10‰ range typical of groundwater samples recently recharged and impacted by plant activity, most likely C4 plants (grass). These Igneous Aquifer samples also show the clear trend of lightest $\delta^{13}\text{C}$ values being associated with lowest TDS (plot not shown). Balmorhea area springs values are intermediate between these two end members. Note that the August 2004 rainfall event is visible and expressed by a drop in the DIC carbon isotope to lighter values, close to that of the Igneous Aquifer samples, other clear evidence of the impact of local groundwater on the Springs. Sandia springs $\delta^{13}\text{C}$ values seem to be lighter by 2 or 3 units that those of SS-PL-G. Impact from the Igneous Aquifer through mixing cannot explain this difference because Sandia Spring TDS is typically higher. A possible explanation may be local recharge taking the imprint of soil $\delta^{13}\text{C}$ as it infiltrates. Another explanation may be related to the sampling approach, in which samples are taken in the spring pond not at the emergence of the spring water from the rock. Biological activity, either by plants or microorganisms, would draw $\delta^{13}\text{C}$ to lighter values.

6.4.2 Light hydrocarbons

Sampling of dissolved gases in groundwater in the vicinity of unconventional wells has become routine as a result of studies undertaken in the past 20 years, which concluded that contamination

of fresh-water aquifers by methane and other light hydrocarbons could be an environmental threat. These findings have been challenged with several subsequent studies showing that, at many locations where it is found, CH₄ turns out to be of natural origin. In another study, BEG sampled ~20 water supply wells in Loving County and vicinity (unpublished data) with no evidence of methane contamination except next to a blow out in Mentone, Loving County. Similarly, BEG analyzed for dissolved methane and other light hydrocarbons in all sampled locations including Balmorhea area springs. Only one outlier has significant dissolved methane, the BEG Cherry Canyon Deep MW well drilled into the organic-rich Boquillas Fm., which is the western equivalent to the oil-producing Eagle Ford Fm. in the Texas Gulf Coast plains. Two samples yielded 27 and 21 mg/L dissolved methane, relatively high values but below the saturation level at that depth and pressure. However, the samples clearly fall into the biogenic field with very small amounts of ethane and propane detected as well as a diagnostic light $\delta^{13}\text{C}$ at -75.7‰ and -73.0‰. Values for δD of methane (-233.1‰ and -231.0‰, respectively) suggests methane is sourced from organic material in the formation through the well-known mechanism of CO₂-reduction (e.g., Milkov and Etiope, 2018). There is no evidence that CH₄ as a product of CO₂ reduction (by Archae) is being utilized as an energy source by sulfate-reducing bacteria. Sulfate concentration is naturally low, and no methane shift to heavier carbon is visible.

Most samples have estimated CH₄ concentrations <3ppb or non-detect (detection limit is generally accepted to be ~1ppb). One Giffin Spring sample had 4ppb and one Hamilton well sample had 22 ppb whereas other samples from this latter location did not contain measurable methane. Wells with the highest dissolved methane concentrations are from the Rustler and other deep wells, generally >10 ppb with a maximum of 78 ppb. All these concentrations were too low for the labs to measure isotope ratios of C and H. However, ethane and propane are both very low and at their detection limits, also pointing to a biogenic origin of these low methane concentrations. Ammonium and dissolved methane are loosely positively correlated. They both imply biological activity in anoxic conditions but at a low level given the low concentrations of these reaction products.

There is currently no data in the Balmorhea area suggesting that natural gas present in the Woodford and associated formations would migrate naturally or otherwise into the Permian and younger age aquifers.

6.5 Chloride-bromide ratio

The Cl/Br ratio have been used to discriminate between Cl resulting from long-term evolution of groundwater and from dissolution of halite. Sea water Cl/Br mass ratio is ~290, whereas freshwater aquifer values vary with proximity of the recharge zone to the ocean but should be in the 100-200 range in West Texas (Davis et al., 1998, 2004). On the other hand, halite does not accept much Br in its crystal network. A water sample at equilibrium with halite will have a high TDS and a high Cl/Br ratio (>1000). Another indicator of halite dissolution is stoichiometric Na and Cl.

6.5.1 Balmorhea area springs

The Cl/Br mass ratio of Balmorhea area spring water and associated wells (Hamilton WM, BEG Sandia Shallow MW, and BEG BSP MW as well as Lake Balmorhea) is larger than that of current sea water (Figure 40) and is a strong indicator that the source of Cl is halite. The Na/Cl ratio is also close to 1 but slightly higher (~1.1), which is likely related to the concomitant dissolution of gypsum and subsequent ion exchange driving Na up and Ca down. Ca/SO₄ ratio

also strongly suggests gypsum dissolution, with Ca driven down by ion exchange (because $\text{Na/Cl} > 1$) and likely calcite precipitation (because some Ca still missing).

6.5.2 Igneous springs and related groundwater

The Cl/Br ratios are mostly in the 50-100 range, consistent with the continental locations of the recently recharged samples.

6.5.3 Produced water

Cl/Br ratios of produced water carry the signature of brine evolved from sea water (ratio $< \sim 300$) for 5 of the 7 producing wells. Their TDS range from 77k to 88k ppm. The other 2 wells with a Cl/Br ratio slightly above that of sea water would conventionally show a minor influence of halite dissolution, which seems to contradict their lower TDS at 42k and 57k ppm. The source of these brines can then be explained at least partly by addition of meteoric water that dissolved some halite. This hypothesis is supported by (1) a Na/Cl molar ratio close to 1 (or closer to 1), and (2) the relatively low water isotopes ($\delta^{18}\text{O}$ at +0.20 and -1.17, respectively, compared to $\sim +4.0$ for the other 5 samples) (Figure 35). A simple mixing model (end members of typical brine at $\delta^{18}\text{O} = 4\text{‰}$ and old meteoric water analogous to Balmorhea spring water at $\delta^{18}\text{O} = -9\text{‰}$) suggests that the two PW samples with lower TDS are 9/13 = 69% brine and 30% meteoric water. A similar computation with δD provides a similar mixing ratio ($\delta\text{D} = -21\text{‰}$ for brines, -60‰ for Balmorhea spring water, and -35‰ for the low TDS produced water samples) of 25/39 = 64%. The ratio approximately holds for the TDS too: $((69+64)/2)\%$ of 82k is 54k. Such occurrences are common in brines of the Delaware Basin (Nicot et al., 2020).

6.6 Chlorine isotopes

6.6.1 Background

Natural chlorine consists mostly of two common natural stable isotopes: ^{35}Cl (75.8% of total Cl) and ^{37}Cl (24.2%). A third radioactive isotope with a relatively long half-life ^{36}Cl is used to age-date groundwater. The three isotopes are very conservative (stay in solution) and are little fractionated through common processes such as evaporite precipitation or molecular diffusion but sufficiently so to be helpful as a tracer. $\delta^{37}\text{Cl}$ values (ratios of ^{37}Cl to ^{35}Cl) are calculated relative to the standard SMOC (Standard Mean Ocean Chloride) and are typically single digit unlike other elements involved in highly-fractionated biological reactions such as ^{13}C or ^{34}S (Clark and Fritz, 1994). Halite is slightly enriched in the heavy isotope (^{37}Cl) during precipitation from brine ($\sim 0.24\text{‰}$ at 20°C). Diffusion along a concentration gradient will favor ^{35}Cl whereas membrane filtration can slow down the motion of ^{37}Cl , which is already impeded for Cl ions because of the negatively-charged rock matrix. Pore waters and formation waters tend to have a negative $\delta^{37}\text{Cl}$ (Barnes and Sharp, 2017).

6.6.2 Analysis

A total of 13 samples were analyzed for $\delta^{37}\text{Cl}$: Balmorhea springs and associated wells (n=5), Igneous wells and igneous springs (n=5), Rustler (n=1), and so-called Cretaceous wells (n=2) (McIntire and Duncan Camp). $\delta^{37}\text{Cl}$ values stays close to 0‰ and vary between +0.4 and -0.7‰ (median and average of -0.1‰) (Figure 41). These values are close to the expected accuracy of 0.2‰ of $\delta^{37}\text{Cl}$ analyses (Barnes and Sharp, 2017). Chlorine isotope analyses were initially ordered to dismiss any exotic sources of chloride. No strong trend is discernable; data mildly suggest that average Balmorhea area spring values heavier than average, possibly denoting some halite dissolution along the long flow path to the springs.

Diffusion and membrane filtration do not appear to be controlling mechanisms of aquifer ionic composition; variations in $\delta^{37}\text{Cl}$ are likely related to halite precipitation and dissolution, possibly in several cycles, and NaCl-rich marine aerosol deposition. Another commonly used tracer to track halite dissolution is the Cl/Br ratio, which increases with the fraction of Cl originating from halite dissolution. It follows that in a system controlled by halite, $\delta^{37}\text{Cl}$ and Cl/Br should be positively correlated. Igneous samples with a low Cl/Br ratio (Figure 40) tend to also have a low $\delta^{37}\text{Cl}$ whereas Balmorhea-area spring samples with a higher Cl/Br ratio tend to have a higher $\delta^{37}\text{Cl}$ but the crossplot is noisy. Overall, no real insight was gained from these analyses.

6.7 Sulfate isotopes

6.7.1 Background

Of the four stable sulfur isotopes, ^{32}S (95% of total S) and ^{34}S (4.2%) are the most abundant. They are also fractionated in many abiotic and microbial reactions. The standard $\delta^{34}\text{S}$ (i.e., = 0‰) is a meteorite, the so-called Vienna Canyon Diablo Troilite (VCDT). The ratio spans ~60‰ units (from -30‰ to +30‰). Common sources of sulfur in the context of this study are sulfate evaporites and sulfides such as pyrite to which we can add sulfur from atmospheric deposition. Atmospheric deposition, through precipitation and then recharge, is an important component of dissolved solids in unconfined aquifers, particularly clastic aquifers. When combined with $\delta^{18}\text{O}$ of sulfate, sulfur isotopes of sulfate are very discriminatory. Seawater sulfate isotopes have fluctuated through time and have correlatively impacted the sulfate isotopes of evaporites. Permian seawater had the lowest (i.e., lightest) $\delta^{34}\text{S}$ (at ~+12‰) and $\delta^{18}\text{O}$ (at ~+10‰) of the entire Phanerozoic era with quick increases on either side of this minimum (Clark and Fritz, 1994). Note that oxygen exchanges with water are negligible at aquifer temperatures. Eight West Texas Ochoan (Permian) anhydrite samples yielded values ranging from +9.6 to +11.5 ‰ whereas 14 samples from the Permian Basin Leonardian and Guadalupian ranged from +10.6 to 13.0‰ (Thode and Monster, 1965; Claypool et al., 1980). Precipitation of gypsum may slightly favor ^{34}S (maybe by 1‰), but this fractionation effect would be lost in the quickly varying seawater sulfate isotopes during the Permian period. On the other hand, $\delta^{34}\text{S}$ of biogenic pyrite (shales and carbonates) is lighter with negative values (-25 to 0‰ range). Sulfate from pyrite oxidation would result in a similar signal. Sulfate $\delta^{18}\text{O}$ would depend on the exact reaction mechanism, which involves both O_2 and H_2O , but is generally understood as being negative relative to VSMOW. Atmospheric deposition originates as sea spray ($\delta^{34}\text{S} = +20‰$; $\delta^{18}\text{O} = +10‰$) and anthropogenic sources (petroleum and coal, $\delta^{34}\text{S}$ from -5 to +10‰). Note that microbial action on the sulfate (sulfate reduction) would make both S and O isotope ratios heavier in the remaining sulfate.

6.7.2 Analysis

Our dataset (10 samples), complemented by TWDB-TPWD (2005, 8 samples) and Finch (2017, 4 samples) clearly shows that high sulfate is dominated by anhydrite dissolution (Figure 42), whereas the low sulfate in Igneous samples likely result from atmospheric deposition, not from anhydrite dissolution. In the details, SS-PL-G springs as well as Hamilton WM well (tapping the karst system of Phantom Lake spring) are consistent with a $\delta^{34}\text{S}$ of 10.5-10.6‰ and $\delta^{18}\text{O}$ of sulfate at 12.2-12.4‰, which is indicative of Permian evaporite sulfate (Clark and Fritz, 1994) and consistent with results by Chowdhury et al. (2004) and TWDB-TPWD (2005). Results from these authors and Gobble Hole well tapping the Rustler indicate that Rustler sulfate is slightly isotopically heavier than that of the springs at ~11-12‰. Two other Cretaceous wells (McIntire

and BOR windmill) also show a Permian evaporite signature. Two igneous wells (Davis Mountains SP WSW and Huelster #1) show a lower $\delta^{18}\text{O}$ of sulfate but very low sulfate concentrations (13 and 9 mg/L, respectively) and are possibly related to dry deposition (aerosols) or rain input whereas the 4J Wildcat well has $\delta^{34}\text{S}$ at -6.5‰ and relatively low sulfate (64 mg/L). The combination of negative $\delta^{34}\text{S}$ and negative $\delta^{18}\text{O}$ is often seen as indicative of oxidation of sulfides (pyrite), which is also probably the origin of some of the low sulfate in the Igneous samples (current ORP suggest that redox conditions are favorable for pyrite oxidation). However, the positive $\delta^{18}\text{O}$ values point either to pyrite oxidation in the vadose zone or shallow subsurface mostly by dissolved atmospheric O_2 and not in suboxic conditions (Clark and Fritz, 1997, Fig. 6-4) [$\text{FeS}_2 + 3.5 \text{O}_2 + \text{H}_2\text{O} \Rightarrow 2 \text{SO}_4^{2-} + \text{Fe}^{2+} + 2\text{H}^+$], or to a large contribution from atmospheric dry deposition. The samples chosen for sulfate isotope analysis show no microbial sulfate consumption but such mechanism was described in TWDB-TPWD (2005).

7 Physical hydrogeological results

This section relies on logger data collected by BEG and historical data from the TWDB. Examples of streams, springs, and well logger data are displayed in Figure 43, Figure 44, and Figure 45, respectively. Figure 46 shows examples of unprocessed WellIntel[®] data.

7.1 Groundwater levels and potentiometric surfaces

The springs near Balmorhea, TX, discharge water from fractured Cretaceous-age rocks, in places overlain by recent alluvium. Multiple sources of the spring water have been postulated by numerous workers since at least the early 1940s (e.g., White et al., 1941; Olgibee et al., 1962; Couch, 1978). To date, the more definitive evidence of recharge of groundwater discharging in the springs, along both long-distance (100+ miles to the west) regional, and local (Davis Mountains) flow paths, has primarily been hydrogeochemistry-based. Previous works have ranged from measurements of temperature and TDS to studies of stable and radiogenic isotopes (e.g. Neilson and Sharp, 1985; LaFave and Sharp, 1987; Uliana and Sharp, 2001; Chowdhury et al., 2005; Uliana et al., 2007). Early on, White et al. (1941) identified local spring water sources through observation of “heavy seepage losses” from streams in the foothills of the Davis Mountains (Big Aguja, Little Aguja, Madera, and Cherry Canyon); they also described extensive faulting of Lower Cretaceous carbonate rocks in the vicinity of the springs. As noted by Chowdhury et al. (2004), Couch (1978) proposed a regional spring-water-source – groundwater from the Capitan Reef aquifer “west of the Pecos River” flowing into down-faulted Lower Cretaceous rocks. Hence the importance of documenting cross-formational groundwater flow, both distally and in the vicinity of the major Balmorhea-area springs.

Previous efforts to enhance documentation of regional and local recharge to the spring systems using physical hydrogeologic data have been limited by sparse measurements of water levels in wells tapping single – or even known – geologic strata (e.g., Ashworth et al., 1997; Chowdhury et al., 2005). Locations of all wells used for water level and potentiometric surfaces are shown with associated water level elevations (Figure 16). Usable water levels and their specific units from oldest to youngest are:

Permian (Capitan, Rustler, Permian undivided): Central and northwestern part of study area; the Capitan and Rustler are not thought to be hydrologically connected.

Cretaceous (Edwards-Trinity Plateau): Central and northeastern part of study area; it is unconfined along a NW-SE trending valley between the northern foothills of the Davis Mountains and Interstate 10 (I-10), but becomes confined where overlain by the Pecos Valley

alluvial aquifer throughout most of the southern half of Reeves County. ~2-miles north of I-10 in the Balmorhea area. The most common host groundwater transport occurs along bedding planes. Cenozoic Igneous: Central and southern part of study area; the majority of Jeff Davis County, the Davis Mountains and southeastern corner of Reeves County coincident with the Barilla Mountains. This is a fractured rock aquifer.

Recent Pecos Valley Alluvium: Northeastern part of study area; The Pecos River cuts across the northeast corner of the study area in Pecos, TX, ~40 miles northeast of Balmorhea, TX. The Pecos Trough segment of the Pecos Valley alluvial aquifer

Recent West Texas Bolson: Western part of study area.

BEG Balmorhea area, or major spring, monitoring sites are located, from southwest to northeast, in Phantom Lake cave (water level elevation = 3470 ft amsl), Giffin Spring (water level elevation = 3327 ft amsl, San Solomon spring at Balmorhea State Park (water level elevation = 3320 ft amsl), and East Sandia Spring (water level elevation = 3159 ft amsl). Elevations at the springs represent surface water levels, but roughly coincide with nearby groundwater levels in Cretaceous wells. In Figure 47, the same well locations as in Figure 16, but without associated water level elevations, are superimposed on the same base map layer of topography plus cultural features overlain by simplified surface geology plus surface faults. We have contoured groundwater equipotential lines, color-coded to match those of geologic units in which corresponding wells are completed. The 2010-2020 Permian (blue) and Cretaceous (green) water level data points are limited to the extent that only one contour line can be drawn for each. Multiple contours are possible for Igneous (red), West Texas Bolson (brown), and Pecos Valley (yellow/light brown) surfaces.

Groundwater flow inferred from the potentiometric contours (Figure 47) is as expected from previous studies, indicated by higher elevation water levels in the Davis Mountains (6000 to 4000 ft amsl) trending toward lower water levels in the topographically lower West Texas Bolson (4300 to 3700 ft amsl) and Pecos Valley (2700 to 2500 ft amsl) regions. For the units with multiple contour lines, we see (i) near radial flow coming off the Davis Mountains igneous terrain (semi-concentric red curves at bottom center), (ii) flow possibly originating from the southwestern edge of the Davis Mountains then up to the north-northwest in West Texas Bolson toward Van Horn, TX (dark brown contours at lower left), and (iii) flow in Pecos Valley alluvium trending from south near Balmorhea, TX down-gradient and northward into the Toyah Basin/toward Pecos, TX and the Pecos River. The progression of groundwater elevations from the 4,000-ft Permian and Igneous contours toward the 3000-ft Cretaceous contour is also consistent with previous work. The described flow directions are inferred because there are not enough data points to discern the influence of faulting. The contours are dashed where approximated, but are constrained by water levels in nearby wells, albeit completed in different aquifer units.

A zoomed in view of water level elevations in select wells northeast of Balmorhea, TX reveals the typical decrease from southeast to northwest toward the Pecos River (Figure 48). Exceptions to expected water level elevation trends occur for several reasons. For example, two Pecos Valley alluvial (PVA) wells each within 1,200 ft of Toyah and Sandia creeks have water levels higher than other nearby PVA wells and two Cretaceous wells sandwiched between them (circled area in Figure 48). An explanation for the higher levels in PVA wells is hydrologic connection with the nearby creeks. Another reason for unexpected trends in water level

elevations, area-wide, is the way water supply wells in the region are often completed in more than one water-bearing interval to maximize water production.

Examination of the potentiometric data shows anecdotal evidence of potential for vertical flow. As with potentiometric surfaces, wells used to document vertical flow between stacked water-bearing units will ideally be constructed within a single unit; hence providing a clear signal for flow from higher to lower potential. Most existing wells in the region have been installed to maximize water production, so they are commonly screened across multiple aquifer zones. Regardless, water level elevations in multiple sets of closely spaced wells, which we have assigned to different aquifer units, indicate potential for vertical, cross-formational flow.

Examples of cross formational flow (Figure 49):

- Example A – Upward flow from Cretaceous to Pecos Valley (one well set);
- Example B – Upward flow from Permian and Cretaceous to Pecos Valley (one well set);
- Example C – Downward flow from Cretaceous to Permian (two well sets north of I-10 and down-gradient from major springs);
- Example D – Upward flow from Permian to Cretaceous (two well sets south of I-10 and up-gradient from major springs);
- Example E – Downward flow from Cenozoic Igneous to Cretaceous (two well sets SW and south of major springs).

Example A: Upward vertical flow potential from Cretaceous to Pecos Valley. North of I-10.

ID	Unit	WL Elevation (ft) (WL Date)	Head difference (ft)	Total Depth (ft)	Distance between wells	Location
SWN 4659508 (drilled in 1954)	Cretaceous	2717 (01/2020)		690		Approx. 4-miles north of Balmorhea, TX
SDR 501327 (20 gpm well) (annular seal other than SC)	Pecos Valley	2630 (12/2018)		425		
			87		~2-miles	

Example B: Upward vertical flow potential from Permian (Rustler) and Cretaceous to Pecos Valley. Southeast of Balmorhea. Water level elevations in a Permian/PVA well set indicate upward flow potential from Permian to PVA.

ID	Unit	WL Elevation (ft) (WL Date)	Head difference (ft)	Total Depth (ft)	Distance between wells	Location
SDR 465044	Permian (Rustler)	2864 (06/2017)		2407		Approx. 7-miles SE of Balmorhea, TX
SWN 5203302	Pecos Valley	2727 (2020)		400		
			137		~2-miles	

SDR 465044, well tapping the Rustler: Apache water supply well (Gobbler WSW) with annular cement from surface to 1,945 ft (2500 bags of cement); definitely Rustler only well - 4mi2 area centered on gobbler, top of Rustler ranges from 1614 to 1841 ft depth. 600gpm.

SWN 5203302, stock well tapping the PVA and installed in 1952; 665 gpm in 1959

Example C: Downward vertical flow potential from Cretaceous to Permian (Rustler). NE of Balmorhea and north of I-10 and regional E-W structures.

ID	Unit	WL Elevation (ft) (WL date)	Head difference (ft)	Total Depth (ft)	Distance between wells	Location
SDR 335021	Cretaceous	2829 (01/2012)		380		Approx. 18 miles ENE of Balmorhea (N of I-10)
SDR 282953	Permian	2690 (03/2012)		1275		
			139		~4,000 ft	
SDR 304813	Cretaceous	2842 (11/2012)		320		Approx. 19 miles east of Balmorhea (N of I-10)
SDR 371736	Permian	2711 (06/2014)		1543		
			131		~1,700 ft	

SDR 335021 – no annular cement; 90gpm

SDR 282953 – annular seal surface – 100 ft; 500+ gpm

SDR 304813 – no annular seal; filter pack 80-320 ft; 80 gpm

SDR 371736 – annular seal surface – 1165 ft; 500-650 gpm

Example D: Upward vertical flow potential from Permian (Rustler) to Cretaceous. SE of Balmorhea, TX and south of I-10 and regional E-W structures. Approximately 20 miles to the southeast of Balmorhea several wells completed in Permian strata (probably Rustler) were flowing at the surface within hours of being constructed. One flowing well (SDR 313076) was drilled and completed to a depth of 1,140 ft in January 2013; it has an annular seal from surface to 1,015 ft. The SDR documents drilling through limestone.

ID	Unit	WL Elevation (ft) (WL date)	Head difference (ft)	Total Depth (ft)	Distance between wells	Location
SDR 313076	Permian	3303* (01/2013)		1140		Approx. 20 miles ESE of Balmorhea (S of I-10)
SDR 260043	Cretaceous	2948 (06/2011)		428		
			355		~1,800ft	
SDR 434120	Permian	3573* (09/2016)		1416		Approx. 22 miles SE of Balmorhea (S of I-10)
SWN 5213801	Cretaceous	3075 (04/2020)		485		
			498		~1.8 miles	

* Well is flowing at surface (artesian)

SDR 313076 – annular seal surface to 1015 ft; artesian well; 700 gpm

SDR 260043 – no annular seal; 20 gpm

SDR 434120 – annular seal surface to 1078; artesian well; 620 gpm

SWN 5213801 & SDR 97819– annular seal surface to 44 ft; 100+ gpm

Example E: Downward vertical flow potential from Cenozoic Igneous to K units. SW of Balmorhea.

ID	Unit	WL Elevation (ft)	Head difference (ft)	Total Depth (ft)	Distance between wells	Location
BEG Pole Pen (SWN 5201404)	Igneous	4015		275		Approx. 14 miles SW of Balmorhea, TX
BEG Wildcat (SDR 96566)	Cretaceous	3651		1025		
			364		~1.2-miles	

BEG Limpia Shallow	Igneous	4059		75		Approx. 14 miles south of Balmorhea, TX
BEG Limpia Deep	Cretaceous	3935		163		
			124		40 feet	

SWN 5201404 – no annular seal; WL dates (WNT) = 10/1/2020 – 3/25/2021; classified as Cretaceous in TWDB GWB, but chemistry shows the groundwater in this well (Piper Plot) is clearly igneous composition with TDS < 400.

SDR 96566 – Rig Supply well; no annular seal below 22 ft.; WL dates (WNT) = 10/1/2020 – 3/25/2021; 220+ gpm; limestone from 20 ft to TD.

7.2 Spring response: Analysis of historical records of recharge events

San Solomon Spring flow rates were recorded daily by the USGS from October 1931 to September 1965 (35 water years) with a few measurements before 1930 and between 4 and 17 measurements a year from 1967 to 2017 but with a 15-year gap between 1987 and 2000 (Figure 50). From mid-May 2017 on, USGS recorded stage (flow rate) at a 15-minute interval. Phantom Lake Spring had daily measurements in 1932 and 1933, then a gap to ~1949, from which year between 4 and 12 measurements a year were taken up to 2010. Giffin Spring has a few pre-1930 measurements and then daily measurements during the 1931-1932 water year, then a gap to 1941 after which between 3 and 7 measurements were taken every year with a gap between 1958 and 1966. Starting in August 2002, 15-minute measurements have been recorded. East and West Sandia springs have a combined 34 measurements from 1931 to 1996 in addition to ~daily measurements during the 1931-33 water years for West Sandia spring. Saragosa Spring has a total of 28 measurements during the same period (data from White, 1941, and Schuster, 1997). The earliest measurements are found in Meinzer (1927) where he stated that flow rate at Phantom Lake was 46 cfs on Sept. 5, 1900 and on July 21, 1904. San Solomon flow rate was 36 cfs on those same days, but the text is unclear.

Plotting flow rates against day of the year reveals that larger precipitation events typically occur in September or October with lingering effects at San Solomon Spring but are flashier at Phantom Lake spring (Figure 51 and Figure 52). Phantom Lake shows a 5x increase at the sharp peak relative to baseflow whereas San Solomon show a 2x increase in flow rate with a much broader peak. Giffin Spring stays steady and does not seem to respond much to extreme events (Figure 53) although this apparent lack of response may be due to the coarseness of the measurements. There was still a 30-50% drop relative to base flow during the 1931 and 1932 events although actual baseflow at the time is uncertain due to limited data. Although they do not report data, White et al. (1938) stated that Saragosa flow rate increased at the onset of the event but not that of East and West Sandia springs.

Historical data show two large extreme events in the span of 15 years with large increases in spring flow (1932 and 1941) and five less extreme relatively minor events (Figure 54 for San Solomon; Figure 55 shows two of these events for Phantom Lake). The total flow above baseflow during the Fall 1932 can be computed by integrating the curves in Figure 51 and Figure 52. The first event started on August 30, peaked on September 2-3, and started leveling off. Then a second rain event on September 4 and 9 led to a higher peak. A broader peak at San Solomon suggests contributions from various sources with different arrival times. A faster decrease from the maximum at Phantom Lake suggests a more restricted drainage area (under the assumption that the rain event was regional in nature). Assuming the event started on August 30, 1932 (2.06” and 2.72” in Alpine and Balmorhea on that day but 3.9” and 5.05” in Fort Davis on August 27

and 29, 1932, respectively) and lasted until approximate return to baseflow conditions on February 28, 1933. The three weather stations (Alpine, Balmorhea, and Fort Davis) recorded a cumulative total of 1.68", 6.51", and 7.2" in excess of 1" early during this period (only the fraction of daily measurements in excess of 1" is considered). The 1-inch threshold is somewhat arbitrary but an examination of the data shows that daily precipitation events below 1" do not significantly impact the flow rate (Figure 56). We then assume that the entire watersheds received similar cumulative excess precipitation of 7" (178 mm). This is likely an underestimate as precipitation is likely higher on the reliefs of the Davis Mountains.

Still focusing on the Fall 1932 event and assuming that the springs drain the following watersheds: Cheery Creek, Madera Canyon, and Little and Big Aguja, they represent, respectively, $226 + 298 + 131 + 215 = 870 \text{ km}^2$. The excess rain volume is then $\sim 5.5 \text{ billion ft}^3$ ($870 \times 10^6 \times 0.178 / (10^9) / 28.3$). The excess volume that flowed through the springs during this extreme major rain event was $\sim 290 \text{ million ft}^3$ and $\sim 260 \text{ million ft}^3$ at San Solomon and Phantom Lake, respectively, which scaled by the watershed areas amount to 9.5 and 8.4 mm. These two springs have largely independent drainage systems, otherwise San Solomon flow rate would drop much faster (and would have dried out). If this is truly the case, $\sim 10\%$ of this extreme rain event flowed through the springs.

USGS daily measurements recorded significant flow increase at San Solomon Spring in 1932 and 1941 (Figure 57) with several noteworthy pulses in 1933 and 1942-1946 (Figure 58). The following 20 years of daily measurements did not detect any significant flow increase (Figure 4), fact certainly related to the drought of record of the 1950's. When high flow rates are again observed at the springs, there is no average daily measurement available to capture their evolution through time. If there were only three weather stations operational during the Fall 1932 event (Alpine, Balmorhea and Fort Davis), the Fall 1941 event included two more (Van Horn and Mount Locke). However, only San Solomon daily data were recorded for this event, not Phantom Lake. As seen in Figure 54, the Fall 1932 and Fall 1941 events are of comparable stormflow intensity as observed at the spring but the Fall 1941 event has a longer tail that may be due to steadier precipitation over the area (Figure 57).

The Sept.-Dec. 1933 event shows an increase of 50% with a month-long flat peak (Figure 58a). The start of the flow increase corresponds to a precipitation event in Alpine (1.59") and to an almost concomitant smaller one in Balmorhea, however two subsequent events visible in the Alpine (1.58") and Balmorhea (1.72") stations are not reflected in the spring flow rate, showing the difficulty of extrapolating rainfall on the recharge watersheds from the weather stations. The pulse is fully attenuated after 3 months. Interpretation of the next four following events (1942-1946) can take advantage of two additional weather stations (a total of five, clockwise, Van Horn, Balmorhea, Fort Davis, Alpine and Mount Locke). The Sept.-Dec. 1942 event (Figure 58b) shows a $\sim 25\%$ flow increase pulse with a round peak and tail that lingers on for two additional months. The pulse is possibly related to precipitation captured by the Mount Locke station ($\sim 1"$) although another event two weeks later ($\sim 1"$) is barely perceptible on the spring flow rate. A larger intervening event at Balmorhea (1.8") refreshed the peak that slowly decays to base flow in early December, three months after the start of the event. The Sept.-Dec. 1944 event (Figure 58c) with an increase in flow rate of $\sim 50\%$ shows better behaved peaks because precipitation events were regional in nature (daily rate from all stations overlap). A smaller peak (2.22" at Mount Locke) is followed by a bigger peak (1.55" at Mount Locke and 2.05" at

Balmorhea) with a long tail back to base flow conditions in early 1945, more than 4 months after the initial event.

The July-Dec. 1945 event (Figure 58d) showing a single precipitation pulse and concomitant spring flow rate peak (50% increase) followed by a slow decay to base flow after ~4 months is probably the cleanest recorded extreme event. The five weather stations show large precipitation on July 2 and 3 (including 2.99" at Mount Locke and 2.45" and 2.18" at Balmorhea). Subsequent rain events, including some slightly >1" over a day, hardly impacted spring flow decay. Calculating the excess spring volume is that event (~120 millions ft³) and scaling it to the same watersheds as previously yields 3.9 mm. Making the assumptions that average excess precipitation is 1.5" (fraction above 1") (37.2 mm) and that Phantom Lake flow volume in response to the same event was similar, we arrive at the higher value of ~20% of the precipitation event going through the springs, a higher fraction than calculated during the Fall 1932 major extreme event. The 10% (7" average precipitation above the 1" threshold) and 20% (1.5" average precipitation above the 1" threshold) suggests that a higher fraction of precipitation fallen in the relevant Davis Mountains watersheds makes its way through the springs during minor extreme events (but still less volume in absolute values). The smallish event of Sept.-Dec. 1942 (Figure 58b) confirms it with a volume of 88 million ft³ above baseline (or 2.8 mm) for excess precipitation of approximately 0.5" (12.4 mm), that is a fraction ~40%, accounting for Phantom Lake. These values of 10, 20, and 40% are very approximative as an actual water budget would account for evapotranspiration and other mechanisms; but they suggest that a higher fraction of the runoff is captured in smaller events, which is corroborated by the observations that, in such case, creek beds remain dry passed where the Lower Cretaceous is exposed at the foot of the Davis Mountains. Note that the 1" threshold is arbitrary and that, although using a value of, for example, 0.8" would change the values, it would not change the trend.

The Oct.-Dec. 1946 event (Figure 58e) is preceded by several precipitation events <1" that do not seem to lift San Solomon flow rate from baseflow until end of September 1946 when flow rate increases by ~35% and generates an excess volume of ~60 million ft³ (2 mm). It has a complex peak related to three closely spaced distinct events, each ~0.1" above the 1" threshold, that is, a total of 0.3" (7.4 mm) or >50 % of the excess precipitation volume.

TDS information during and after the extreme precipitation event is limited but provides useful insight (Figure 56b and Figure 59). Observed TDS values are lower than a simple TDS-weighted mixing of baseflow and stormflow suggesting that some of baseflow cannot reach the springs and is somehow deflected. This suggests that large rain events supercharge the Cretaceous aquifer with Igneous water-type water that is then slowly released through time. It is also possible that the basal volcanic layers, reputedly more porous, retain some of the water and release it slowly. No measurements from wells in the Davis Mountains were taken at the time. However, this is less likely because Phantom Lake would also benefit from this storage. A clear difference between San Solomon and Phantom Lake locations is the amount of alluvium. Alluvium, although not very thick south of I-10, can store significant amounts of water. White et al. (1941) report that several wells located in close proximity to the springs but upstream from them and drilled into the alluvium responded strongly to the heavy precipitations and that the water level dropped slowly in the course of the following months suggesting that surficial alluvium can also store water. They also reported the puzzling fact (to us) that East and West Sandia did not respond to the heavy precipitation. As noted by TWDB-TPWD (2005), the lack of

impact of the drought of record of the 1950's on the average flow rate of the spring strongly suggests that a decrease in precipitation volume is not the proximal cause of the spring flow rate decline.

High-frequency spring measurements by the USGS (instantaneous 15-minute increment instead of average daily flow of the 1931-1965 period) resumed in May 2017 (Figure 60) with the caveat that pool operations mask somewhat the actual spring flow rate. Average baseline flow rate is currently considerably less than the 1930's and 1940's but San Solomon spring still responds to precipitation events, in particular to a regional relatively large event on September 22, 2019 (3.76" Mount Locke, 1.75" Balmorhea, 1.24" Fort Davis) as discussed next (beginning of the Early Fall 2019 event). The flow rate increases from 19 to 26 cfs, almost a 40% increase (Figure 61). However the increase is small at 7 cfs from the base of the spike or 10 cfs from the local minimum attained two months earlier. This absolute increase is smaller than what would be expected for an event of this size (see Figure 58a-e). The much higher sampling frequency allows for better time resolution and also demonstrates that some small precipitation events (<1") can have a small impact (a few cfs) on the San Solomon Spring flow rate.

Estimation of baseflow vs. stormflow by previous authors shows a considerable range, mostly because it depends on the time scale. Fraction of stormflow following a large storm event will clearly be higher than before the storm event. One way to estimate long-term contribution of baseflow is to assume a constant baseflow rate and that any larger flow is due to stormflow (simplified approach of the baseflow separation on stream hydrographs). An alternative way would be to follow a similar approach with TDS / specific conductivity or, better still, combine both approaches. Unfortunately, specific conductivity data were not as systematically recorded as flow rate. An extreme calculation of stormflow can be computed from the Fall 1932 event at Phantom Lake during which the spring flow rate jumped from 12 to 100+ cfs. Concluding that baseflow is only 10% of springflow is clearly wrong. A better approach is to use the entire 1932-33 period in which case Phantom Lake baseflow is 2/3 of spring flow (assuming a long-term baseflow of 13 cfs). Applying the same approach to the San Solomon spring (average daily rate from January 1932 to December 1933 by USGS) yields an estimate of 83% baseflow when assuming a long term baseflow of 35 cfs (75% for a long-term baseflow of 30 cfs). The next period with daily data at San Solomon is 1941 to 1965 yielding a baseflow contribution of ~90% (assuming long-term baseflow of 30 cfs). This is a higher baseflow contribution than calculated previously; very likely, the drought of the 1950's limited the stormflow contribution. More recent hourly data from May 2017 to May 2021 also suggests a baseflow contribution of ~90%. However, the complexity of operational activities at the pool (built in 1936) compounded by the current location of the USGS gauge adds considerable uncertainty to these raw estimates. A reasoned estimate of the long-term baseflow contribution at San Solomon Springs is in the order of ~80%.

7.3 Spring response: Analysis of logger data

Comparison of rainfall measured at five gauging stations within the study area (Balmorhea, Fort Davis, Kent, Van Horn, and Mount Locke) and USGS-gauged discharge from San Solomon and Giffin springs shows correlation between significant rainfall and increased spring discharge. Between January 2018 and January 2021, larger rainfall events (over 1.5") occurred from June to October of each year with a notable peak (over 3.5") in September 2019. This is consistent with the typical Summer monsoonal rainfall patterns characteristic of the region. Less typical larger rainfall over 1.5-inch occurred in November 2019 and March 2020.

Interpretation of increases in spring discharge in response to larger rainfall events has been complicated during the study period by draining of the pool at BSP during TPWD maintenance; for example from Fall 2018 to early 2019. The most significant correlation between rainfall and increased discharge in both San Solomon and Giffin springs is coincident with >3.5” (and soon after) rainfall in late September/early October 2019 (Figure 60). BEG has recognized events in many of the InSitu[®] logger data sets. We define a “rainfall event” as when records of rainfall measured in regional gauges correspond with significant changes in BEG InSitu[®] logger pressure, specific conductivity, and sometimes temperature. Below the September 2019 event is documented further with specific examples from BEG logger data.

7.3.1 Logger examination

Surface and groundwater flowing from the Davis Mountains toward springs in the Balmorhea area after large rainfall events have been noted to contribute to increases in discharge. To date, evidence for this relationship has primarily been based on geochemical data. Analyses of InSitu[®] logger data from BEG monitoring locations along five watersheds in the Davis Mountains (Figure 5) corroborate the relationship between rainfall and increased spring flow. The BEG loggers are placed along five major watersheds extending from uppermost elevations of the Davis Mountains northeastward toward the Balmorhea springs area. The watersheds are from west to east (1) Cherry Creek, (2) Madera Canyon (upper and middle), (3) Little Aguja/Lower Madera canyons, (4) Big Aguja Canyon, and (5) composite Limpia creek watersheds. Downgradient ends of watersheds (2), (3), and (4) converge in the San Solomon Creek – Toyah Creek watershed. The Upper Cherry Creek watershed (1) and others to the west end at short distances downgradient of NW-SE trending regional structures. Multiple sub-units of the Limpia Creek composite watershed (5) have an unclear relationship to the Balmorhea-area springs. Time series perturbations in logger data can be used to track pulses of rainwater flowing through multiple watersheds to the Balmorhea area springs. However, signal interpretations are complicated by differences in physical settings of the loggers and, even variations within the physical groupings. A summary of variations in BEG logger responses in spring, stream, and well installations follows. Where springs discharge into water that is artificially pooled like at BSP, sensor responses are muted; e.g., an increase in pressure reflecting a change in height of water over the logger will dissipate in all directions. This is one reason why multiple methods of gauging discharge around Balmorhea areas springs is needed. Temperature and specific conductivity responses of loggers installed in larger pools of water are also diluted.

Logger responses are also altered when springs have been artificially enclosed, like with the concrete spring box at Willow spring in Cherry Canyon. When water levels drop below the logger mount in the spring box, it appears as if the spring had stopped flowing, but this is an artificial response. Another misleading logger response is associated with the pressure spike resulting from the late September 2019 rainfall event where we see a coincident increase in specific conductivity, which is followed by a sharp drop in specific conductivity (Figure 43a). This appears to result from rainfall mobilizing sediment from upstream or steeply sloping streambanks, increasing suspended solids (turbidity) within the spring box before being flushed by subsequent water flow (also noted by Chowdhury et al., 2004). In other logger locations, rainfall-induced pressure spikes are accompanied by coincident declines in specific conductivity. Daily temperature data variations are buffered in spring boxes where loggers are usually submerged. When spring discharge is reduced so that water levels fall below the logger; for example, in Seven Springs in the summer of 2020, temperature variations greatly increase (Figure 43b).

Most stream logger installations are in dry stream beds. Daily temperature variations are large (from approximately 20 to 55°C in summer and -5 to 25°C in winter) until a rainfall-induced pulse of water covers the logger and insulates it from temperature fluctuations (e.g. Little Aguja, Limpia Upper, Limpia Lower, Madera Lower, and Cherry Lower). Pressure spikes from rainfall pulses in dry streams are obvious in otherwise noisy datasets as in the Little Aguja Stream plots (Figure 44a). A reduced amplitude of the temperature signal coincident with the late September 2019 pressure spike can also be seen at this location where water has been observed to pond for several months after major rainfall events. (Figure 44a). In other stream locations such as Cherry Creek Lower, the September 2019 pressure spike is more obvious than the temperature buffering because the logger was installed away from an area where water can flow or pond for short periods after rainfall (Figure 44b). The Limpia Upper Stream logger is more representative of a spring, since it was installed in a nearly constant-level, spring-fed pool. The September 2019 rainfall event is evident in the January 2018 to January 2020 plots, with a higher pool level following almost a year after the event (Figure 44c).

We observe different logger responses in unused wells versus those being pumped. None of the 11 BEG-installed monitoring wells are currently being pumped and data record durations are too short to interpret at this point. Regardless, rainfall responses in wells differ depending on whether or not the well is being pumped, and show a subdued response compared to spring or stream loggers. Water level in the Cherry Lower Well declined from December 2018 until the late September 2019 rainfall event as indicated by a positive pressure response (~0.75 meter). Pressure/water level remained elevated until it declined again in summer 2020 (Figure 45a), possibly related to groundwater storage in the alluvium. The overall decline in water level throughout the study period is consistent with increasing drought conditions in the region. A possible explanation for the longer term temperature and specific conductivity trends in Figure 45a is sensor drift. Two of the wells with data loggers have been used for water supply throughout the study period, Hamilton WM Well and the Madera Valley Water Supply Corporation (MVWSC) Huelster #3 well. Responses to rainfall events are not as obvious in logger data from wells. Data from Huelster #3 (Figure 45b) show lower water levels and higher temperatures in summer, but responses to rainfall events are overshadowed by daily pumping signals (i.e., small changes in pumping and recovery cycles).

7.3.2 Early Fall 2019 event

The most obvious correlation between a period of heavy rainfall and increased discharge in Balmorhea area springs – during this study period of January 2018 to December 2020 – took place in late September/early October 2019 (Figure 62). Coincident responses in BEG InSitu[®] logger pressure data can be used to track contributing water pulses flowing downstream along the northern flanks of the Davis Mountains. Rainfall events are also evident in the datasets in June 2018 and 2019, but are not as significant as those in September/October 2019.

Pressure, temperature, and specific conductivity responses to the Fall 2019 rainfall events are noted in several series of loggers along five major watersheds draining the northern Davis Mountains (loggers sorted from high to low elevation) as summarized below and detailed in the following paragraphs:

- Headwaters and Upper Cherry Canyon Watershed: Cherry Upper Stream (RT), Cherry Willow Spring (AT), Cherry Lower Stream (RT), and Cherry Lower Well (AT);
- Upper and Middle Madera Canyon Watershed: Madera Upper Stream (RT), Madera Lower Stream (RT), and Hamilton WM Well (AT)

- Little Aguja/Lower Madera Canyon Watershed: Little Aguja Stream (RT) and Huelster #3 Well (AT)
- Upper and Lower Big Aguja Canyon Watershed: Big Aguja Stream/Spring (AT) and Seven Springs (AT)
- Composite Limpia Creek Watershed: Limpia Upper Stream (RT) and Limpia Lower Stream (RT)

Early Fall 2019 rainfall was concentrated in two intervals. First, a cumulative 5.9” was measured at the Mount Locke station for 10 days (September 17-26), lower but significant cumulative amounts were measured at Balmorhea (2.1”) and Fort Davis (1.6”) and relatively small amounts were measured west of the Balmorhea area at the Van Horn (1”) and Kent (0.3”) stations. The second interval (six days from September 28 to October 3) was slightly less intense, centered west of the Balmorhea area (2” at Van Horn) but more evenly distributed (0.9” at Fort Davis, 0.8” at Balmorhea, 0.7” at Kent, and 0.6” at Mount Locke) (Figure 63b).

Data loggers in the more easterly watersheds (Little Aguja and lower Limpia canyons) showed stronger responses to September 17 – 26, 2019 rainfall concentrated over gauges in central and eastern portions of the study area (Mount Locke, Fort Davis, and Balmorhea). Loggers in more westerly portions of the study area (Cherry Canyon) show strong pressure responses to September 28 – October 3, 2019 rainfall concentrated over Van Horn. The logger in Lower Limpia Stream showed responses after both periods of rainfall (Figure 63c). Runoff from mid- to late-September rainfall triggered short duration (minutes to hours) logger responses in monitored watersheds, triggering a response in Balmorhea area springs on September 25th. Larger pulses of water can be seen in data from Little Aguja followed by Limpia and Madera watersheds (Figure 63a). Unfortunately, the logger in Madera Lower Stream was not functioning during this period of rainfall.

Logger data from Little Aguja to Lower Madera canyons watershed shows short duration pressure (and associated stage) spikes in response to rainfall between September 17 and 26, 2019. The Little Aguja Stream logger plots (Figure 64a) show two larger pressure spikes on September 21st and 22nd, representing stage increases up to 1.28 m (4.2 ft) (Figure 63a), which are preceded and followed by smaller peaks. The temperature curve demonstrates that the logger was submerged by ponding of water from September 13th through October 20th (Figure 64a). There are also indications of contemporaneous stage increases in data from the Huelster #3 well logger indicating a slow release of the precipitation that had fallen earlier.

Logger data from the composite Limpia Canyon watersheds also show short duration pressure (and associated stage) spikes in response to rainfall between September 17 and 26, 2019. In plots of logger data from both the Upper Limpia Stream (Figure 64b) and Lower Limpia Stream (Figure 64c) locations, there are also multiple pressure spikes on September 21st and 22nd, representing stage increases up to 1.16 m (3.8 ft) (Figure 63a). The Limpia Upper Stream logger is in a spring-fed pool, which is reflected by the continued stage elevation after the first set of pressure spikes. There is also a second, smaller pressure spike in Limpia Upper that corresponds with the September 28 – October 3, 2019 period of rainfall (Figure 64b). In the full timescale plot of the Limpia Upper Stream location (Appendix B), we can see that the higher pond level following this rain event persisted until March of 2020. In the normally dry stream bed location of the Lower Limpia Stream logger, such ponding did not occur (Figure 64c). We think the temperature plot at the Limpia Upper Stream location (Figure 64b) indicates stagnant pool conditions prior to the rainfall event followed by sustained spring flow. Time differences

between the start of logger responses in Upper and Lower Limpia Stream loggers suggest that it took 50 minutes for a stormwater runoff pulse to travel between the two locations (Figure 63a).

Data from both Madera Upper Stream and Madera Lower Stream loggers in Upper and Middle Madera Canyon watersheds show short duration pressure (and associated stage) spikes prior to the September 17 and 26, 2019 period (Figure 64d,e). These early peaks represent stage increases up to 0.48 m (1.6 ft) and 0.24 m (0.8 ft) at the upper and lower logger locations (Figure 63a). Water is able to pond at both these logger locations; hence the sustained pressure/stage levels seen prior to the September 17-26, 2019 rainfall period. A following stage increase at Madera Upper Stream was only 0.16 m (0.5 ft) compared to an increase of 0.44 m (1.4 ft) at the Madera Lower Stream location on September 21st. Time differences between the start of logger responses in Upper and Lower Madera Stream loggers suggest that it took only 11 minutes for a stormwater runoff pulse to travel between the two locations (Figure 63a). The larger pulse of water at the lower logger could be explained by heavier rainfall at that location.

Runoff from late September to early October rainfall triggered slightly longer duration logger responses (generally hours to days) in Cherry Creek, Madera Canyon, and Limpia Creek watersheds (Figure 64f) compared to shorter responses (minutes to hours) observed after the September 17-26, 2019 rainfall period (Figure 63a). Locations of loggers that responded to this later rainfall period are concentrated in more westerly watersheds (Cherry Creek and Madera Canyon) and in the uppermost Limpia Canyon watershed. (Figure 64i). It appears that loggers in these locations showed a greater response to rainfall from the Van Horn area. We posit here that the smaller scale, late September to early October logger responses in the Balmorhea area springs indicate higher flow from more distant, regional rainfall rather than that falling over higher elevations of the Davis Mountains.

InSitu[®] logger data from both Cherry Willow Spring and Cherry Lower Stream in the headwaters and upper reaches of the Cherry Creek watershed (Upper Cherry Creek) show pressure spikes in early October 2019 (Figure 64f,g). Willow Spring is confined by a spring box so there was an initial increase of 0.14 m starting on September 27th, which was followed by a faster 0.63 m pulse on October 2, 2019 (Figure 64i). As a result of artificial water ponding, it took over a month for both the temperature and pressure sensors to re-equilibrate in the Cherry Willow Spring logger (Figure 64h). A short duration (4 hours), 0.73 m (2.4 ft) pulse passed over the Cherry Lower Stream logger, also on October 2, 2019. Time differences between the start of logger responses in Cherry Willow Spring and Cherry Lower Stream suggest that it took two hours and 15 minutes for a stormwater runoff pulse to travel between the two locations (Figure 64i). The larger pulse of water at the lower elevation location could be a result of geometric constraints of the spring box, and/or higher accumulated rainfall runoff downstream. Sensor responses in the logger in Cherry Lower Well differ from those in the spring box and dry streambed and have been influenced by processes discussed above (Figure 64h). But the increase in pressure/stage in the well also began on October 2, 2019. In this case, the water level rose 0.81 m (2.7 ft) over two months.

As discussed previously, loggers near San Solomon Springs in the pool at Balmorhea State Park show only subtle responses to changes in discharge or chemistry of spring flow. Regardless, over a 70-minute period (from 18:25 to 19:35) on September 25, 2019, stage in the pool increased by 0.04 m (0.13 ft) and remained at that approximate level for 12 days. On September 25th, specific conductivity started out at 3370 $\mu\text{S}/\text{cm}$, dropped to as low as 2937 $\mu\text{S}/\text{cm}$ on September 29th, and had rebounded to 3313 $\mu\text{S}/\text{cm}$ by October 6, 2019. Temperature dropped 0.18°C during the same

interval (Figure 65a, red ovals). In a plot of USGS gauge data from the BSP outlet (proxy for San Solomon Springs) and Giffin Spring in combination with rainfall events from five regional gauges, peak discharge dates and magnitude differ slightly at the two locations (Figure 65b). At San Solomon, spring discharge peaked on September 25-26 and October 6, 2019. Discharge peaked at Giffin spring on September 21, 24, and October 3, 2019.

USGS gauge data collected at the Balmorhea State Park pool outlet (a proxy for San Solomon spring flow) shows increased discharge of 7.5 cfs from September 20th to 26th and a smaller increase on October 7, 2019 that is truncated by a data gap (Figure 65c). On the same plot discharge peaks at Giffin occur on September 25th and October 3, 2019. InSitu[®] AT logger responses in Phantom Lake Cave are small, but correspond to signals seen in other logger locations. Relative stage (corrected pressure signal) increased by 0.03m (0.01 ft) over seven days beginning at 0825 on September 20, 2019. Temperature and specific conductivity fell simultaneously at 2005 on September 21, 2019 by 0.13°C in 40 minutes and 69 µS/cm, respectively. Additional drops in specific conductivity (28 to 75 µS/cm) took place at various times between October 1-4, 2019, but there are not obvious changes in pressure and temperature on these later dates (red ovals on Figure 65d, Figure 65g).

The Hamilton WM Well AT logger data show pressure spikes and contemporaneous drops in temperature and specific conductivity at multiple intervals between April and December 2019 (Figure 65e); but here we only discuss the Fall 2019 events. The most obvious logger response occurred on September 21, 2019 as indicated by red ovals in Figure 65e. Casing from the Hamilton WM well extends down into Phantom Cave, reportedly into a shallow pool. In fact, BEG has measured the water column in the well (distance between well total depth and water level) to be as little as 0.5 ft. Mineral precipitation observed on the logger when it is retrieved for downloading indicates active evaporation. We lost a logger here due to corrosion of the ferrules sometime prior to the October 2020 download. The point being that specific conductivity measurements are erratic at this location (Figure 65e).

Figure 65f is a zoomed-in view of the stage data for the Hamilton WM well. The curves reflect daily cycles from the solar pump. As noted above in Figure 65e, the most obvious (September 21) logger response corresponds to the nighttime pressure spike inside the red oval (Figure 65f). Another obvious pressure response took place during the daytime on September 24. Each of these spikes represent close to 1m (3.3 ft) of water level rise over the logger (Figure 63a and Figure 65g). Multiple additional daytime pressure pulses took place between September 27 and October 9; however, the largest ones happened before September 25, 2019.

The greatest Balmorhea area spring flow responses appear to have occurred in late September 2019 contemporaneously with rainfall concentrated over the Davis Mountains (Mount Locke, Fort Davis) (Figure 63a, Figure 64i, Figure 65g), and pulses of rainfall runoff are noted in BEG InSitu[®] loggers along multiple watersheds.

7.4 Spring Response: Analysis of watershed precipitation

Precipitation recorded at weather stations cannot reveal the exact extent and timing of rain events at the watershed level. Rather we turn to radar data, which provide estimates of daily precipitation over the larger study area (see Figure 1 for geographic references), from Van Horn to the west to Fort Davis to the southeast and from the Presidio-Jeff Davis County line to the south to the City of Pecos to the north (Figure 66). An examination of the radar data and the corresponding weather station data show that they mostly coincide but the overlap is not perfect

(Figure 67). Some precipitation events detected by radar were not captured in any of the weather stations and some actual precipitation events seen at a weather station did not show up in the processed radar data. Robertson et al. (2019) described some of the difficulties of dealing with radar data. The objective of this present analysis is to identify rain events that would be localized to a watershed and isolate the impact of this watershed or group of watersheds on spring flow rate responses. We extracted radar information for the period from April to December 2019, which includes the largest event seen during the study period (end of September 2019, Early Fall 2019 event).

Most of the precipitation events of the period did not impact San Solomon Spring flow rate (Figure 68). Pool operations seem to have had more impact on the flow rate than small precipitation events. The data are made noisier by runoff generated locally. In April 2019, precipitation does not appreciably affect springs. The May 7 and 12-13 rain events in lower Limpia may have caused slight San Solomon Spring response but this might be reading too much in the data. These events also created antecedent moisture which wetted up the system so that June rain caused Madera Creek to flow. The June 1-5 rain events may have caused an instantaneous increase in flow rate of ~1 cfs at the gauge location, likely related to local runoff. The true impact on the spring is seen a few days later thanks to a TDS decrease on June 11 when the flow rate was already on the declining limb. The June 17-18 events were overall more intense (Figure 66c and Figure 67). Madera Creek flowed on June 19, 2020 (evening) and an increase of ~2 cfs in flow rate was observed at the SSS. A few rain events in July, August (radar data missing for the month of August), and first half of September 2019 did not generate much flow rate changes at the spring. However, the high-intensity rainfall of September 22 translated into a sharp increase in flow rate almost by 10 cfs. The slow decline curve shows a few small secondary peaks related to a couple of rain events in October. The decline continues in October and November. There is a large gauge response on December 11 (Figure 68), likely related to the December 10 rain event (Figure 66h). As observed earlier, several weather stations have to register daily precipitation >1" to observe a response at the springs. This might be the amount of rain needed to have enough runoff in the watershed for the water to reach the spring recharge zone over the karsted Buda Limestone.

An initial estimate of recharge using a rate of 5% of precipitation is likely too high but confirms that recharge originating only from local watersheds in the immediate upgradient areas to Balmorea-area springs is insufficient to produce observed discharge rates (i.e., 25-30 cfs at San Solomon Springs; Robertson et al., 2019; Sharp et al., 2003). For comparison, Beach et al. (2004) recharge estimates varied from 1.2–2.0 % of precipitation for mean annual precipitation (MAP) >12 in/year (i.e., no recharge below ~3,000 ft). Despite limitations of this initial recharge analysis, it reveals the potential importance of recharge originating in Limpia Creek, Adobe Draw, and Herds Pass Draw, as these watersheds have the highest mean annual volume (MAV) and could potentially contribute to spring flow.

Over the entire study area, mean annual precipitation (MAP) is 350 mm while the ephemeral drainages range from 405 mm at Herds Pass to 466 mm in Little Aguja. When summed over each watershed, we can estimate total mean annual volume (MAV) which ranges from 16,400 AF in Little Aguja (note its smaller area) to 104,000 AF in Limpia Creek (Table 1-1). In general, MAP decreases to the northwest and away from the Davis Mountains whose orographic relief causes air masses to rise, cool and condense into precipitation. After Limpia Creek, Adobe Draw and Herds Pass have the next largest MAV of 69,600 and 41,400 AF, respectively, but they also

have considerable larger basin areas and longer paths to the springs. If we assume 95% loss of MAP to evapotranspiration (which is highly variable in both time and space), the ranking of instantaneous flux range from 3–19 cfs. San Solomon, the largest of Trans-Pecos springs, has consistent discharge ranging from 25–30 cfs (Robertson et al., 2019). These channels are unlikely to be the dominant source of sustained flow, but they do have the fastest flow path compared to the regional flow path.

8 Discussion

8.1 Discussion of geochemical results

What is(are) the ultimate source(s) of the long-term baseflow component? Although it is accepted that the Salt Basin flats are significant contributors to Balmorhea area spring flow (as strongly suggested by geochemical observations), the exact source(s) remain elusive. More attention must be given to collecting water samples in a broad area along I-10 from Van Horn to Balmorhea. The following elements can be teased out from this study:

The six Balmorhea area spring waters are characterized by a relatively high TDS at 2000-3000 mg/L, mixed anion (Cl-SO₄) – mixed cation (Ca-Na) water type with high Sr isotope ratio emphasizing their external source. The spring waters have been described as originating from four end member sources: (1) up-gradient Wildhorse Flat (low TDS, Na/Ca-HCO₃); (2) Rustler Hills (moderate-high TDS, Ca-SO₄); (3) Davis Mountains (low TDS, Ca-HCO₃); and possibly (4) nearby upwelling deep basin brines (high TDS, Na-Cl). However, the high Cl/Br ratio as well as the nearly stoichiometric Na-Cl and Ca-SO₄ suggests halite and gypsum dissolution as the source of the relatively high TDS rather than invasion from deep brines (i.e., coming from formations older than the Ochoan [Permian] evaporites), which have a low Cl/Br ratio and are not particularly impacted by halite and even less gypsum dissolution (Nicot et al., 2020). The heavy water isotopes associated with deep brines also negate (Figure 35a) the upwelling hypothesis. More generally, there is no evidence of contribution from basinal brines to the springs. The observed stoichiometric characteristics can result from direct exposure to halite and gypsum or mixing with waters that were exposed to these rocks.

The source of these major ions in Balmorhea area spring waters could be the Rustler, Salado, and Castile Fms, in any combination. Anhydrite is abundant in the Rustler and Castile Fms. and flow through either can explain the Ca-SO₄ nature of the spring water (including sulfate isotopes). However, the Salado Fm. does not exist in the drainage area of the springs and halite in the Rustler Fm. has been described as abundant only in the NE sections of its footprint toward the New Mexico-Texas state line, leaving only the Castile Fm. as a viable source. Anhydrite is dominant in the Castile Fm. relative to halite but this abundance is balanced by the higher solubility of halite. Uliana and Sharp (2001) individualized a small “NW Davis” sample group of the Na-Cl water type at the location where halite dissolution likely takes place. Kirkland et al. (2000) and Anderson (1981) stated that about 1/3rd of the formation is currently halite after a significant amount had already been dissolved, chiefly along the western side of the basin. The limited number of samples analyzed for sulfate isotopes tenuously suggest that sulfate of Rustler water samples is slightly heavier than that of spring samples, possibly hinting at a way to firm up the origin of the major ions, but more samples need to be analyzed to reach statistical significance.

Balmorhea spring water isotopes are lighter than the average rainfall but not as light as the lightest of the rain water. Although some rain water isotopes (winter time) can be lighter than the

Balmorhea area springs (Figure 34 and Figure 35), Davis Mountains igneous springs and alluvium wells, presumably isotopically similar to the meteoric contribution to the springs, exhibit heavier water isotopes than the Balmorhea area springs, pointing to a water source external to the spring area.

It is clear that the artesian springs share similar geochemistry whereas water table / gravity springs, East and West Sandia springs on one side and Saragosa Spring on the other side show different geochemical characteristics indicative of the influence of a shallower source. Lower average temperature and larger seasonal swings are the most obvious parameter showing that the gravity springs drain mostly shallower groundwater. There are other parameters supporting the mostly shallow source of the non-artesian springs: higher nitrate, heavier water isotopes, lower strontium isotopic ratio, elevated silica, and slightly lighter carbon isotope of DIC. It should be noted that a principal component analysis (PCA) on the Balmorhea area springs by Nunu (2020) shows that major ion chemistry is discriminatory (they are all weighted similarly in the Principal Component #1) emphasizing the role of varying TDS whereas Principal Component #2 is composed of nitrate and dissolved silica. Nitrate is high in the non-artesian springs and their dissolved silica originates from either the Davis Mountains stormwater directly flowing through the alluvium or from the alluvium, which is composed of igneous rock debris eroded from the Davis Mountains.

Nitrate is typically higher in the gravity spring samples than in the artesian springs (Figure 27) and at higher values that would happen mechanically by adjusting the TDS. Nitrate (oxidation product of ammonium) and phosphate are typical indicators of septic waste. However, the chemical analyses never revealed any phosphate (except for a Madera Creek sample at 0.4 ppm), which agrees with recent NCKRI sampling. Another useful tracer of septic tank plumes is boron (found in laundry detergents), but the Sandia springs are not particularly enriched in boron. Nunu (2020) analyzed for $\delta^{11}\text{B}$, which is generally used as a marker of surface contamination, from which analysis no conclusion can be drawn. The spring samples are not particularly enriched in potassium (K) either, K along with nitrate is an indicator of fertilizer use. The settling basins of the Balmorhea water treatment plant might be a potential origin. There is no strong seasonality in the nitrate (Figure 28) as would be expected for a natural origin. The nitrate issue remains somewhat unresolved, however, the fact that artesian springs show an increase in nitrate during significant precipitation events (Figure 29) suggests that nitrate could originate from the Davis Mountains and impact the alluvium. That would explain the lack of seasonality in the nitrate observations. In addition, although the Sandia Springs Sr ratio is close to that of the artesian springs (Figure 37), it is slightly lower, which again is consistent with some input from water other than that of the artesian springs (possibly from irrigation).

Stable water isotopes of the gravity springs are slightly higher than in the artesian springs (Figure 35) but do not markedly deviate from the meteoric water line suggesting that the slightly higher values are related to a contribution from water of Igneous chemistry, which is also consistent with the nitrate distribution observation. This is corroborated by slightly higher silica concentrations in the gravity springs (Figure 30), a typical indicator of the presence of water from the Igneous category, as well as a slightly lighter carbon of DIC (Figure 39), suggesting less impact from carbonate dissolution or, alternatively, some impact of water from the Igneous category.

In conclusion, the gravity springs exhibit signals from the Igneous category that can be interpreted as water originating from the Davis Mountains and stored in the shallow alluvium of

the Balmorhea area (e.g., Huelster well) during large storm events or slow storm baseflow in between large events. The conundrum is that the presence of Igneous indicators would imply that the Igneous contribution would decrease the TDS of the gravity springs whose main contributor is the seepage from the artesian springs. However, TDS of the gravity springs is higher than that of the artesian springs. It is tempting to assume that Sandia springs are fed by Lake Balmorhea whose evaporative contribution would explain the higher TDS. Guided by rhyolite outcrops, an overflow drainage ditch from Lake Balmorhea seems to disappear in the area between East and West Sandia Springs. But this explanation is not satisfying. Sandia springs samples do not show any obvious evaporation trend—simply a step inching toward the water isotope values of the Igneous category. An alternative explanation is the potential presence of solutes that had accumulated in the shallow subsurface through secular evapotranspiration in between drainage channels (Scanlon et al., 2010a,b) and that would be mobilized by percolating irrigation waters. A limited soil coring campaign would test this hypothesis.

We do not have a history of TDS at Lake Balmorhea but the few samples (unfortunately not taken in the summer time) show that their TDS is lower than that of the springs, particularly that of the Saragosa Spring, which is not in the path of the Lake Balmorhea outlets. The position of Lake Balmorhea stable water isotopes away from the GMWL strongly suggests evaporation, which is not seen in the potentially gravity springs. Lake Balmorhea samples do not show nitrate or only low concentrations on par with the geochemistry of the artesian springs. Sr epsilon ranges from $\epsilon_{Sr} = 7-9\text{‰}$ for the Sandia springs, slightly lower than that of the artesian springs at $\epsilon_{Sr} = 10-11\text{‰}$ but much higher than Lake Balmorhea at $\epsilon_{Sr} = \sim 1.2\text{‰}$ (with the caveat that we do not have many samples). Such observations are compatible with additional contributions (in addition to artesian spring outflow and Igneous water from alluvium) from a deeper source to be determined, which suggests that the springs are located on different fault lines or within different fault compartments.

8.2 Discussion of physical results

Despite all the studies performed in the past 50 years and earlier, many aspects of the springs are still unknown with unanswered questions, including:

- (1) Which watershed(s) contribute the most to the short-term stormflow component of spring flow?
- (2) Can the Limpia watershed, a large watershed apparently located downgradient of the springs, contribute to spring flow?
- (3) Do storm events and recharge in the Apache Mountains directly impact spring flow? What is the importance of local distributed recharge or low-level base flow from the Davis Mountains?
- (4) Are springs responding independently, but at the same time, to external factors or do they feed each other, that is, are they on the same flowpath or in different fault compartments? What is the impact of faults as flow barriers or flow pathways.
- (5) How widespread is cross-formational flow? What are the relationships between the water-bearing formations along the faulted mountain front and the Rounsaville Syncline?

We tentatively address these questions below:

- (1) Knowing the ultimate sources and their pathways to the springs is a key element to protecting the spring environmental health the same way the wellhead protection program works. In this context, it is important to determine the contributions of each watershed. Isolated but intense rain

events in combination with monitoring of streams and wells (data loggers) can provide the needed information, but it requires multi-year and patient monitoring, and detailed data analysis. The hypothesis of water storing or mounding after large rain events, whose shape is most likely controlled by the contributions of each source watershed, suggests that water withdrawals downgradient of the springs should be somehow timed relative to these events.

(2) Some authors have suggested that recharge from the Limpia watershed contributes to spring flow, mostly on relative elevation arguments. It seems possible that interbasin groundwater flow from lower Limpia Creek via fractured volcanic rocks in the Rounsaville Syncline to Big Aguja Canyon potentially contribute to Balmorhea-area spring discharge. The mouth of Limpia Creek as it emerges from the Davis and Barilla Mountains into the Washita stage (Cretaceous) limestones of the flanks of the Toyah Basin is at a higher elevation than the springs (3400-3500 ft vs. 3200-3300 ft). The low TDS of a Rustler well in the Toyah Basin which is diluted by Limpia stream water (Hidalgo) show the strength of storm events in the watershed. White et al. (1941) suggested Limpia contributions to spring flow might happen. Robertson et al. (2019) using NEXRAD data also suggested Limpia recharge. However, the geology does not seem to favor such a hypothesis. Examination of the Fort Stockton GAT sheet (as well as idealized cross-section by Eifler, 1951) strongly suggests that the Cenozoic volcanic rocks cover thick marly Upper Cretaceous units, which crop out piecemeal on the western, northern, and eastern flanks of the Barilla Mountain. The karsted layers of the Fredericksburg and Wachita stages are not accessible to potential losing stream recharge until the creek reaches the alluvial plain. Even then, the domal nature of the Barilla Mountains makes it difficult, even in an artesian system, for the recharging water to move west to the springs. However, it is possible that the fractured volcanic rocks of the Star Mountain (Tsm of GAT sheets) and Huelster (Th of GAT sheets) formations exposed in the syncline between Star Mountain and the Barilla Mountains provide a pathway to the basal Jeff conglomerate that could discharge into Big Aguja Creek through tributaries, but again artesian flow in that direction would be difficult. Careful land survey and drilling of a few monitoring wells would help resolve the issue.

(3) Precipitation and subsequent recharge in the Apache Mountains could provide dilute water to the springs after a storm event in addition to that of the Davis Mountains and contribute to the longevity of the slow return back to baseflow. Careful and long-term monitoring is needed to understand the role of the Apache Mountains on the spring flow rate. Similarly, it is often assumed that local contributions are from mountain-front recharge and not from distributed recharge from rain events in close proximity to the springs. Work by various authors have demonstrated that, in West Texas, recharge occurs only when rain events on topographic highs are strong enough to produce ephemeral flow that percolates through the alluvium at the mountain front below the root zone (e.g., Scanlon, 1991). Where is that shallow recharge (as opposed to the Cretaceous recharge) going, is it all captured by the springs?

A related issue is the nature of the pre-Cenozoic basement underneath the Davis Mountains. Although the potential presence of Upper Cretaceous clays may prevent any connection with the underlying formations, if they are absent or deeply fractured, hydraulic connection is possible. Beach et al. (2004) shows several oil wells penetrating the Permian (all dry holes) and makes use of proprietary work to draw cross-sections through the Davis Mountains. Consulting the IHS Enerdeq database and cursory interpretation of well logs shows the presence of Permian rocks below the Davis Mountains. Examination of Well #42-243-00001 (completed in 1958) suggests that post-Buda Limestone Upper Cretaceous was observed whereas well #42-243-00017 (completed in 1962) describes only the Lower Cretaceous (Figure 69). A subcrop map of pre-

Cretaceous formations in Brown (2019) suggests they overlie progressively older Permian rocks (Guadalupian to Wolfcampian). Sampling the water present in these formations or finding archived samples to age-date them may help to determine if any contribution exists from the pre-Cenozoic rocks of the Davis Mountains that would be immune to increased pumping.

(4) Although it is clear that the springs share a generalized common source, details reveal that they are not sources from a common reservoir. The three groups of springs (SS-G-PL, ES-WS, and Saragosa) are on different fault lines (Chowdhuri et al., 2004) and may not receive recharge coming transversally from the Davis Mountains in a similar way. In this context, potentiometric maps can be misleading if the permeability field is strongly anisotropic, in which case, flow cannot be simply inferred from isolines and can even be almost parallel to them with strong anisotropy (e.g., Edwards Aquifer on the Balcones Fault Zone). In the Balmorhea area, studies suggest that the maximum horizontal stress (SH_{max}) in the southern Delaware Basin is NW-SE to WNW-ESE (Lund-Snee and Zoback, 2018; Heidbach et al., 2018), which is supported by the main orientation of the Alpine High play horizontal well laterals (NNE-SSW; data from IHS Markit) allowing the hydraulic fractures to open along SH_{max} as they should. This suggests that natural fractures and faults in the Stocks Fault zone, as well as other faults sharing similar orientation, are favorably oriented for enhanced permeability. It would also suggest that flow in SW-NE-oriented fractures could be impeded, if not following conduits. The contrast in behavior between closely located Giffin and San Solomon springs suggests complexity of the karstic network. However, the paucity of data limits further analysis on the regional anisotropy of the flow system.

(5) Effective cross-formational flow requires two elements: a driving force, the head difference between the two aquifers, and a pathway to move the water from one aquifer to the other. The GAM models provided some information about vertical gradient and potential vertical flow. However the modeling results are generalized from regional models. The Rustler GAM shows a patchwork of up and down gradients (Ewing et al., 2012) that were actually computed from very limited data in the Balmorhea Springs area and mostly extrapolated. Our water level data analysis shows the same, both up and downward gradients between closely spaced wells. Several authors have concluded that at least in the Fort Stockton / Belding irrigation area water can potentially flow from the Capitan (eastern arm) to the Rustler to the Edwards-Trinity (Bumgarner et al., 2012; Mace et al., 2020). Common pathways are diffuse fractures leading to a distributed invasion, in particular, in areas where the intervening aquitard is thin, or localized fault zones. Several authors have hypothesized that Rustler water locally invades and mixes with overlying Edwards-Trinity water in the Leon-Belding irrigation area and more generally in the Monument Trough (Kreitler et al., 2013) and in the vicinity of the Diamond Y Spring (Boghici, 1997), both locations are in Pecos County.

The exact relationships between the Capitan, Rustler, Castile, and Edwards Group are complex; their stratigraphic relationships are clear but depositional, erosional, and structural boundaries make it such that any two of these formations can be in direct vertical contact. Cross-sections proposed by Finch (2017) and by Standen et al. (2009) suggest that, at the eastern extent of the Stocks Fault where the Capitan foreereef and some of its core are still on the downdropped side of the fault, Cretaceous limestones (and Cox Sandstone and Yearwood Fm.) directly overlie the section of the Capitan connected to the Salt Flat as well as the Castile Fm.. The buried down-throw compartment of the Capitan north of the Stocks Fault seems to have higher head than the exposed compartment to the south of the Fault, and as high as it is in the likely recharge zone in

the Patterson Hills (Jones 2016a). The Capitan south of the Stocks Fault is now in lateral contact with the Cretaceous formations. Another cross-section by Pearson (1985) in the Balmorhea Springs area where the fault throws are considerably less also shows the Lower Cretaceous resting directly on top of the Capitan. It does not seem that Cretaceous layers are in direct contact with the DMG basinal deposits (coeval of the Capitan). Traveling farther to the SE and approaching the Balmorhea area springs from the NW along the mountain front, the relationships between the Rustler and Castile Fms. are uncertain as they both pinch out towards the structural boundary of the basin. In particular, it is unclear which formation pinches out the farthest to the SW. Limited data seems to indicate that it is the Rustler, which then would be in vertical and lateral contact with the Capitan.

The various questions posed at the beginning of the section all assume that the declining flow rate observed in the past decades is related to pumping and that a better knowledge of the regional flow system and of the individual contributions to the spring complex could guide decisions on water withdrawal. Phantom Lake ceased to flow in 1990, SSS flow rate has been declining steadily. TWDB-TPWD (2005) noted a disconnect between spring flow rate and pumping rates and stated that flow rate decline started before heavy irrigation pumping. Clearly the lack of data on pumping locations and amounts of water withdrawn at the beginning of the 20th century impedes a full examination of this hypothesis. The lack of accurate water withdrawal metering/reporting is still an issue. A numerical flow model centered on the Balmorhea Spring Complex that includes sections of the following GAM models: West Texas Bolsons, Igneous, Edwards-Trinity, Rustler, and Capitan Aquifers, to which Permian formations of the Diablo Platform (Artesia Group) and of the Basin (DMG) are added, would help to decipher the impact of early pumping.

A simple use of the pressure diffusion relationship approximates how fast a pressure disturbance travels ($t=d^2/D$ where t is characteristic time, d is length scale or distance, and D is hydraulic diffusivity; $D = K/S_s$, is defined as the ratio of conductivity K [L^2t] to specific storage S_s [L^{-1}]). The average hydraulic conductivity can be estimated at 0.75 m/day (which is approximately equivalent to a permeability $k=1$ darcy) from the travel time ($\sim 12,000$ years), distance (80 km), topographic gradient between the salt flats and the spring area (0.0025), and porosity (10%). Now, assuming a specific storage of 10^{-5} m^{-1} , D is 75×10^3 m^2/day and $t = 64 \times 10^8 / 75 \times 10^3 = 230$ years, which is only a rough approximation but that suggests that it takes decades to centuries for a pressure change (recharge, pumping) to propagate from the Salt Basin to the springs. Considering disturbances closer to the Balmorhea spring complex, at the eastern edge of the Apache Mountains as the feature connect to the Toyah Basin (~ 40 km), would translate into a travel time of ~ 120 years. However, we caution against reading too much into these numbers. They simply suggest that it is admissible that a strong pressure signal initiated somewhere between the Salt Flats and Balmorhea would have reached the springs a few decades ago. As pressure signals travel, they are typically attenuated and blurred by merging with other signals so that only the low frequency signals travel far (e.g., change in climate but not a drought of a few years). Given the complexity of the regional system involving at least seven aquifers, several of which show evidence of cross-formational flow, analytical solutions, even sophisticated, and piecemeal disconnected numerical models are unlikely to provide satisfying answers to the questions raised. Although, ultimately such a numerical model is needed, it cannot move forward before more long-term non-geochemical data are collected.

Other hypotheses to explain the flow rate decline suffer from lack of evidence. A spring flow decrease due to local cones of depression decreasing the head at the spring has been suggested to explain the drying up of Phantom Lake Spring (windmill pumping; Sharp, 2003). However, such explanation lacks generality as San Solomon Spring flow rate does not show seasonality, suggesting a distal origin for the decline. A change in vegetation pattern with an increase in phreatophyte extent (encroachment of salt cedars near the outlet and historical pool area at Phantom Lake Spring) would benefit from a study of time-stamped aerial photos and satellite images that may validate or invalidate this hypothesis. A vegetation change is more likely to have a local impact, for example, at the Sandia or Saragosa springs with much vegetation rooted in the shallow aquifer. The earthquake hypothesis (TWDB-TPWD, 2005) is unlikely for two reasons: (1) the Valentine earthquake (Doser, 1987) happened in August 1931, and the USGS/TWDB study (White et al., 1938, 1941) started around the same time, any unusual behavior of the springs would have been noted by the local population and reported to the USGS team; and (2) if flow rates (Sneed et al., 2003; Fleeger et al., 1999; Manga et al., 2016) and geochemical changes (Nanni et al., 2020; Claesson et al., 2007) are reported following seismic events in an area, they are often reversed in a matter of days, weeks, months, or years.

9 Conclusions and future work

This study agrees with most of the previous work on the Balmorhea area springs but not all of it since conflicting hypotheses have been proposed by various researchers. Examination of historical data and of data collected during this study led us to conclude: (1) the most likely distal origin of a significant fraction of baseflow is in the northern section of the Salt Flats (Salt Basin), hypothesis initially promoted by Chowdhury et al. (2004) and TWDB (2005); then the flow interacts with the Castile Fm. in the vicinity of the Apache Mountains where it acquires its geochemical signature before reaching the springs; and (2) each regional precipitation event of relatively high intensity (>1-2" per day for a few not necessarily contiguous days as recorded by local weather stations) results in storage of large water volumes upflow from the Balmorhea area springs, which are slowly released in the following months. The recharge mound could also possibly deflect some of the baseflow.

Insufficient rainfall events during the study period and the lack of a strong signal limited the usefulness of the data loggers in the course of this study. TWDB-TPWD (2005) made a similar comment after completion of their 3-year study. Longer time series and heavy rainfall in the Davis Mountains are needed to identify changes in spring water physio-chemistry and correlate these changes with potential recharge areas. Rainfall statistics (Figure 70) clearly support the need for multi-year data collection. As of July 2021, the InSitu[®] loggers are still recording spring, stream, and well parameters (unprocessed data were downloaded during the field trips of late December 2020 and of June 2021 and will be during the planned trip of December 2021 / January 2022).

Several important points could not be resolved in this study. For example, what is the impact of cross-formational flow, either natural or due to well completion, on the springs; in particular what is the potential of mixed completion wells to depressurize the Cretaceous aquifer and contribute to the observed reduction in spring flow? Potential for cross-formational flow either upward or downward has been clearly established and also strongly suggested through GAM modeling, but there are limited data on vertical flow in the Balmorhea area. A few pump tests, aimed toward assessing vertical flow, would be useful.

In order to build on this study, there is a need to deploy well monitoring equipment on existing wells upstream of the springs to the west and northwest up to the eastern edge of the Apache Mountains. There is also a need to sample aquifers for natural tracers such as water, strontium and sulfate isotopes along the presumed path of the baseflow all the way to the Salt Flats. Work by Uliana and several other researchers focused on the bolsons south of I-10. Minor geochemical tasks such as additional analyses of produced water and other brines sampled in the general vicinity of the Balmorhea area are needed to fully confirm their lack of connection with the springs.

In the medium term two numerical flow models need to be developed, a regional model focusing on the baseflow and the complexity of the faulted boundary of the southern Delaware Basin, with the spring complex its focus and at its center (unlike all current GAM models) and a more local, finer-resolution model focusing on the recharge pulses from the Davis Mountains (Cretaceous, alluvium) and transient mounding. The current study was not geared towards developing numerical flow models and an extensive data collection must take place along with a refining of the conceptual flow model presented here.

Supplementary Information

The companion electronic folder (<https://doi.org/10.18738/T8/RENGP9>), available in the public domain, contains the following files:

- Analytical results from the BEG geochemical sampling
- Compilation of previous geochemical data
- Raw logger data
- Official record of driller logs and other information of BEG monitoring wells

References

- Anaya, R., and Jones, I., 2009, Groundwater Availability Model for the Edwards-Trinity (Plateau) and Pecos Valley Aquifers of Texas: Texas Water Development Board, Report #373.
- Anderson, R.Y., 1981, Deep-seated salt dissolution in the Delaware basin, Texas and New Mexico, in Wells, S.G. and Lambert, W. (eds.), New Mexico Geological Society, Albuquerque, NM, Special Publication #10, p.133-145.
- Angle, E.S., 2001, Hydrogeology of the Salt Basin, *in* Mace, R. E., Mullican, W. F., and Angle, E. S., eds., Aquifers of West Texas. Report #356. Texas Water Development Board: Austin, TX, Texas Water Development Board, p. 232-247.
- Appelo, C.A.J. and Postma, 2005, Geochemistry, groundwater and pollution, A.A. Balkema Publishers, London, UK, 2nd edition, 649pp.
- Ashworth, J.B., 1990, Evaluation of ground-water resources in parts of Loving, Pecos, Reeves, and Winkler Counties, Texas, Texas Water Development Board Report #317, 51pp.
- Ashworth, J.B., D.B. Coker, and W. Tschirhart, 1997, Evaluation of diminished spring flows in the Toyah Creek Valley, Texas, Texas Water Development Board Open File Report 97-03,
- Barker, D.S., 1977, Northern Trans-Pecos magmatic province: Introduction and comparison with the Kenya rift: GSA Bulletin, v. 88, no. 10, p. 1421-1427.
- Barker, D.S., 1979, Cenozoic Magmatism in the Trans-Pecos Province: Relation to the Rio Grande Rift, in Riecker, R. E., ed., Rio Grande Rift: Tectonics and Magmatism, Volume 14: Washington, DC, American Geophysical Union.

- Barker, D.S., 1987, Tertiary alkaline magmatism in Trans-Pecos Texas. Geological Society, London, Special Publications 30, no. 1, p. 415-431.
- Barker, R.A., and Ardis, A.F., 1992, Configuration of the base of the Edwards-Trinity Aquifer System and hydrogeology of the underlying pre-Cretaceous Rocks, west-central Texas, U.S. Geological Survey Water-Resources Investigations Report 91-4071, 33p.
- Barker, R.A., P.W. Bush, and E.T. Baker, Jr., 1994, Geologic history and hydrogeologic setting of the Edwards-Trinity Aquifer System, west-central Texas, U.S. Geological Survey Water-Resources Investigations Report 94-4039, 51p.
- Barnes, J.D. and Z.D. Sharp, 2017, Chlorine Isotope Geochemistry, *Reviews in Mineralogy & Geochemistry*, 82(1), p.345-378, <http://dx.doi.org/10.2138/rmg.2017.82.9>.
- Beach, J.A., Ashworth, J.B., Finch, S.T., Jr., Chastain-Howley, A., Calhoun, K., Urbanczyk, K. M., Sharp, J.M., Jr., and Olson, J., 2004, Groundwater Availability Model for the Igneous and parts of the West Texas Bolsons (Wild Horse Flat, Michigan Flat, Ryan Flat and Lobo Flat) Aquifers, variously paginated.
- Behl, N., Bohm, B., Bruton, M., Fleming, S., and Vance, S., 2018, Case Study: Apache's Approach to Societal Responsibility thru the Environmental Media Monitoring Program for the Alpine High Play, Annual Technical Conference and Exhibition, Dallas, Texas, USA, September 2018, <https://doi-org.ezproxy.lib.utexas.edu/10.2118/191589-MS>.
- Boghici, R., 1997, Hydrogeological investigations at Diamond Y Springs and surrounding area, Pecos County, Texas, Master's Thesis, The University of Texas at Austin.
- Boghici, R., and Van Broekhoven, N.G., 2001, Hydrogeology of the Rustler Aquifer, Trans-Pecos Texas, *in* Aquifers of West Texas, Texas Water Development Board Report #356, p.207-225.
- Boren, R., 2012, The Early Archaic Cultural Period in Eastern Trans-Pecos Texas: *Journal of Big Bend Studies*, v. 24.
- Boyd, F.M. and C.W. Kreitler, 1986, Hydrogeology of a Gypsum Playa, Northern Salt Basin, Texas, The University of Texas at Austin Bureau of Economic Geology Report of Investigations No.158, 37p.
- Bradley, R. G., and Kalaswad, S., 2003, Groundwater resources of the Dockum Aquifer in Texas. Texas Water Development Board. Report 359, Texas Water Development Board.
- Brand, J.P. and R.K. DeFord, 1962, Geologic map of eastern half of Kent quadrangle, Culberson, Reeves and Jeff Davis Counties, Texas. 1:63,360, Virtual Landscapes of Texas, University of Texas at Austin, Bureau of Economic Geology, Geol. Quad. Map, no. 24.
- Brown, A., 2019, Post-Permian history of the greater Permian Basin area, *in* Ruppel, S. C., ed., *Anatomy of a Paleozoic basin: the Permian Basin, USA* (vol. 1, ch. 5): The University of Texas at Austin, Bureau of Economic Geology Report of Investigations 285; AAPG Memoir 118, p. 97–134.
- Brune, G., 1975, Major and Historical Springs of Texas, Texas Water Development Board Report #189, 94pp.

- Bumgarner, J.R., Stanton, G.P., Teeple, A.P., Thomas, J.V., Houston, N.A., Payne, J.D., and Musgrove, M., 2012, A conceptual model of the hydrogeologic framework, geochemistry, and groundwater-flow system of the Edwards-Trinity and related aquifers in the Pecos County Region, Texas. U.S. Geological Survey, Scientific Investigations Report 2012-5124, 74p., <https://doi.org/10.3133/sir20125124>.
- Bureau of Economic Geology, 1976, Pecos sheet, 1:250,000, Geological Atlas of Texas, GA00025, The University of Texas, by G.K. Eifler, Jr.
- Bureau of Economic Geology, 1979, Marfa sheet, 1:250,000, Geological Atlas of Texas, GA00022, The University of Texas, by P.C. Twiss.
- Bureau of Economic Geology, 1982, Fort Stockton sheet, 1:250,000, Geological Atlas of Texas, GA00016, The University of Texas, by J.E. Anderson, Jr., J.B. Brown, J.C. Gries, E.M.P. Lovejoy, D. McKalips, and V.E. Barnes
- Bureau of Economic Geology, 1983, Van Horn-El Paso sheet, 1:250,000, Geological Atlas of Texas, GA00036, The University of Texas, by J.W. Dietrich, D.E. Owen, C.A. Shelby, and V.E. Barnes.
- Burke W.H., Denison R.E., Hetherington E.A., Koepnick R.B., Nelson H.F., and Otto J.B., 1982, Variation of seawater $^{87}\text{Sr}/^{86}\text{Sr}$ throughout Phanerozoic time, *Geology*, 10, p.516–519, [https://doi.org/10.1130/0091-7613\(1982\)10<516:VOSSTP>2.0.CO;2](https://doi.org/10.1130/0091-7613(1982)10<516:VOSSTP>2.0.CO;2).
- Bush, P.W., Ardis, A.E., and Wynn, K.H., 1993, Historical potentiometric surface of the Edwards-Trinity aquifer system and contiguous hydraulically connected units, west-central Texas: U.S. Geological Survey, Water-Resources Invest. Rept. 92-4055, 3 plates, <https://doi.org/10.3133/wri924055>.
- Bush, P.W., Ulery, R.L., and Rittmaster, R.L., 1994, Dissolved-solids concentrations and hydrochemical facies in water of the Edwards-Trinity aquifer system, west-central Texas, U.S. Geological Survey, Water-Resources Investigations Report 93-4126, 29p. + 2 plates, <https://doi.org/10.3133/wri934126>.
- Cameron, K.L., Parker, D.F., and Sampson, D.E., 1996, Testing crustal melting models for the origin of flood rhyolites: A Nd-Pb-Sr isotopic study of the Tertiary Davis Mountains volcanic field, west Texas, *J. Geophys. Res.*, 101(B9), 20407– 20422, <https://doi.org/10.1029/96JB00935>.
- Chowdhury, A.H., C. Ridgeway, and R.E. Mace, 2004, Origin of the waters in the San Solomon Spring system, Trans-Pecos Texas, Texas Water Development Board 360, p.315-344
- Claesson, L., Skelton, A., Graham, C. And Mörth, C.-M., 2007, The timescale and mechanisms of fault sealing and water-rock interaction after an earthquake. *Geofluids*, 7, p.427-440, <https://doi.org/10.1111/j.1468-8123.2007.00197.x>
- Clark, I.D. and P. Fritz, 1997, Environmental isotopes in hydrogeology, CRC Press/Lewis Publishers, Boca Raton, ISBN: 156670249, 328pp.
- Clark, B.R., Bumgarner, J.R., Houston, N.A., and Foster, A.L., 2014, Simulation of groundwater flow in the Edwards-Trinity and related aquifers in the Pecos County region, Texas. U.S. Geological Survey Scientific Investigations Report 2013–5228, 9781411309.

- Claypool, G.E., W.T. Holser, I.R. Kaplan, H. Sakai, and I. Zak, 1980, The age curves of sulfur and oxygen isotopes in marine sulfate and their mutual interpretation, *Chemical Geology*, 28, p.199-260, [https://doi.org/10.1016/0009-2541\(80\)90047-9](https://doi.org/10.1016/0009-2541(80)90047-9).
- Corbet, T.F., 2000, A groundwater-basin approach to conceptualize and simulate post-Pleistocene subsurface flow in a semi-arid region, southeastern New Mexico and western Texas, USA, *Hydrogeology Journal*, 8(3), p.310-327, <https://doi.org/10.1007/s100400000067>. = WIPP
- Couch, H.E., 1978, Study of the lower Cretaceous and associated aquifers in the Balmorhea district of Trans-Pecos, Texas: Department of Water Resources, Report, 61 p.
- Daly, C.M., Halbleib, J.I., Smith, W.P., Gibson, M.K., Doggett, G.H., Taylor, J.C., and Pasteris, P.P., 2008, Physiographically sensitive mapping of climatological temperature and precipitation across the conterminous United States, *International Journal of Climatology*, v. 28, p. 2031-2064, <https://doi.org/10.1002/joc.1688>.
- Darling, B.K., 2017, Integration of carbon-14 and oxygen-18 as a basis for differentiating between late Pleistocene and post-Pleistocene groundwater ages along flow paths of two west Texas bolson aquifers, *Geological Society of America Abstracts with Programs*, 49(6), <https://doi.org/10.1130/abs/2017AM-294991>.
- Davis, M.E., and Leggat, E.R., 1965, Reconnaissance investigation of the ground-water resources of the upper Rio Grande Basin, Texas: Texas Water Commission Bulletin 6502, 99p.+Appendices.
- Davis, S.N., Whittemore, D.O. and Fabryka-Martin, J., 1998, Uses of Chloride/Bromide Ratios in Studies of Potable Water. *Groundwater*, 36(2), p.338-350, <https://doi.org/10.1111/j.1745-6584.1998.tb01099.x>.
- Davis, S.N., J.T. Fabryka-Martin, and L.E. Wolfsberg, 2004, Variations of Bromide in Potable Ground Water in the United States, *Groundwater*, 42(6), p. 902-909, <https://doi.org/10.1111/j.1745-6584.2004.t01-8-.x>.
- Denison, R.E., D.W. Kirkland and R. Evans, 1998, Using Strontium Isotopes to Determine the Age and Origin of Gypsum and Anhydrite Beds, *The Journal of Geology*, 106(1), p.1-18, <https://doi.org/10.1086/515996>
- Doser, D. I., 1987, The 16 August 1931 Valentine, Texas, earthquake: Evidence for normal faulting in west Texas, *Bulletin of the Seismological Society of America*, 77(6), p.2005-2017.
- Dowell, C.L. and S.D. Breeding, 1967, Dams and Reservoirs in Texas - Historical and Descriptive Information December 31, 1966, Texas Water Development Board, Report 48, June 1967, 267pp.
- Dubrovsky, N.M., Burow, K.R., Clark, G.M., Gronberg, J.M., Hamilton P.A., Hitt, K.J., Mueller, D.K., Munn, M.D., Nolan, B.T., Puckett, L.J., Rupert, M.G., Short, T.M., Spahr, N.E., Sprague, L.A., and Wilber, W.G., 2010, The quality of our Nation's waters—Nutrients in the Nation's streams and groundwater, 1992–2004: U.S. Geological Survey Circular 1350, 174 p., <http://water.usgs.gov/nawqa/nutrients/pubs/circ1350>.
- Eifler, G.K., Jr., 1951, Geology of the Barrilla Mountains, Texas, *Geological Society of America Bulletin*, 62(4), p.339-353, [https://doi-org.ezproxy.lib.utexas.edu/10.1130/0016-7606\(1951\)62\[339:GOTBMT\]2.0.CO;2](https://doi-org.ezproxy.lib.utexas.edu/10.1130/0016-7606(1951)62[339:GOTBMT]2.0.CO;2).

- Engle, M.A., F.R. Reyes, M.S. Varonka, W.H. Orem, L. Ma, A.J. Ianno, T.M. Schell, P. Xu, and K.C. Carroll, 2016, Geochemistry of formation waters from the Wolfcamp and “Cline” shales: Insights into brine origin, reservoir connectivity, and fluid flow in the Permian Basin, USA, *Chemical Geology*, 425, p.76-92, <https://doi.org/10.1016/j.chemgeo.2016.01.025>.
- Ewing, J. E., Jones, T. L., Yan, T., M. Vreugdenhil, A., Fryar, D. G., Pickens, J. F., Gordon, K., Nicot, J.-P., Scanlon, B. R., Ashworth, J. B., and Beach, J., 2008, Final groundwater availability model report for the Dockum Aquifer. Prepared for: Texas Water Development Board.
- Ewing, J.E., V.A. Kelley, Toya L. Jones, T. Yan, A. Singh, Ph.D., D.W. Powers, R.M. Holt, and J. M. Sharp, 2012, Final Groundwater Availability Model Report for the Rustler Aquifer, Texas Water Development Board contract report, variously paginated.
- Ewing, T.E., 2016, *Texas Through Time: Lone Star Geology, Landscapes, and Resources: The University of Texas at Austin, Bureau of Economic Geology Udden Series No. 6*, 431pp.
- Finch, Jr., S.T., 2017, Hydrogeologic evaluation and development of groundwater flow model for Capitan Reef Complex Aquifer, Apache Ranch, Culberson County, Texas, John Shomaker & Associates, Inc., Albuquerque, New Mexico, Report prepared for Hughes Apache Ranches, Culberson County, Texas, March 29, 2017, 32pp. + illustrations and appendices [unpublished]
- Finch, S.T. and Bennett, J.B., 2002, Hydrogeology evaluation of the northern part of Culberson County Groundwater Conservation District, Culberson County, Texas: Consultant report prepared for Culberson County Groundwater Conservation District by John Shomaker and Associates, Inc., 24 p.
- Fleeger, G.M., Goode, D. J., Buckwalter, T.F., and Risser, D.W., 1999, Hydrologic effects of the Pymatuning Earthquake of September 25, 1998, in Northwestern Pennsylvania: U.S. Geological Survey Water-Resources Investigations Report 99-4170, 8 p.
- FWS, 2004, U.S. Fish and Wildlife Service, Biological opinion on construction of a dam and pumping system at Phantom Lake Spring (Consultation No. 2-15-04-F-02840).
- Ge, J., J.-P. Nicot, P.H. Hennings, K.M. Smye, S.A. Hosseini, R.S. Gao, and C.L. Breton, 2021, Recent Water Disposal and Pore Pressure Evolution in the Delaware Mountain Group, Delaware Basin, Southeast New Mexico and West Texas, submitted for review
- Halverson, G.P. and L. Théou-Hubert, 2015, Seawater Sr Curve, *in* Encyclopedia of Scientific Dating Methods, W.J. Rink and J.W. Thompson (eds), Encyclopedia of Earth Sciences Series, Springer, Dordrecht 10pp., https://doi.org/10.1007/978-94-007-6326-5_143-1.
- Harden, R.W., 1972, Groundwater conditions in the vicinity of Phantom Lake, Giffin, and San Solomon springs, Reeves and Jeff Davis counties, Texas: consultant report to Texas Water Rights Commission on behalf of the Reeves County Water Improvement District 1.
- Harrington, R., Rainville, K., and Blandford, T. N., 2017, Comment on “Drawdown ‘Triggers’: A Misguided Strategy for Protecting Groundwater-Fed Streams and Springs,” by Matthew J. Currell, 2016, v. 54, no. 5: 619–622: *Groundwater*, v. 55, no. 2, p. 152-153, <https://doi.org/10.1111/gwat.12503>.
- Hart, M.A., 1992, *The Hydrogeology of the Davis Mountains, Trans-Pecos Texas*, M.A. Thesis, The University of Texas at Austin, 157 p.

- Heidbach, O., Rajabi, M., Cui, X., Fuchs, K., Müller, B., Reinecker, J., Reiter, K., Tingay, M., Wenzel, F., Xie, F., Ziegler, M. O., Zoback, M.-L., and Zoback, M., 2018, The World Stress Map database release 2016: crustal stress pattern across scales: *Tectonophysics*, v. 744, p. 484–498, <https://doi.org/10.1016/j.tecto.2018.07.007>.
- Heitmuller, F.T., Reece, B.D., 2003. Database of Historically Documented Springs and Spring Flow Measurements in Texas (USGS Numbered Series No. 2003–315), Open-File Report. U.S. Geological Survey.
- Hem, J.D., 1985, Study and Interpretation of the Chemical Characteristics of Natural Water, U.S. Geological Survey Water Supply Paper 2254, 263pp.
- Henry, C.D., Price, J.G., Rubin, J.N., Parker, D.F., Wolff, J.A., Self, S., Franklin, R., and Barker, D.S., 1988, Widespread, lavalike silicic volcanic rocks of Trans-Pecos Texas: *Geology*, v. 16, no. 6, p. 509-512.
- Hershler, R., Landye, J. J., Liu, H.-P., Maza—Benignos, M. D. I., Ornelas, P., and Carson, E. W., 2014, New Species and Records of Chihuahuan Desert Springsnails, With a New Combination for *Tryonia brunei*: *Western North American Naturalist*, 74(1), p.47-65, <http://www.bioone.org/doi/full/10.3398/064.074.0105>.
- Hibbs, B.J., 2020, Long Term Climate Change and Environmental Implications of Aquifer Flow Capacity in Arid Groundwater Basins, World Environmental and Water Resources Congress 2020: Groundwater, Sustainability, Hydro-Climate/Climate Change, and Environmental Engineering, p.89-96, <https://doi.org/10.1061/9780784482964.009>.
- Hiss, W.L., 1976, Structure of the Permian Guadalupian Capitan aquifer, southeastern New Mexico and western Texas: U. S. Geological Survey Open-File Report 76-0053, 338 p.
- Horne, E.A., Hennings, P.H., and Zahm, C.K., 2021, Basement-rooted faults of the Delaware Basin and Central Basin Platform, Permian Basin, West Texas and southeastern New Mexico, in Callahan, O. A., and Eichhubl, P., eds., *The geologic basement of Texas: a volume in honor of Peter T. Flawn*: The University of Texas, Bureau of Economic Geology Report of Investigations No. 286, <http://doi.org/10.23867/RI0286C6>.
- Hutchinson, W.R., I.C. Jones, and R. Anaya, 2011, Update of the Groundwater Availability Model for the Edwards-Trinity (Plateau) and Pecos Valley Aquifers of Texas, Texas Water Development Board, 59p.
- Jasechko, S., 2019), Global isotope hydrogeology—review. *Reviews of Geophysics*, 57, p.835-965, <https://doi.org/10.1029/2018RG000627>.
- Jones, I.C., 2016a, Conceptual Model: Eastern Arm of the Capitan Reef Complex Aquifer of Texas, Texas Water Development Board.
- Jones, I.C., 2016b, Groundwater Availability Model: Eastern Arm of the Capitan Reef Complex Aquifer of Texas, Texas Water Development Board.
- Jones, M., 2020, San Solomon Springs Baseflow Period Hydrochemistry Data Set [Data set]. Zenodo. <http://doi.org/10.5281/zenodo.3897198>
- Kirkland, D.W., R.E. Denison, and W.E. Dean, 2000, Parent brine of the Castile evaporites (Upper Permian), Texas and New Mexico, *Journal of Sedimentary Research*, 70(3), p.749–761, <https://doi.org/10.1306/2DC40935-0E47-11D7-8643000102C1865D>.

- Knowles, D.B., and Lang, J.W., 1947, Preliminary Report on the Geology and Ground-Water Resources of Reeves County Texas, Texas Board of Engineers report M226, 87pp.
- Korte, C., Kozur, H.W., Bruckschen, P., Veizer, J., 2003, Strontium isotope evolution of Late Permian and Triassic seawater, *Geochimica et Cosmochimica Acta*, 67(1), p.47–62, [https://doi.org/10.1016/S0016-7037\(02\)01035-9](https://doi.org/10.1016/S0016-7037(02)01035-9).
- Korte, C., T. Jasper, H.W. Kozur, and J. Veizer, 2006, 87Sr/86Sr record of Permian seawater, *Palaeogeography, Palaeoclimatology, Palaeoecology*, 240(1–2), p.89-107, <https://doi.org/10.1016/j.palaeo.2006.03.047>.
- Kreitler, C.W., Beach, J.A., Symank, L., Uliana, M.M., Bassett, R., Ewing, J.E., and Kelley, V.A., 2013, Evaluation of Hydrochemical and Isotopic Data in Groundwater Management Areas 3 and 7, contract report prepared for the Texas Water Development Board by LBG-Guyton, Austin, TX, 265pp., https://www.twdb.texas.gov/publications/reports/contracted_reports/doc/1148301235.pdf.
- Kuniansky, E.L. and Holligan, K.Q., 1994, Simulations of flow in the Edwards-Trinity aquifer system and contiguous hydraulically connected units, West-Central Texas: U.S. Geological Survey Water-Resources Investigations Report 93-4039, 40p, <http://pubs.er.usgs.gov/publication/wri934039>.
- LaFave, J.I., and Sharp, J.M., 1987, Origins of groundwater discharging at the springs of Balmorhea: West Texas Geological Society, v.26, p. 5-14.
- Land, L., M. Jones, and G. Veni, 2020, Using electrical resistivity methods to map cave passages and conduits in the San Solomon Springs karstic aquifer system, west Texas, USA, NCKRI Symposium #8, Proceedings of the 16th Multidisciplinary Conference on Sinkholes and the Engineering and Environmental Impacts of Karst, L. Land, C. Kromhout, and M.J. Byle, Eds, p.93-104.
- Land, L., and Veni, G., 2018, Karst Hydrogeology Scoping Investigation of the San Solomon Spring Area: Culberson, Jeff Davis, and Reeves Counties, National Cave and Karst Research Institute, Report of Investigations #8, 20pp.
- Larkin, T.J., and Bomar, G.W., 1983, Climatic atlas of Texas: Texas Department of Water Resources Report LP-192, 151 p.
- Lewis, R.H., Allan, N.L., Stoops, S.B., Garrett, G.P., Kroll, C.W., West, J., and Deaton, R., 2013, Status of the Endangered Pecos Gambusia (*Gambusia nobilis*) and Comanche Springs Pupfish (*Cyprinodon elegans*) in Phantom Lake Spring, Texas: *The Southwestern Naturalist*, v. 58, no. 2, p. 234-238.
- Lund Snee, J.-E., and Zoback, M.D., 2017, State of stress in the Permian Basin, Texas and New Mexico: implications for induced seismicity: *The Leading Edge*, v. 37, no. 2, p. 127–134, <https://doi.org/10.1190/tle37020127.1>.
- Lupton, D., Kelley, V., Powers, D., and Torres-Verdin, C., 2016, Identification of potential brackish groundwater production areas -- Rustler aquifer, Texas Water Development Board contract report, 358pp.
- Mace, R.E, S. Leurig, H. Seely, and D.A. Wierman, 2020, Bringing Back Comanche Springs: An Analysis of the History, Hydrogeology, Policy, and Economics, Texas Water Trade and The

- Meadows Center, Texas State University, Report #2020-08, 153pp., <https://gato-docs.its.txstate.edu/jcr:d07544be-530b-4a04-8494-8e715f50c930>.
- Manga, M., Wang, C.-Y., and Shirzaei, M., 2016, Increased stream discharge after the 3 September 2016 Mw 5.8 Pawnee, Oklahoma earthquake, *Geophys. Res. Lett.*, 43, 11,588–11,594, <https://doi.org/10.1002/2016GL071268>.
- Matchus, E.J. and T.S. Jones, co-chairmen, 1984, East-West cross-section through Permian Basin of West Texas: prepared by Stratigraphic Problems Committee of the West Texas Geological Society, Publication 84-79, 1 sheet.
- Meinzer, O.E., 1927, Large springs in the United States, USGS Water Supply Paper 557, 119p., <https://doi.org/10.3133/wsp557>.
- Meyer, J.E., Wise, M.R., and Kalaswad, S., 2012, Pecos Valley Aquifer, West Texas: Structure and Brackish Groundwater, Texas Water Development Board Report #382, 86p.
- Meyer, J.E., 2020, Brackish Resources Aquifer Characterization System Database Data Dictionary, Fifth Edition, TWDB Open File Report 12-02, April 2020, <https://www.twdb.texas.gov/innovativewater/bracs/database.asp>.
- Milkov, A.V. and G. Etiope, 2018, Revised genetic diagrams for natural gases based on a global dataset of >20,000 samples, *Organic Geochemistry*, 125, p.109-120, <https://doi.org/10.1016/j.orggeochem.2018.09.002>.
- MRLC, 2018, Multi-Resolution Land Characteristics Consortium (MRLC), National Land Cover Database (NLCD). <http://www.mrlc.gov/>, accessed August 13, 2018.
- Nanni, T., Vivalda, P.M., Palpacelli, S., Marcellini, M., and Tazioli, A., 2020, Groundwater circulation and earthquake-related changes in hydrogeological karst environments: a case study of the Sibillini Mountains (central Italy) involving artificial tracers, *Hydrogeology Journal*, 28, p.2409–2428, <https://doi.org/10.1007/s10040-020-02207-w>.
- Neilson, P. D. and Sharp, J. M., Jr., 1985, Tectonic controls on the hydrogeology of the salt basin, Trans-Pecos, Texas: in Dickerson, P.W., and Muehlberger, W.R., eds., *Structure and tectonics of Trans-Pecos Texas: West Texas Geological Society Special Publication*, p. 231-234.
- Nicot, J.-P., R. Darvari, P. Eichhubl, B.R. Scanlon, B.A. Elliott, L.T. Bryndzia, J.F.W. Gale, and A. Fall, 2020, Origin of low salinity, high volume produced waters in the Wolfcamp Shale (Permian), Delaware Basin, USA, *Applied Geochemistry*, 122, 104771, <https://doi.org/10.1016/j.apgeochem.2020.104771>.
- Nunu, R.R., 2020, Using Geochemical and Statistical Analyses to Identify Local and Regional Flow to a Multi-Outlet Spring System: San Solomon Springs, Texas, USA, Master's Thesis, The University of Texas at San Antonio, 72p.
- Nunu, R.R., and Green, R., 2020, Development of a geochemical framework to characterize complex aquifer recharge-discharge relations: trans-Pecos, Texas, USA (abs.), GSA 2020 Connects Online 253-15.
- Ogilbee, W. and Wesselman, J.B., 1962, Geology and ground-water resources of Reeves County, Texas: Texas Water Commission Bulletin 6214, Volume I, 196pp. and Volume II, 243pp.

- Parker, D.F., 1988, The Davis Mountains volcanic field, west Texas, in Hayward, O.T., ed., DNAG, Centennial Field Guide, Volume 4, South-Central Section of the Geological Society of America: Denver, CO, Geological Society of America, p. 407-410.
- Parker, D.F., J.C. White, M. Ren, and M. Barnes, 2017, Basement control of alkalic flood rhyolite magmatism of the Davis Mountains volcanic field, Trans-Pecos Texas, U.S.A., *Lithos*, 292–293, p.234-249, <https://doi.org/10.1016/j.lithos.2017.09.011>.
- Pearson, B.T., 1985, Tertiary structural trends along the northeast flank of the Davis Mountains: in Dickerson, P.W. and Muehlberger, W.R., eds., *Structure and Tectonics of Trans-Pecos Texas: West Texas Geol. Soc. Publ.* 85-81, p.153-156.
- Piper, A.M., 1944, A graphic procedure in the geochemical interpretation of water-analyses, *Eos Trans. AGU*, 25(6), p.914–928, <https://doi.org/10.1029/TR025i006p00914>.
- Plummer, L.N., Busby, J.F., Lee, R.W., and Hanshaw, B.B., 1990, Geochemical Modeling of the Madison Aquifer in Parts of Montana, Wyoming, and South Dakota, *Water Resources Research*, 26(9), p.1981– 2014, <https://doi.org/10.1029/WR026i009p01981>.
- PRISM, 2018, PRISM Climate Group. Average Annual Precipitation for Texas (West) (1981-2010). http://prism.oregonstate.edu/projects/gallery_view.php?state=TX_W. Accessed August 13, 2018.
- Rees, R. and Buckner, A.W., 1980, Occurrence and quality of ground water in the Edwards-Trinity (Plateau) aquifer in the Trans-Pecos Region of Texas. Texas Department of Water Resources Report 255.
- Register, J.K., Brookins, D.G., 1980. Rb-Sr Isochron Age of Evaporite Minerals from the Salado Formation (Late Permian), vol. 29. southeastern New Mexico: Isochron-West, pp. 39–42.
- Robertson, W.M., Allen, J.T., Wolaver, B.D., and Sharp, J.M., 2019, Arid land spring response to mesoscale precipitation: implications for groundwater-dependent ecosystem sustainability, *Journal of Hydrology*, , Vol. 570, p.850-862, <https://doi.org/10.1016/j.jhydrol.2018.12.074>.
- Robertson, W.M. and Sharp, J.M. Jr., 2013, Variability of groundwater nitrate concentrations over time in arid basin aquifers: Sources, mechanisms of transport, and implications for conceptual models. *Environment and Earth Science*, 69, p.2415–2426, <https://doi.org/10.1007/s12665-012-2069-1>.
- Ruppel, S.C., Ed., 2019, Anatomy of a Paleozoic basin: the Permian Basin, USA, vol. 1, The University of Texas at Austin, Bureau of Economic Geology Report of Investigations 285; AAPG Memoir 118, 399p., <https://doi.org/10.23867/RI0285-1>.
- Ruppel, S.C., Ed., 2020, Anatomy of a Paleozoic Basin: The Permian Basin, USA, vol. 2, The University of Texas at Austin, Bureau of Economic Geology Report of Investigations 285; AAPG Memoir 118, 526p., <https://doi.org/10.23867/RI0285-2>.
- Saller, A. and A.M. Stueber, 2018, Evolution of formation waters in the Permian Basin, United States: Late Permian evaporated seawater to Neogene meteoric water. *AAPG Bull.*, 102(3), p.401–428, <https://doi.org/10.1306/0504171612517157>.
- Scanlon, B.R., Reedy, R.C., and Gates, J.B., 2010a, Effects of irrigated agroecosystems: 1. Quantity of soil water and groundwater in the southern High Plains, Texas, *Water Resour. Res.*, 46, W09537, <https://doi.org/10.1029/2009WR008427>.

- Scanlon, B.R., Gates, J.B., Reedy, R.C., Jackson, W.A., and Bordovsky, J.P., 2010b, Effects of irrigated agroecosystems: 2. Quality of soil water and groundwater in the southern High Plains, Texas, *Water Resour. Res.*, 46, W09538, <https://doi.org/10.1029/2009WR008428>.
- Scanlon, B.R., 1991, Evaluation of moisture flux from chloride data in desert soils, *Journal of Hydrology*, 128, p.137–156, [https://doi.org/10.1016/0022-1694\(91\)90135-5](https://doi.org/10.1016/0022-1694(91)90135-5).
- Schuster, S.K., 1997, Hydrogeology and local recharge analysis in the Toyah basin aquifer, Master's thesis, the University of Texas at Austin, 130pp.
- Sharp, J.M. Jr., 1989, Regional ground-water systems in northern Trans-Pecos Texas, *in* Muehlberger, W.R. and Dickerson, P.W., editors, *Structure and Stratigraphy of Trans-Pecos Texas*, 28th International Geological Congress Field Trip Guidebook T317, p.123-130.
- Sharp, J. M, Jr., 1990, Regional groundwater systems in northern Trans-Pecos Texas: *in* Kreitler, C. W. and Sharp, J. M., Eds, *Hydrogeology of Trans-Pecos Texas: The University of Texas at Austin, Bureau of Economic Geology, Guidebook 25*, p. 113-120.
- Sharp, J.M., Jr., Boghici, R., and Uliana, M., 2003, Groundwater systems feeding the springs of West Texas, *in* Garrett, G.P., and Allan, N.L., eds., *Aquatic fauna of the Northern Chihuahuan Desert. Special publications. Museum of Texas Tech University. Contributed papers form a special session within the thirty-third annual symposium of the Desert Fishes Council. 17 November 2001. Sul Ross State University, Alpine, Texas, Volume 46*, p. 1-11.
- Siegel, M.D., S.J. Lambert, and K.L. Robinson, 1991, *Hydrogeochemical Studies of the Rustler Formation and Related Rocks in the Waste Isolation Pilot Plant Area, Southeastern New Mexico*, Sandia National Laboratories report #SAND88-0196, variously paginated.
- Simonds, W.J., 1996, Balmorhea Project. *Historic Reclamation Projects. Bureau of Reclamation*, 21p.
- Small, T.A. and G.B. Ozuna, 1993, *Ground-water conditions in Pecos County, Texas, 1987*, U.S.G.S. Water-Resources Investigations Report 92-4190, 63p. <https://doi.org/10.3133/wri924190>.
- Smye, K., D.A. Banerji, R. Eastwood, G. McDaid, and P. Hennings, 2021, *Facies and Reservoir Properties of the Delaware Mountain Group of the Delaware Basin and Implications for Saltwater Disposal*, *Journal of Sedimentary Research*, in 2nd review
- Sneed, M., D.L. Galloway, and W.L. Cunningham, 2003, *Earthquakes-rattling the Earth's Plumbing System*, USGS Fact Sheet 096-03, 5pp.
- Standen, A., Finch, S., Williams, R., Lee-Brand, B., and Kirby, P., 2009, *Capitan reef complex structure and stratigraphy*, prepared for the Texas Water Development Board.
- Sun, C., Shanahan, T.M., and Partin, J., (2019), *Controls on the isotopic composition of precipitation in the south-central United States*, *Journal of Geophysical Research: Atmospheres*, 124, p.8320–8335, <https://doi.org/10.1029/2018JD029306>.
- TCEQ, 2017, Texas Commission on Environmental Quality (TCEQ). *Water Well Report Viewer v3.6*. <https://gisweb.tceq.texas.gov/waterwellpublic/>.
- TCEQ, 2019, Texas Commission on Environmental Quality (TCEQ), *Balmorhea Pool Discharge Canal C808*, https://www.tceq.texas.gov/cgi-bin/compliance/monops/water_site_photo.pl?cams=808, accessed March 1, 2019.

Thode, H.G. and J. Monster, 1965, Sulfur-isotope geochemistry of petroleum, evaporites, and ancient seas, *in* Fluids in Subsurface Environments, A. Young and J.E. Galley (Eds), p.369-377, <https://doi.org/10.1306/M4360C15>.

Thomas, J.V., Stanton, G.P., Bumgarner, J.R., Pearson, D.K., Teeple, A.P., Houston, N.A., Payne, J.D., and Musgrove, M., 2013, A conceptual hydrogeologic model for the hydrogeologic framework, geochemistry, and groundwater-flow system of the Edwards-Trinity and related aquifers in the Pecos County region, Texas, U.S. Geological Survey Fact Sheet 2013–3024, 6pp.

TWDB, 2005, Diminished spring flows in the San Solomon Springs System, Trans-Pecos, Texas, report prepared for Texas Parks & Wildlife, [very similar to Chowdhury et al. (2004)]

TWDB, n.d.1, Groundwater Database, <https://www.twdb.texas.gov/groundwater/data/gwdbbrpt.asp>, last accessed on April 2021.

TWDB, n.d.2, Brackish Resources Aquifer Characterization System (BRACS) Database, <https://www.twdb.texas.gov/innovativewater/bracs/database.asp>, last accessed on April 2021.

TWDB, 2017, Texas Water Development Board, Submitted Driller's Report Database. <http://www.twdb.texas.gov/groundwater/data/drillersdb.asp>.

TWDB, 2019a, Texas Water Development Board (TWDB), Automated Groundwater Level Wells. State Well Numbers 4644501, 4652404. <https://waterdatafortexas.org/groundwater>, accessed October 19, 2018.

TWDB, 2019b, Texas Water Development Board (TWDB), Submitted Drillers Reports (SDR) Database. <https://www.twdb.texas.gov/groundwater/data/drillersdb.asp>, accessed Feb 1, 2019.

TWDB, 2019c, Texas Water Development Board, Groundwater Database. <http://www.twdb.texas.gov/groundwater/data/gwdbbrpt.asp>, accessed February 1, 2019.

Tyler, R.C., 2020, Trans-Pecos desert legends and rugged grandeur, *in* Chapman, B.R., and Bolen, E.G., 2018, The Natural History of Texas, Chapter 9, Texas A&M University Press, College Station, Texas, 390pp., p.170-200.

Uliana, M.M., 2000, Delineation of regional groundwater flow paths and their relation to structural features in the Salt and Toyah basins, Trans-Pecos Texas, The University of Texas at Austin PhD dissertation, 215pp., available online.

Uliana, M.M. and Sharp, J.M. Jr., 2001, Tracing regional flow paths to major springs in Trans-Pecos Texas using geochemical data and geochemical models, *Chemical Geology*, 179, p.53-72, [https://doi.org/10.1016/S0009-2541\(01\)00315-1](https://doi.org/10.1016/S0009-2541(01)00315-1).

Uliana, M.M., Banner, J.L., and Sharp J.M. Jr., 2007, Regional groundwater flow paths in Trans-Pecos, Texas inferred from oxygen, hydrogen and strontium isotopes, *Journal of Hydrology*, 334, p.334-346, <https://doi.org/10.1016/j.jhydrol.2006.10.015>.

Uliana, M.M., 2001, The geology and hydrogeology of the Capitan Aquifer: A brief overview, Chapter 11 *in* Mace, R. E., Mullican, W. F., and Angle, E. S., eds., *Aquifers of West Texas*. Report 356. Texas Water Development Board: Austin, TX, Texas Water Development Board, p.153-166.

- Unmack, P.J. and Minckley, W. L., 2008, The demise of desert springs, *in* L.E. Stevens and V.J. Meretsky (eds), *Arid land springs in North America: ecology and conservation*, University of Arizona Press, Tucson, Chapter 2, 25pp.
- Urbanczyk, K., Rohr, D., and White, J. C., 2001, Geologic History of West Texas, *in* Mace, R. E., Mullican, W.F., and Angle, E.S. (eds), *Aquifers of West Texas*. Report 356, Chapter 2. Texas Water Development Board, Austin, TX, p.17-25.
- Veizer, J., 1989. Strontium isotopes in seawater through time, *Annual Review of Earth and Planetary Science*, 17, p.141-167, <https://doi.org/10.1146/annurev.ea.17.050189.001041>.
- Veizer, J., D. Ala, K. Azmy, et al., 1999, $^{87}\text{Sr}/^{86}\text{Sr}$, $\delta^{13}\text{C}$ and $\delta^{18}\text{O}$ evolution of Phanerozoic seawater, *Chemical Geology*, 161(1–3), p.59-88, [https://doi.org/10.1016/S0009-2541\(99\)00081-9](https://doi.org/10.1016/S0009-2541(99)00081-9).
- Veni, G., 2013, Impact of climate change on human and ecological use of karst groundwater resources: A case study from the southwestern USA, *NCKRI Symposium 3, 20th National Cave and Karst Management Symposium*, p.51-59.
- Walvoord, M.A. and F.M Phillips, 2004, Identifying areas of basin-floor recharge in the Trans-Pecos region and the link to vegetation, *Journal of Hydrology*, 292, p.59-74, <https://doi.org/10.1016/j.jhydrol.2003.12.029>.
- Warner, N. R., Darrah, T. H., Jackson, R. B., Millot, R., Kloppmann, W., and Vengosh, A., 2014, New Tracers Identify Hydraulic Fracturing Fluids and Accidental Releases from Oil and Gas Operations, *Environmental Science & Technology*, 48(21), p. 12552-12560, <https://doi.org/10.1021/es5032135>.
- White, W.N., H.S. Gale, and S.S. Nye, 1938, *Geology and ground-water resources of the Balmorhea area, western Texas*, Texas Water Development Board report #M011, 80pp.
- White, W.N., H.S. Gale, and S.S. Nye, 1941, *Geology and ground-water resources of the Balmorhea area, western Texas*, U.S. Geological Survey Water Supply Paper 849-C, *in* *Contributions to the hydrology of the United States*, p.83-146, <https://doi.org/10.3133/wsp849C>.
- Wilkins, D. and D. Currey, 1997, Timing and Extent of Late Quaternary Paleolakes in the Trans-Pecos Closed Basin, West Texas and South-Central New Mexico. *Quaternary Research*, 47, p.306-315, <https://doi.org/10.1006/qres.1997.1896>.
- Wolaver, B., A. Sun, T. Caldwell, R. Smyth, P. Mickler, T. Bongiovanni, J. P. Pierre, J. Sharp, M. Uliana, and C. Breton, 2019, Report on Year One Preliminary Results: Hydrogeologic Evaluation and Vulnerability Analysis for Balmorhea-Area Springs, Prepared for Apache Corporation, April 2, 2019, 52pp.
- Wong, C.I., J.L. Banner, M.L. Musgrove, 2015, Holocene climate variability in Texas, USA: An integration of existing paleoclimate data and modeling with a new, high-resolution speleothem record, *Quaternary Science Reviews*, 127, p.155-173, <https://doi.org/10.1016/j.quascirev.2015.06.023>.
- Zhang, J., Howard, K., Langston, C., Kaney, B., Qi, Y. C., Tang, L., Grams, H., Wang, Y. D., Cocks, S., Martinaitis, S., Arthur, A., Cooper, K., Brogden, J., and Kitzen, D., 2016, Multi-Radar Multi-Sensor (MRMS) Quantitative Precipitation Estimation, Initial Operating Capabilities, *Bulletin of the American Meteorological Society*, v. 97, p. 621-637.

Tables

Table 1 BEG monitoring wells

Table 1. BEG monitoring well characteristics.

Well Name	latitude ¹	longitude ¹	Depth Drilled (ft bgl ²)	Screened Interval (ft bgl)	Blank Casing ³ (ft bgl)	Casing Height (ft agl ⁴)	July/Aug 2020 TD (ft btoc ⁵)	July/Aug 2020 WL (ft btoc)	Logger Depth (ft btoc)	Logger Installation Date	Development Flow Rate (gpm ⁶)	BEG WQ Sample ID
BEG Cherry Shallow MW	30.9082	-104.0103	20	0 - 20	0 - 20	1.6	20.3	dry	18	8/1/2020	not developed	--
BEG Cherry Deep MW	30.9081	-104.0103	420	380 - 420	0 - 380	1.0	420.0	318	370	8/1/2020	20	WTX-SRMWD
BEG Cherry Ultra Deep			780			1.0	430.0	dry	Plugged and abandoned on 7/31/2020			
BEG Cherry Lodge MW	30.8635	-104.0481	600	torch slots 560 - 600	steel csg. 10 - 560	1.6	602.2	471	550	8/4/2020	18	WTX-SRMWL
BEG 4J Shallow MW	30.8795	-103.9557	60	0 - 60	n/a	1.7	63.5	dry	60	8/2/2020	not developed	--
BEG 4J Deep MW	30.8794	-103.9557	500	420 - 500	0 - 420	1.6	499.3	379	485	8/2/2020	not developed	--
BEG BigA Shallow MW	30.8171	-103.8359	20	0 - 20	--	1.4	21.1	18	19.5	8/3/2020	not developed	--
BEG BigA Deep MW	30.8170	-103.8361	560	140 - 180 540 - 560	0 - 140 180 - 540	1.0	561.3	dry	500	8/3/2020	1	--
BEG BSP MW	30.9457	-103.7855	40	20-40	0 - 20	1.0	41.8	17	35	7/28/2020	12	WTX-BSPMWS
BEG Sandia Shallow MW	30.9795	-103.7411	80	20-40	0 - 20 40 - 80	1.3	71.0	21	52	7/30/2020	12	WTX-SPMWS
BEG Sandia Deep MW	30.9795	-103.7411	560	open borehole below 60 ft	--	1.0	355.0	52	251	8/3/2020	not developed	--
BEG Limpia Shallow MW	30.7793	-103.7294	83	35 - 75	0 - 35	0.8	75.0	29	60	8/2/2020	12	WTX-LLMWS
BEG Limpia Deep MW	30.7792	-103.7293	200	160 - 200	0 - 160	0.6	199.5	162	185	8/2/2020	2	--

NOTES: 1. measured with Garmin set to WGS-84 datum; 2. bgl = below ground level; 3. 4.5-inch CertaLock PVC; 4. agl = above ground level; 5. btoc = below top of casing; 6. gpm = gallons per minute.

Table 2 Loggers

Table 2. Location and simplified characteristics of the InSitu[®] loggers. Map shown in Figure 13.

Site Name	lat	long	Equipment*	Map symbol	Logger elevation	BaroTROLL Location**
BEG 4J Deep MW	30.87942	-103.95566	AquaTroll200; NV; 60m	green triangle	4062	TNC DMP
Hamilton WM Well	30.93682	-103.85253	AquaTroll200; NV; 60m	yellow triangle	3550	BSP TexNet
Phantom Lake Spring	30.93491	-103.84963	AquaTroll200; NV; 60m	yellow square	3491	BSP TexNet
BEG Limpia Deep MW	30.77921	-103.72929	AquaTroll200; NV; 60m	green triangle	4098	TNC DMP
BEG Limpia Shallow MW	30.77931	-103.72934	AquaTroll200; NV; 60m	red triangle	4091	TNC DMP
Huelster #3 Well	30.91719	-103.84583	AquaTroll200; NV; 60m	red triangle	3507	BSP TexNet
BEG BigA Deep MW	30.81702	-103.83605	AquaTroll200; NV; 60m	green triangle	3852	BSP TexNet
Big Aguja Stream	30.77882	-103.85332	AquaTroll200; NV; 60m	red diamond	4085	TNC DMP
Seven Springs	30.835267	-103.792873	AquaTroll200; NV; 60m	red square	3806	BSP TexNet
Giffin Spring	30.944574	-103.789858	AquaTroll200; NV; 60m	yellow square	3327	BSP TexNet
BEG Cherry Deep MW	30.9081	-104.01026	AquaTroll200; NV; 60m	green triangle	4291	TNC DMP
Cherry Lower Well	30.88781	-104.03017	AquaTroll200; NV; 60m	red triangle	4455	TNC DMP
Willow Spring	30.87003	-104.06337	AquaTroll200; NV; 60m	red square	4744	TNC DMP
BEG BSP MW	30.94572	-103.78548	AquaTroll200; NV; 60m	yellow triangle	3196	BSP TexNet
San Solomon Spring (1)	30.94423	-103.7886	AquaTroll200; NV; 60m	yellow square	3320	BSP TexNet
San Solomon Spring (2)	30.94423	-103.7886	AquaTroll200; NV; 60m	yellow square	3320	BSP TexNet
BEG Sandia Deep MW	30.97951	-103.74106	AquaTroll200; NV; 60m	green triangle	3196	BSP TexNet
BEG Sandia Shallow MW	30.97952	-103.74106	AquaTroll200; NV; 60m	yellow triangle	3196	BSP TexNet
East Sandia Spring	30.990829	-103.729207	AquaTroll200; NV; 60m	yellow square	3159	BSP TexNet
Madera Lower Stream	30.85345	-103.98859	RuggedTroll 100, 30m	red diamond	4324	TNC DMP
Little Aguja Stream	30.81164	-103.94199	RuggedTroll 100, 9m	red diamond	4386	TNC DMP
Limpia Lower Stream	30.76666	-103.75063	RuggedTroll 100, 9m	red diamond	4154	TNC DMP
Cherry Lower Stream	30.87619	-104.04426	RuggedTroll 100, 9m	red diamond	4577	TNC DMP
BSP Drain Canal	30.94531	-103.78529	missing as of 6/2021	yellow diamond	3307	BSP TexNet
Limpia Upper Stream	30.60136	-103.91577	RuggedTroll 100, 9m	red diamond	4921	TNC DMP
Madera Upper Stream	30.69186	-104.12471	RuggedTroll 100, 9m	red diamond	5945	TNC DMP
Cherry Upper Stream	30.76238	-104.11393	RuggedTroll 100, 30m	red diamond	5719	TNC DMP
BEG Lodge MW	30.86346	-104.04812	RuggedTroll; NV; 30m	red triangle	4659	TNC DMP
BEG 4J Shallow MW	30.87946	-103.95571	RuggedTroll; NV; 9m	brown triangle	4062	TNC DMP
BEG BigA Shallow MW	30.81707	-103.8359	RuggedTroll; NV; 9m	red triangle	3852	BSP TexNet
BSP TexNet Baro	30.943702	-103.781092	RuggedBaro TROLL	gray circle	3310	N/A
Madera Creek Baro	30.700711	-104.114657	RuggedBaro TROLL	gray circle	5896	N/A

* NV = non-vented

** TNC DMP = The Nature Conservancy Davis Mountain Preserve; BSP TexNet = Balmorhea State Park TexNet station

Table 3 WellIntelTable 3. BEG WellIntel[®] installations.

Well ID	Name	Total Depth (ft)	Longitude	Latitude	Date Installed	Aquifer	Sensor Elevation (ft amsl)
52-01-301*	MVWSC McIntire #1	450	-103.8976	30.9823	9/24/2019	Cretaceous	1,123
52-02-410*	Huelster Well	230	-103.8514	30.9201	9/24/2019	Alluvial-Igneous	1,075
96566**	Wildcat Draw	1,025	-103.9658	30.9193	9/25/2019	Cretaceous/Igneous	1,228
52-01-404*	Pole Pen	275	-103.9851	30.9217	9/25/2019	Igneous	1,269
52-01-801*	Timber Mountain Ranch	757	-103.9354	30.8770	9/26/2019	Cretaceous	1,239
52-01-201*	HWM2 5201201well	150	-103.9189	30.9591	9/26/2019	Igneous	1,138
N/A***	Weinacht Stock Well	N/A	-103.7727	31.0154	9/25/2019	Alluvial-Cretaceous	983
52-03-323*	Holderman 5203323	699	-103.6289	30.9886	1/28/2020	Alluvial-Cretaceous	905

*: TWDB ID number [State Well Numbers (SWN)]

**: Submitted Drillers Records (SDR) ID number

***: no number (old well)

Table 4 Well data potentiometric

Table 4. Well data (2010-2020) for water table/potentiometric surfaces

Aquifer ID (this report)	Formal Aquifer IDs	# of Wells
Recent Pecos Valley	Alluvial	38
	Pecos Valley	25
	Pecos Valley/Edwards Trinity Plateau	1
	Edwards Trinity Plateau/Other	1
	Total Wells	64
	WL Elevation Range (ft amsl)	2339-2821
Recent West Texas Bolson	Alluvial	10
	West Texas Bolson	29
	West Texas Bolson/Other	7
	Igneous	1
	Other (Alluvial/Cretaceous)	1
	Total Wells	48
WL Elevation Range (ft amsl)	3466-4377	
Cenozoic Igneous	Igneous	85
	Igneous/Other	1
	Cretaceous	1
	Total Wells	87
WL Elevation Range (ft amsl)	3218-6350	
Cretaceous Edwards- Trinity Plateau	Alluvial	6
	Pecos Valley	2
	Pecos Valley/Edwards-Trinity Plateau	1
	Edwards-Trinity Plateau	12
	Cretaceous	15
	Permian Age Aquifer	2
	Other	3
	Not defined	20
	Total Wells	61
WL Elevation Range (ft amsl)	2466-3792	
Permian	Alluvial	1
	Igneous	1
	Permian, undifferentiated	1
	Rustler	5
	Capitan	2
	Not defined	8
	Total Wells	18
WL Elevation Range (ft amsl)	2660-4242	

Figures

Figure 1 Location map

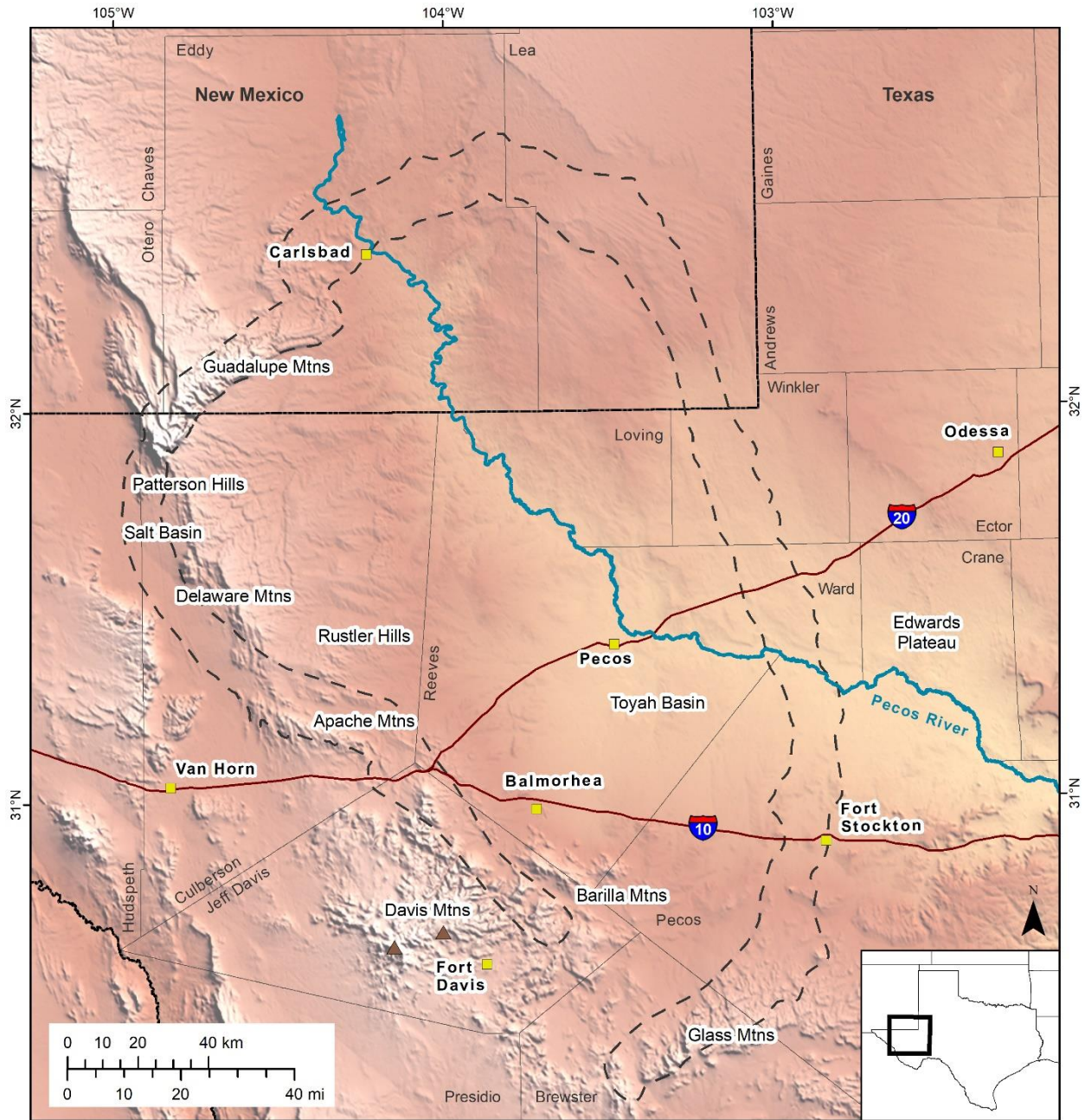


Figure 1. Balmorhea spring location within the Delaware Basin and other geographic and topographic features. The footprint of the Capitan Reef is shown with dotted lines. Mount Locke (east) and Mount Livermore (west) in the Davis Mountains are shown by 2 brown triangles.

Figure 2 West Texas springs

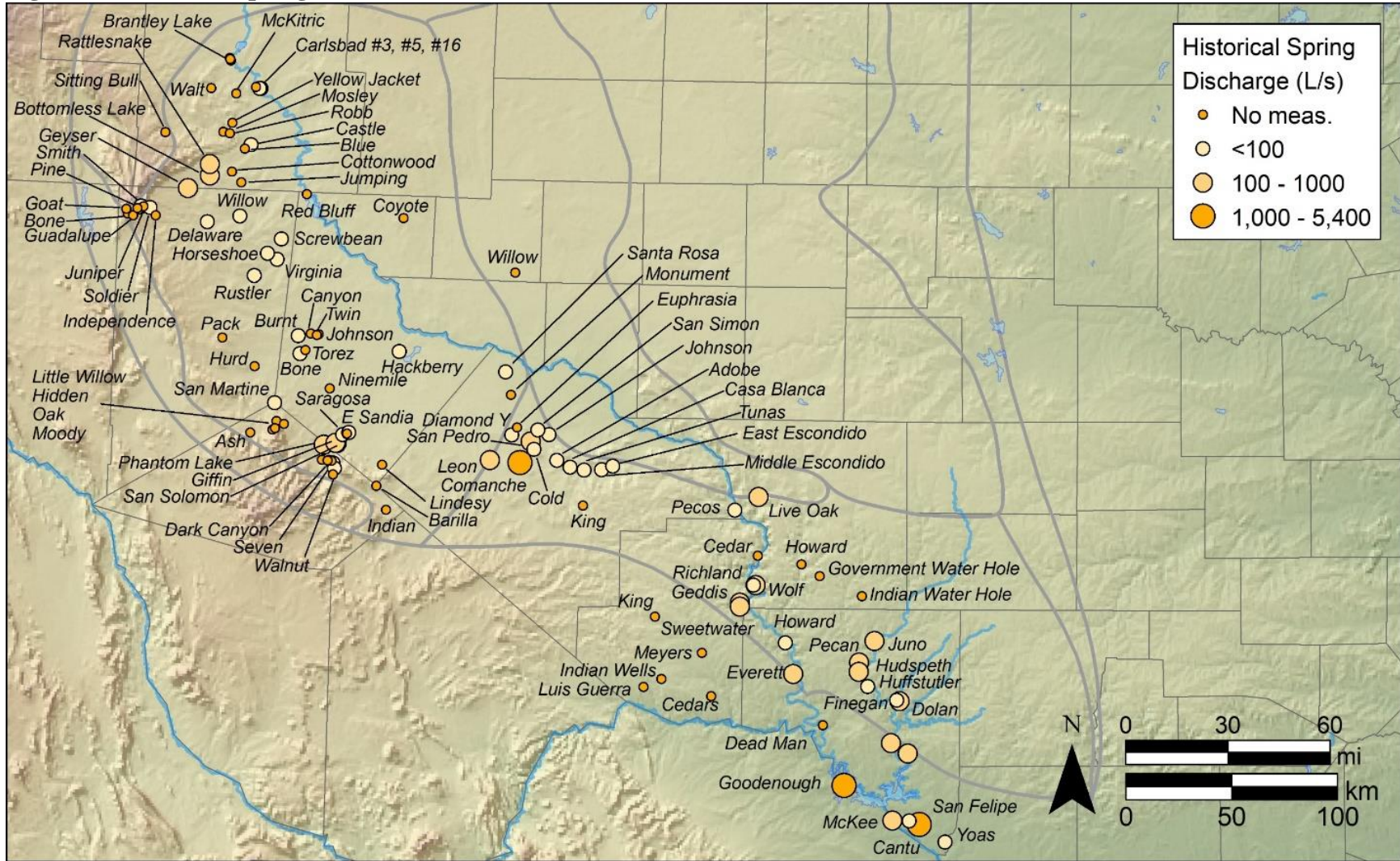


Figure 2. Major Springs of Trans-Pecos Texas. 100 L/s = 3.53 cfs = 1585 gpm.

Figure 3 Precipitation map

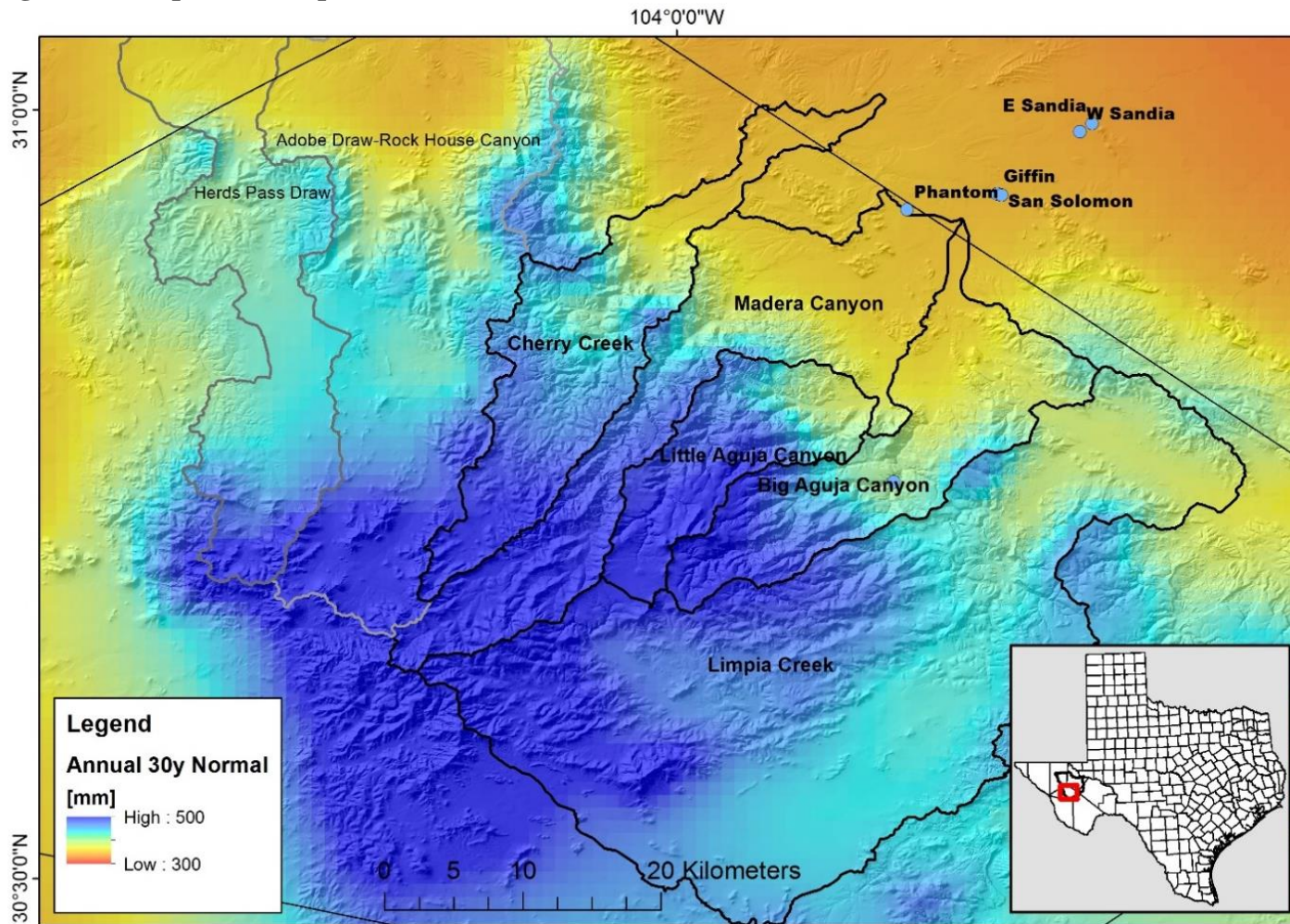


Figure 3. Mean gridded annual precipitation (1981-2010) over the Davis Mountains. The ephemeral recharge component is focusing on Cherry Creek, Madera Canyon, Little and Big Aguja Canyons and Limpia Creek watersheds. Storm waters in these channels are likely fast flow paths to the Balmorhea area springs (blue dots). Source: PRISM (2019, precipitation), USGS (2019, watersheds).

Figure 4 Historical spring flow

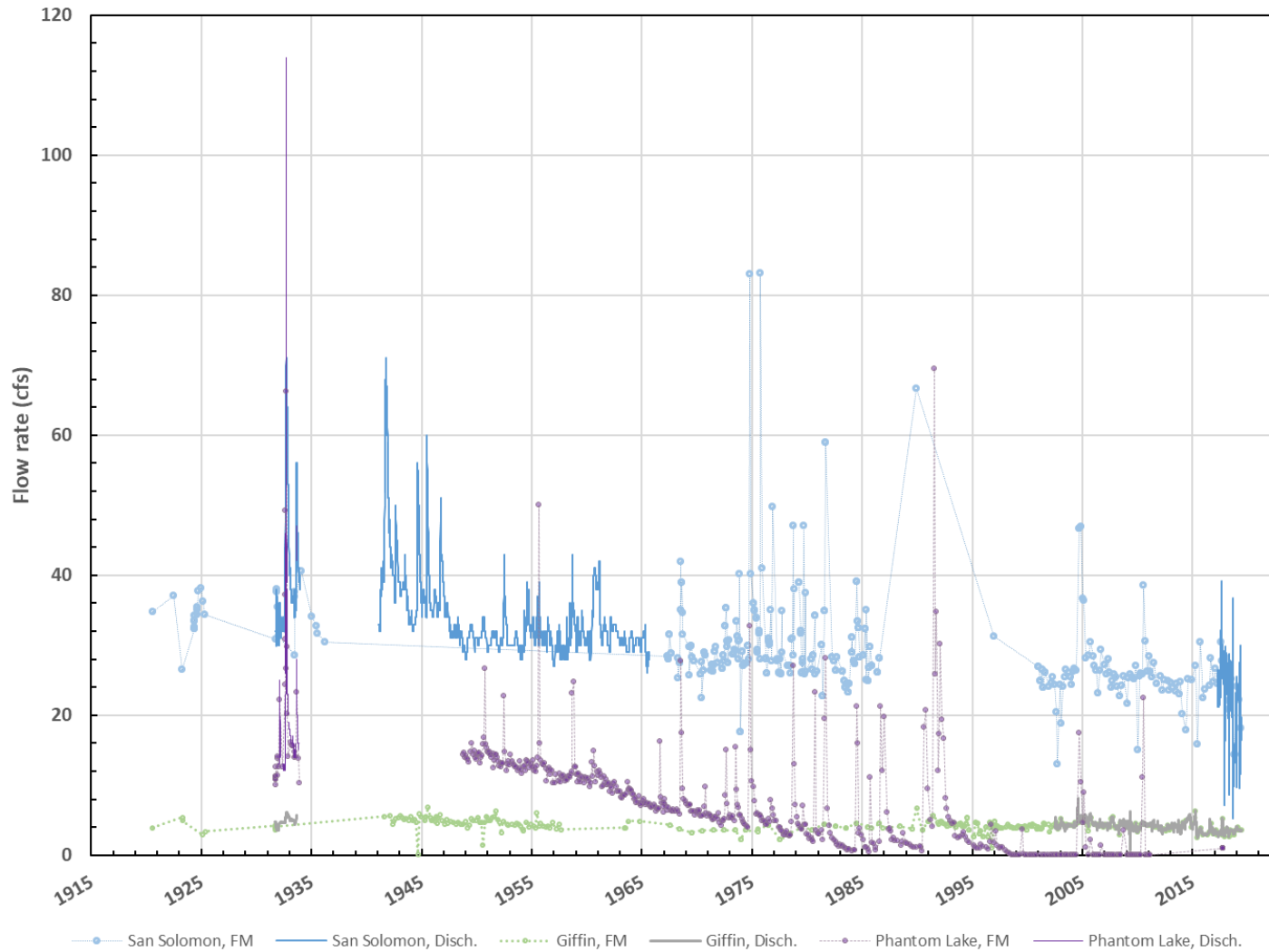


Figure 4. Historical spring flow showing quick decline at Phantom Lake Spring, slow decline at San Solomon Spring, and approximately constant but low flow rate at Giffin Spring. Sources: White et al. (1941), Brune (1976), Sharp et al. (2003), USGS (2020).

Figure 5 Map of watersheds

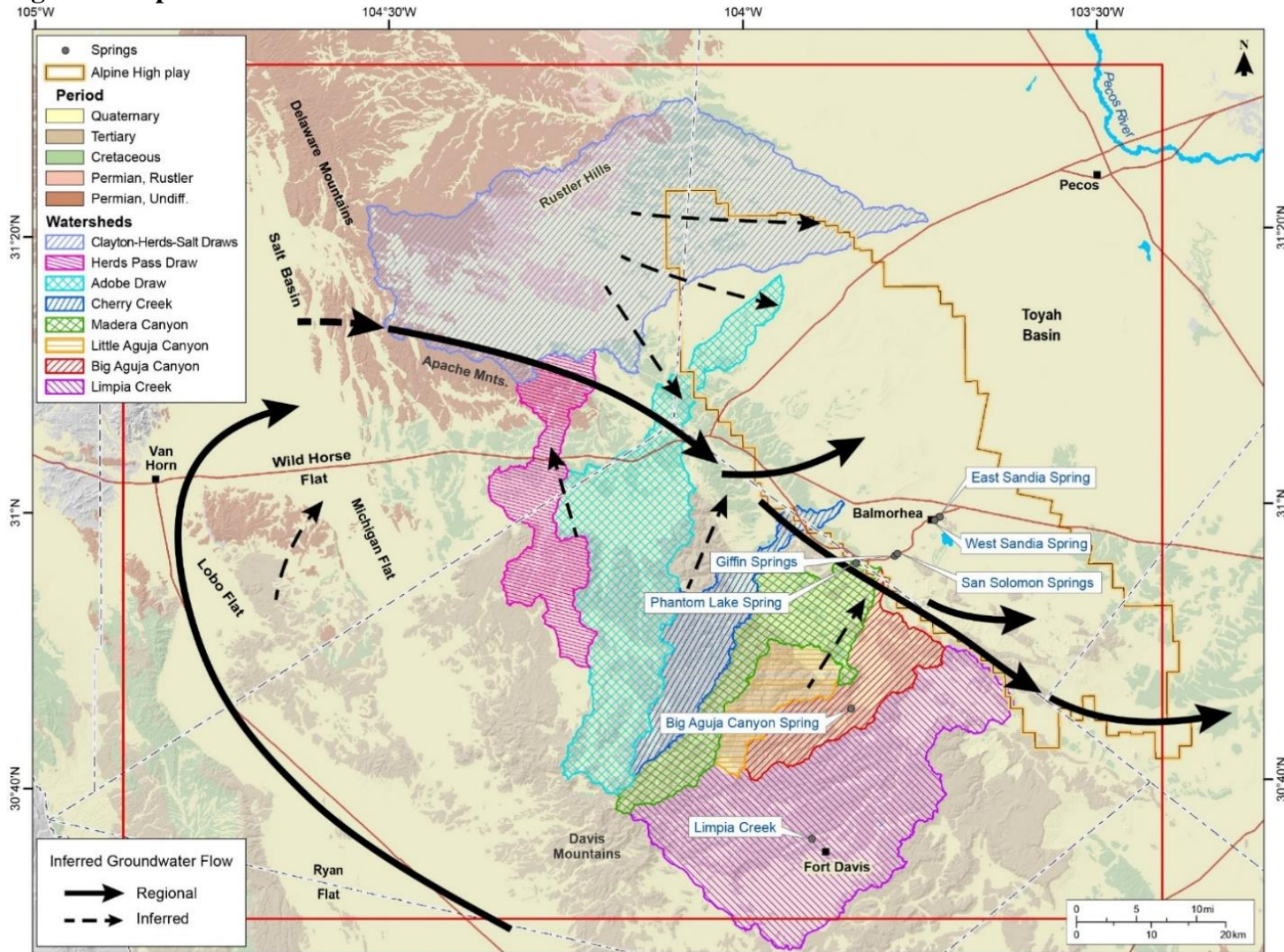
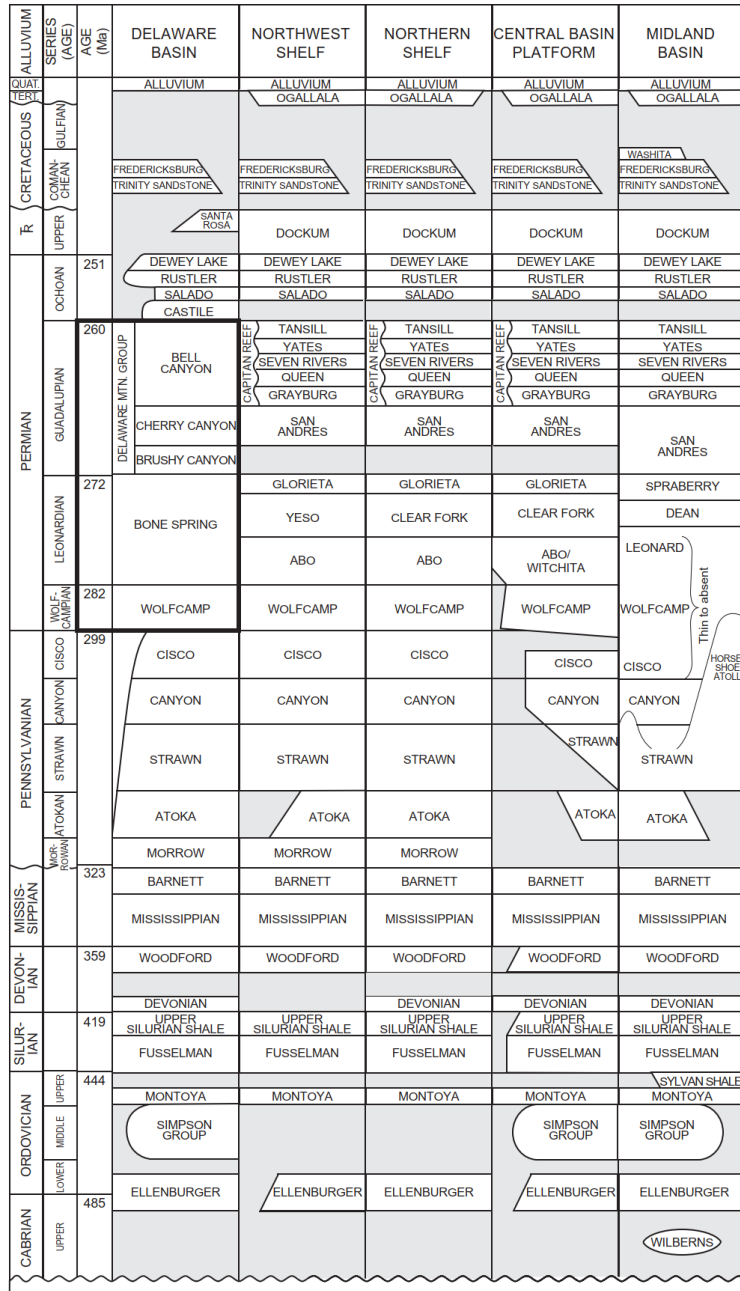


Figure 5. Map of watersheds and historic generally agreed-upon groundwater flow systems. Sources: Darling (1997), Sharp (2001; Fig.3), Sharp et al. (2003; Fig.4-1), Chowdhury et al. (2004; Fig.17-1), Uliana (2001; Fig.1), Uliana et al. (2007; Fig.1).

Figure 6 Stratigraphic column



QAe8613

Figure 6. Stratigraphic column of various components of the Permian Basin. The Balmorhea spring complex is located at the southern edge of the Delaware Basin.

Figure 7 cross section

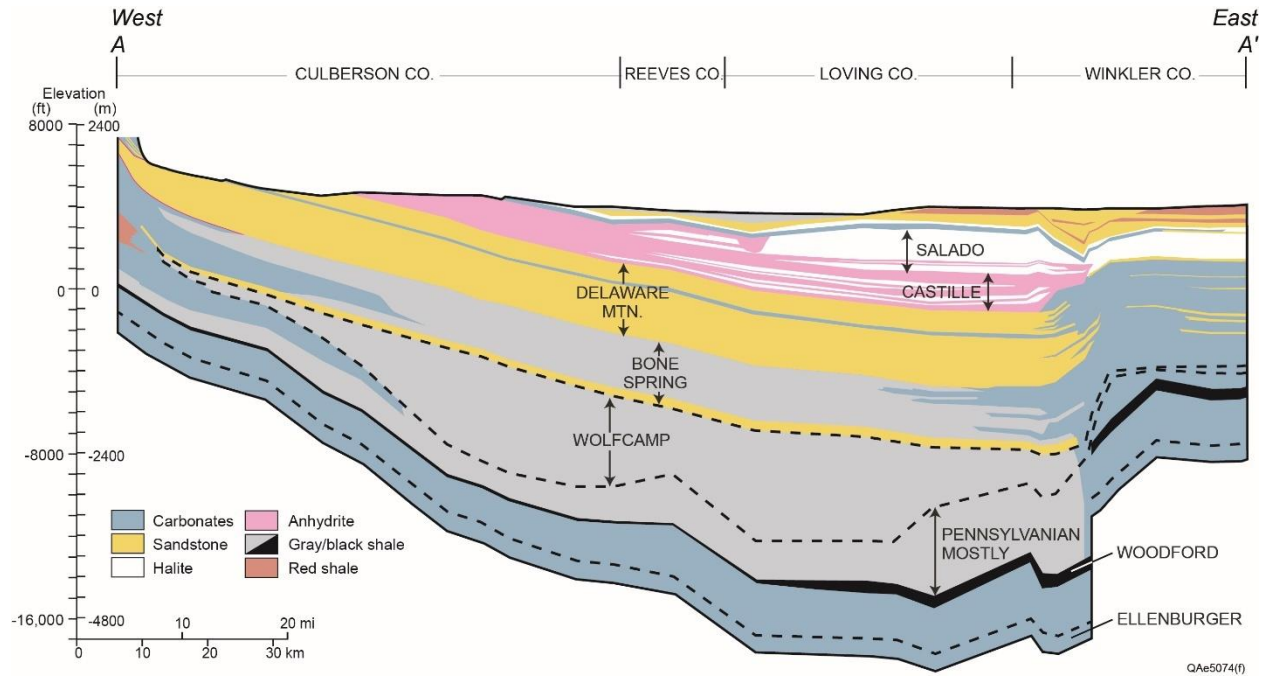


Figure 7. Generalized E-W cross-section of the Delaware Basin (modified from Matchus and Jones, 1984) going through Loving County, south of the Texas-New Mexico state line. The cross section illustrates the relationship between late Permian (Rustler, thin grey strip above the Salado) and post-Permian layers on one side and other Paleozoic layers on the other side. The cross-section shows the Guadalupe Mountains and the Capitan outcrop as well as the DMG and Rustler outcrops. Note that the general topographic slope is to the East. In the Balmorhea area, most of the grey-colored Pennsylvanian, Wolfcamp, and Bone Spring are condensed in a much thinner interval.

Figure 8 Monitoring well locations

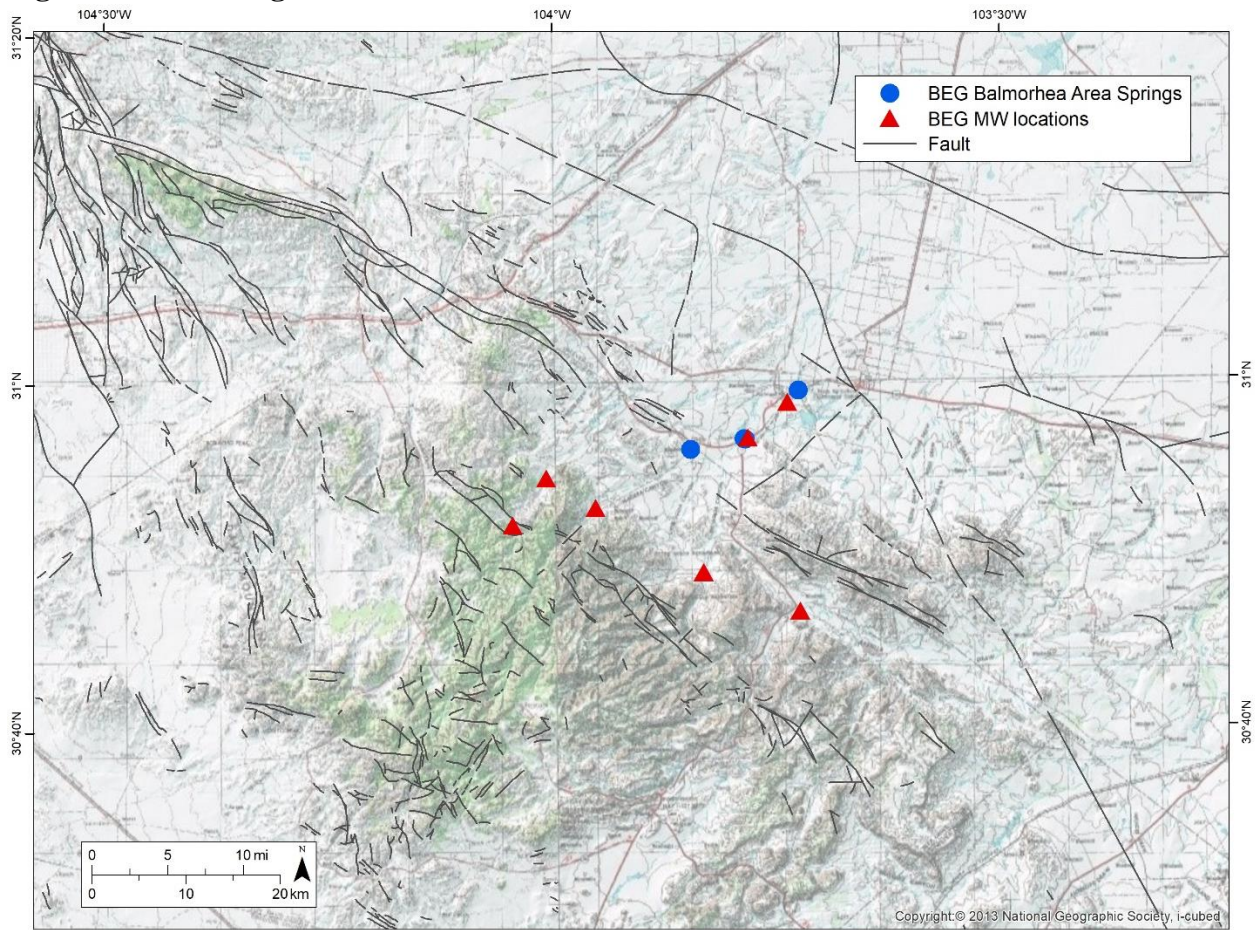


Figure 8. BEG-drilled monitoring well locations.

Figure 9 Depths of BEG wells

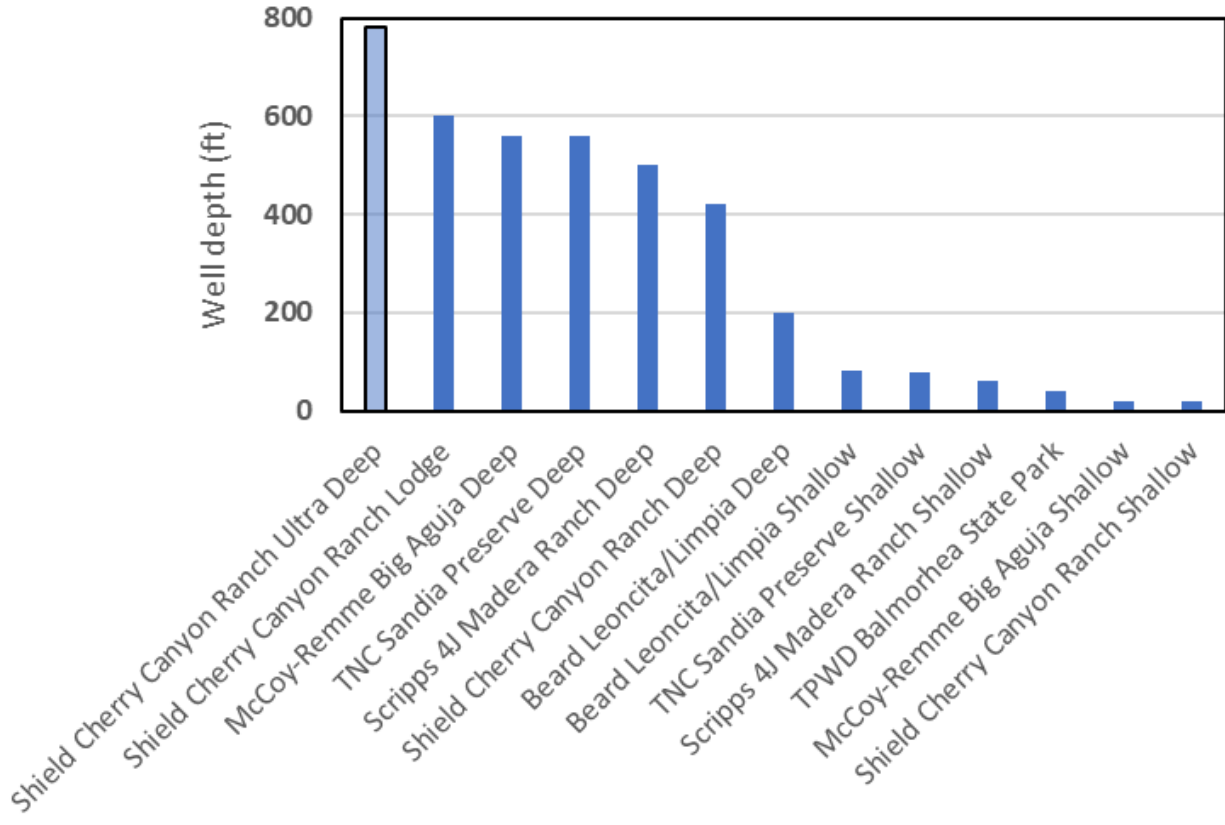


Figure 9. Sorted histogram of BEG-drilled well depths

Figure 10 Map of geochemical samples

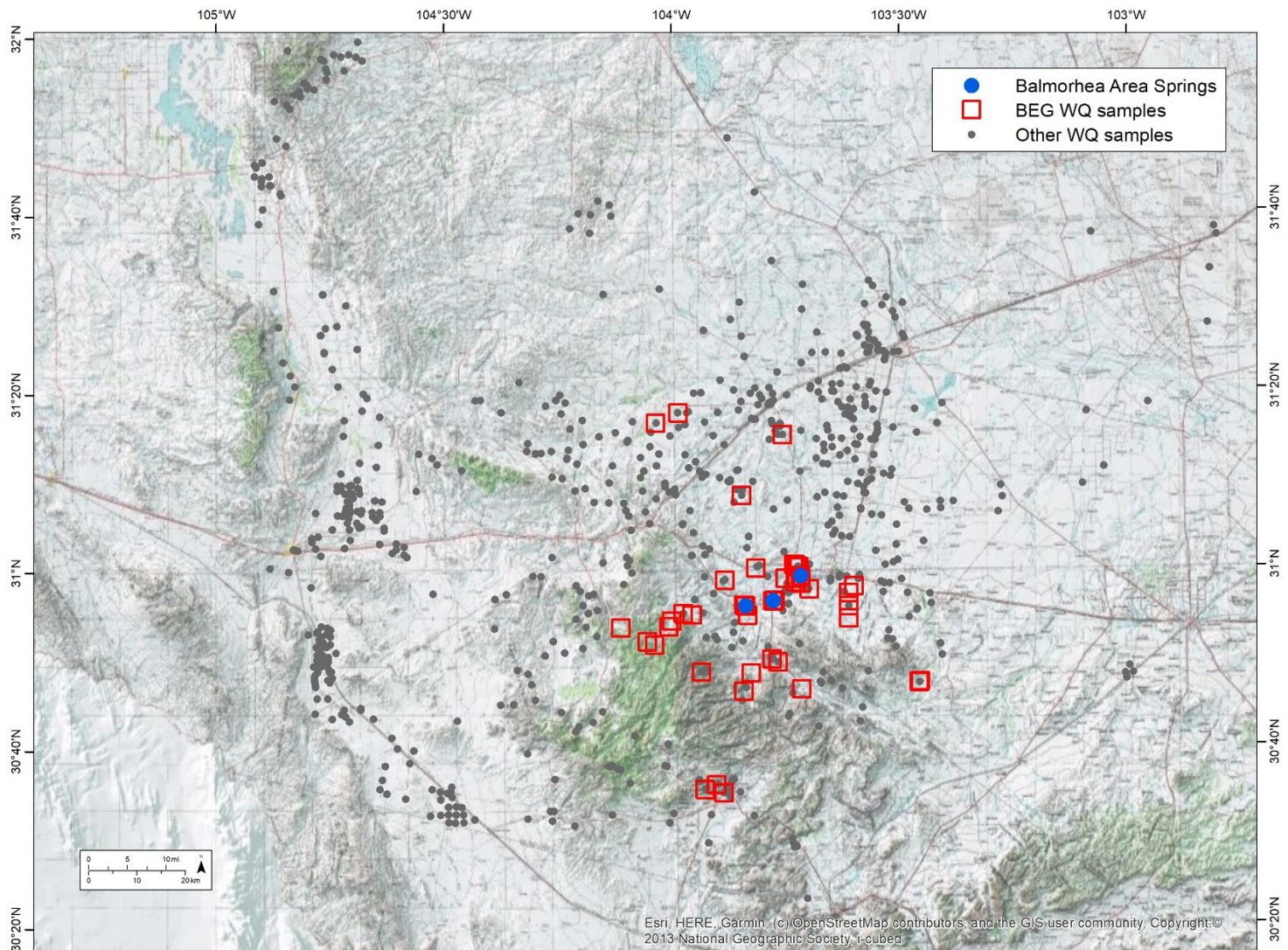


Figure 10. Location map of BEG and other geochemical samples.

Figure 11 Spring sampling

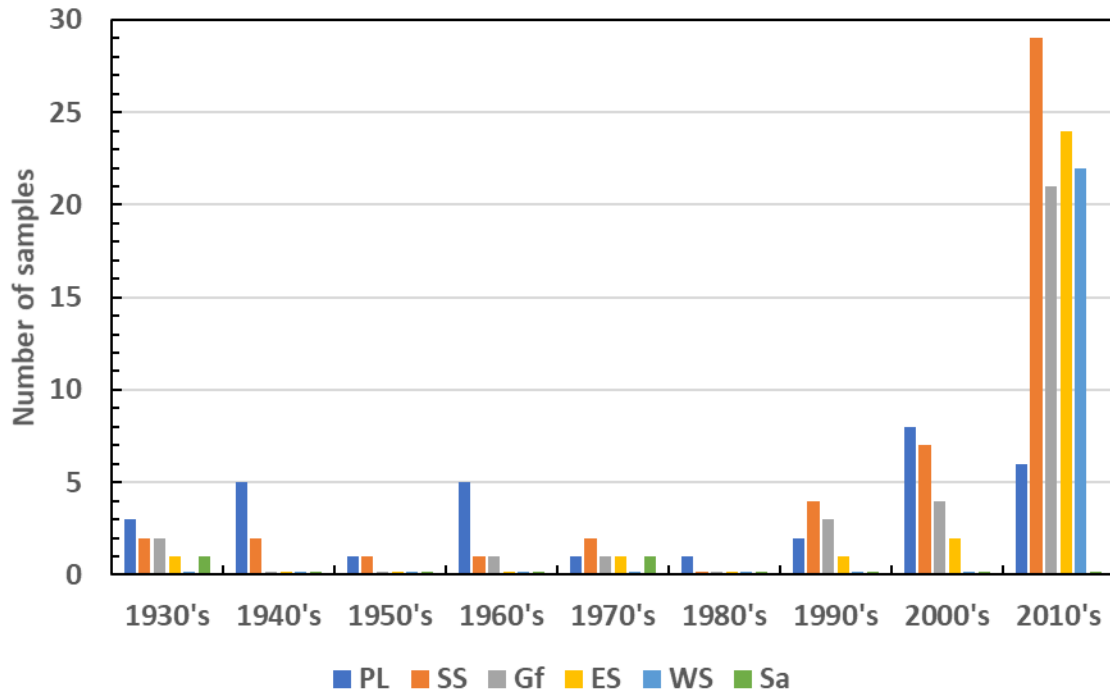
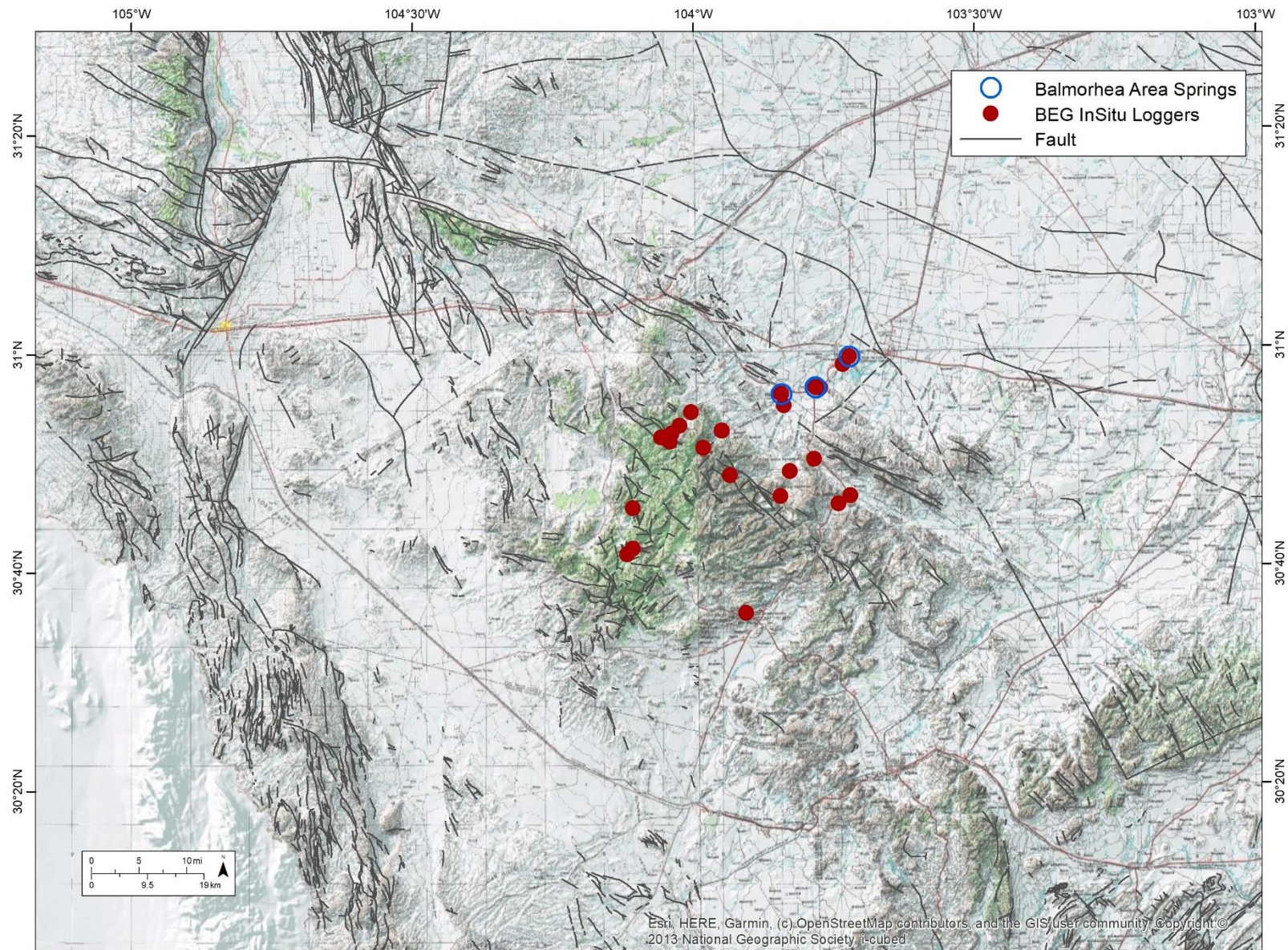


Figure 11. Spring sampling time distribution; PL = Phantom Lake; SS = San Solomon; Gf = Giffin; ES = East Sandia WS = West Sandia; Sa = Saragosa.

Figure 12 Well logger and WellIntel[®] acoustic sounder locations



(a)

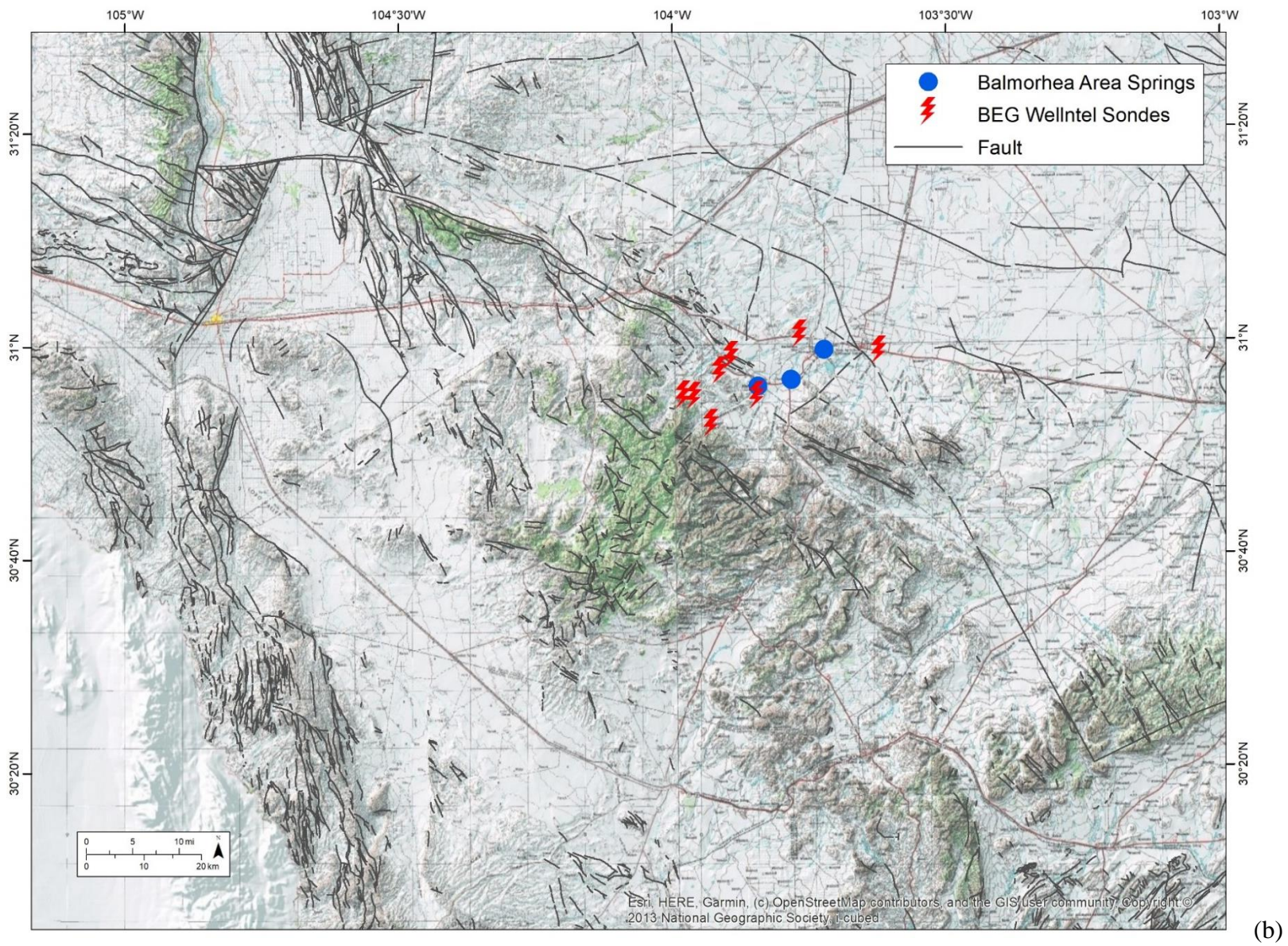


Figure 12. Well loggers (a) and WellIntel® (b) generalized locations.

Figure 13 Well loggers (details)

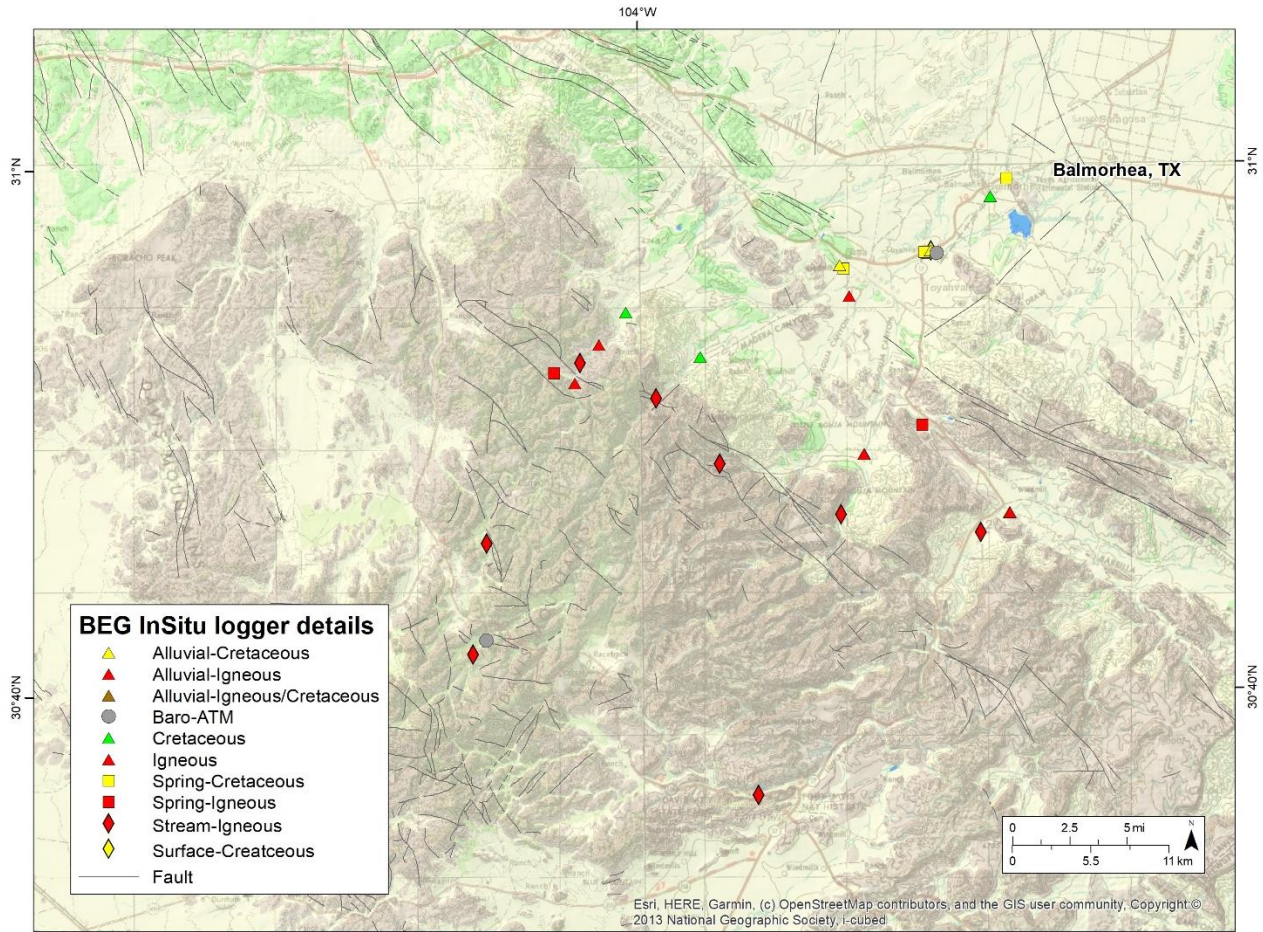


Figure 13. Locations of InSitu[®] loggers. Symbols indicate the following: triangles = wells, circles = barometric control, squares = springs, diamonds = streams or surface water. Color-coding indicates: yellow = alluvial, red = igneous, green = Cretaceous.

Figure 14 Timeline of logger data

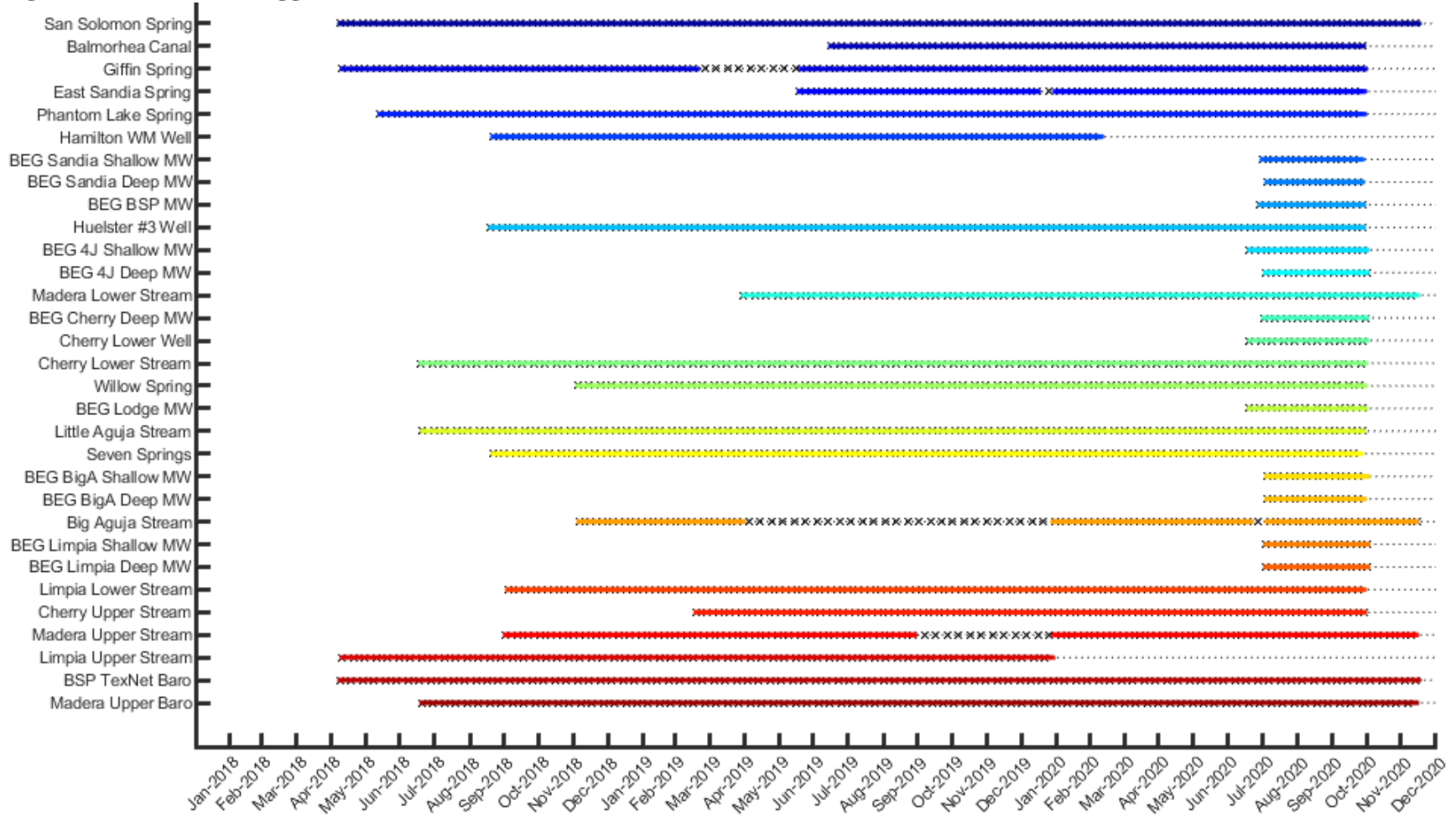


Figure 14. Time line of logger data. Data is still being recorded in 2021 for most loggers but can only be downloaded on site. The symbol “xxx” outlines non-recording periods due to malfunctioning and other factors; the dotted lines with no color represent loggers in place but no data download for the period. Note that many loggers were only recently installed. All loggers are still recording as of early June 2021.

Figure 15 Timeline of WellIntel® sounders

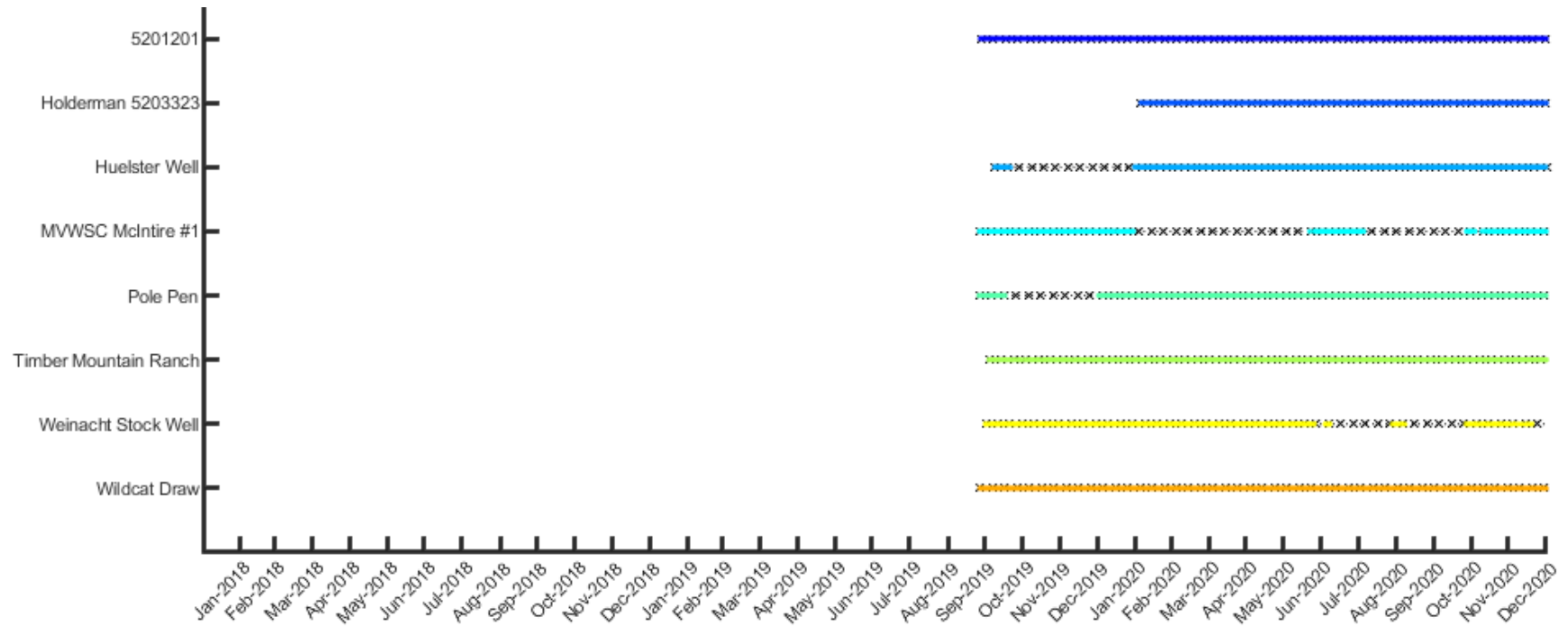


Figure 15. Time line of WellIntel® data. The symbol “xxx” outlines non-recording periods due to malfunctioning and other factors. The WellIntel® system has a remote connection that allows access to the data in real time. Note that the sounders became operational only half-way through the project. All sounders were still operational as of early June 2021.

Figure 16 Map water level wells

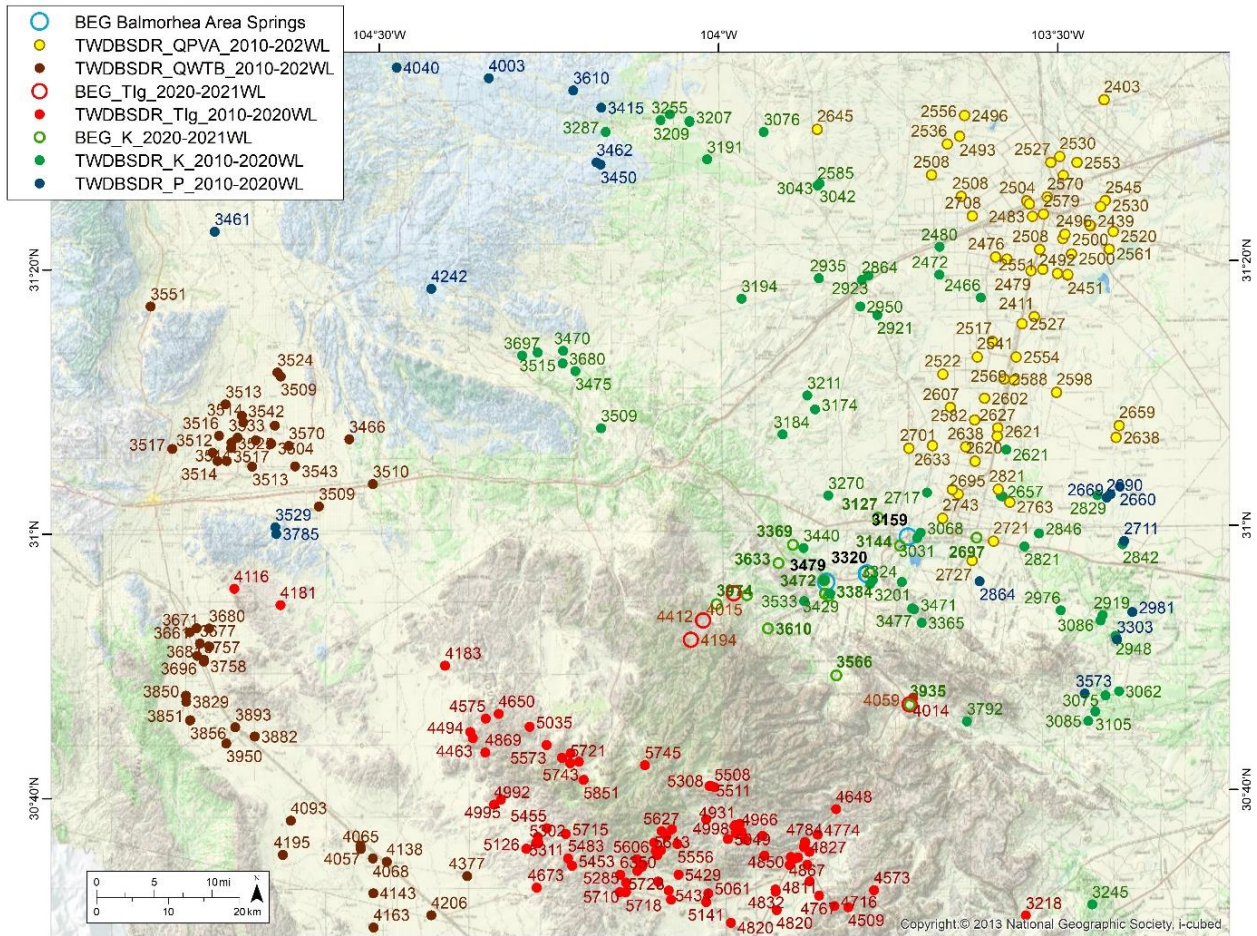


Figure 16. Locations of all wells with useable water level elevations (feet above sea level) measured during winter months (October through April) from 2010 through 2020. Water level elevation data combined from the TWDB and SDR databases are denoted with a TWDBSDR prefix including those completed in Pecos Valley aquifer (QPVA), West Texas Bolson (QWTB), Cenozoic-age Igneous (Tlg), Cretaceous-age (K), and Permian-age (P) aquifers. Well symbols with a BEG-prefix denote locations with BEG-installed water level monitoring equipment in Tlg and K water-bearing zones. The map background is simplified surface geology (beige = recent alluvium; reddish-brown = Cenozoic igneous rocks; green = Cretaceous rocks; and blue = Permian-age rocks) overlying topography and cultural features.

Figure 17 Rain gauge map

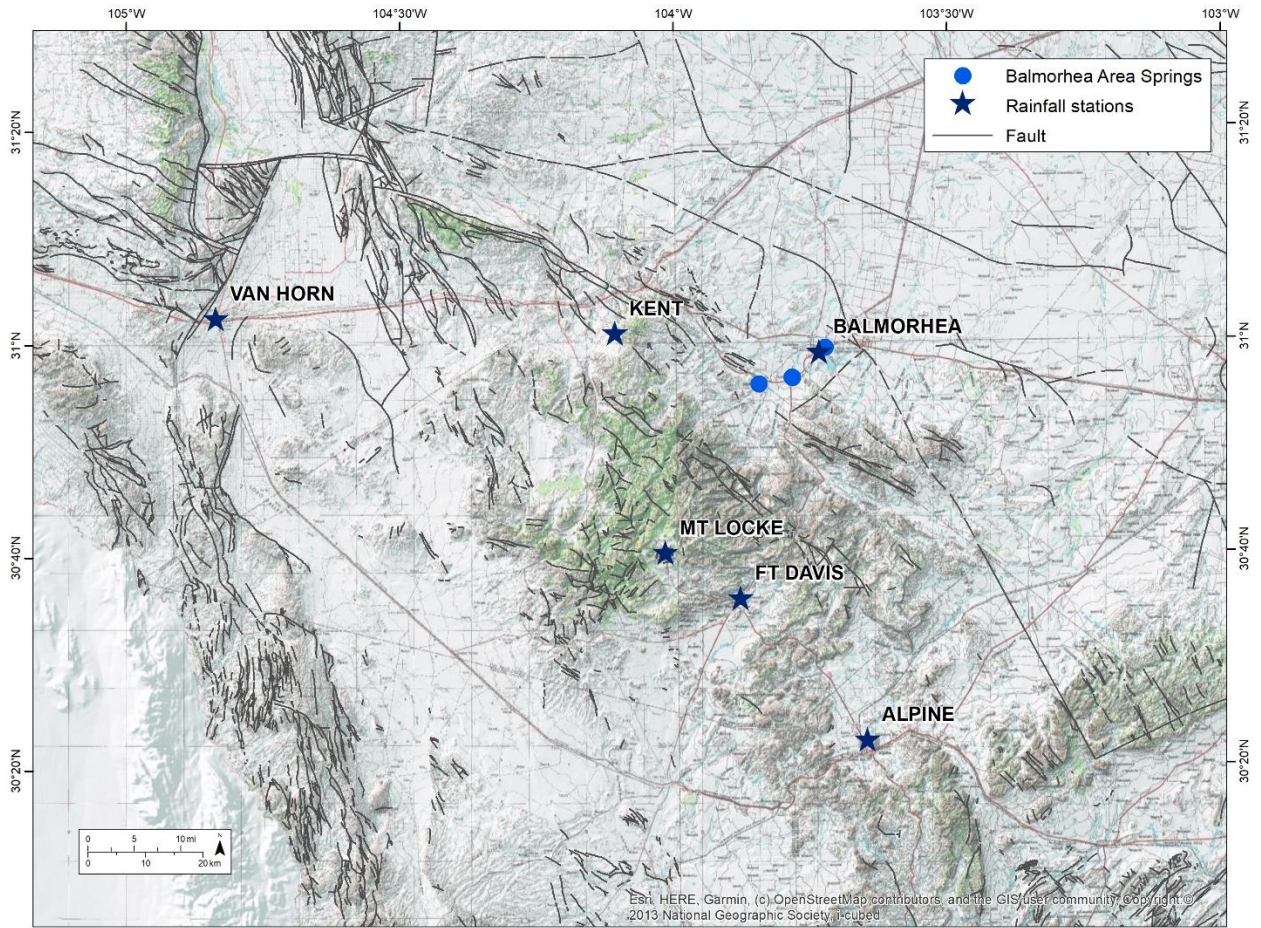


Figure 17. Official rain gauge locations.

Figure 18 Piper plot BEG

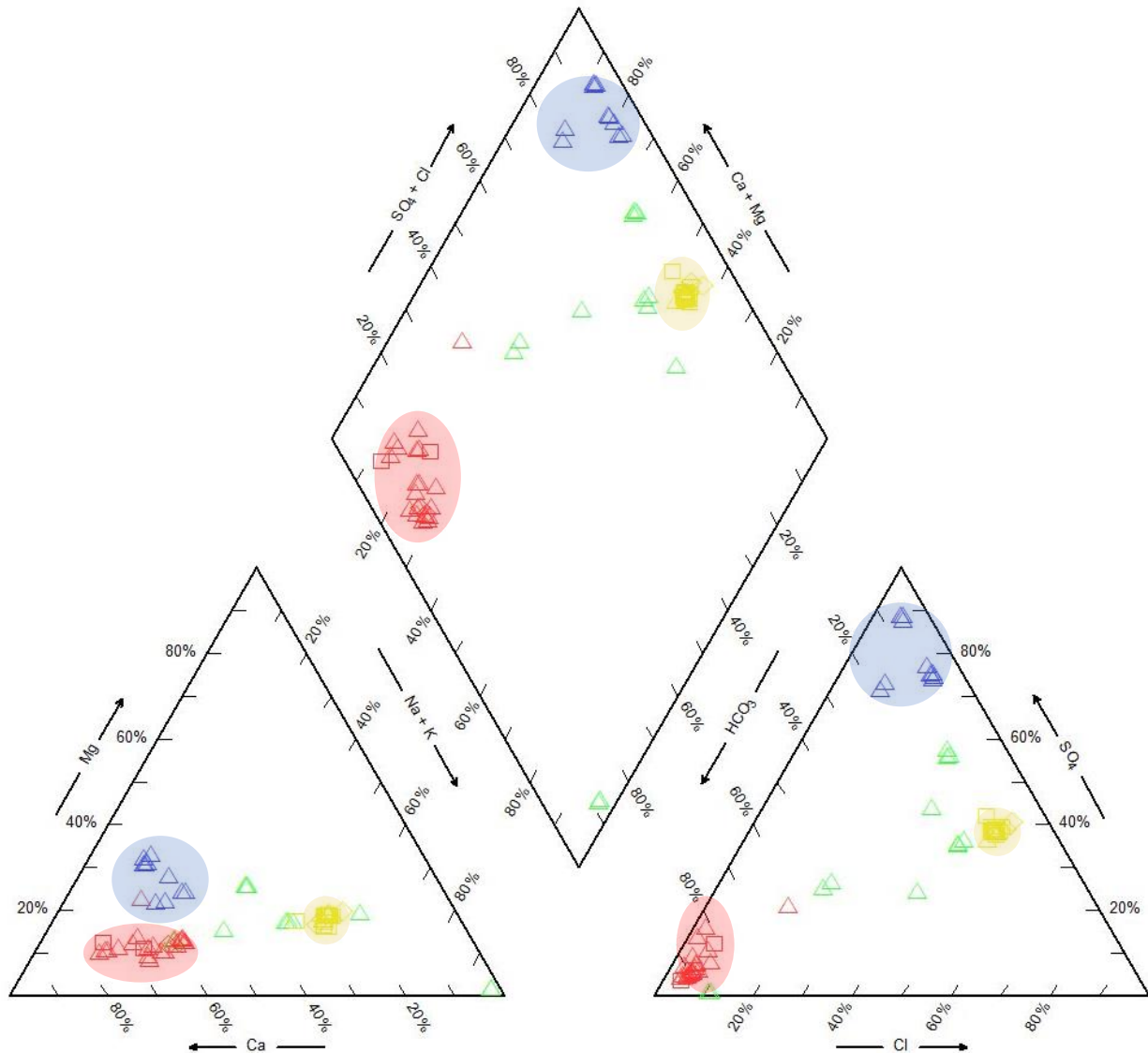


Figure 18. Piper plot of samples collected in this study. Well-defined categories are expressed in red (Igneous), Rustler (blue), the spring complex (yellow), and Cretaceous samples (green).

Figure 19 Map of Stiff diagrams

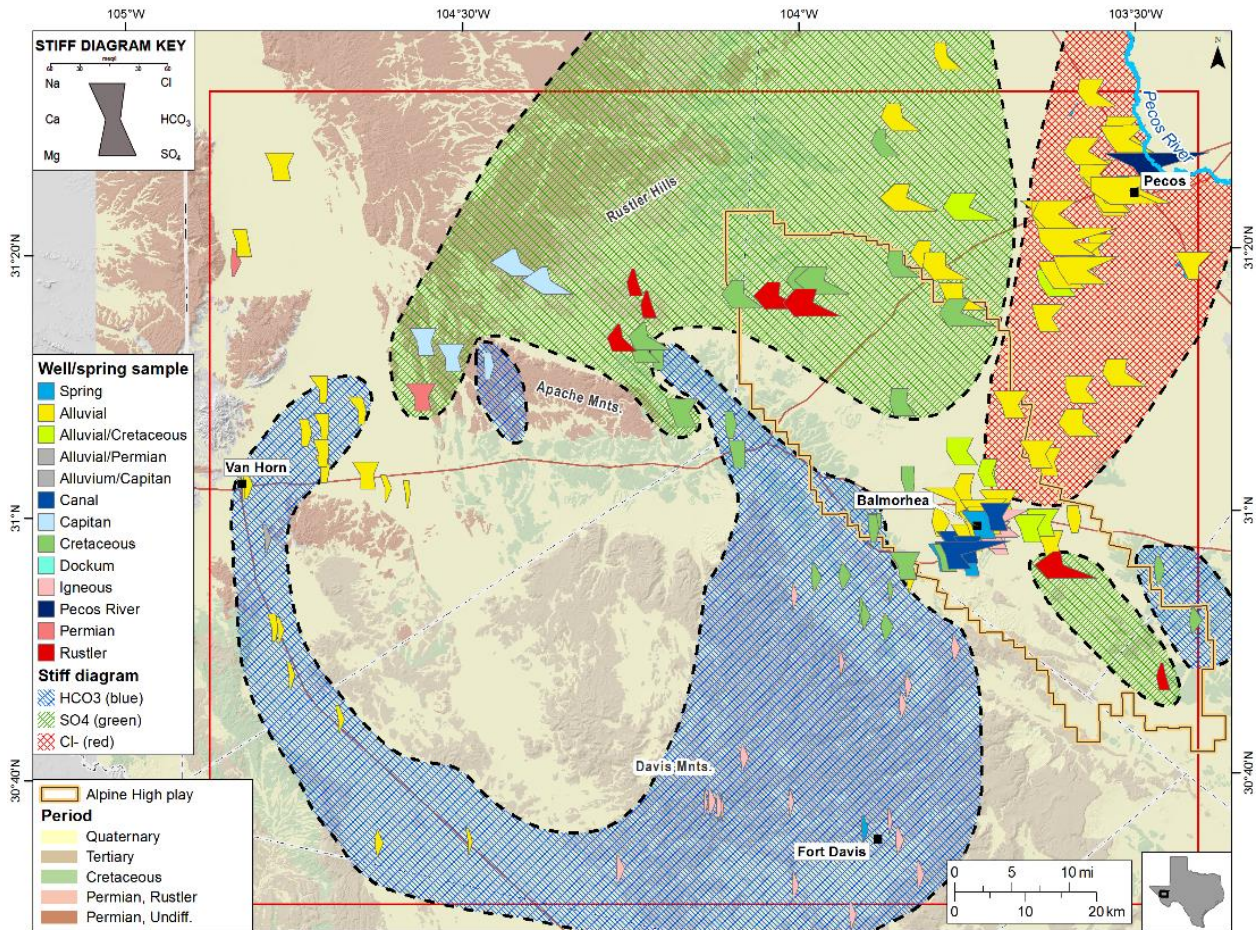


Figure 19. Map of generalized hydrochemical water types with Stiff diagrams. Map generated using post-2000 water quality data compiled by this study.

Figure 20 SI's

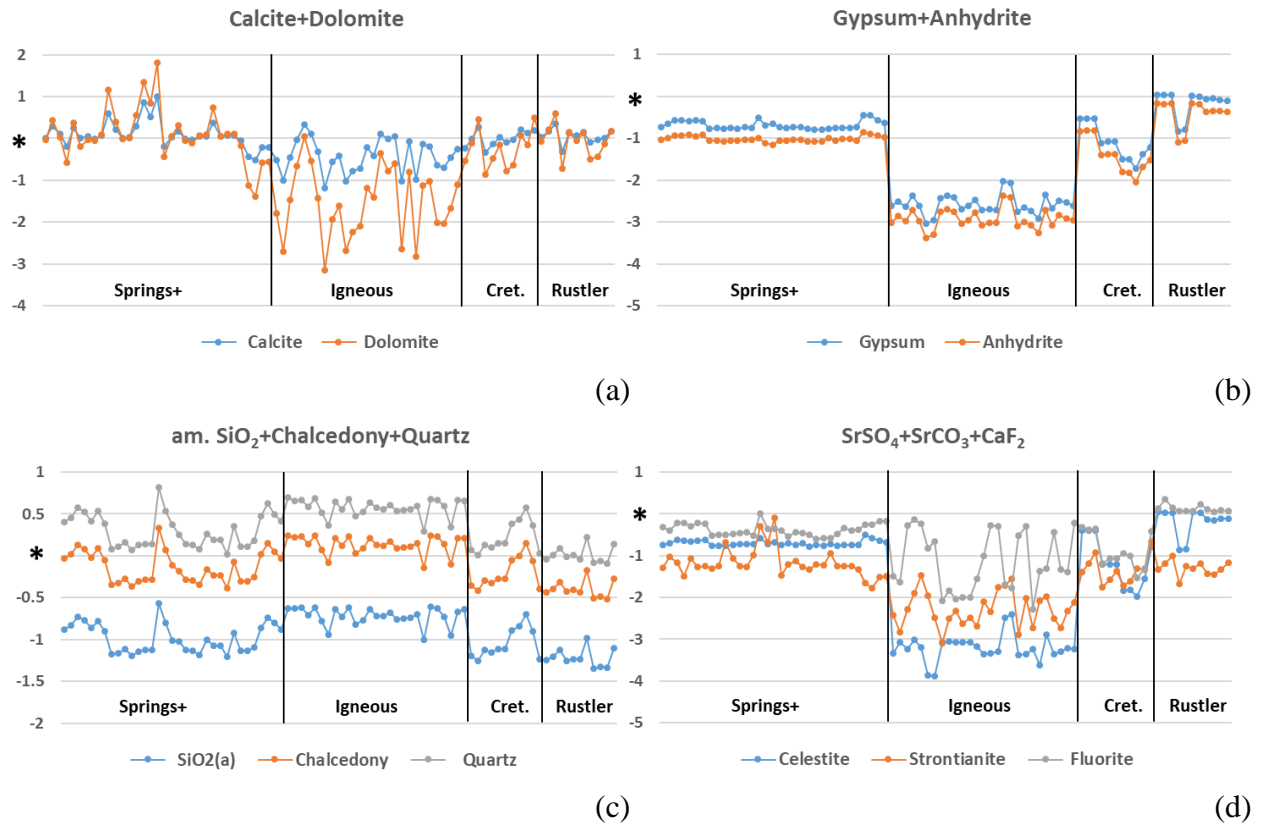
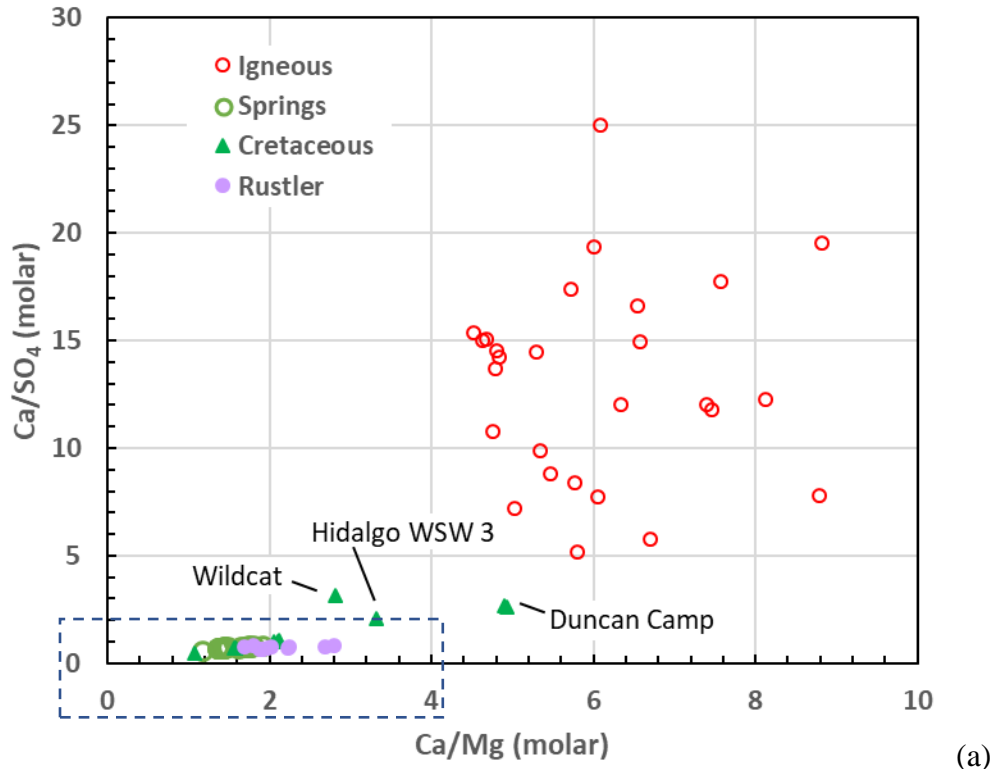
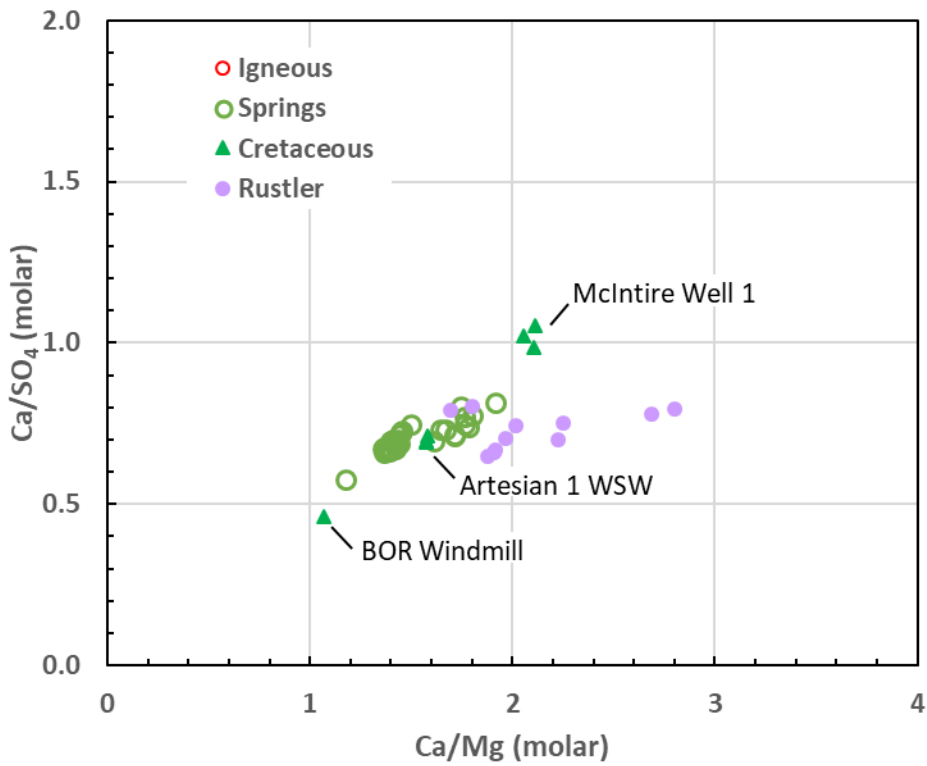


Figure 20. Distribution of saturation indices. The * symbol represents SI=0 and the limit between thermodynamically oversaturated and undersaturated samples.

Figure 21 Ca/Mg vs. Ca/SO₄



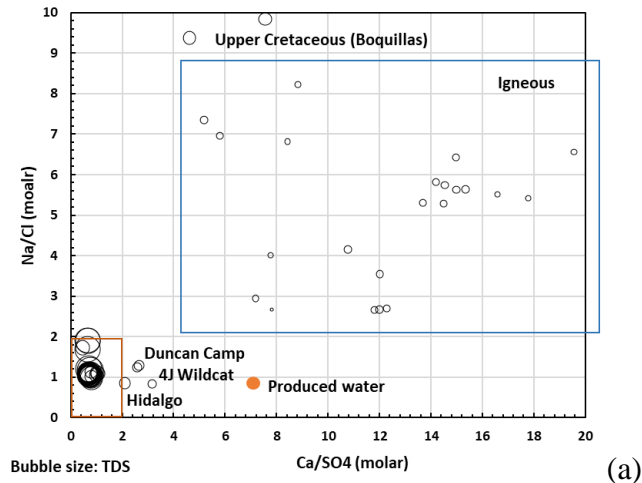
(a)



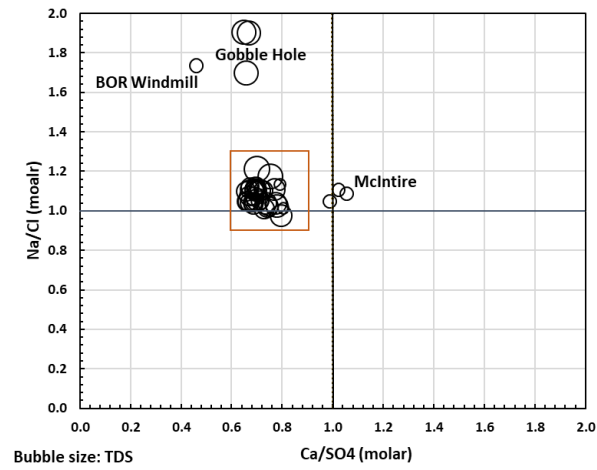
(b)

Figure 21. Ca/Mg vs. Ca/SO₄. Plot (b) is the zoomed-in version of the dotted-line rectangle on plot (a).

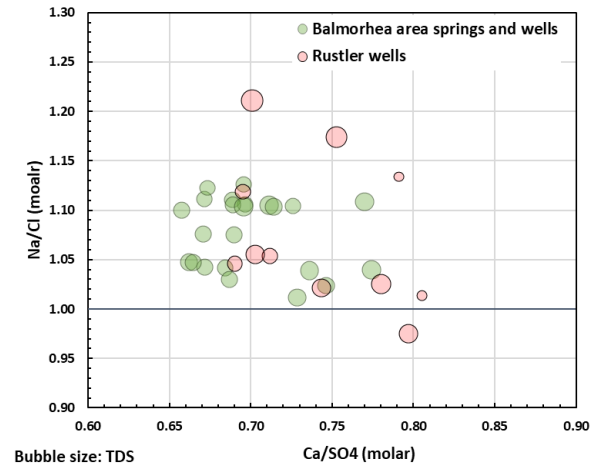
Figure 22 Na/Cl vs. Ca/SO₄



(a)



(b)



(c)

Figure 22. (a) Na/Cl vs. Ca/SO₄. Bubble size = TDS except for produced water samples; (b) Na/Cl vs. Ca/SO₄ zoomed in version, red rectangle in (a); (c) Na/Cl vs. Ca/SO₄ zoomed in version, red rectangle in (b).

Figure 23 spring temperature

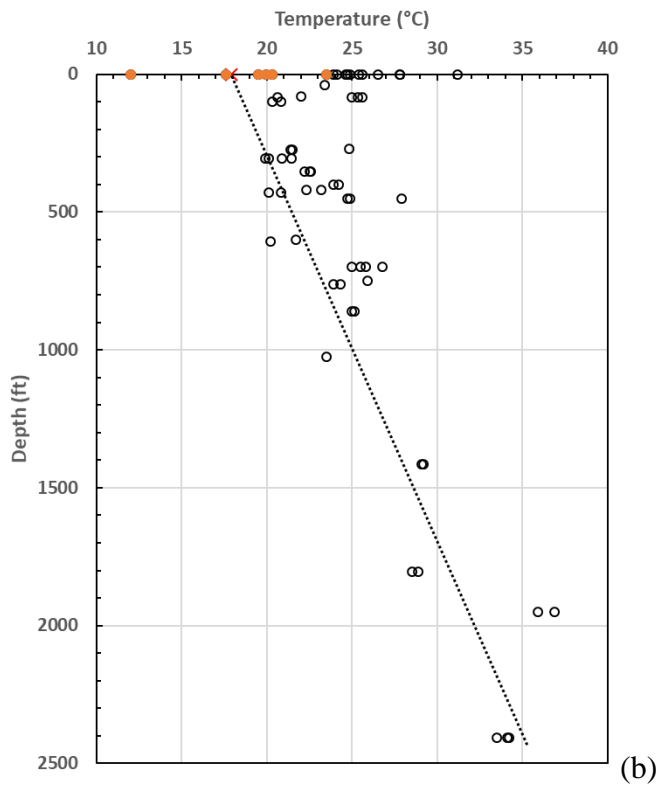
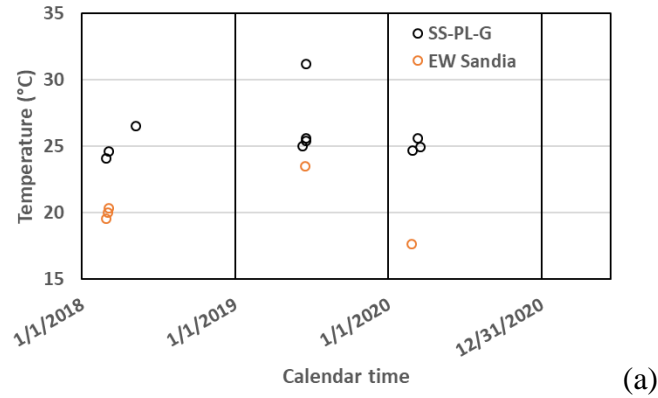


Figure 23. (a) Spring temperature obtained through water samples (including 2 data points from Hamilton well); (b) water sample temperature as a function of depth; red “x” represents the average temperature at Balmorhea whereas the orange dots represent the non-artesian springs (Saragosa at 12°C on Dec. 12, 2020). The dotted line represents a geothermal gradient of 1.25°F/100 ft (22.75°C/km).

Figure 24 SSS TDS through time

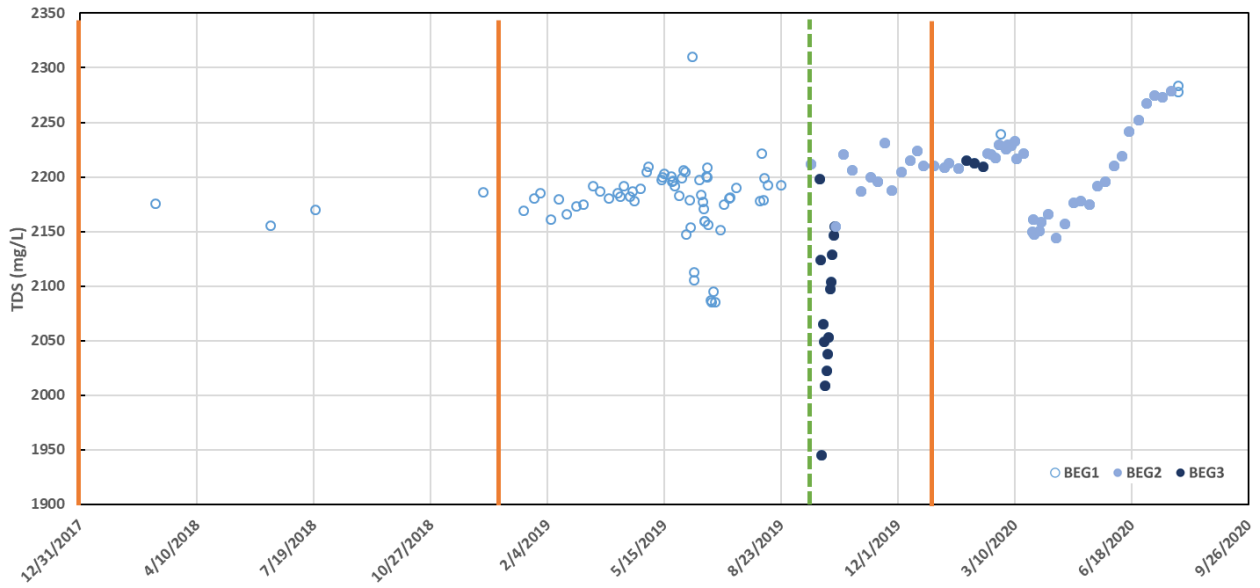
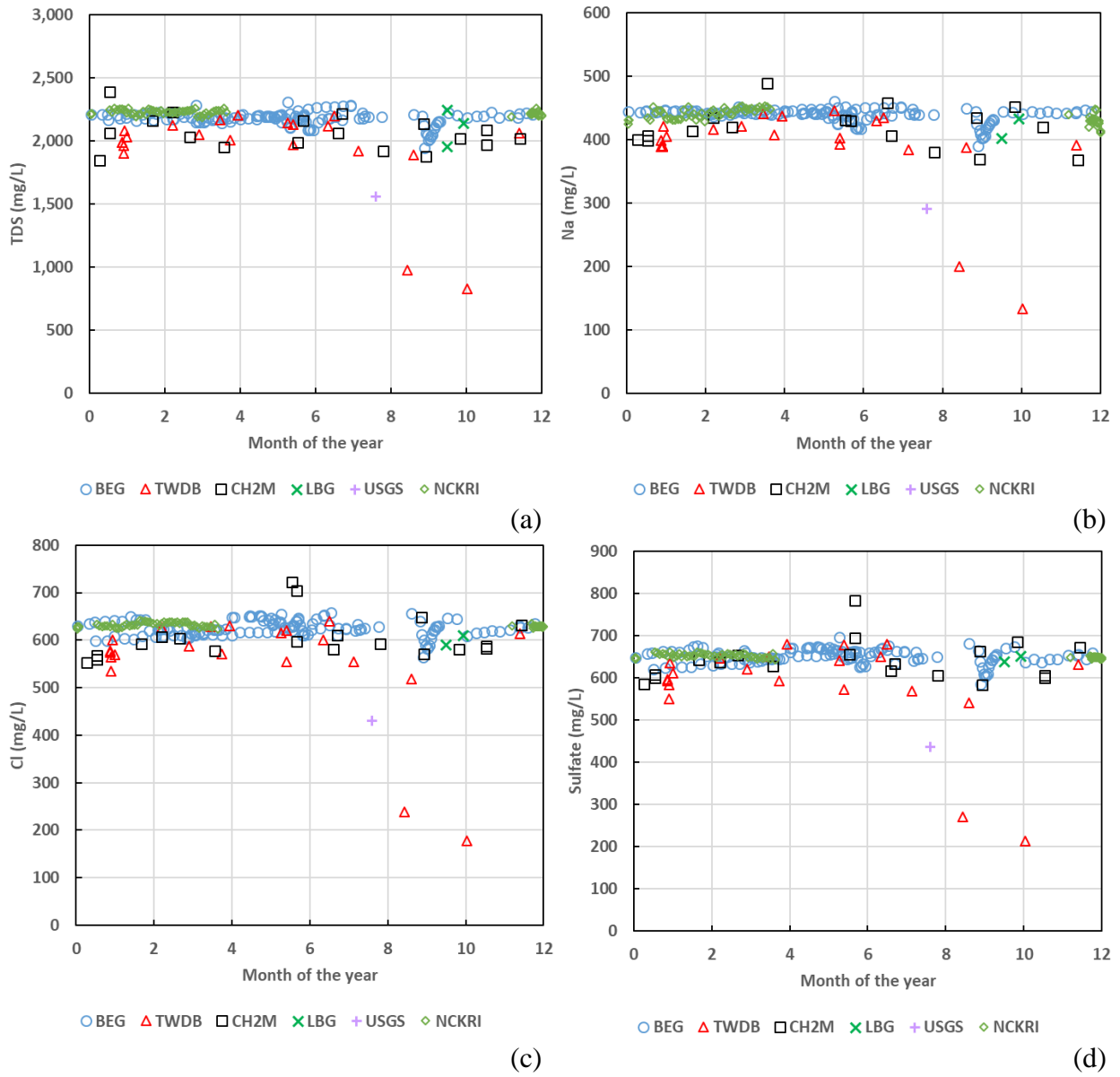


Figure 24. TDS of San Solomon spring samples taken during the study showing sampling point: BEG1 is in the pool, BEG2 is in a canal; and BEG3 is in the canal. The dashed green line represents a major shift in the sampling procedure as well as the gap at the end of March 2020. The solid orange lines simply mark the transition to a new calendar year.

Figure 25 SSS elements and time of the year



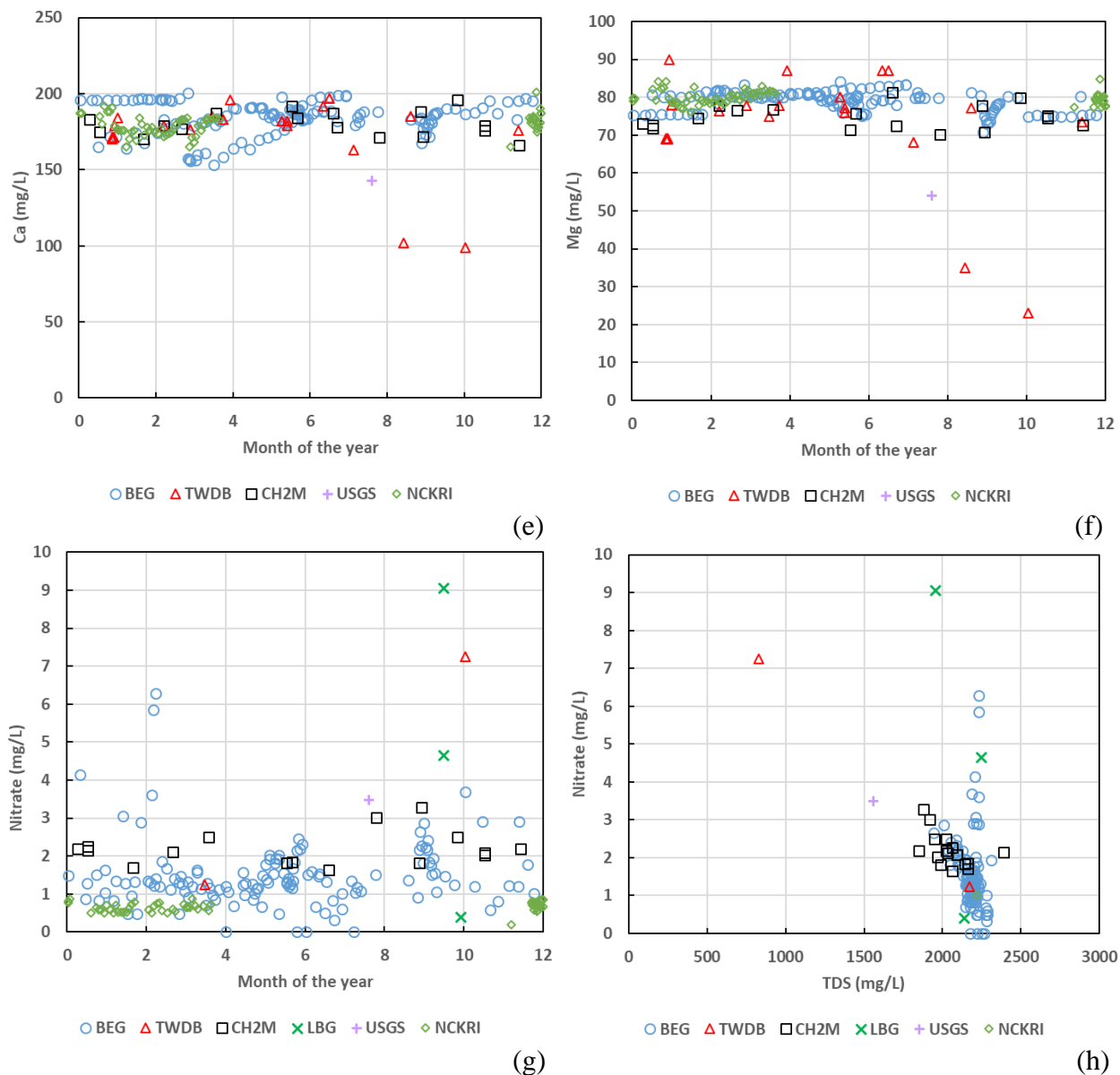


Figure 25. Elements and anions as a function of the time of the year at San Solomon spring (0 and 12 are 12/31 at midnight): (a) TDS; (B) Na; (c) Cl; (d) SO₄; (e) Ca; (f) Mg; (g) nitrate; and (h) nitrate vs. TDS. Sources are this study (BEG) (2018-2020, 134 samples), TWDB databases (1932-2018, 24 samples), Apache consultant (CH2M) (2016-2018, 19 samples), TWDB-sponsored work (LBG) (1930, 1947, 1998, 3 samples), USGS (1 sample (2012) not captured by TWDB databases), and NCKRI (2019-2020, 74 samples). The low-concentration TWDB samples were taken on 9/13/1932 and 11/1/1990. The slightly higher low-concentration USGS sample was taken on 8/18/2010.

Figure 26 Sulfate

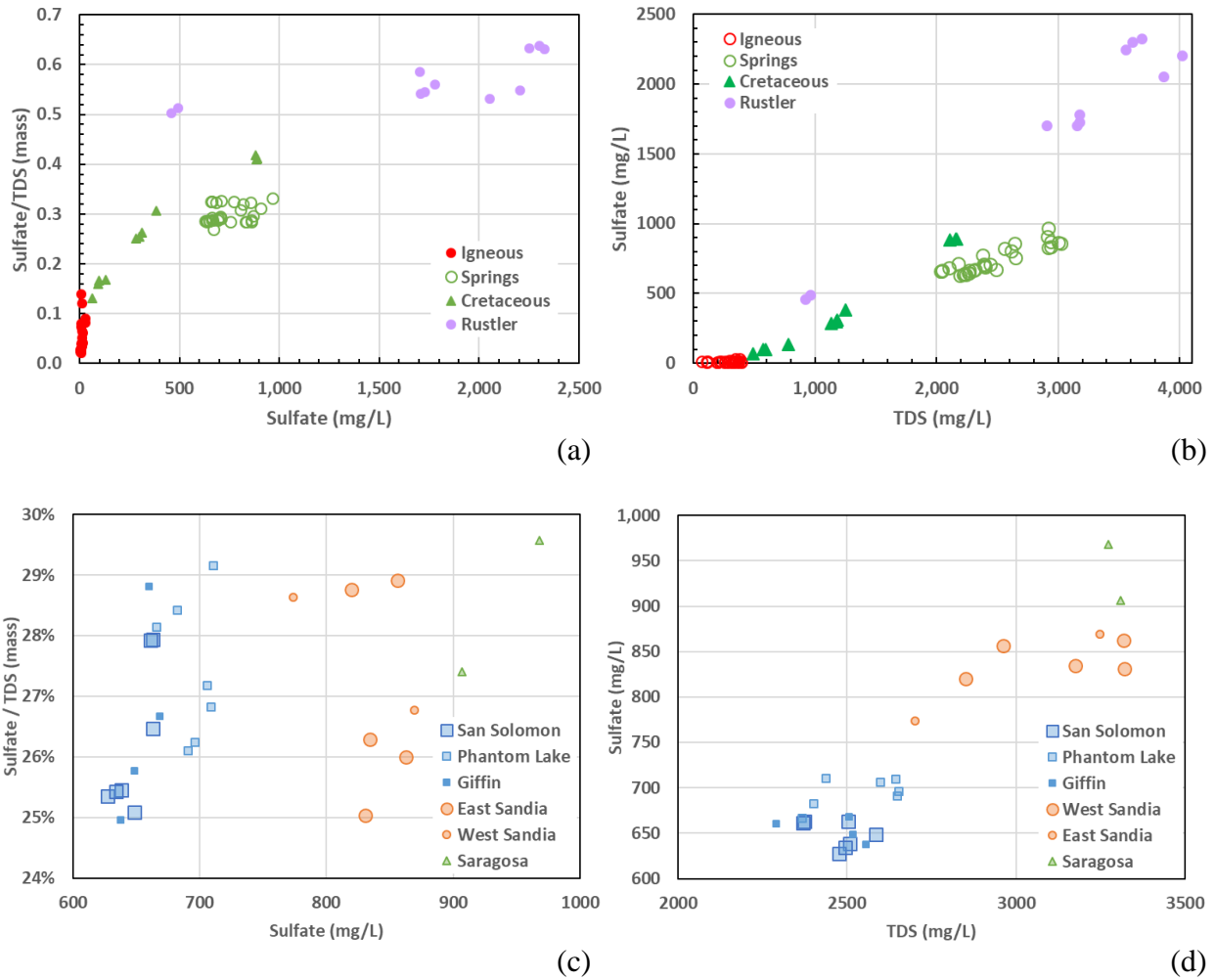


Figure 26. This study sample sulfate distribution: (a) as a fraction of TDS; (b) against TDS. Balmorhea spring sulfate distribution: (c) as a fraction of TDS; (d) against TDS; note the reduced scale.

Figure 27 Nitrate

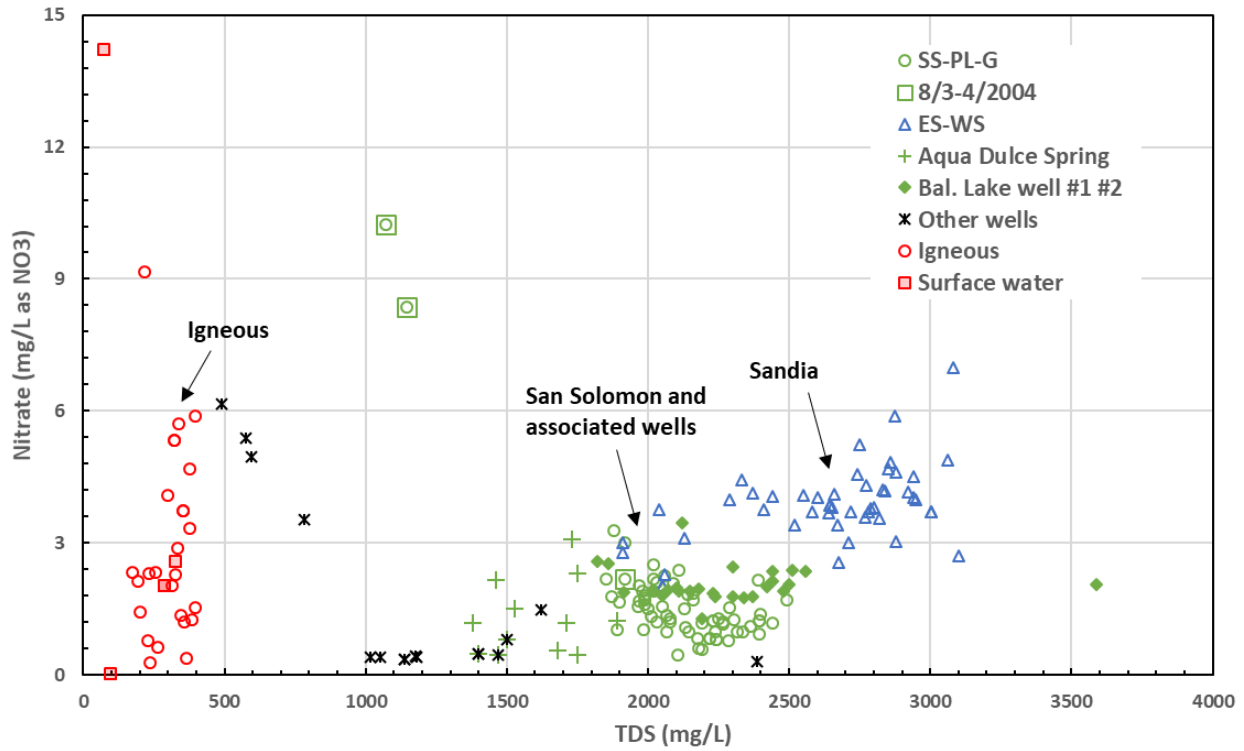


Figure 27. Nitrate (N as nitrate) concentration in all samples (this study and some other available data). Hamilton well and BSP shallow ell are included in the SS-PL-G group and TNC Sandia preserve shallow well included in the ES-WS group. The early August 2004 event is visible with a high nitrate value for PL and G springs but not SSS. The highest value at 14.2 mg/L is observed in Madera Creek, the second highest in surface water / springs is Seven Spring at 9.2 mg/L.

Figure 28 Nitrate and time of the year

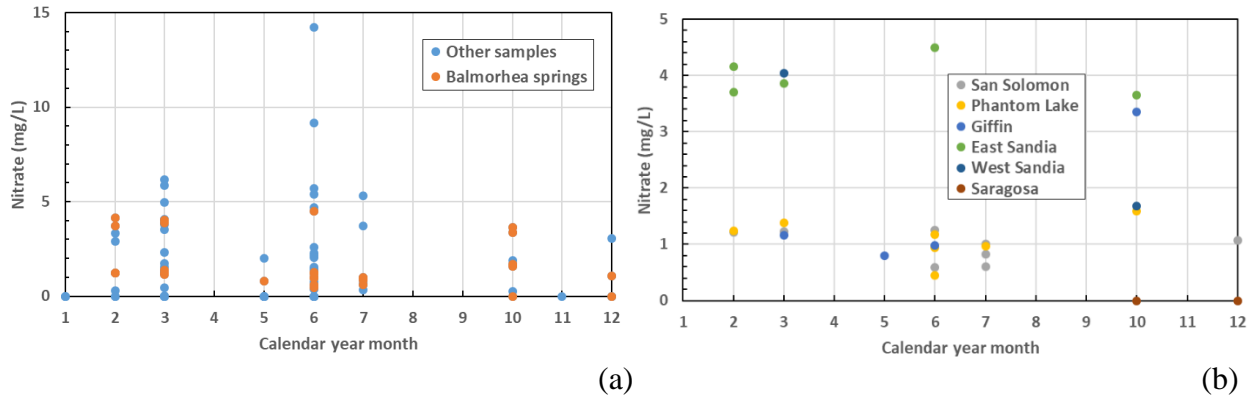


Figure 28. Nitrate concentration vs. month of the year for (a) all samples; and (b) Balmorhea spring samples only.

Figure 29 Nitrate vs. time

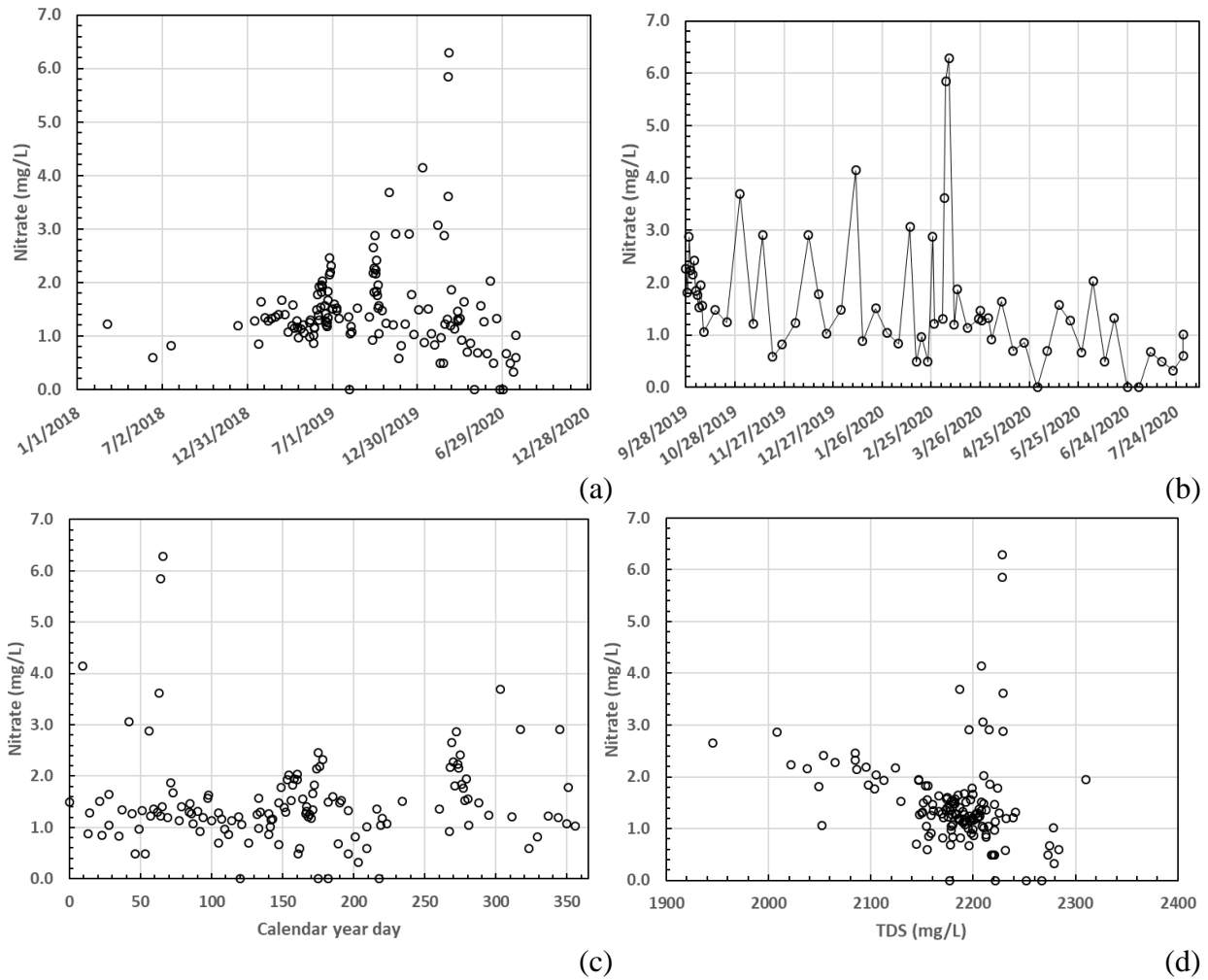


Figure 29. San Solomon Spring nitrate concentration (a) through time; (b) through time with a focus on the nitrate peak values of the dataset (3/4 to 3/7/2020); (c) as a function of the day of the year; and (d) vs. TDS.

Figure 30 Silica

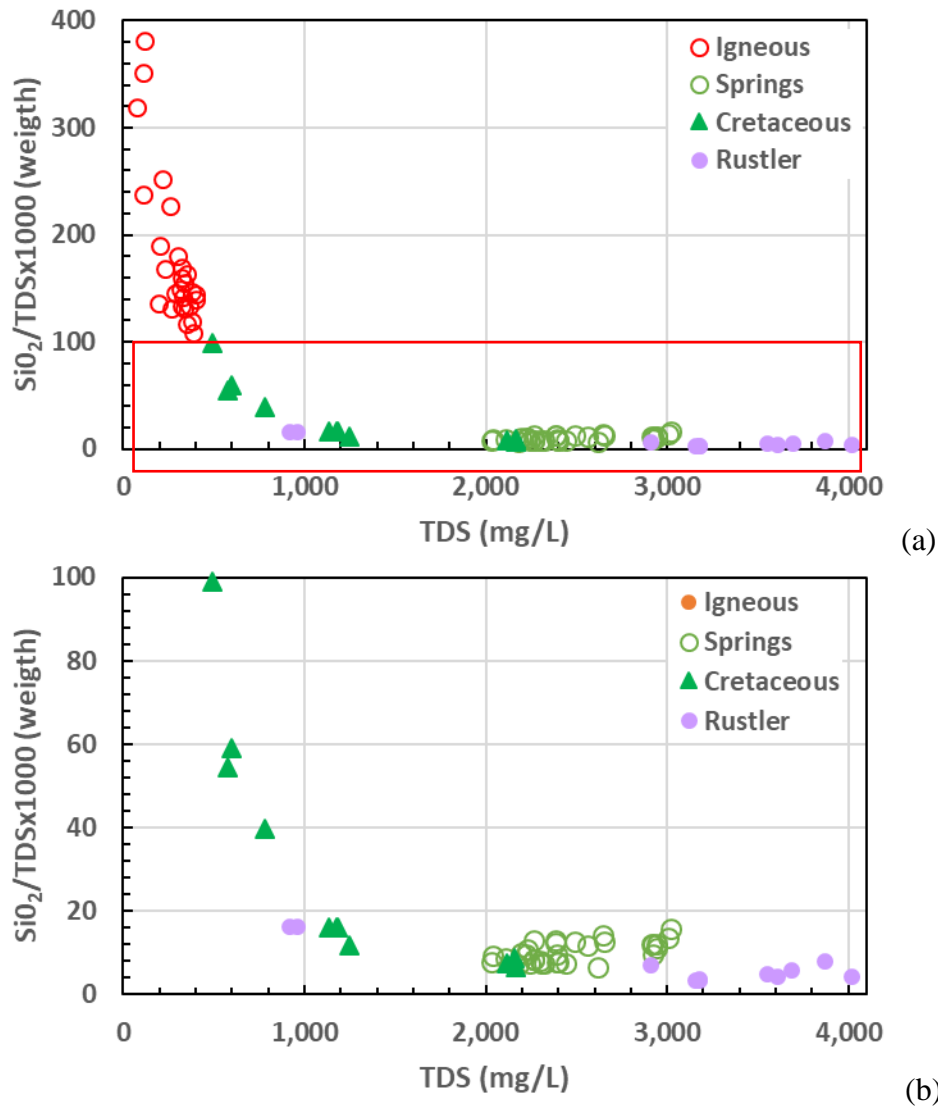


Figure 30. Silica concentrations normalized by TDS as a function of TDS. Red rectangle in (a) represents the extent of (b).

Figure 31 Boron

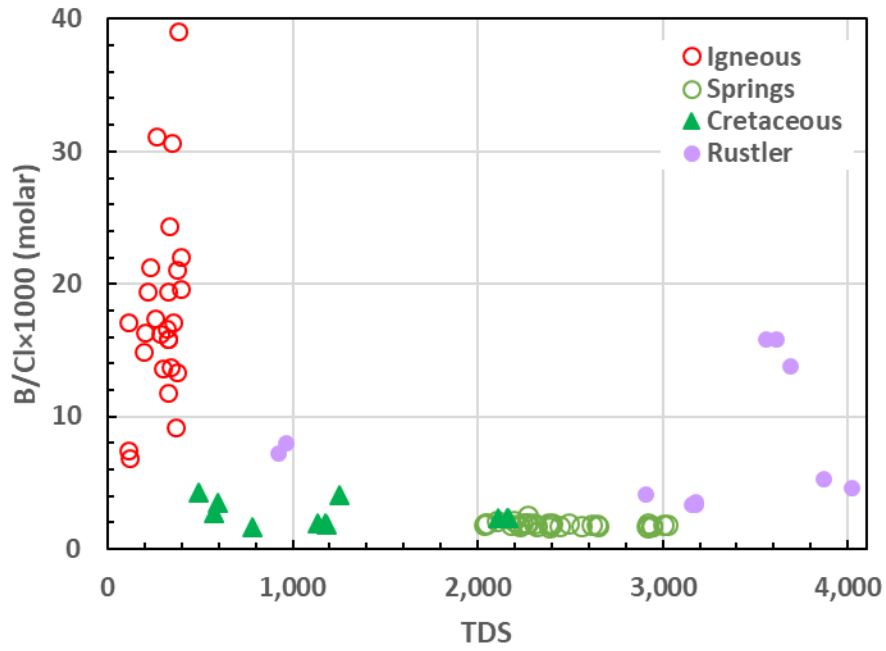


Figure 31. Boron concentrations normalized by Cl as a function of TDS

Figure 32 Silica vs boron

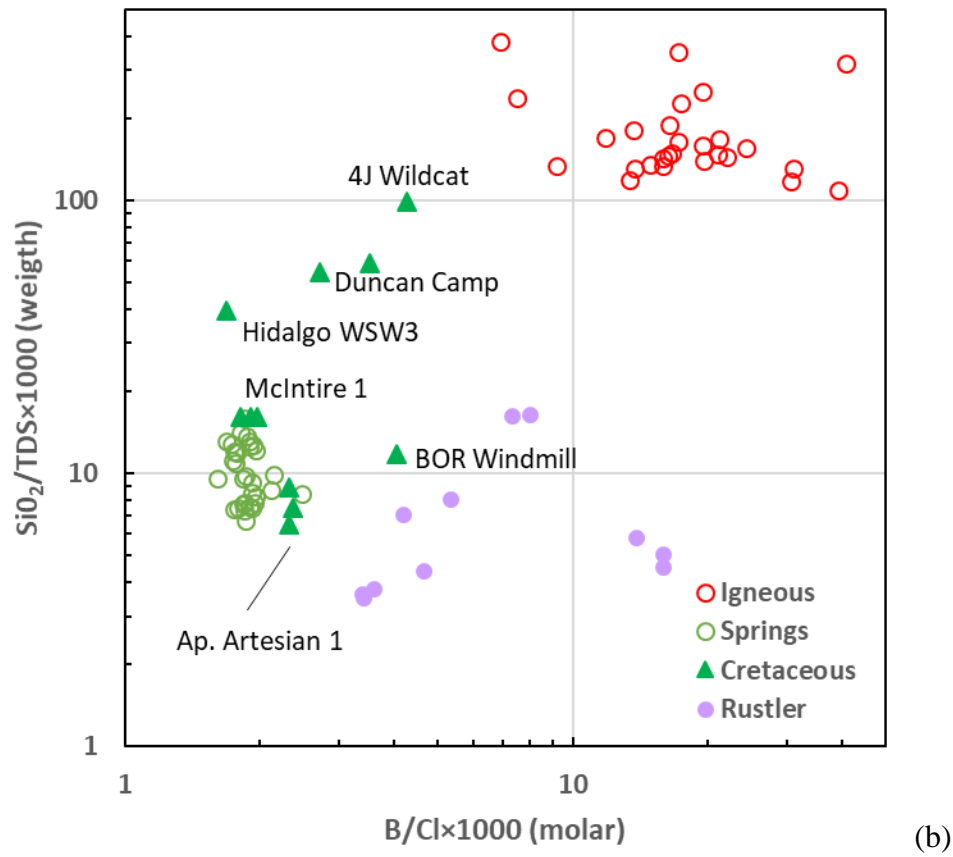
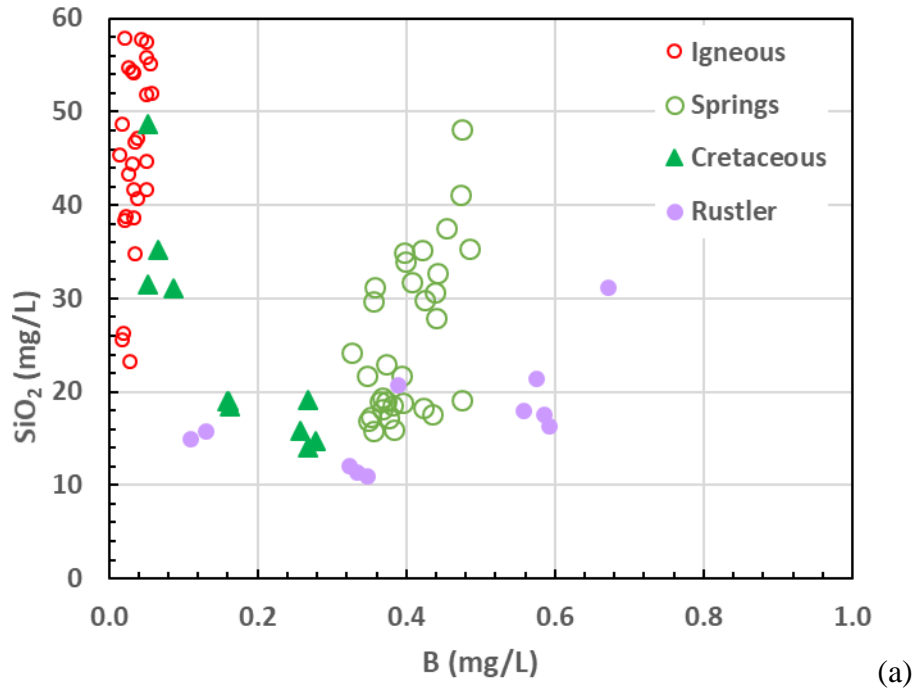


Figure 32. (a) Silica vs. boron; (b) silica normalized by TDS vs. boron normalized by Cl.

Figure 33 Piper plots TWDB

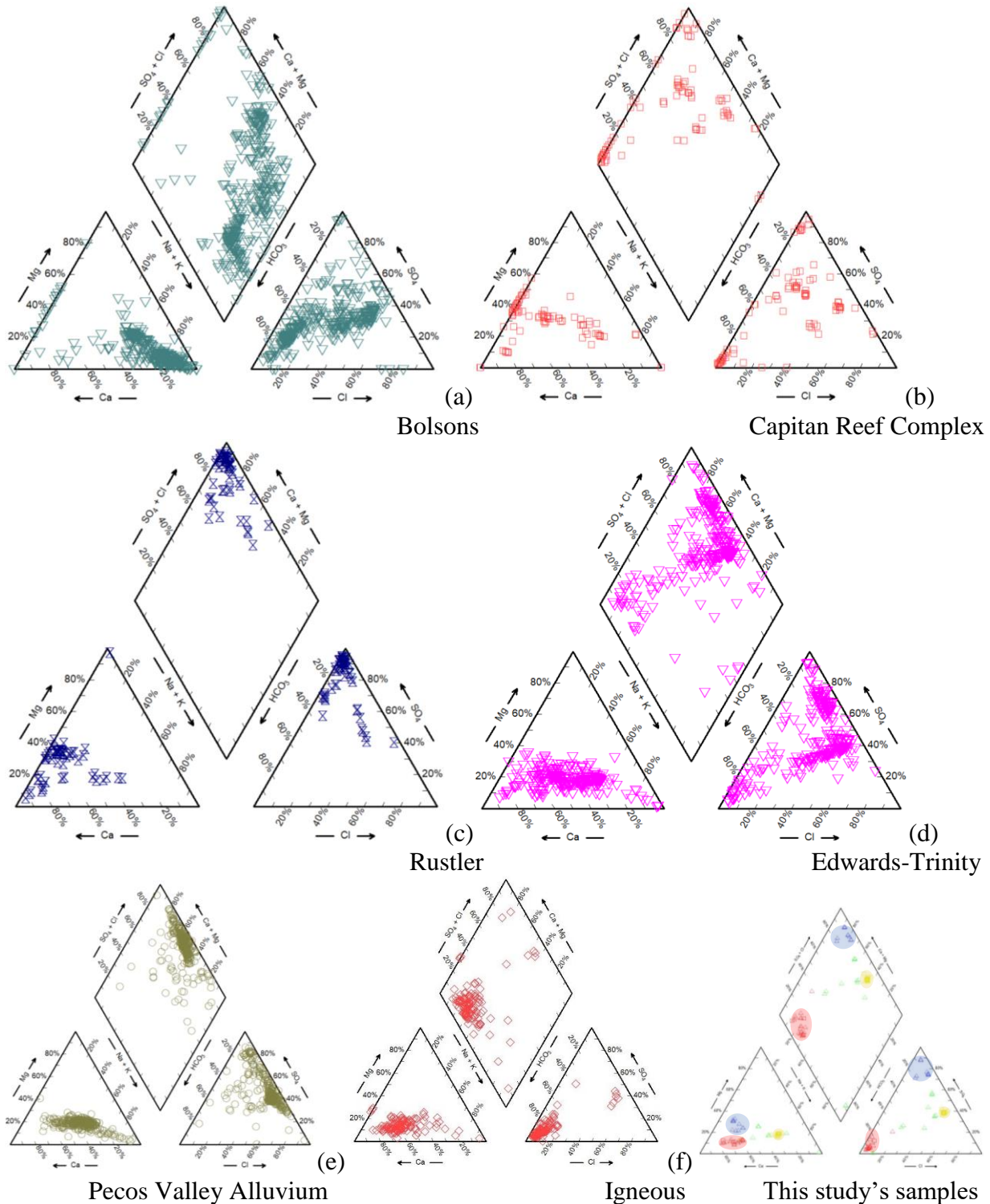
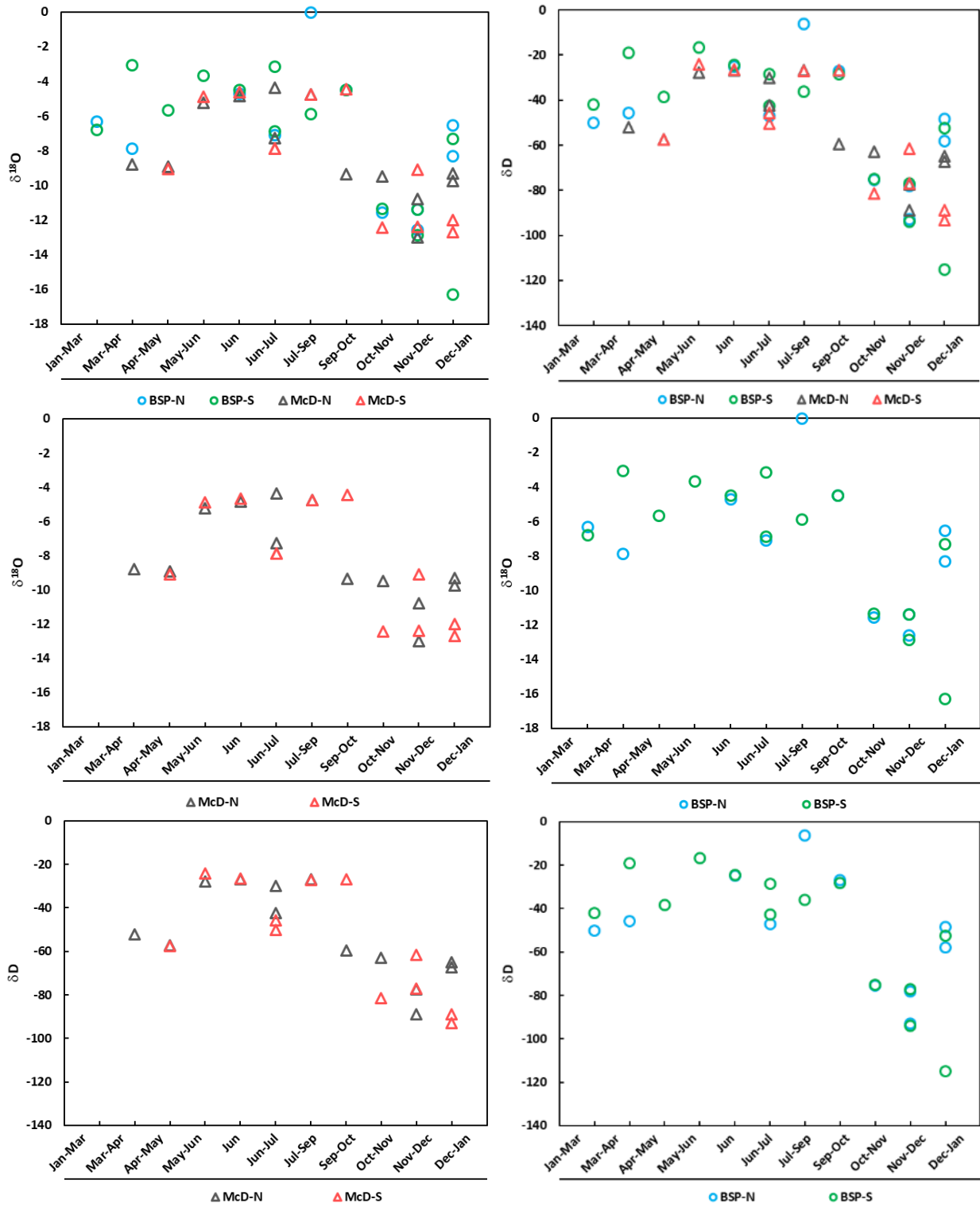
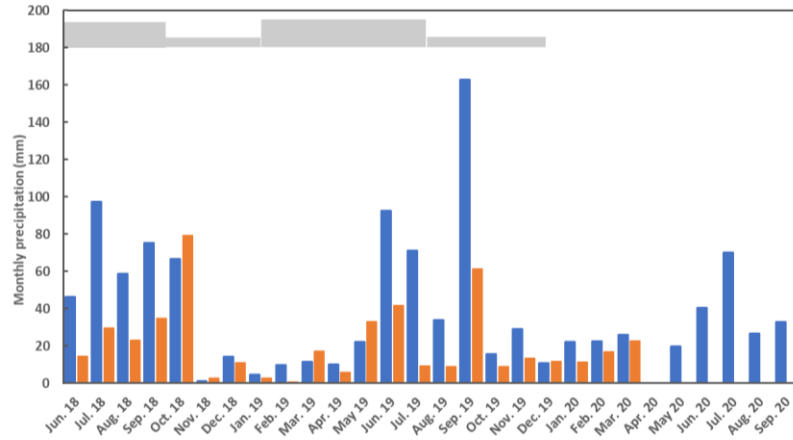


Figure 33. Historical data Piper plots of aquifers: (a) Bolsons (366); (b) Capitan (91); (c) Rustler (56); (d) Edwards-Trinity (313); (e) Pecos Valley Alluvium (303); and (f) Igneous (126). Inset of samples taken in the course of this study shows Rustler (blue), Igneous (red), and Balmorhea Springs (brown) categories. Include data points from multiple sampling at the same location.

Figure 34 Rain water isotopes





Total monthly rainfall at McDonald Observatory (blue, typically but not always larger) and Balmorhea State Park (orange) during this study. On top of the plot, approximate time extent of the water isotopes when sorted in two groups (heavier, thicker line) and lighter (thinner line).

Figure 34. Seasonal variations of rainwater isotopes.

Figure 35 Water isotopes cross-plot

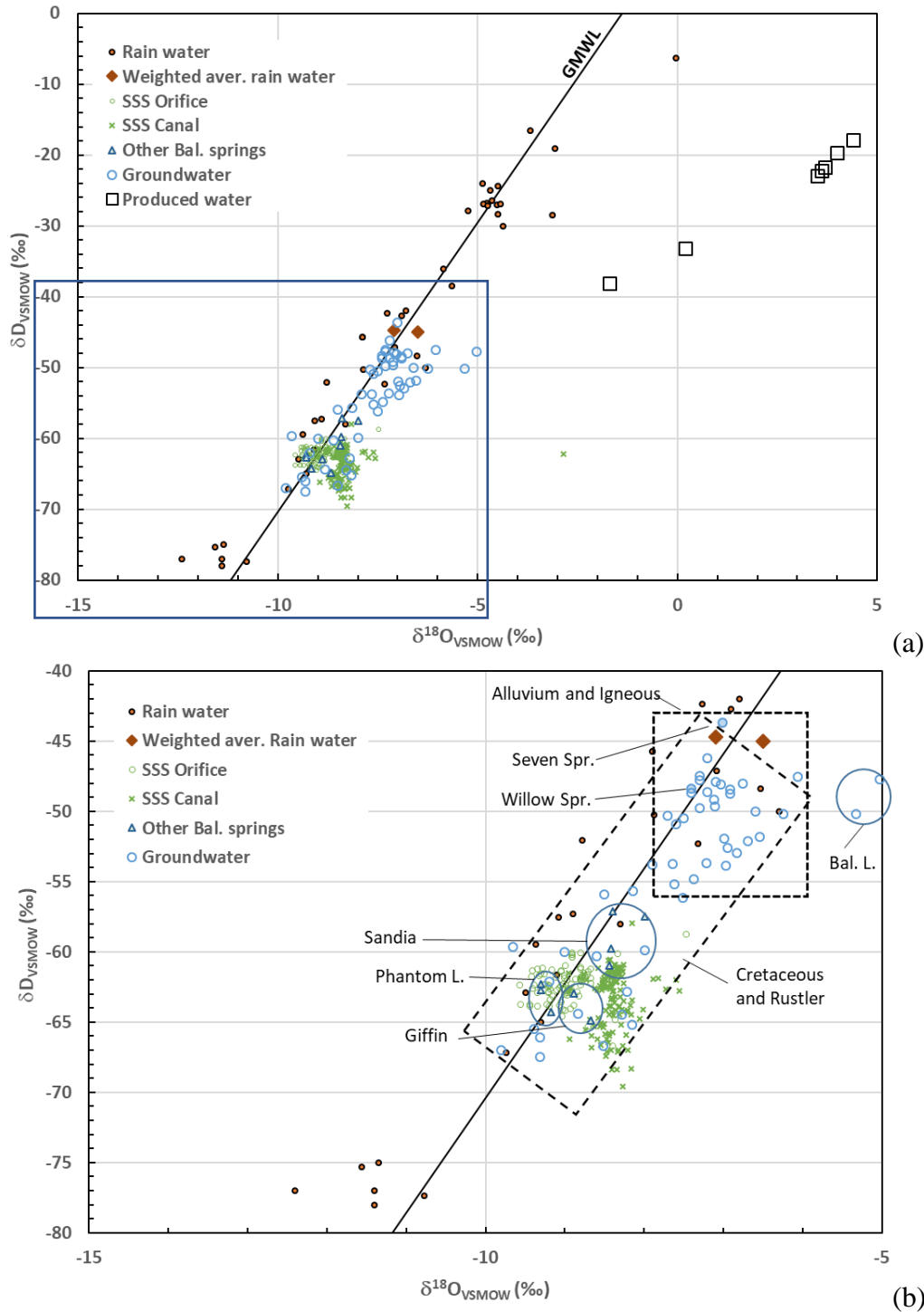
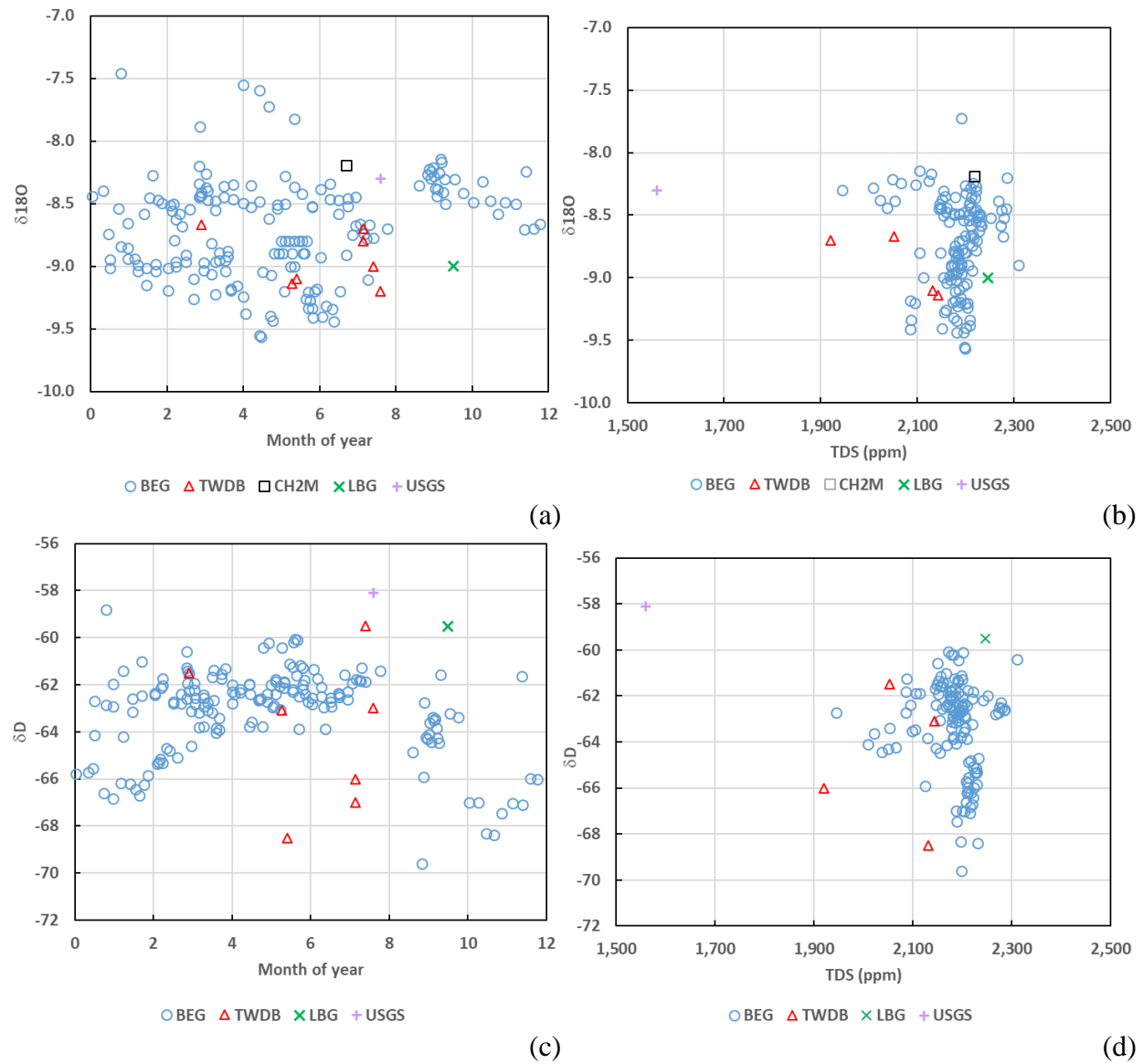


Figure 35. Water isotope cross-plot. The full plot (a) and zoomed-in version (b) include produced water samples, SSS samples taken close to the orifice and then from Sept. 2019 taken from a canal, samples from other springs (Balmorhea area and Davis Mountains), and groundwater samples approximately sorted by aquifer: alluvium and Igneous one side and Cretaceous and Rustler on the other side. This binary sorting is approximate because wells can be completed in

multiple intervals and can also be misattributed. SSS = San Salomon Spring; GMWL = Global Meteoric Water Line; Bal. L. = Lake Balmorhea.

Figure 36 SSS isotopes



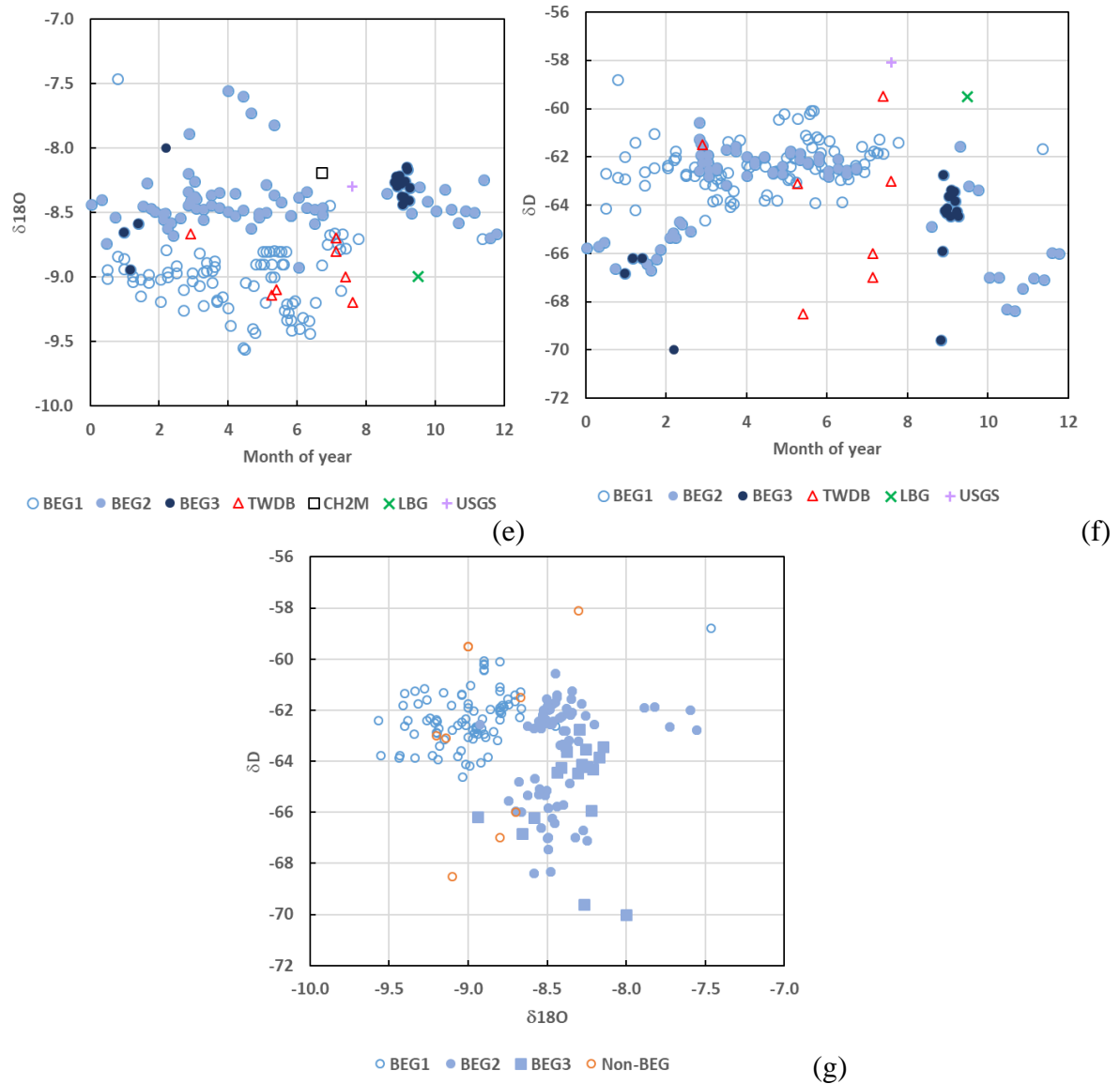


Figure 36. Stable water isotopes as a function of the time of the year at San Solomon spring (0 and 12 are 12/31 at midnight): (a) $\delta^{18}\text{O}$; (b) δD ; (e) and (f) $\delta^{18}\text{O}$ and δD showing sampling point: BEG1 is in the pool, BEG2 is in a canal; and BEG3 is in the canal. Stable water isotopes as a function of TDS: (c) $\delta^{18}\text{O}$; (d) δD ; and (g) $\delta^{18}\text{O}$ vs. δD showing sampling points. Sources are this study (BEG) (2018-2020, 172 samples), TWDB databases (1998-2004, 7 samples), TWDB-sponsored work (LBG) (1998, 1 sample), and USGS (1 sample (2012) not captured by TWDB databases).

Figure 37 Strontium

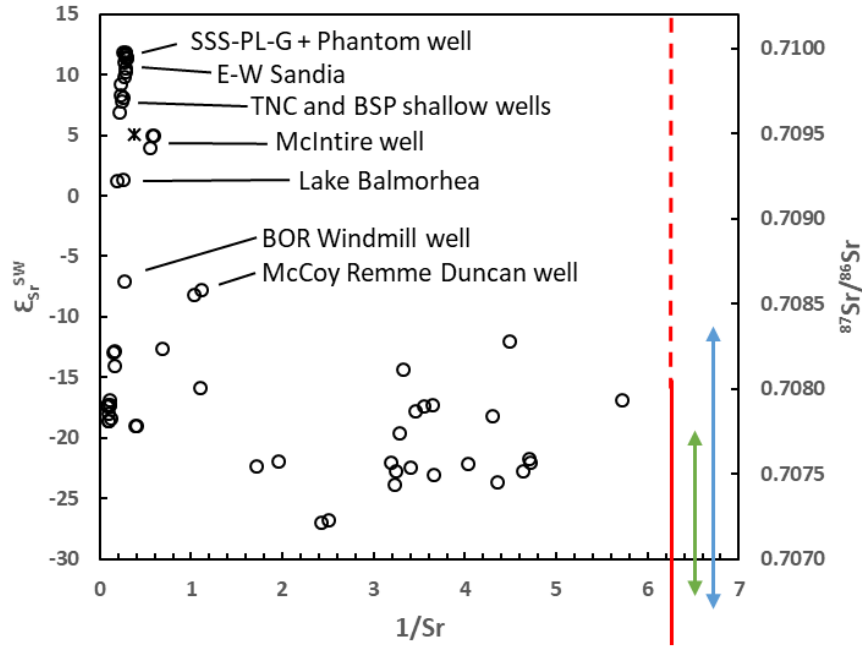


Figure 37. Strontium ratio –Red vertical line represents the range of the Sr ratio in the igneous rocks with some samples observed to have high value. The green line represents range of Cretaceous marine carbonates that show a regular increase during the period from 0.7068 to 0.7077. The blue line represents the range during the Permian period that shows a quick decrease from 0.7084 to 0.7067 with a fast rebound to 0.7074 at the end of the period. Two igneous samples with low Sr ($1/Sr = \sim 10$) are outside of the plot (ϵ of -20.2 and -17.3). The star corresponds to a Saragosa data point from Nunu (2020).

Figure 38 Strontium vs. d18O

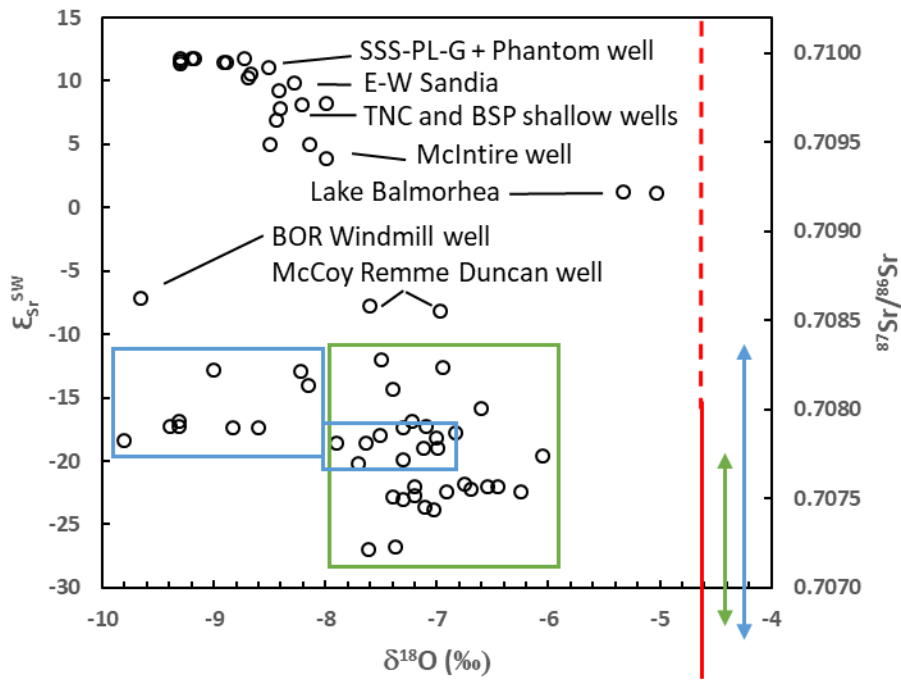


Figure 38. Strontium isotope ratio vs. water oxygen isotope. Red, green, and blue vertical lines represent the range of the Sr ratio in the igneous rocks, Cretaceous marine carbonates and during the Permian period. The green box includes the Cretaceous-hosted water samples and the blue boxes include Permian-hosted water samples.

Figure 39 Bicarbonate C isotopes

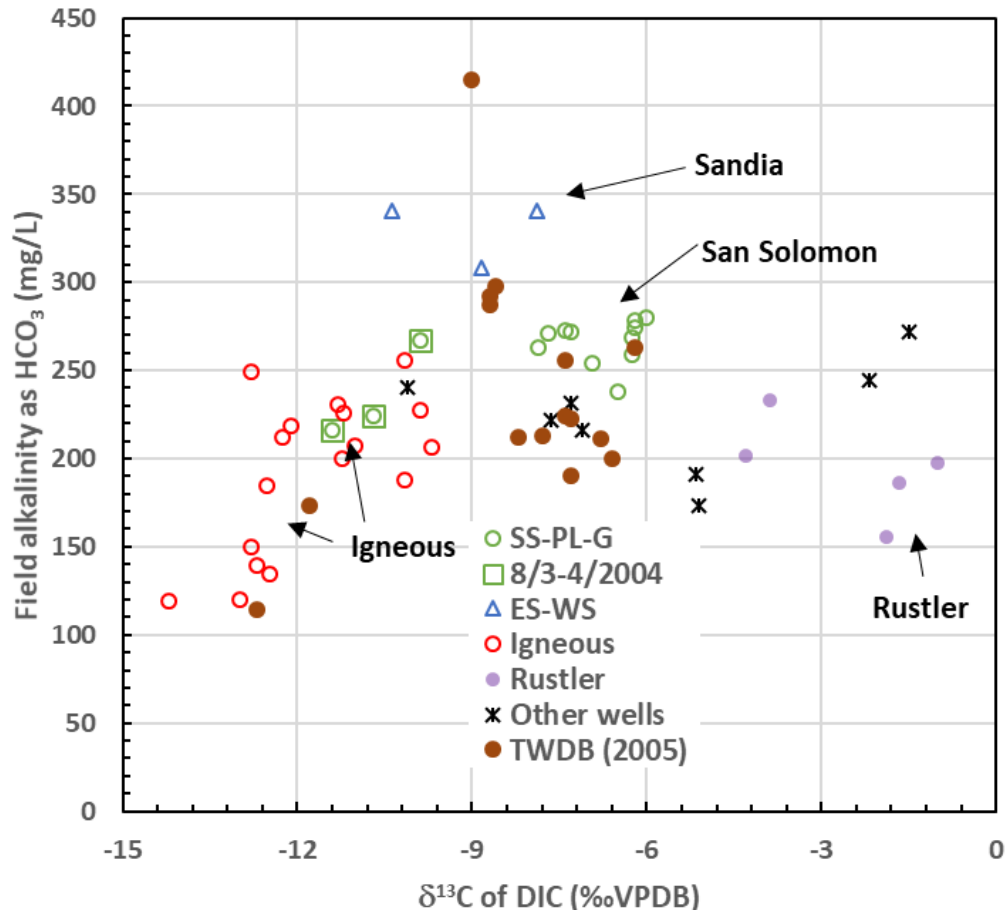


Figure 39. Field alkalinity bicarbonate as a function of the DIC $\delta^{13}\text{C}$. 8/3-4/2004 data from the TWDB database.

Figure 40 Cl/Br ratio

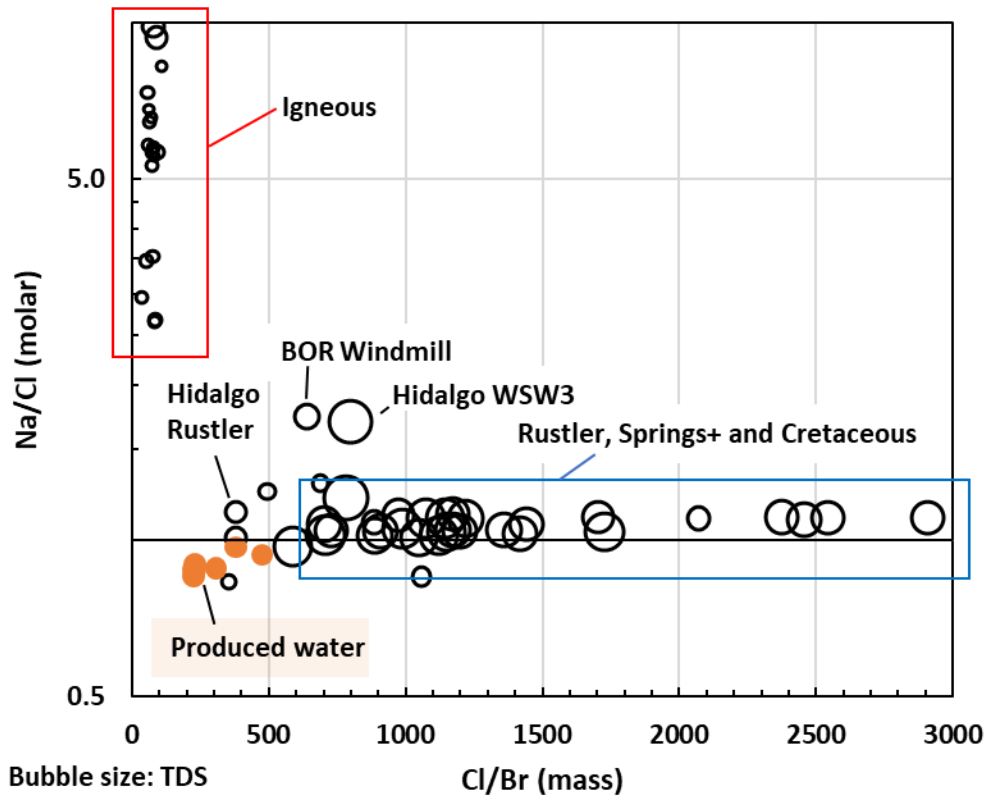


Figure 40. Cl/Br ratio as a function of Na/Cl ratio. Note log scale on the y-axis. Bubble size proportional to TDS except for produced water.

Figure 41 Chlorine isotopes

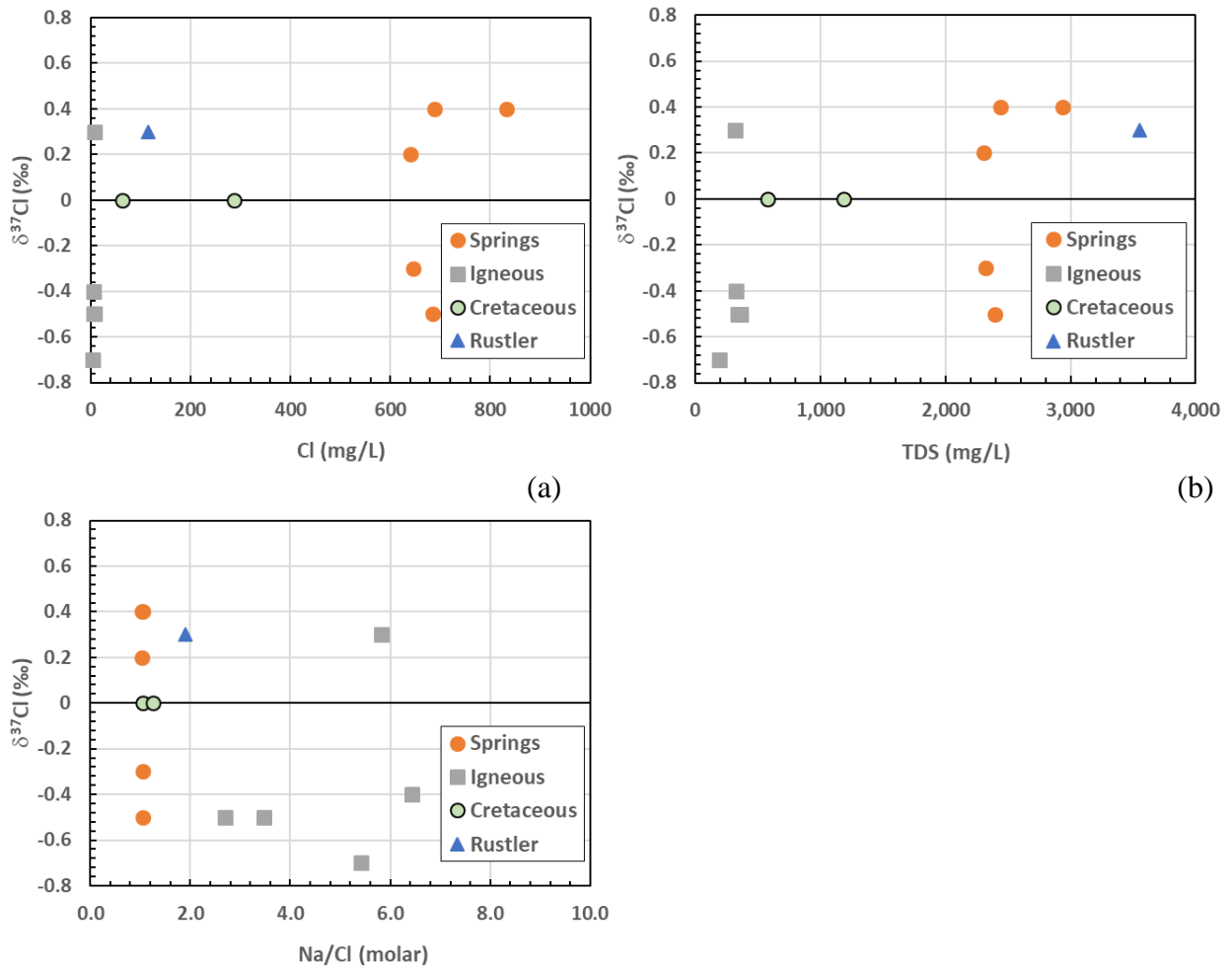


Figure 41. Chlorine isotopes as a function of (a) chloride concentrations, (b) TDS, and (c) Na/Cl ratio.

Figure 42 Sulfate isotopes

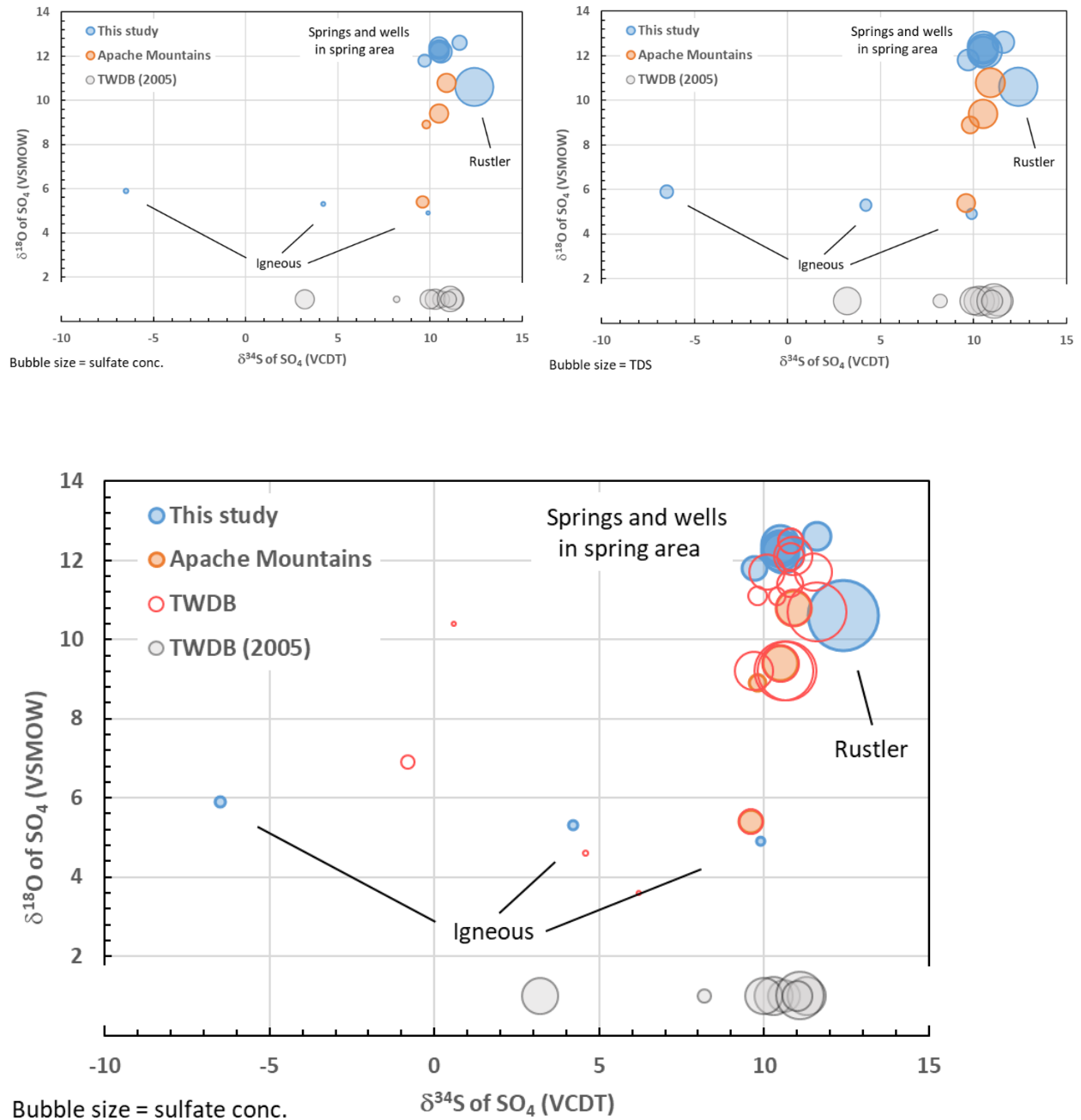


Figure 42. Cross-plot of sulfur and oxygen isotopes of aqueous sulfate with bubble size related to sulfate concentration (a) and TDS (b). Apache mountains dataset (Capitan Reef complex) is from Finch (2017). TWDB is TWDB database (sampling in 2003, 2004, and 2007). Note that the TWDB-TPWD (2005) dataset did not analyze for oxygen isotopes and there is no information on where they fall on the vertical axis.

Figure 43 Spring logger examples

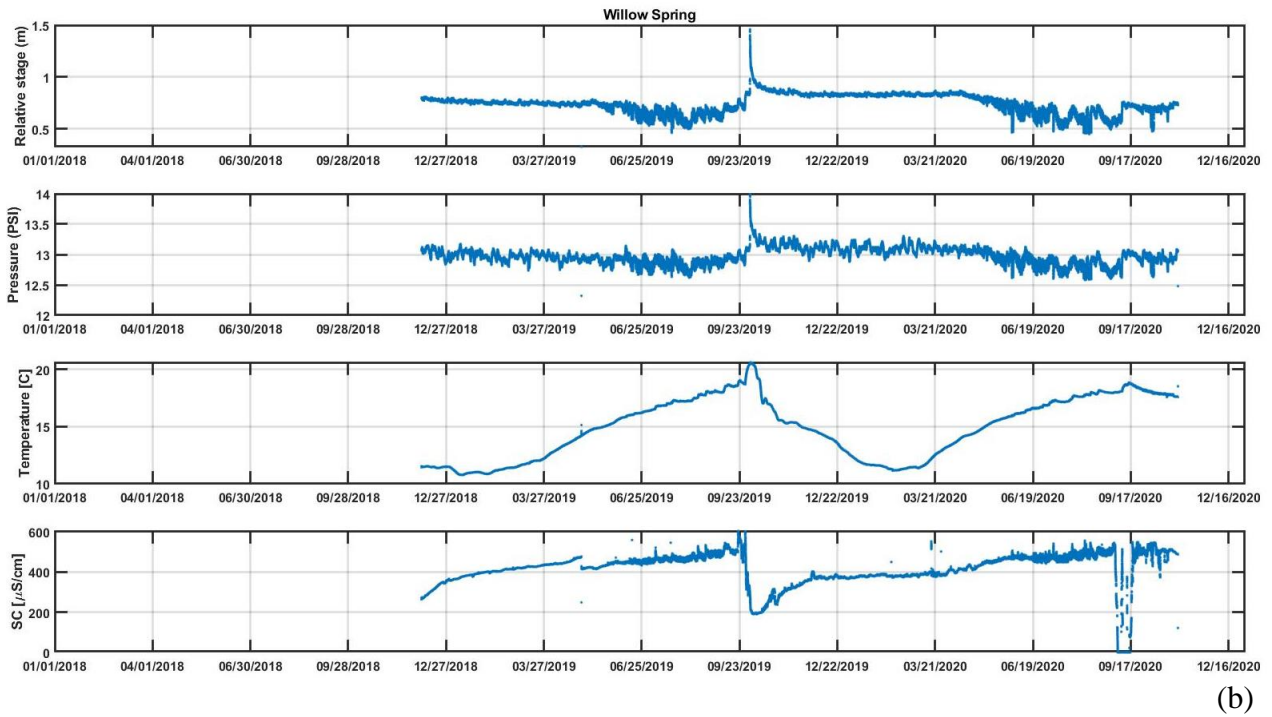
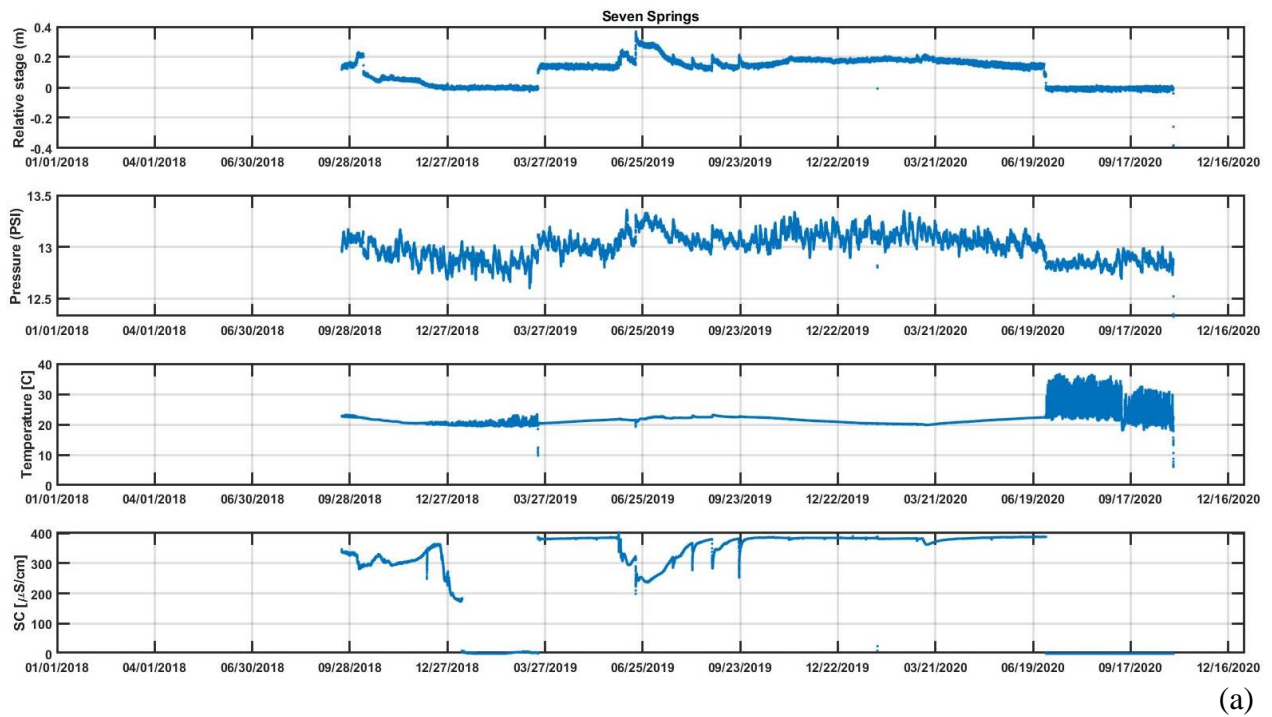


Figure 43. MATLAB[®]-processed logger plots of Davis Mountains springs (Jan. 2018 to Jan. 2020): Seven Springs (a) and Willow Spring (b).

Figure 44 Stream logger examples

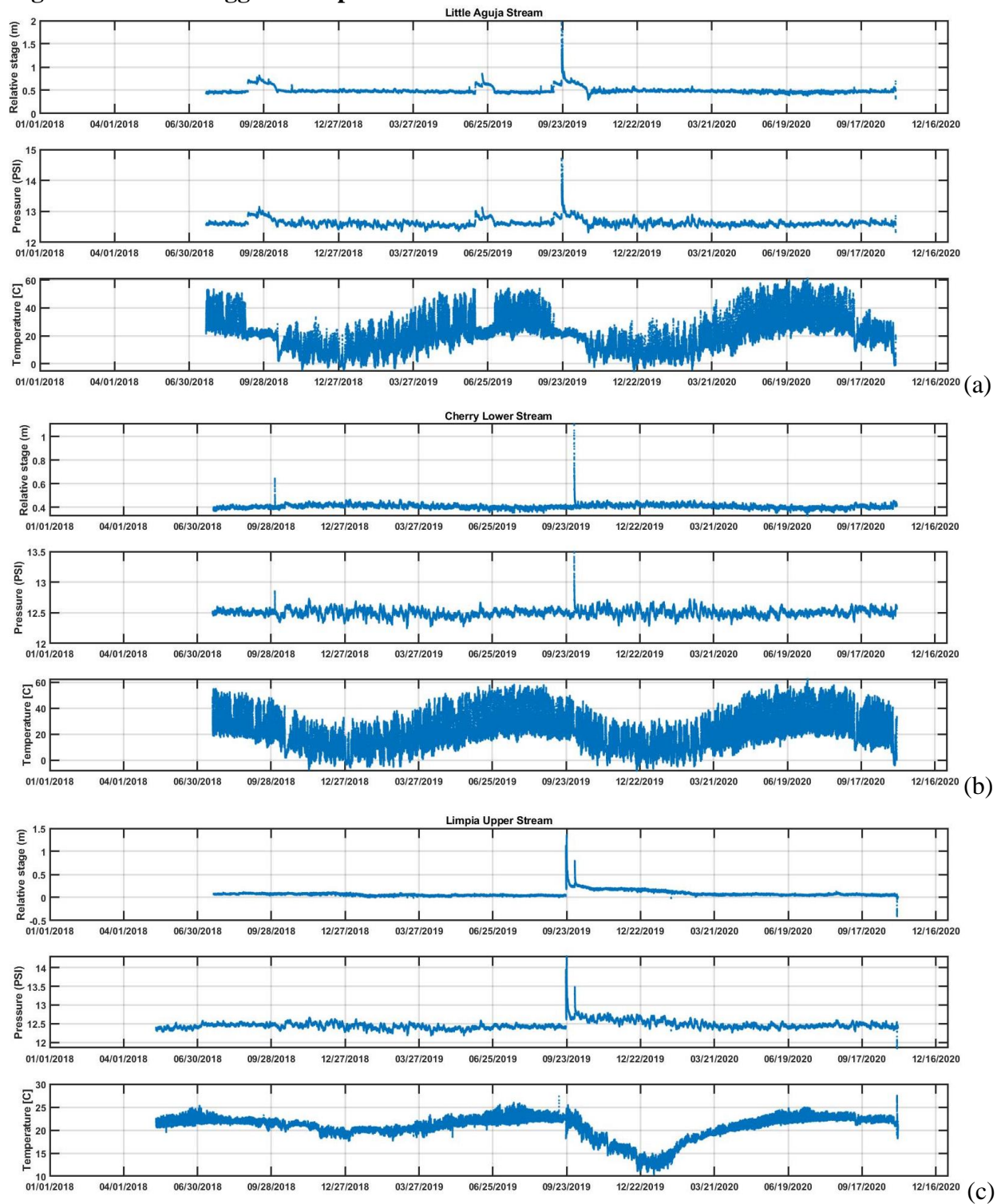


Figure 44. MATLAB[®]-processed logger plots of Davis Mountains stream (Jan. 2018 to Jan. 2020): Little Aguja (a), Lower Cherry (b), and Limpia Upper (c).

Figure 45 Monitoring well logger examples

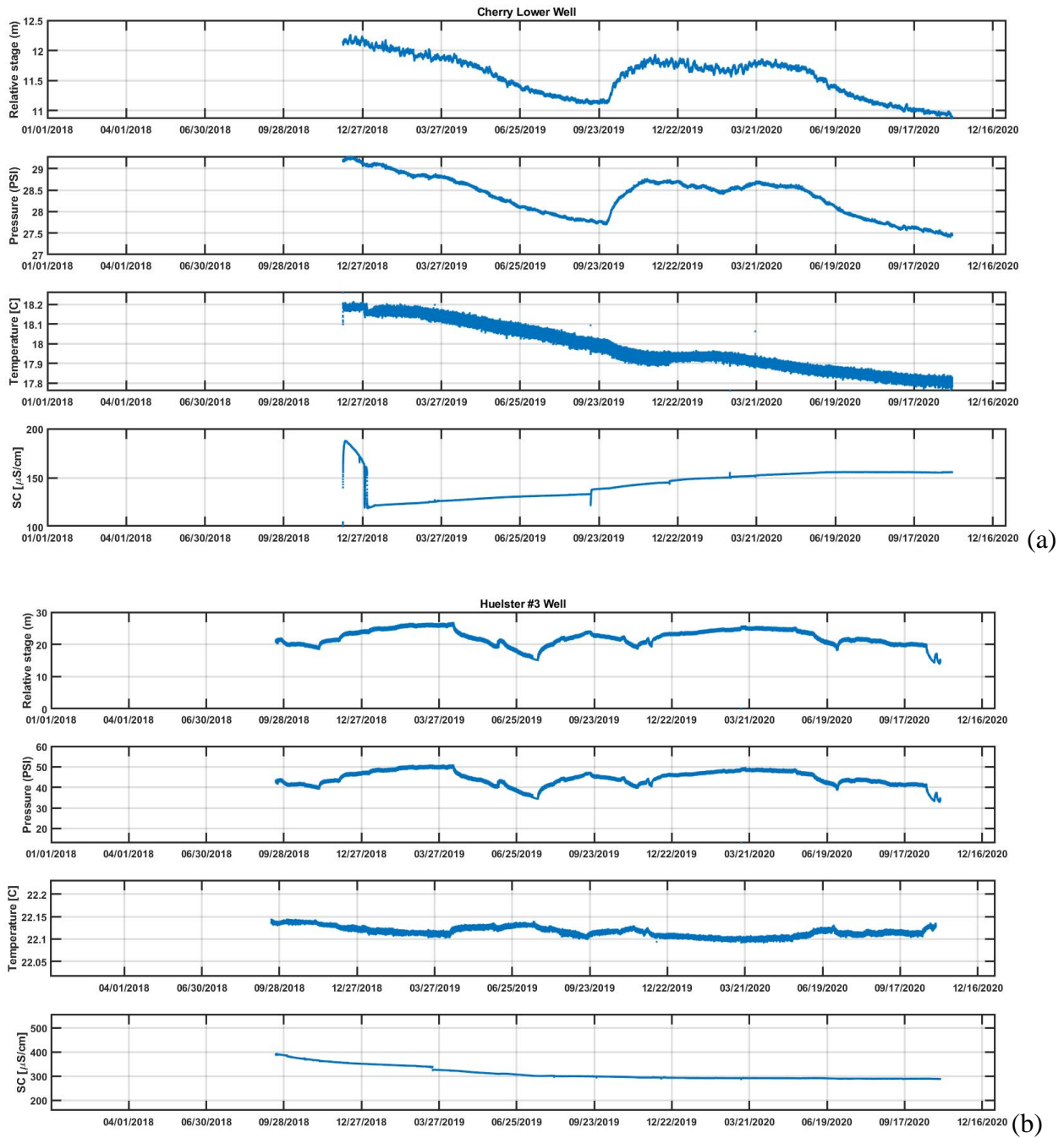


Figure 45. MATLAB[®]-processed logger plots of water wells (Jan. 2018 to Jan. 2020): Cherry Lower (a) and Huelster #3 (b).

Figure 46 Unprocessed WellIntel[®] examples

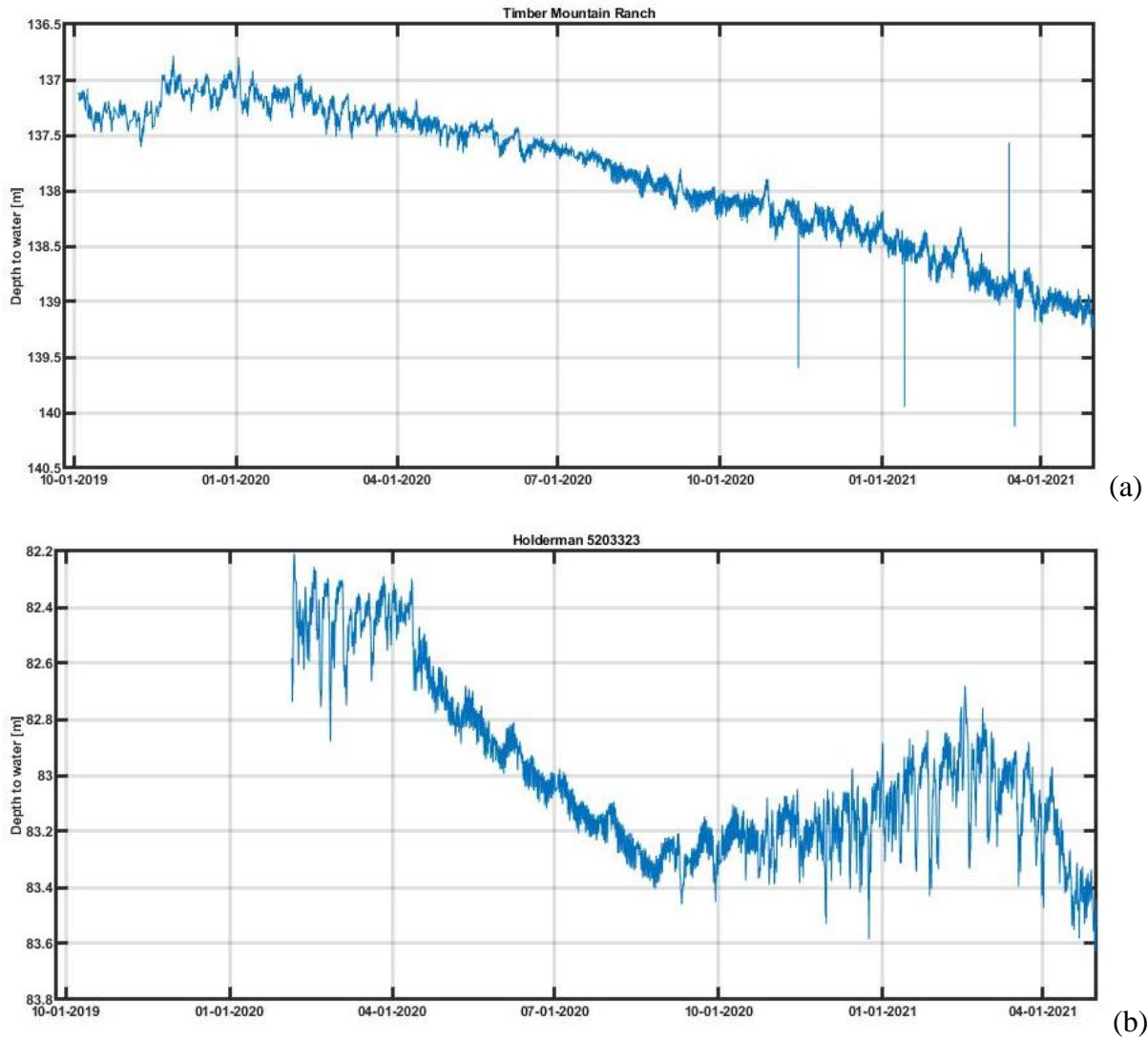


Figure 46. Unprocessed WellIntel[®] measurements (depth to water) on two sounders installed on water wells: (a) Timber Mountain Ranch; and (b) Well 52-03-323 (Holderman).

Figure 47 water levels

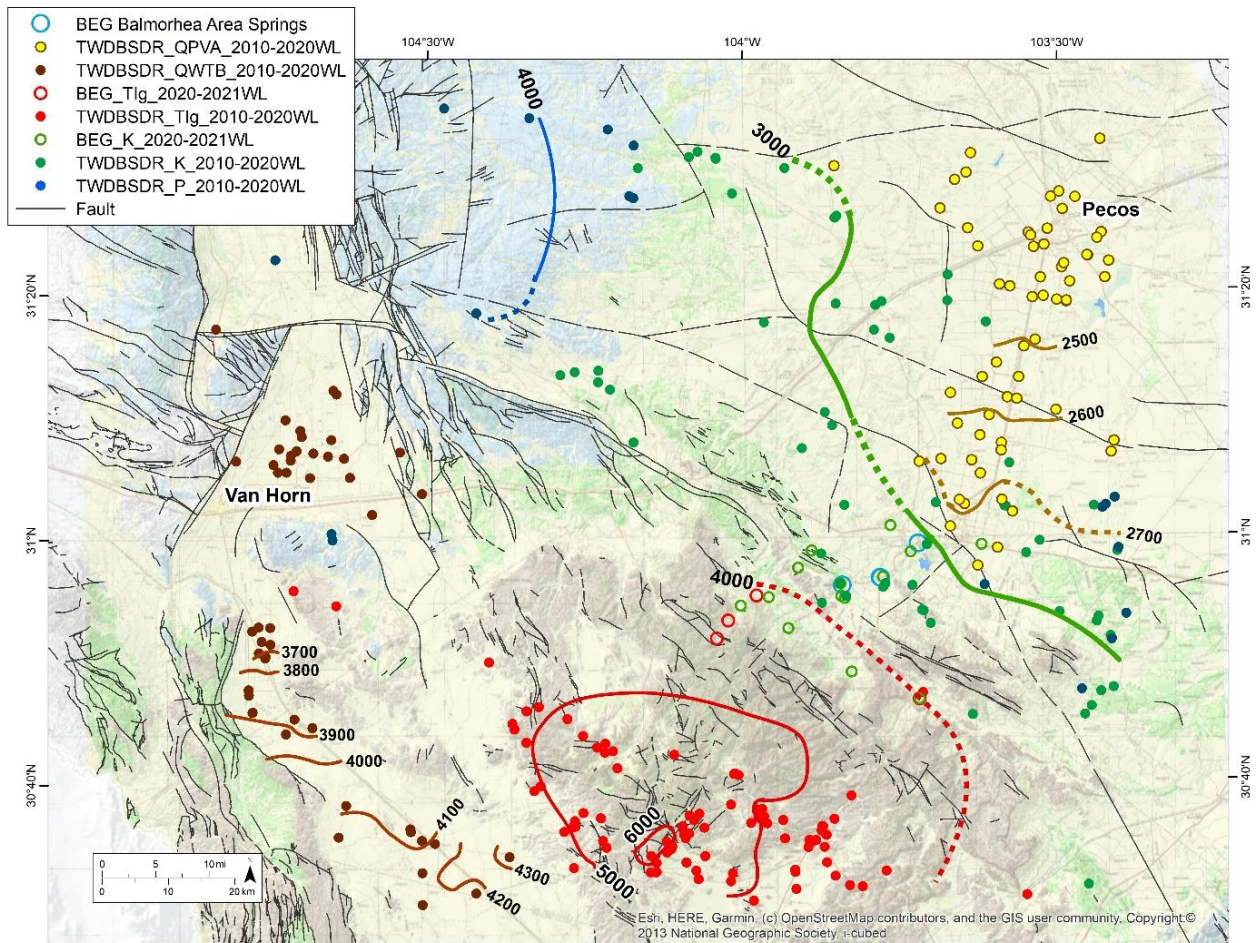


Figure 47. Well locations with groundwater potentiometric contours (feet amsl) based on water level elevation points shown in Figure 16.

Figure 48 Elevated PVA

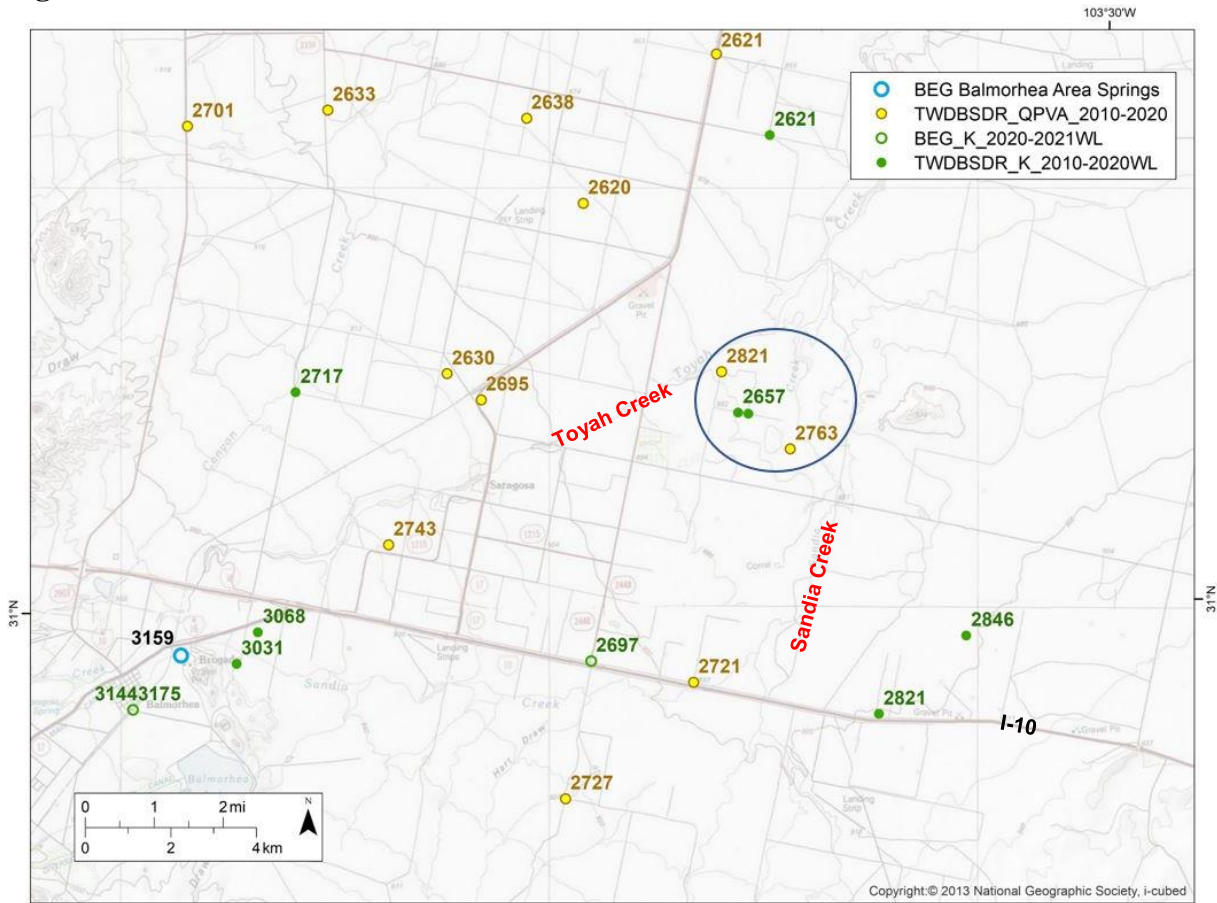


Figure 48. Elevated water levels in Pecos Valley wells adjacent to Toyah and Sandia creeks north of I-10.

Figure 49 X-formatinal flow

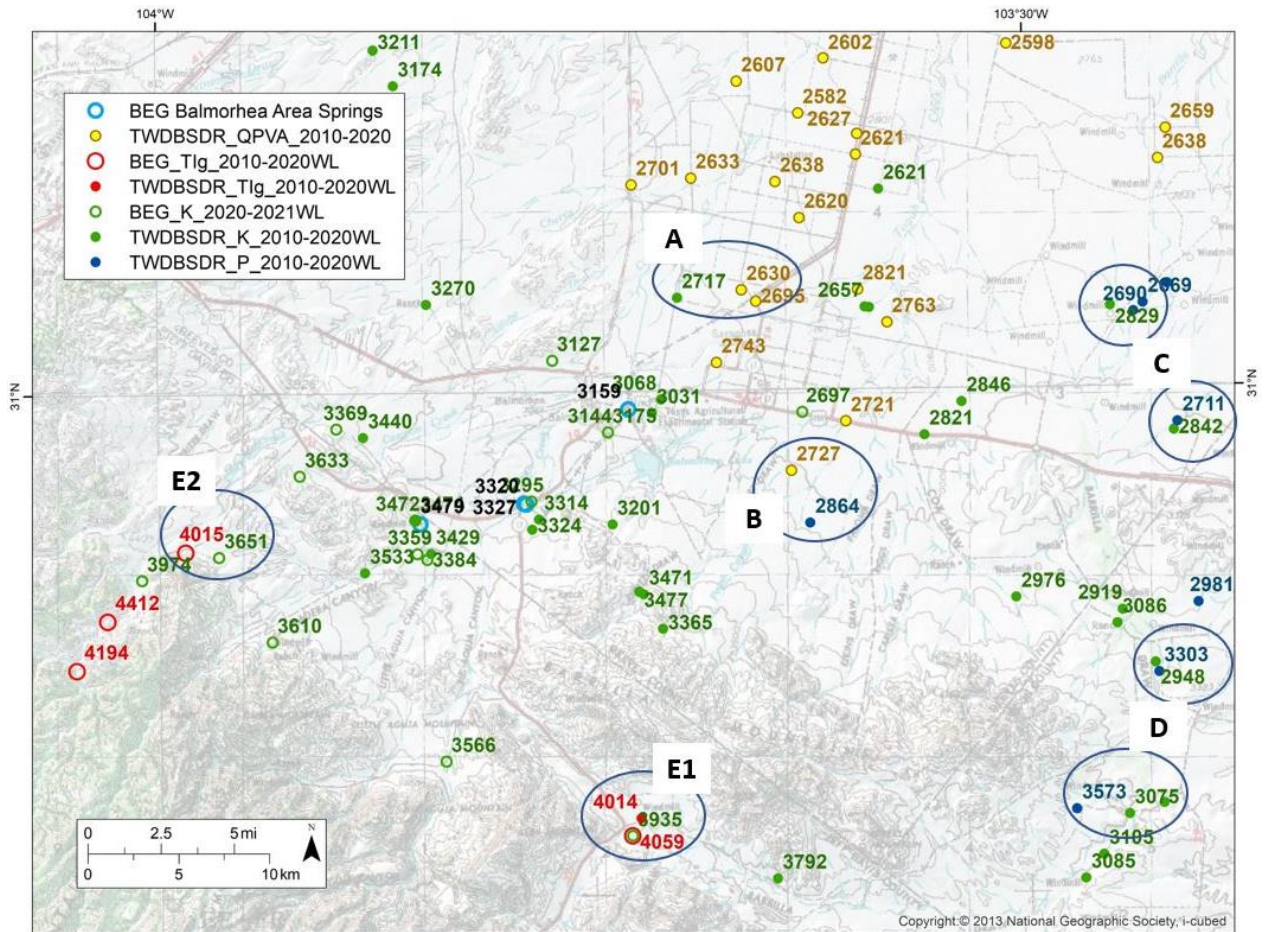


Figure 49. Differences in water level elevations for wells completed in multiple aquifer zones.

Figure 50 Spring flow data point count

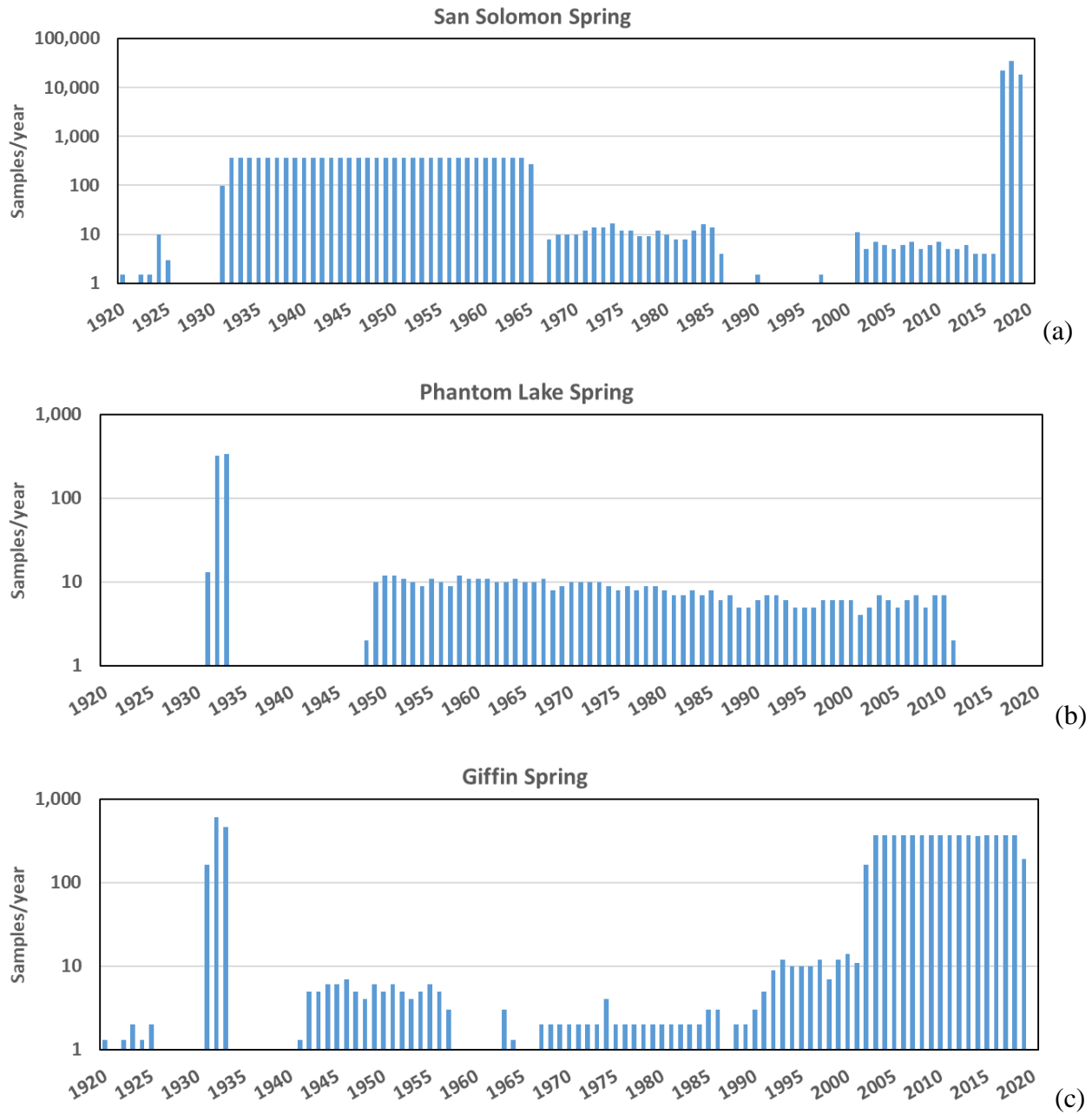


Figure 50. Spring flow measurement temporal density: (a) San Solomon; (b) Phantom Lake; and (c) Giffin springs

Figure 51 SSS calendar day

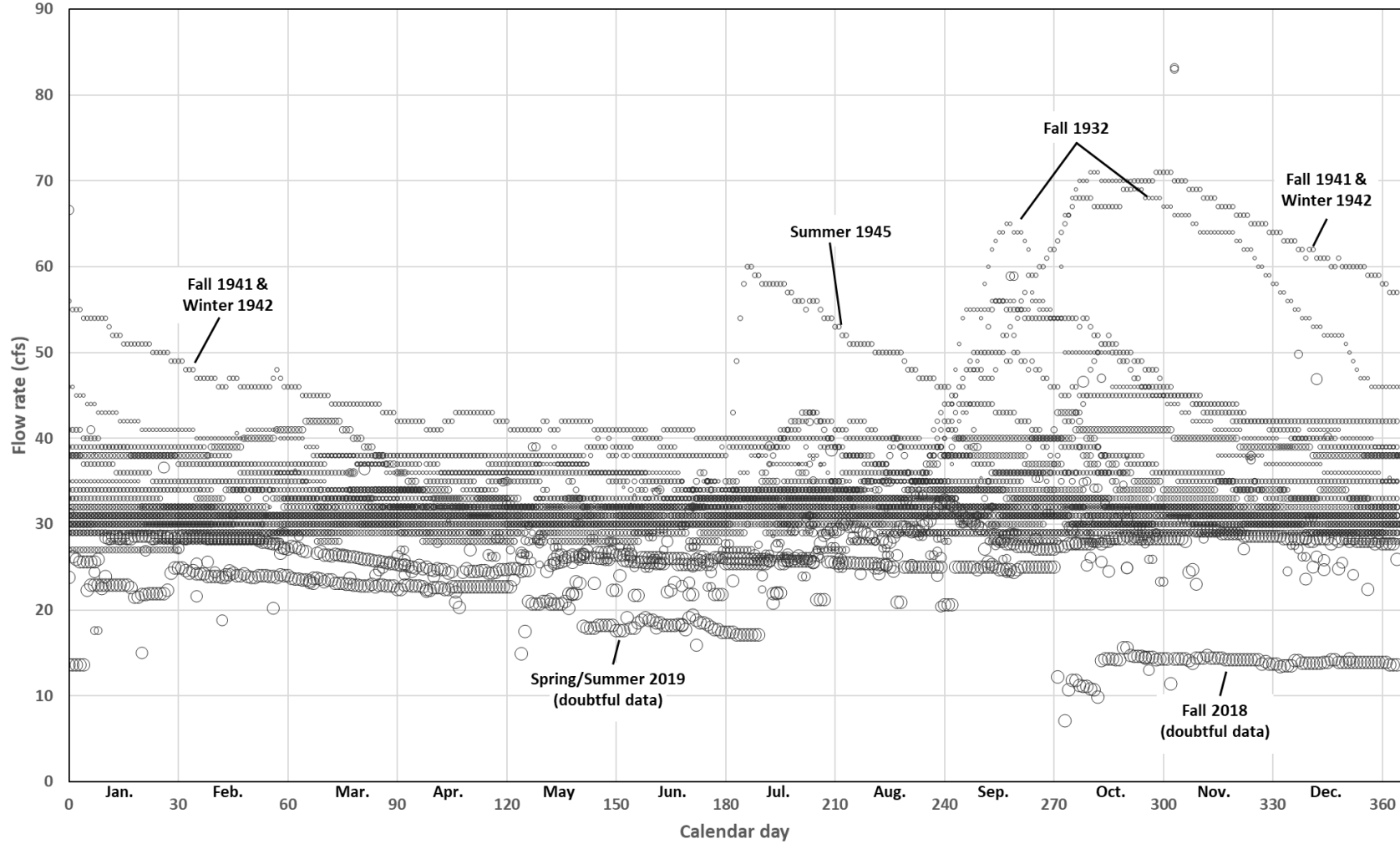


Figure 51. Historical San Solomon spring flow rates as a function of the day of the year (calendar day). Exceptional events stand out and are labeled. Dot size is proportional to sampling time (small initially, growing larger to the present). It can be noted that all captured exceptional events are in the far past and that the flow rate has been declining over the years (bigger dots at lower rates). (13,540 data points)

Figure 52. PL calendar day

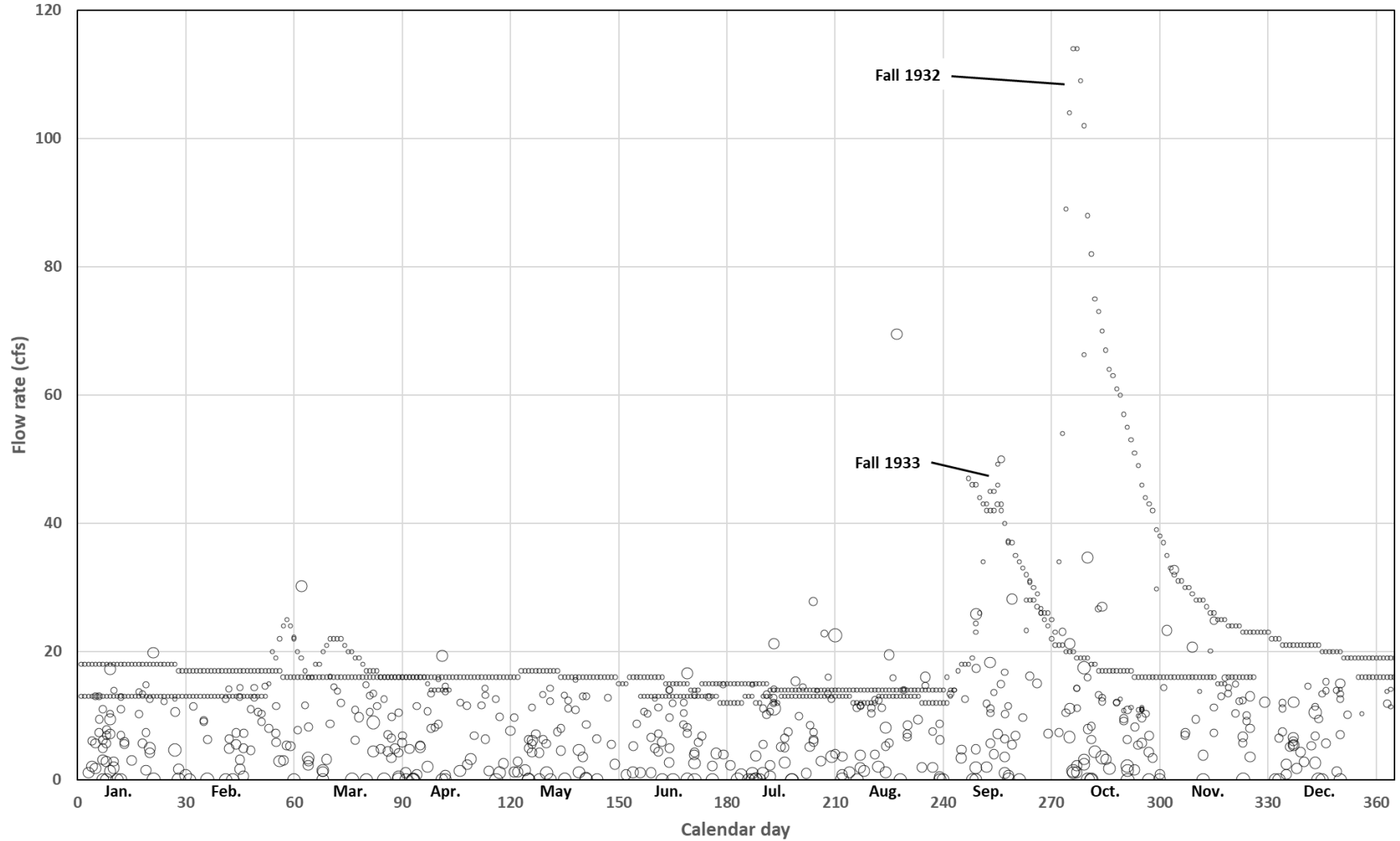


Figure 52. Historical Phantom Lake spring flow rates as a function of the day of the year (calendar day). Exceptional events are labeled. Dot size is proportional to sampling time (small initially, growing larger to the present). It can be noted that flow rate has been declining over the years (bigger dots at lower rates). The spring does not currently flow naturally. (1182 data points).

Figure 53 Giffin calendar day

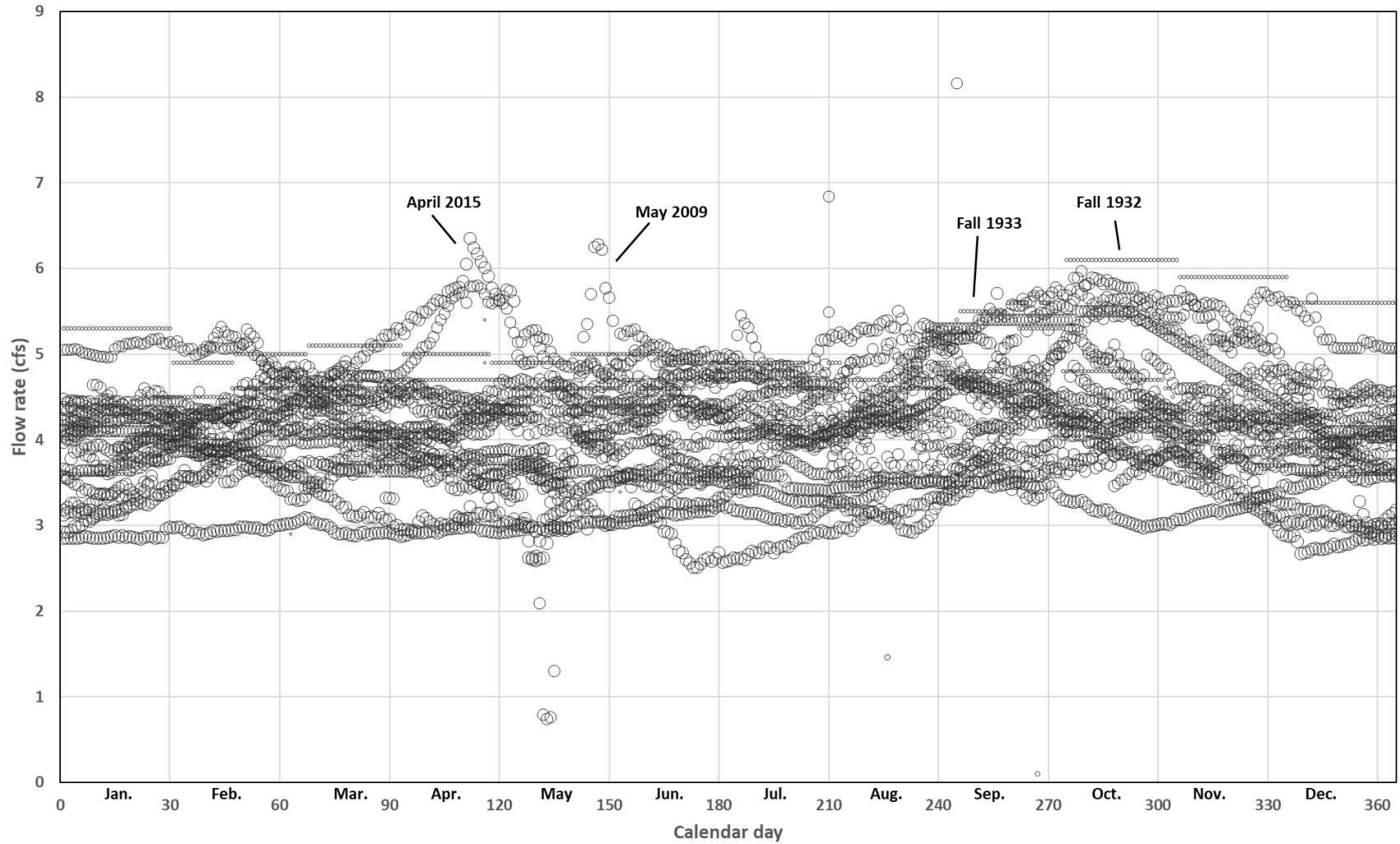


Figure 53. Historical Giffin flow rates as a function of the day of the year (calendar day). Dot size is proportional to sampling time (small initially, growing larger to the present). It can be noted that flow rate has remained relatively steady with possibly a small decline. Two isolated data points at 6.84 and 8.16 cfs are likely measurement errors or due to very local precipitation events. (6923 data points)

Figure 54 SSS extremes

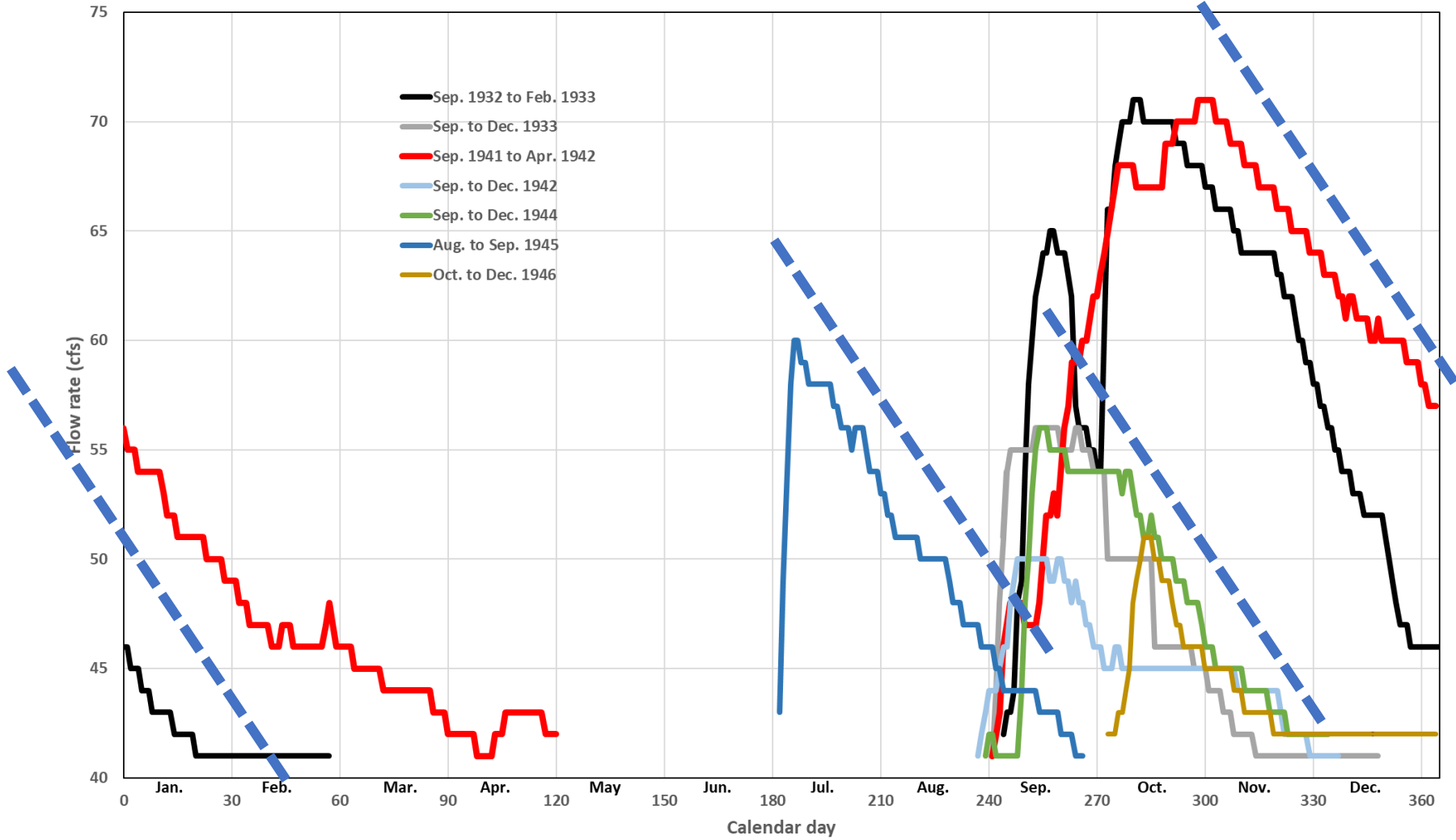


Figure 54. San Solomon above-baseflow historical flow rates as a function of the day of the year (1932-1946). The thick blue dotted lines are all strictly parallel and underline the similar slope of the descending limb, a characteristic of the system.

Figure 55 Ph.L. extreme

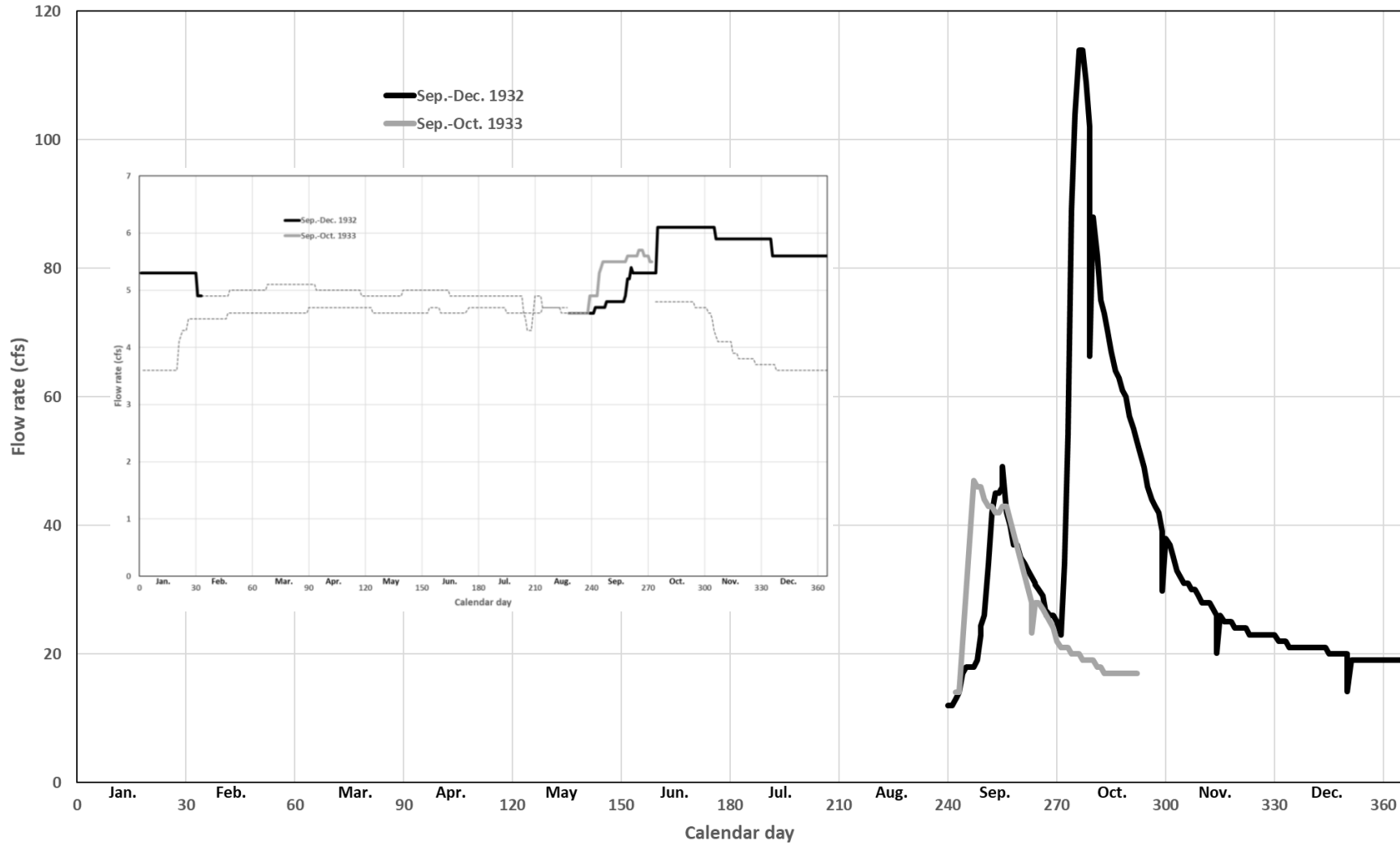
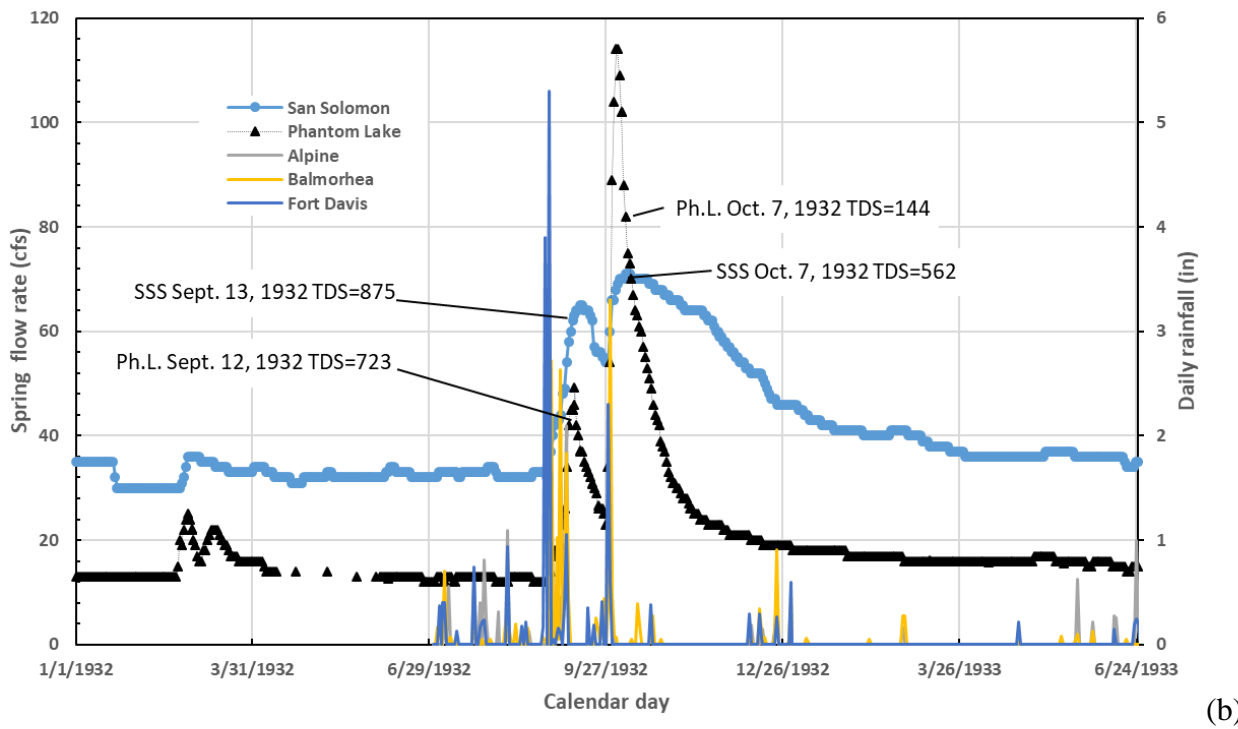
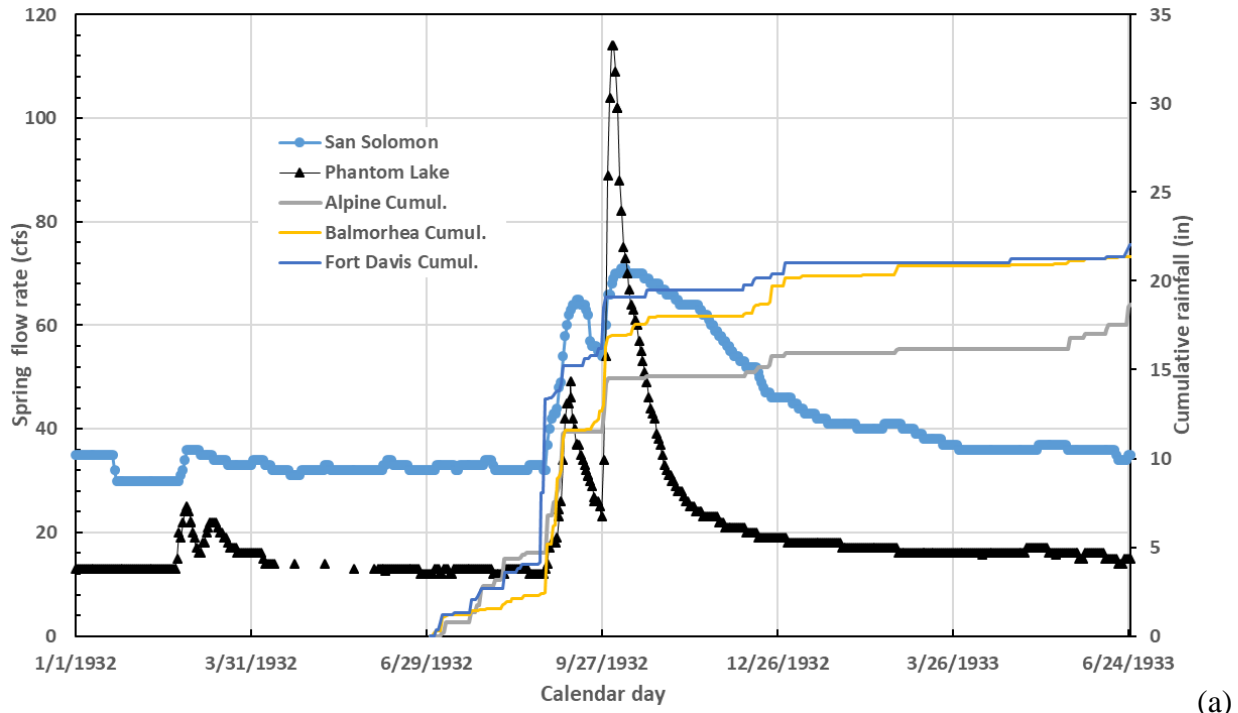
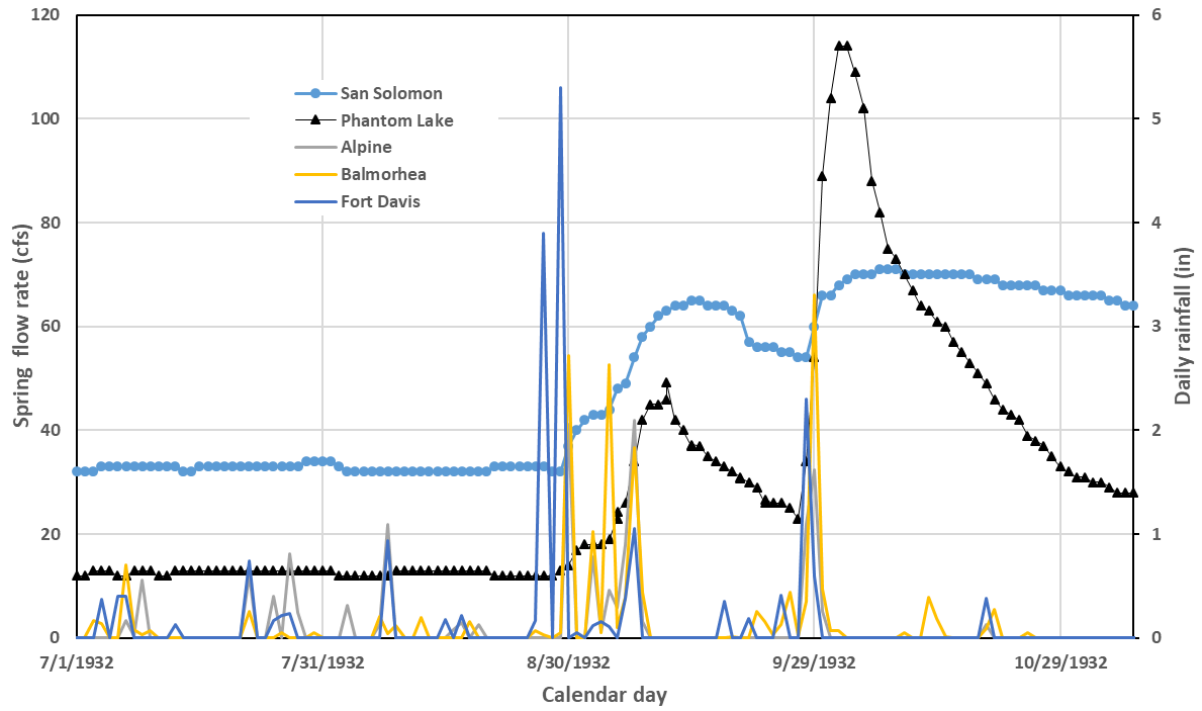


Figure 55. Phantom Lake and Giffin (inset) above-baseflow historical flow rates as a function of the day of the year (1932-1933). Early measurements (5 days) of Phantom Lake 1933 event missing in the dataset.

Figure 56 1932-33 flow and rain

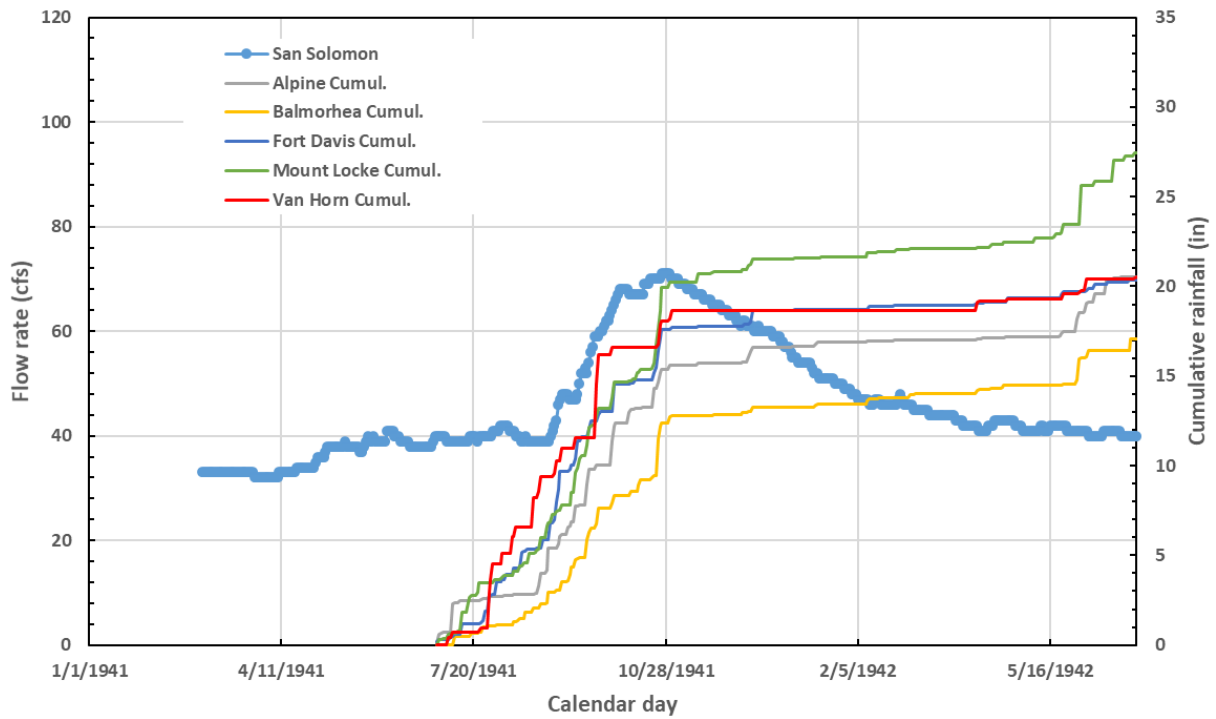




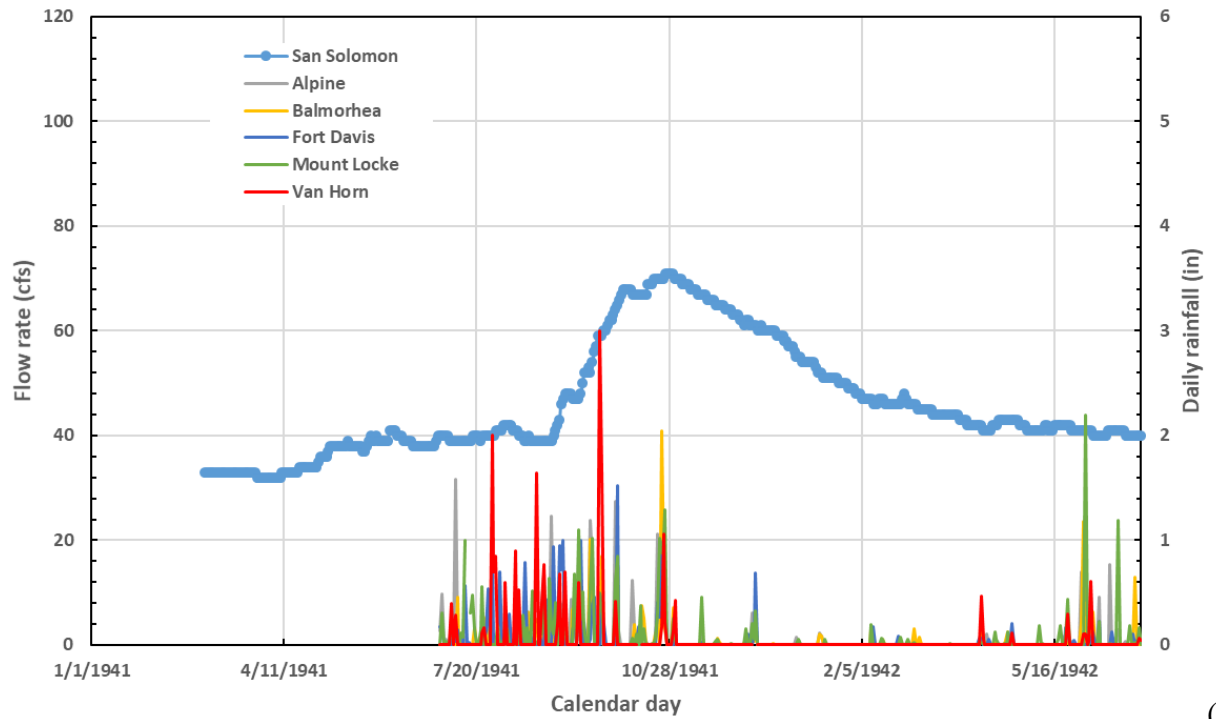
(c)

Figure 56. San Solomon and Phantom Lake extreme event spring flow (1932-33). TDS values from White et al. (1941). (a) daily flow rates and cumulative precipitation; (b) daily flow rates and daily precipitation; and (c) daily flow rates and daily precipitation focusing on the large event.

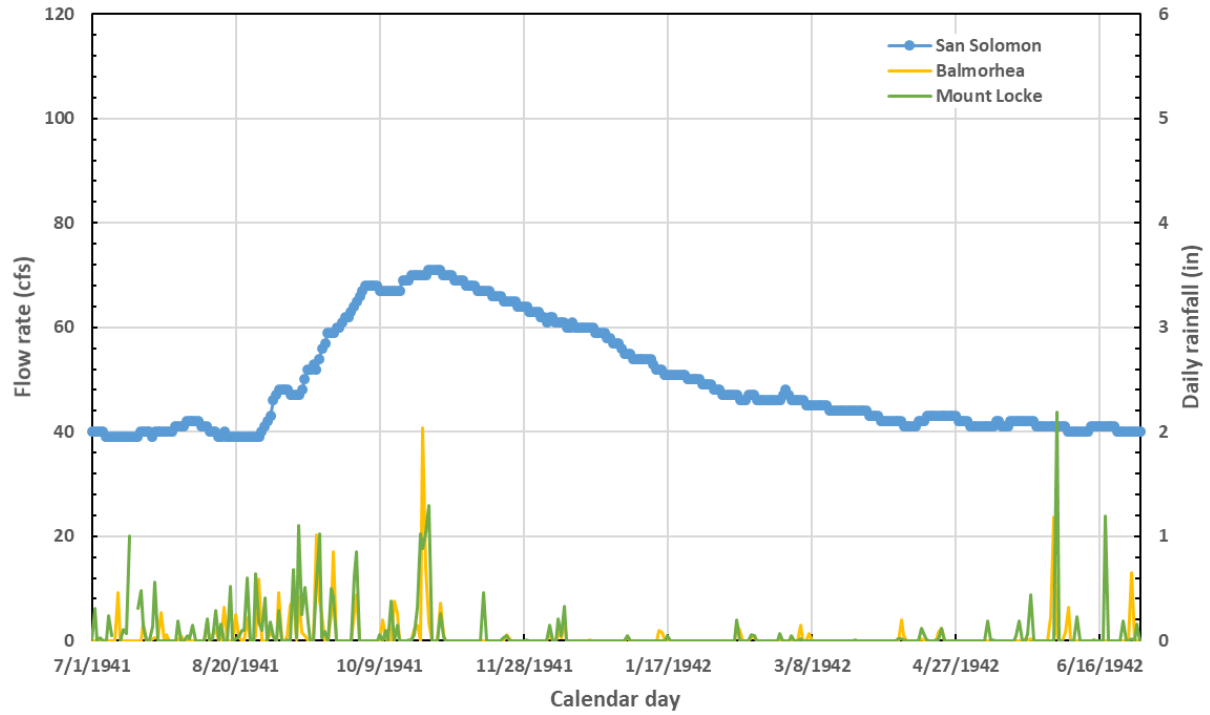
Figure 57 1941-42 flow and rain



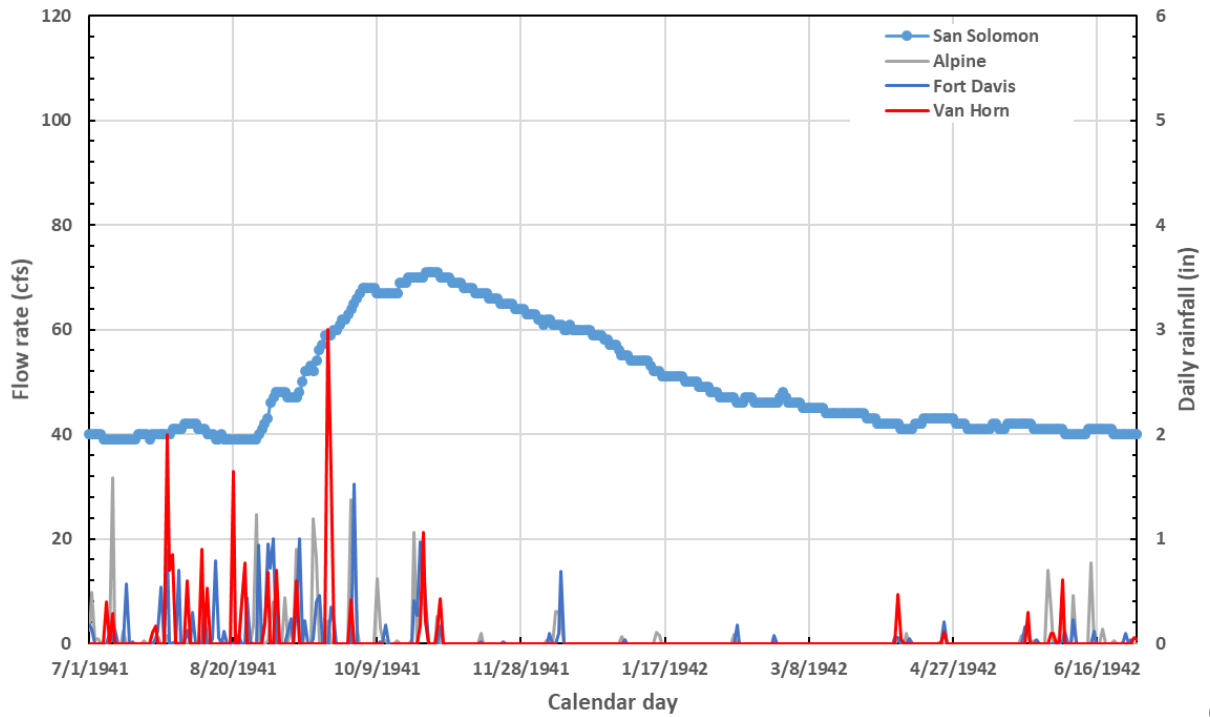
(a)



(b)



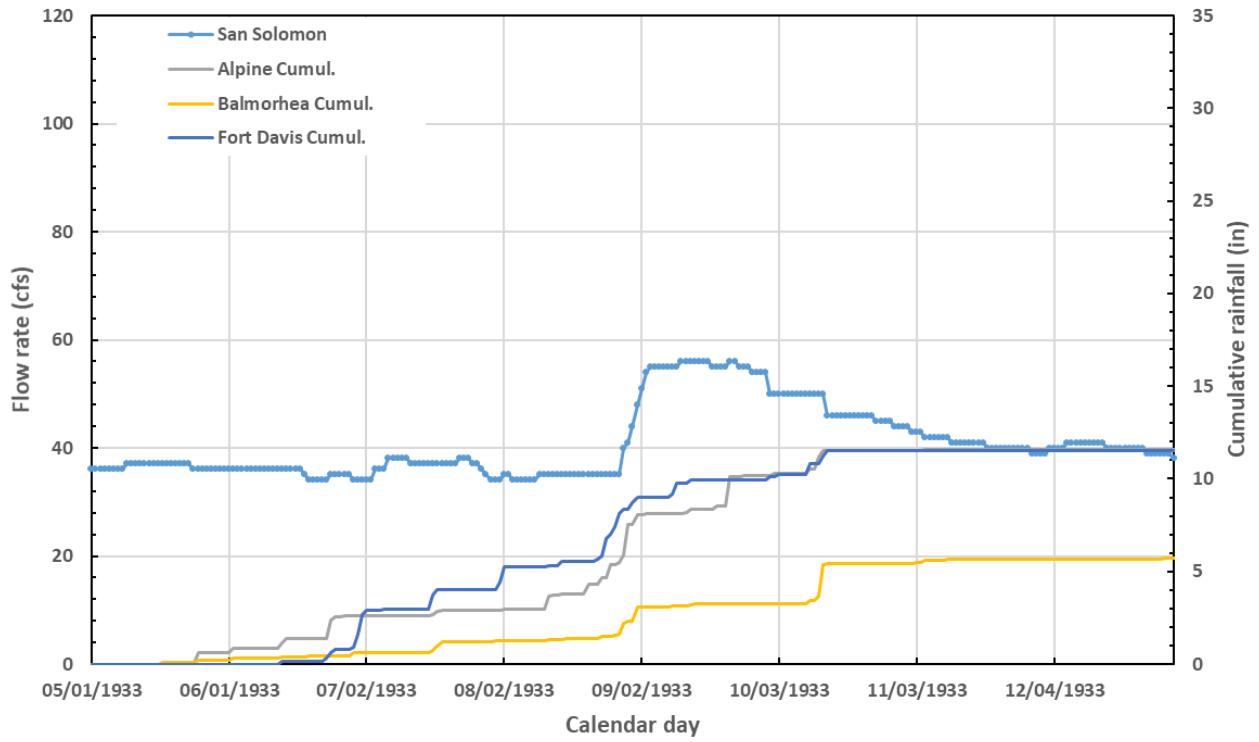
(c)



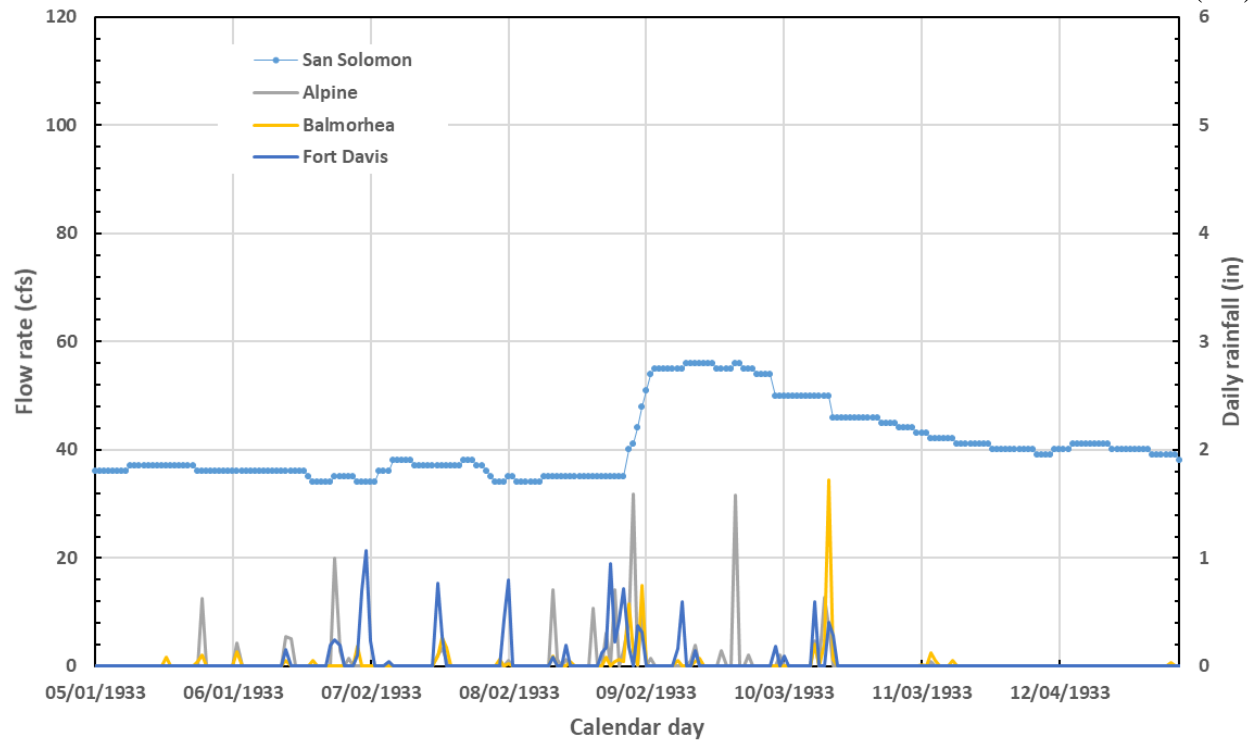
(d)

Figure 57. San Solomon extreme event spring flow (1941-42). (a) daily flow rates and cumulative precipitation; (b) daily flow rates and daily precipitation; (c) daily flow rates and daily precipitation focusing 3 weather stations; and (d) focusing on the other 2 weather stations.

Figure 58 Minor extreme flows

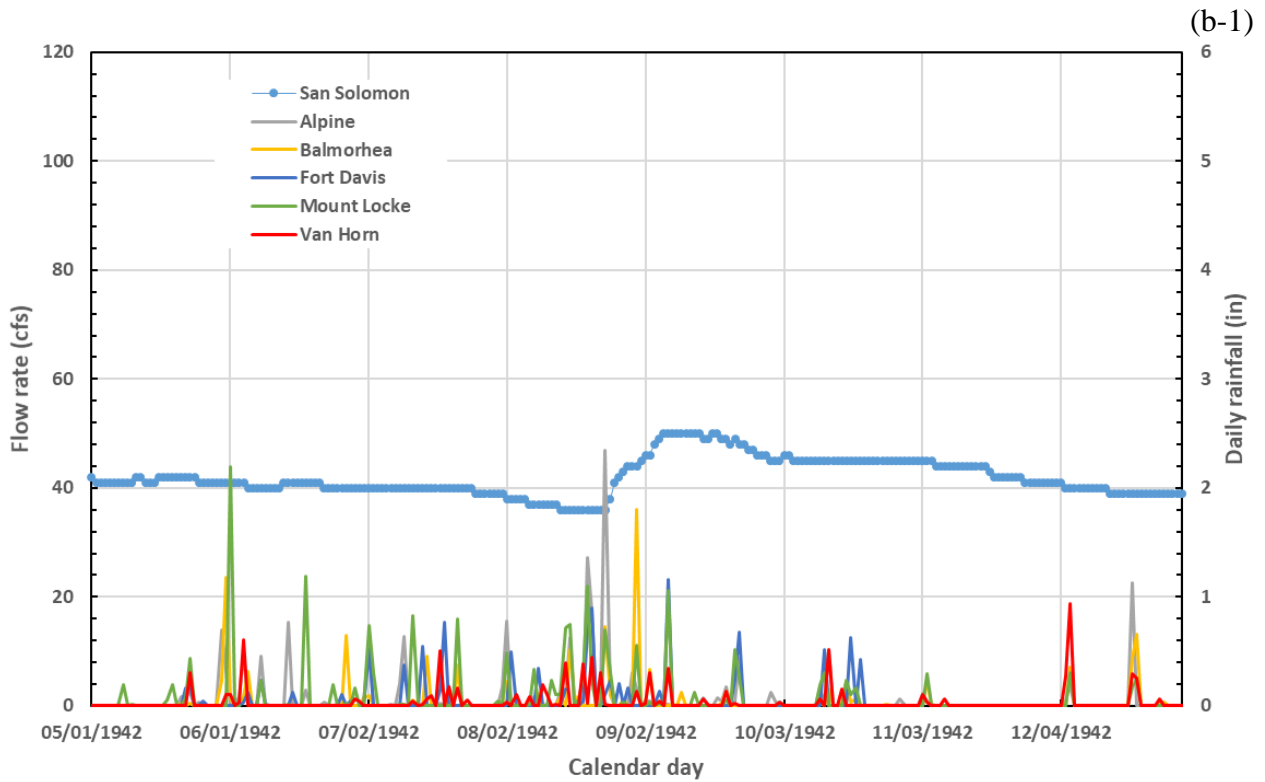
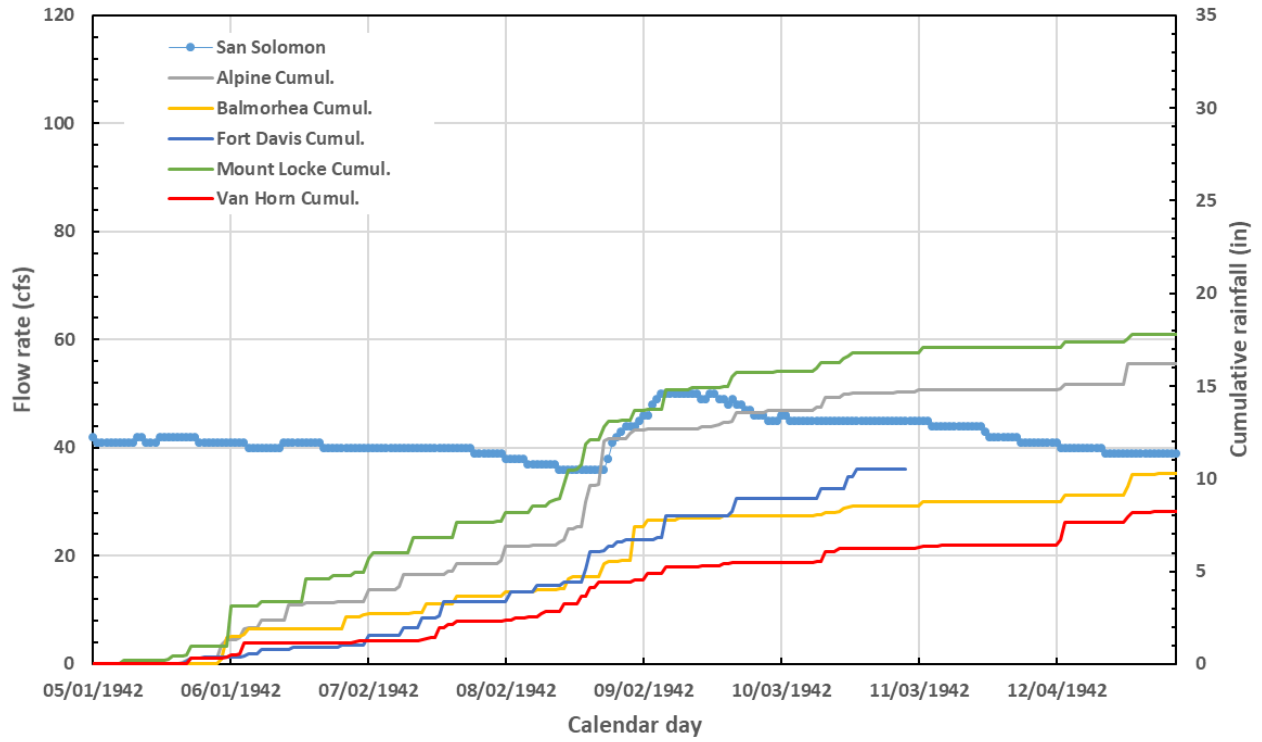


(a-1)

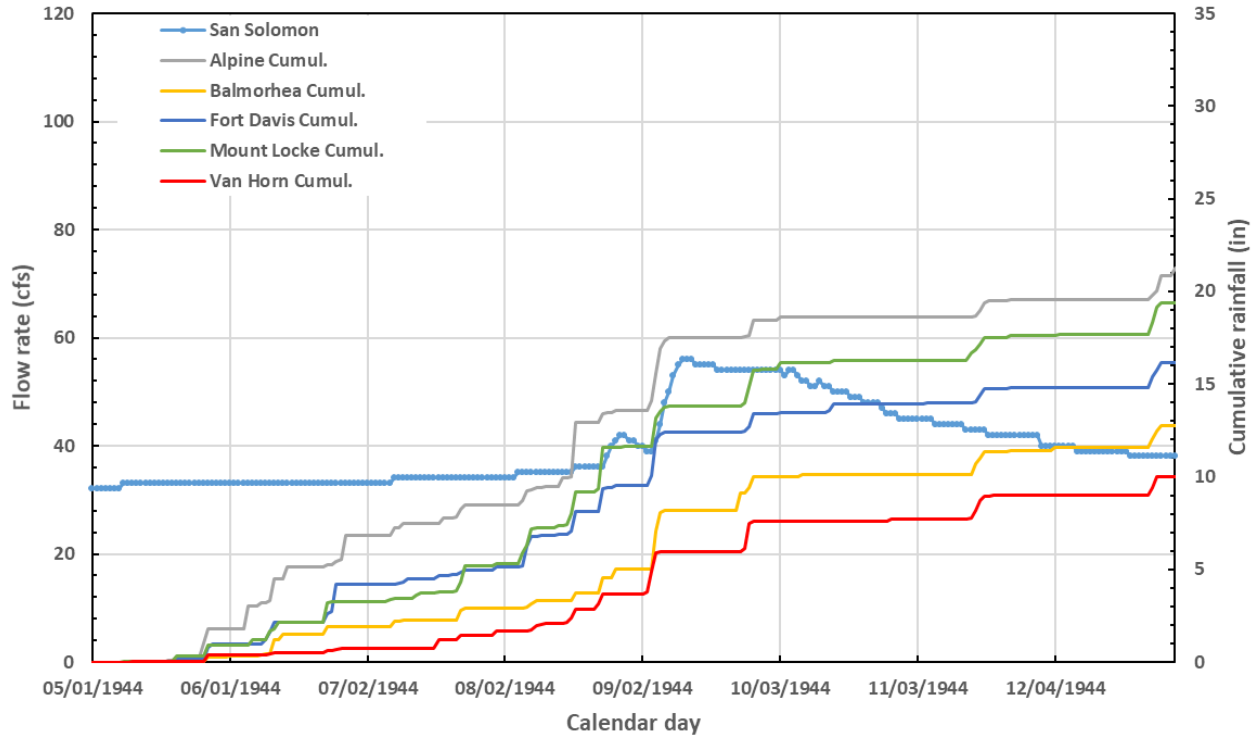


(a-2)

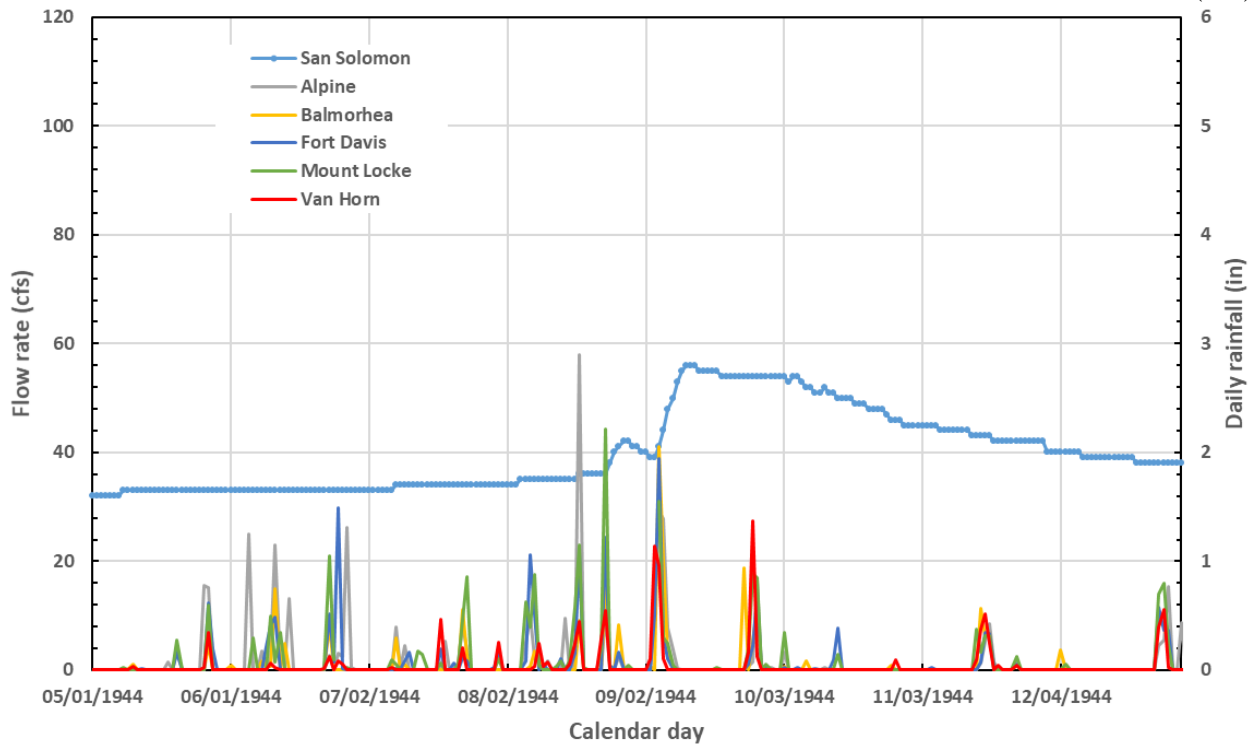
Sept.-Dec. 1933



Sept.-Dec. 1942

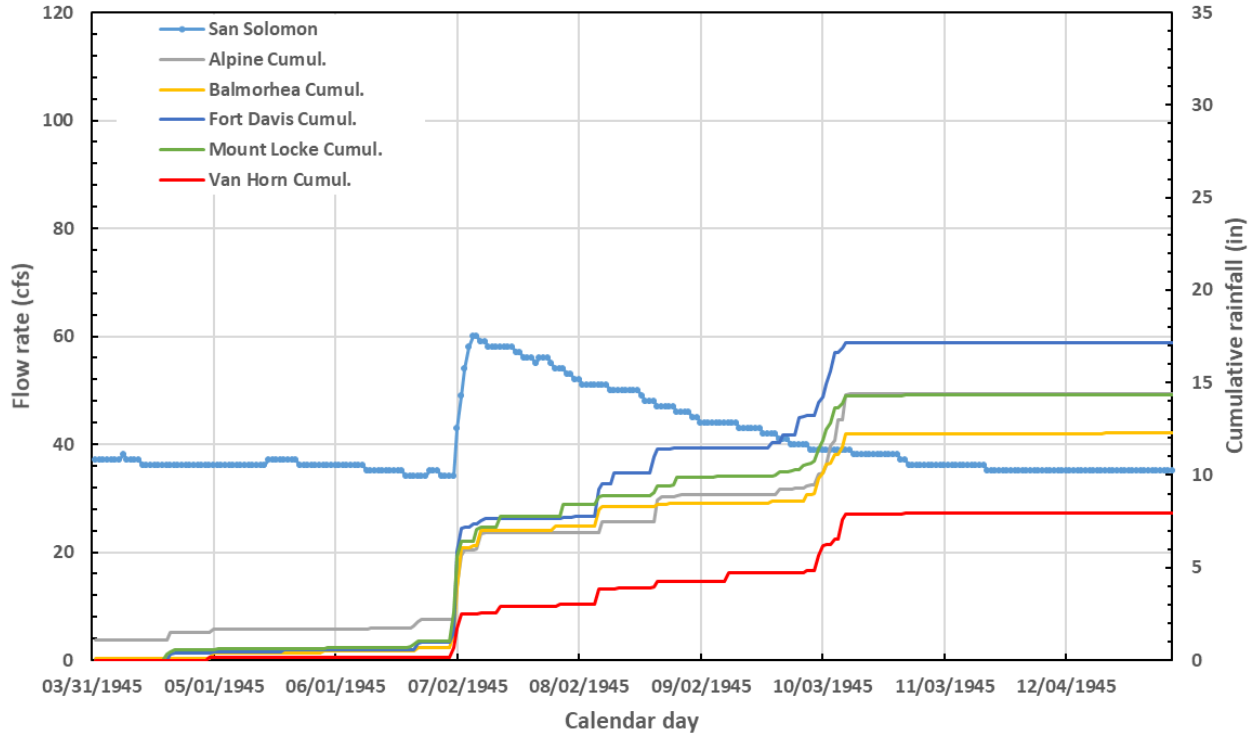


(c-1)

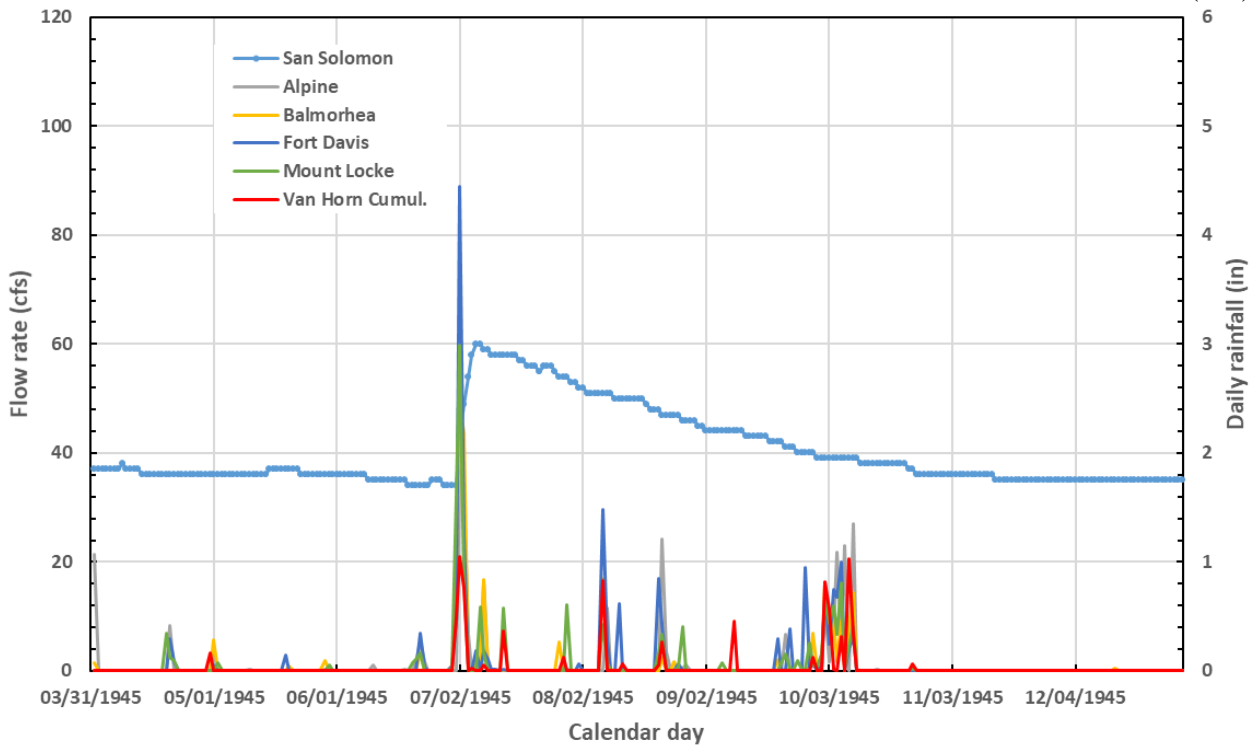


(c-2)

Sept.-Dec. 1944

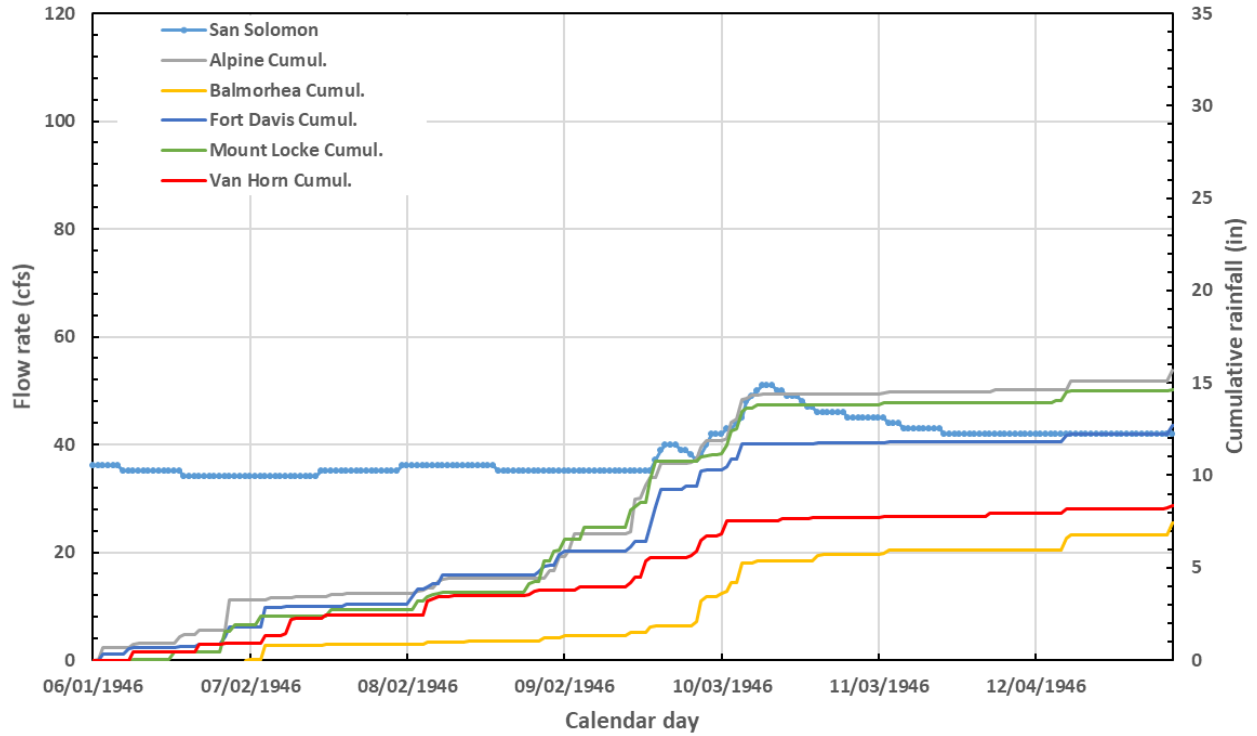


(d-1)

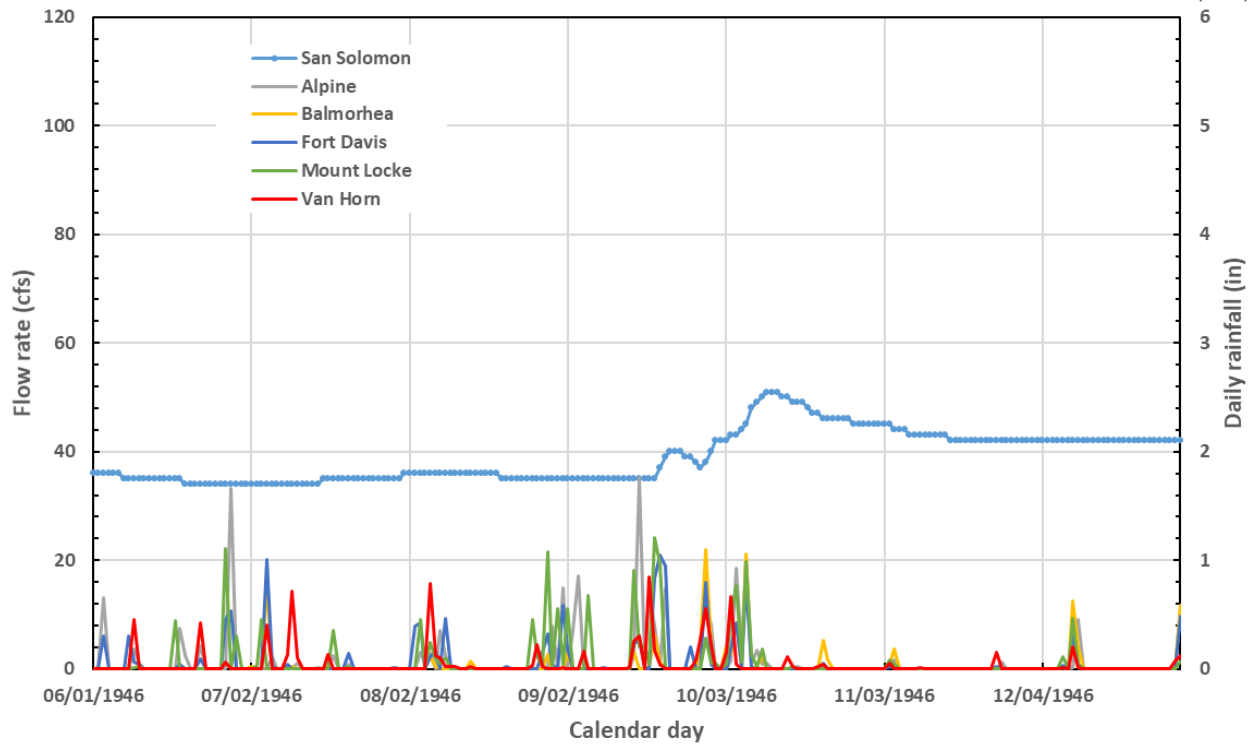


(d-2)

Jul.-Dec. 1945



(e-1)



(e-2)

Oct.-Dec. 1946

Figure 58. San Solomon minor extreme events (1933 and 1942-1946).

Figure 59 spring TDS vs. time

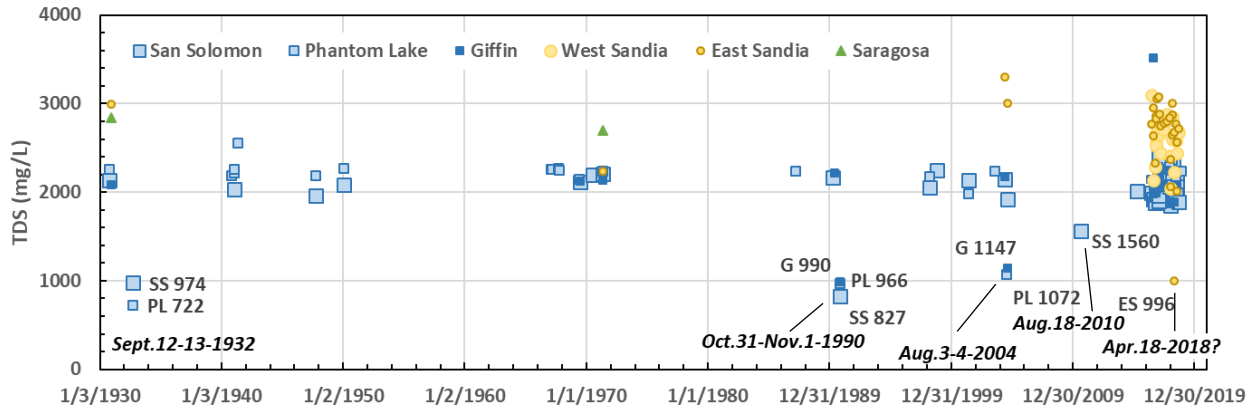


Figure 59. TDS of Balmorhea springs historical water samples. Reported low TDS values are shown next to the spring short names (SS: San Solomon; PL: Phantom Lake; G: Giffin; ES: East Sandia) and sampling date.

Figure 60 SSS daily recent

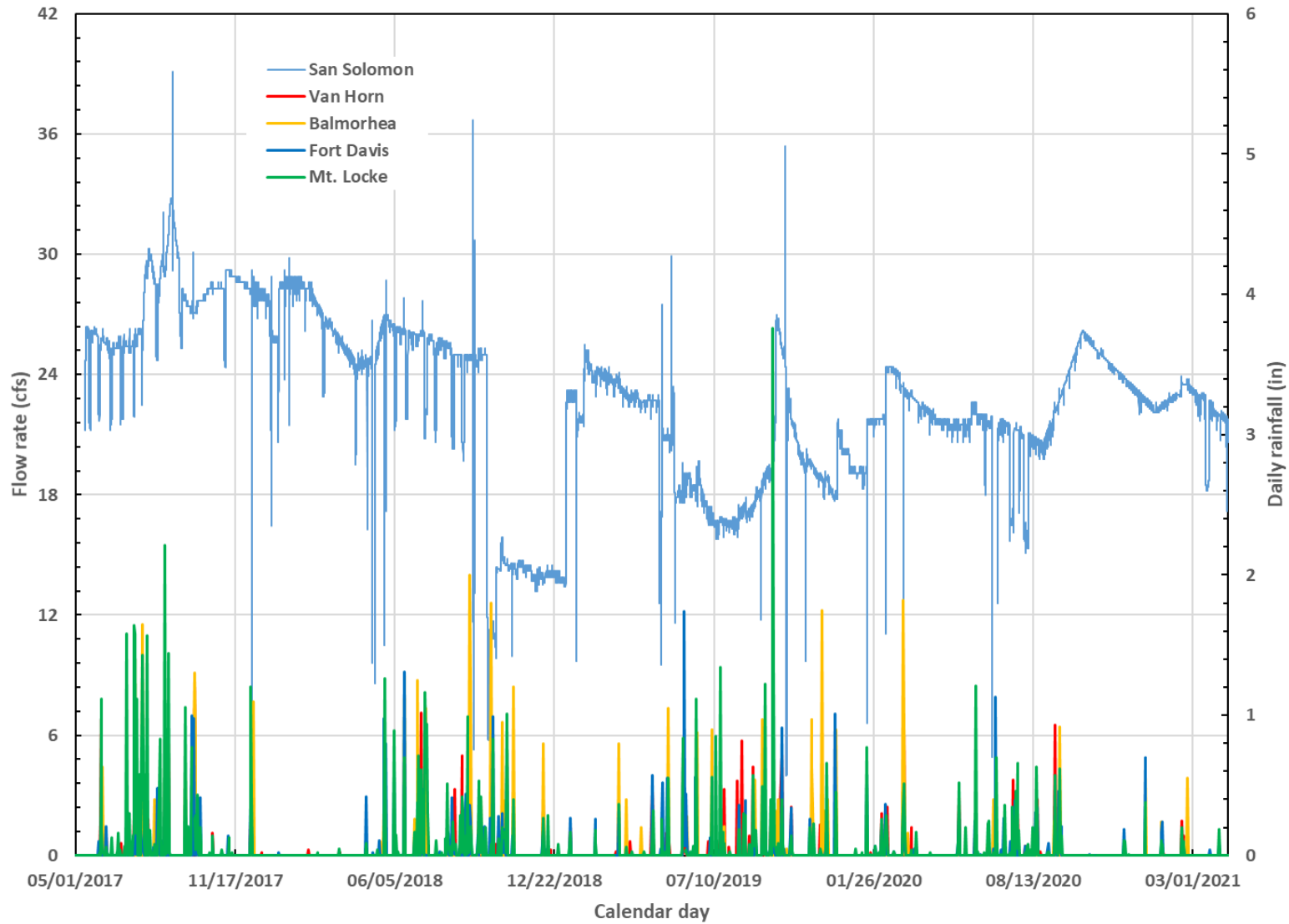


Figure 60. San Solomon daily flow rate and daily precipitation at nearby weather stations (5/2017-3/2021).

Figure 61 SSS 2019 event

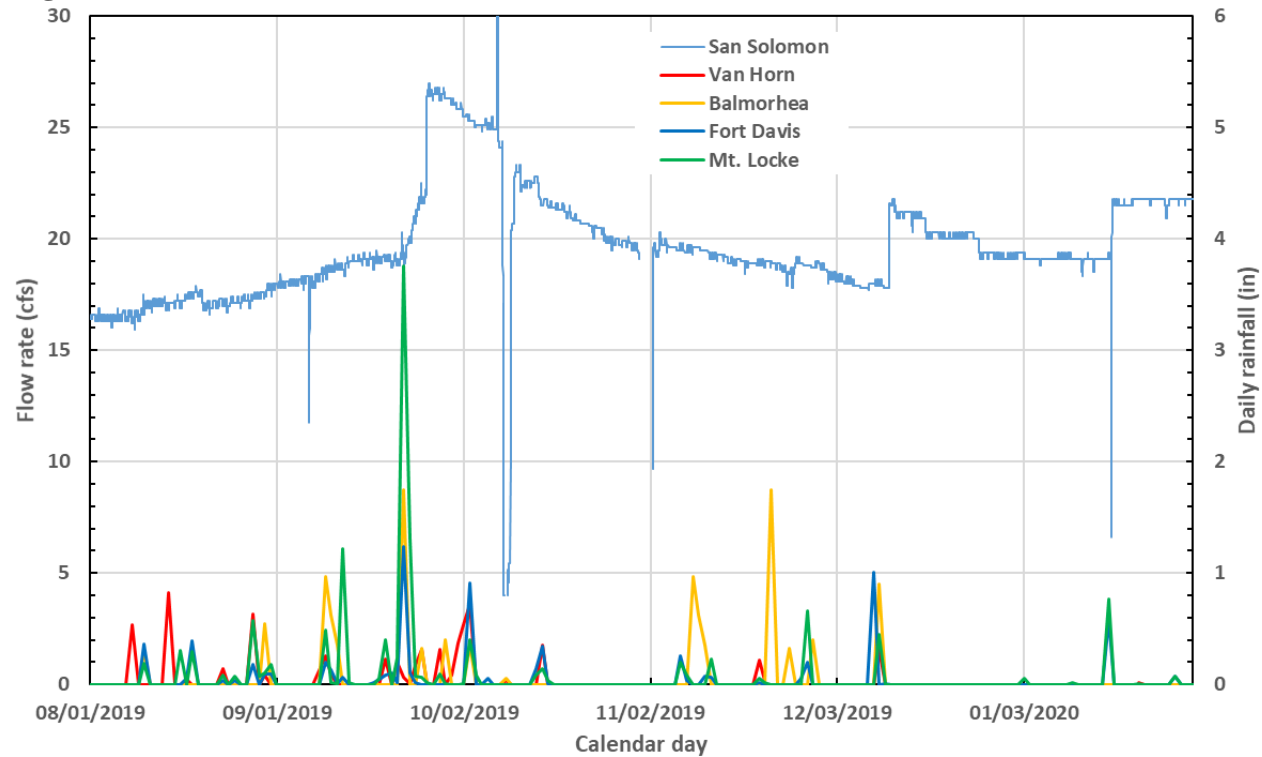


Figure 61. San Solomon daily flow rate and daily precipitation at nearby weather stations during the Fall 2019 event.

Figure 62 USGS+BEG Full period

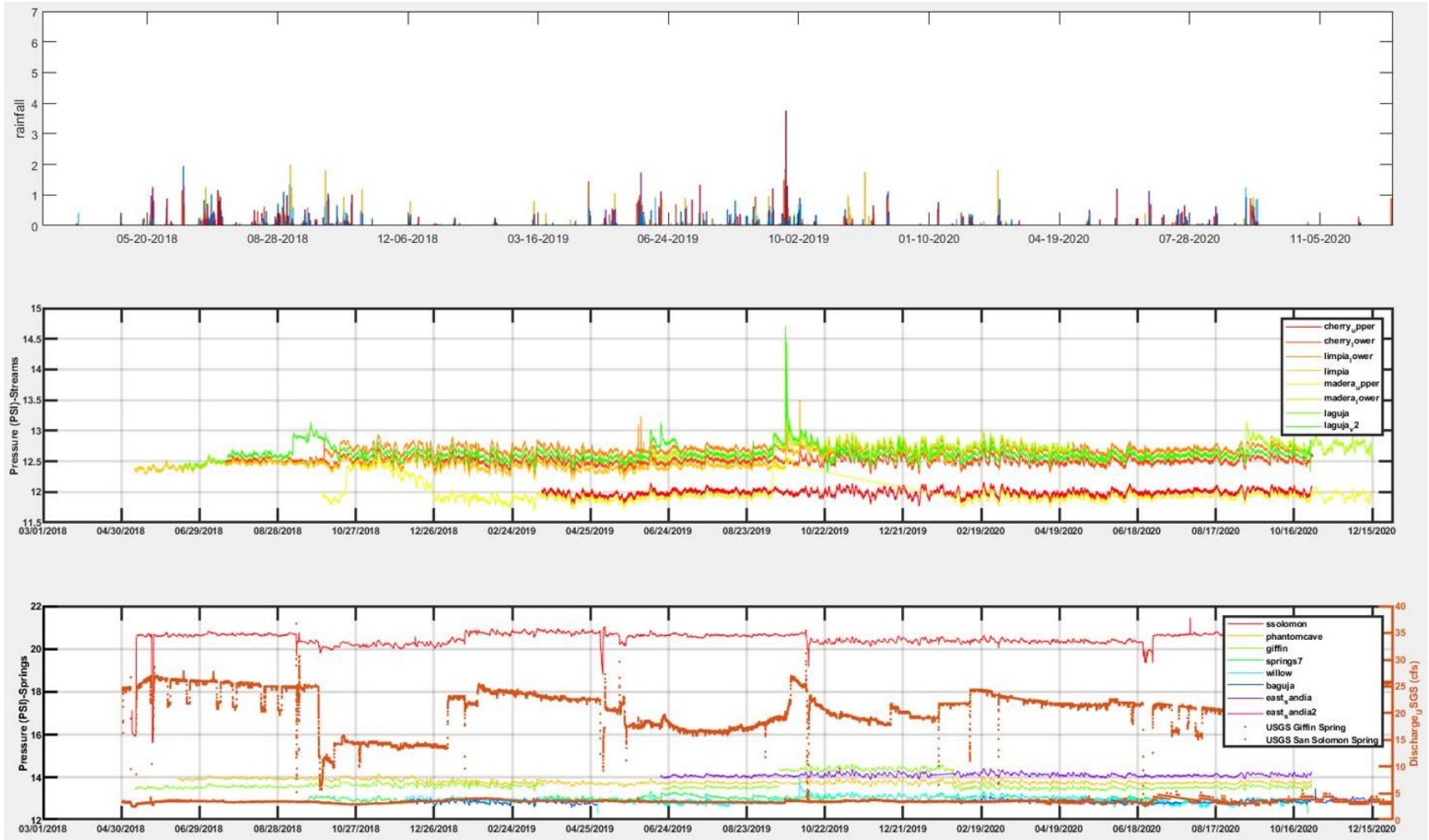
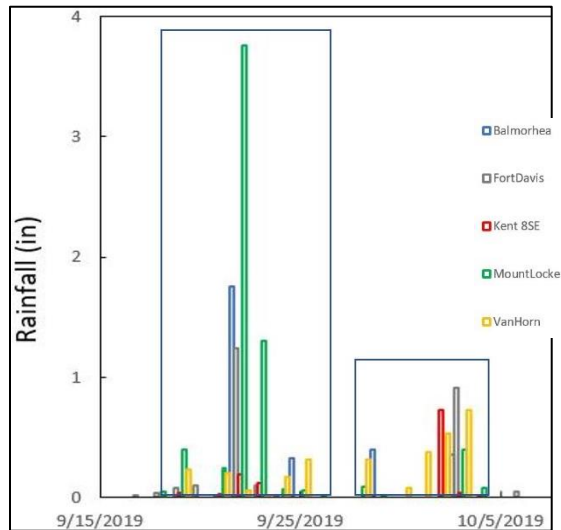


Figure 62. Contemporaneous plots of data from regional rainfall gauges (inch), BEG stream loggers (pressure), and BEG spring loggers (pressure) plus USGS spring gauging stations (discharge) – from January 2018 to December 2020.

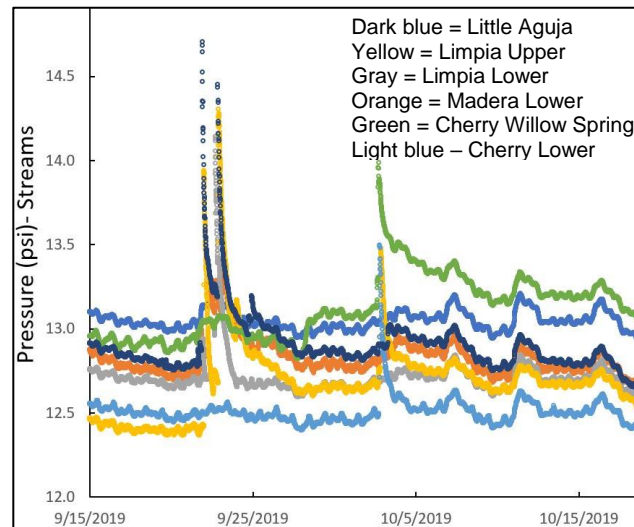
Figure 63 Stream travel time

Watershed	Logger	Date	Start (hr)	Duration	Stage increase.	Comments		
Little Aguja to Lower Madera	Little Aguja	9/21/2019	21:40	20 min	1.28 m			
	Little Aguja	9/22/2019	20:30	20 min	0.88 m			
	Huelster #3	---	---	---	---	Changes in pumping cycles only		
Limpia Creek	Limpia Upper Stream	9/21/2019	23:35	35 min	1.06 m			
	Limpia Upper Stream	9/22/2019	14:10	8 hr	1.16 m			
	Limpia Lower Stream	9/22/2019	15:00	2 hr	1.02 m			
		9/22/2019	Apparent travel time between Limpia Upper and Lower = 50 minutes					
Madera Canyon	Madera Upper Stream	9/21/2019	21:35	70 min	0.48 m	Rainfall began prior to "event" period.		
	Madera Upper Stream	9/21/2019	14:05	21 hr	0.16 m	Water ponded after earlier rainfall.		
	Madera Upper Stream	9/24/2019	11:50	---	---	Logger stopped before end of event		
	Madera Lower Stream	9/21/2019	14:51	6 hr	0.24 m	Rainfall began prior to "event" period.		
	Madera Lower Stream	9/21/2019	14:16	37 hr	0.44 m	Water ponded after earlier rainfall.		
			9/21/2019	Apparent travel time between Madera Upper and Lower = 11 minutes				
	Phantom Lake	9/20/2019	08:25	7 days	0.03 m			
	Phantom Lake	9/27/2019	18:55	---	---	Peak of pressure pulse in pool		
			9/27/2019	Possible travel time between Madera Lower and Phantom Lake = 6 days				
		Hamilton WM Well	9/21/2019	19:30	20 mins	0.9 m		
	Hamilton WM Well	9/24/2019	11:40	2 hrs	0.76			
Big Aguja Canyon	Big Aguja Stream	---	---	---	---	Logger not functioning during event		
	Seven Springs	9/21/2019	17:00	21 hr	0.08 m			

(a)



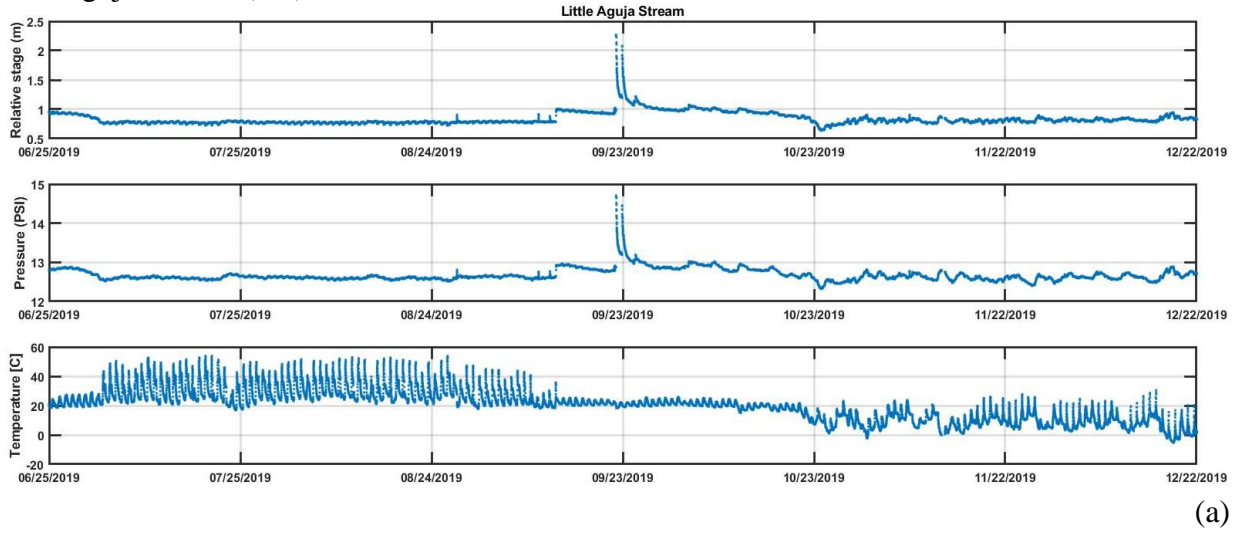
(b)



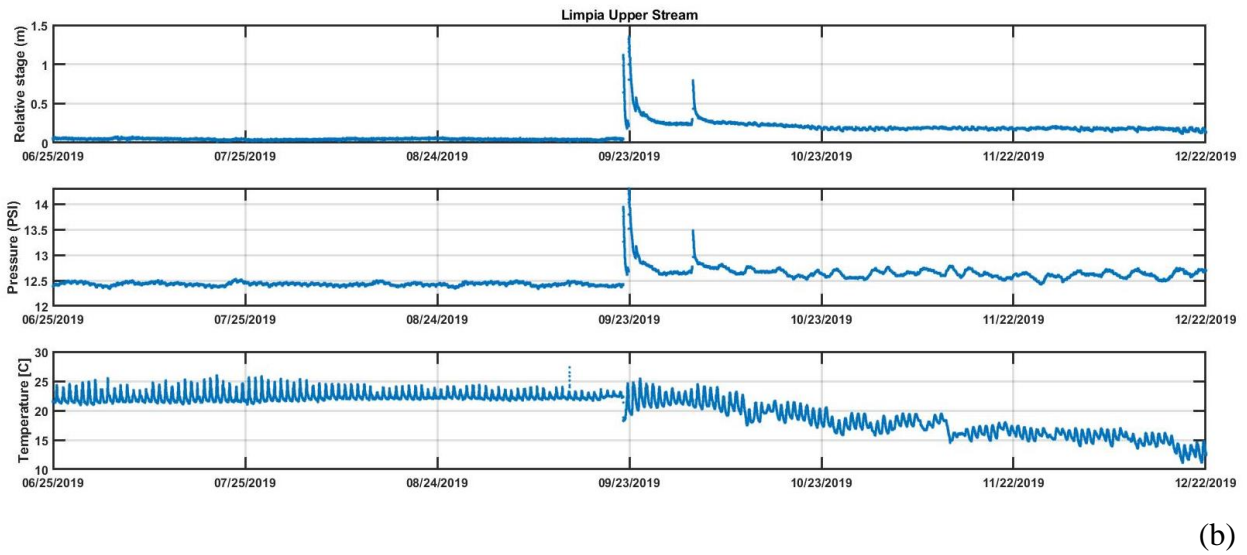
(c)

Figure 63. Logger response to Early Fall 2019 event: (a) calculation table; (b) rainfall; (c) pressure spikes in response to rainfall.

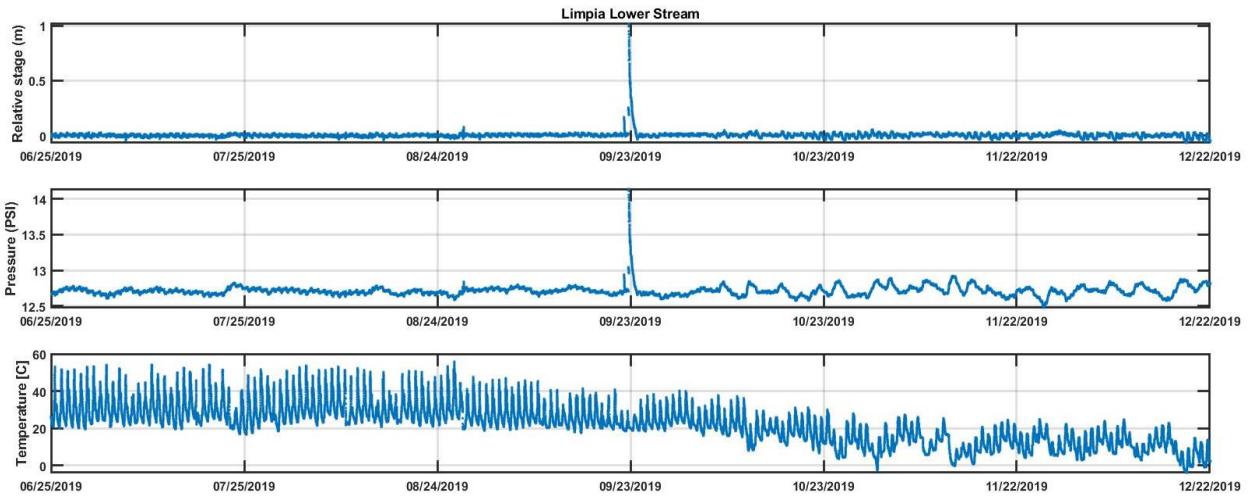
Figure 64 Stream loggers
Little Aguja Stream (RT)



Limpia Upper Stream (RT)

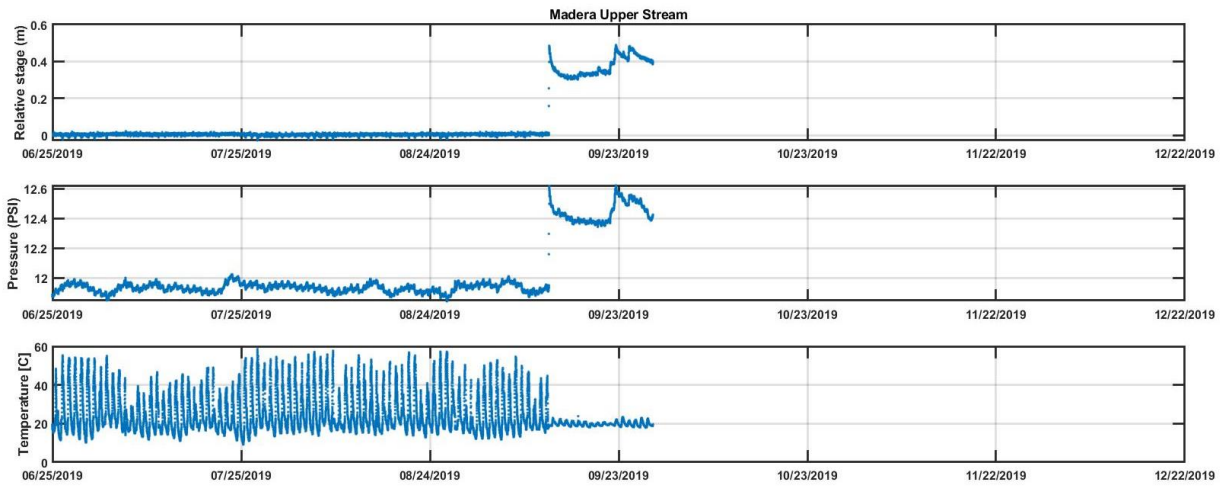


Limpia Lower Stream (RT)



(c)

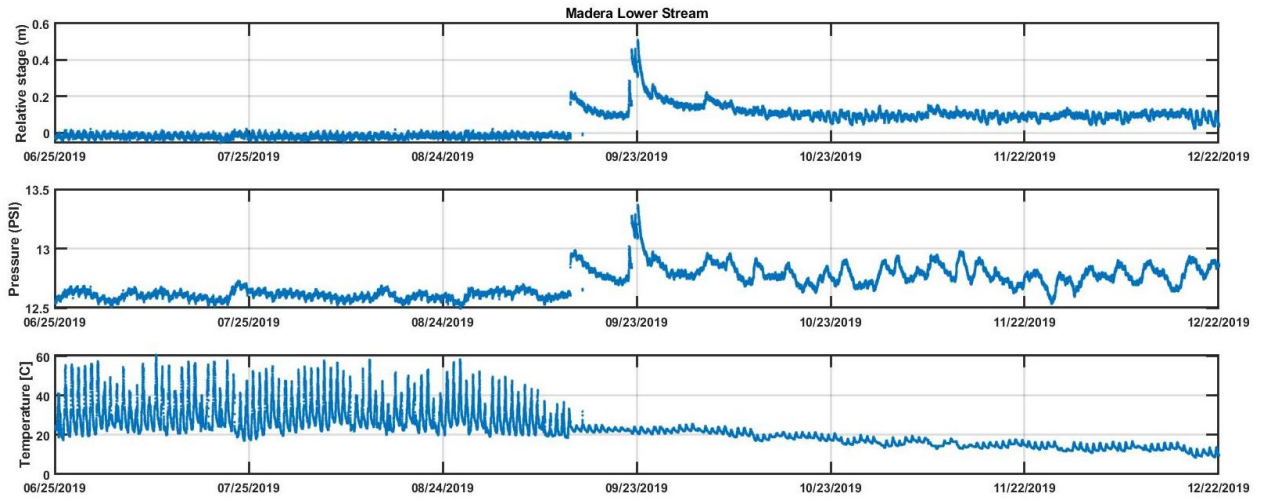
Madera Upper Stream (RT)



(d)

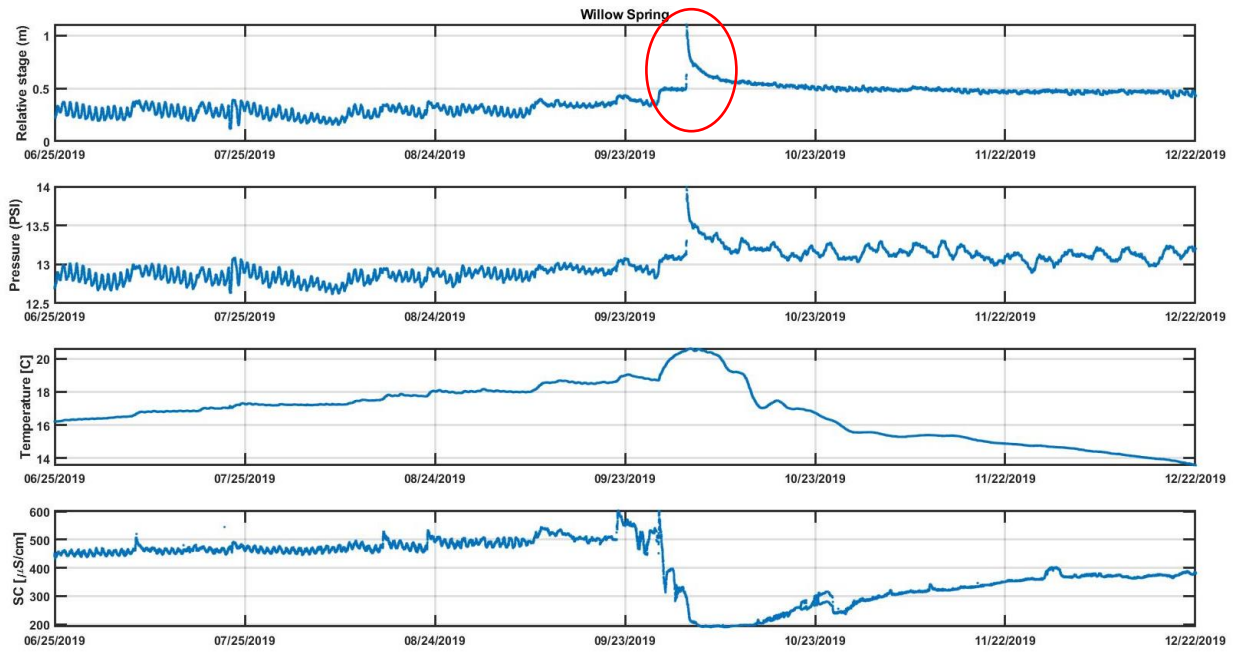
Note that the logger malfunctioned at 08:30 on September 28, 2019 (as illustrated by the straight line connecting to the first data point of 2020) and was not replaced until late January 2020.

Madera Lower Stream (RT)



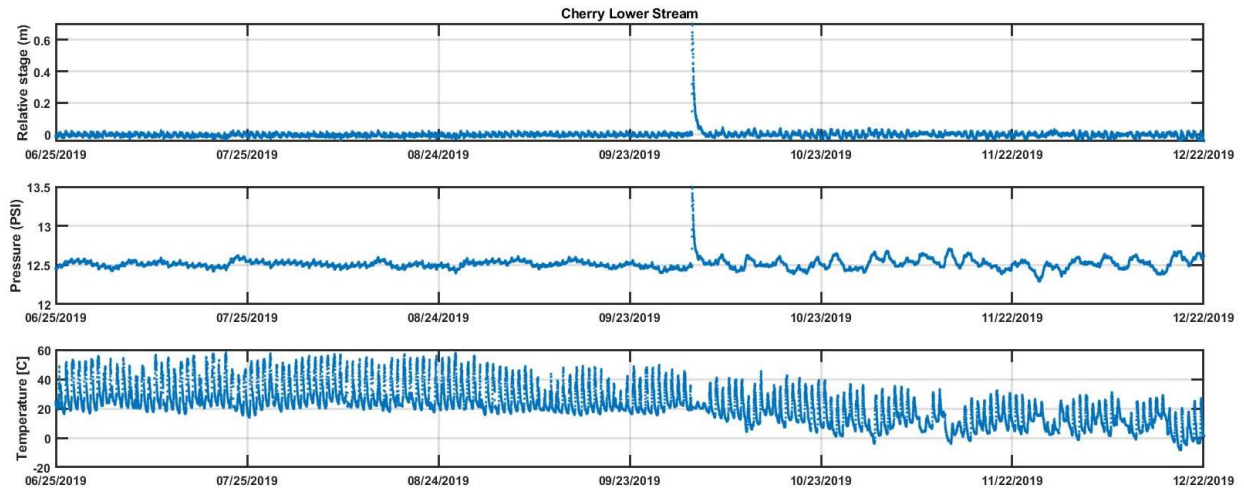
(e)

Cherry Willow Spring (AT)



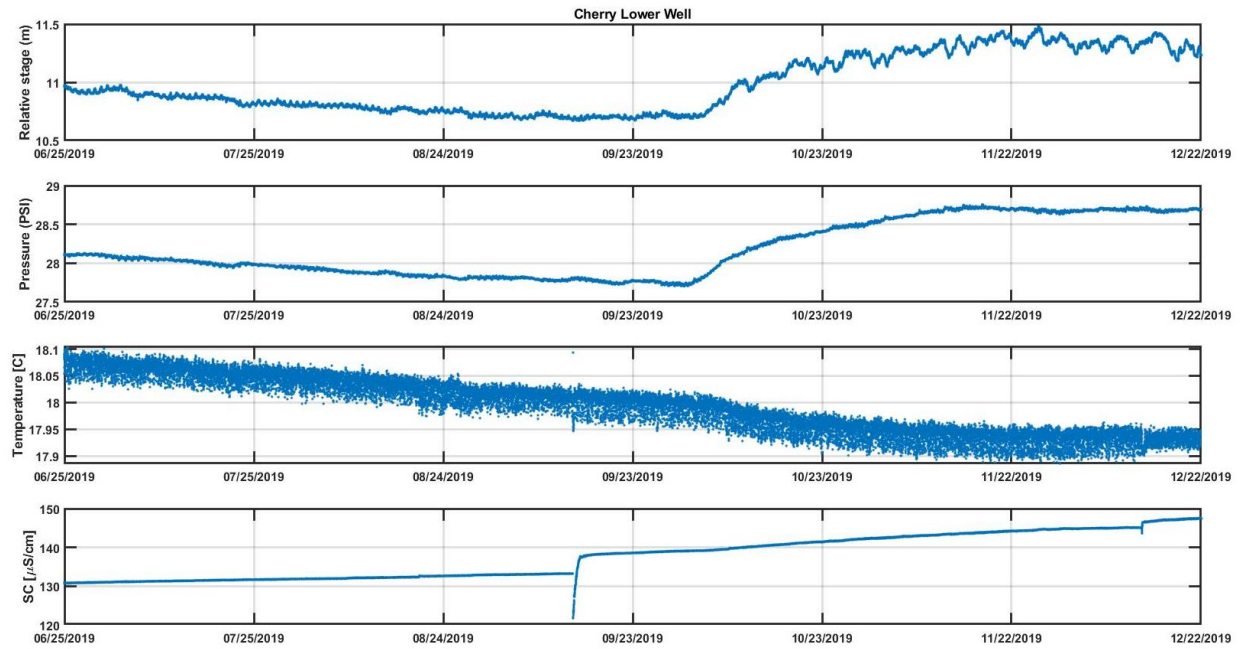
(f)

Cherry Lower Stream (RT)



(g)

Cherry Lower well (RT)



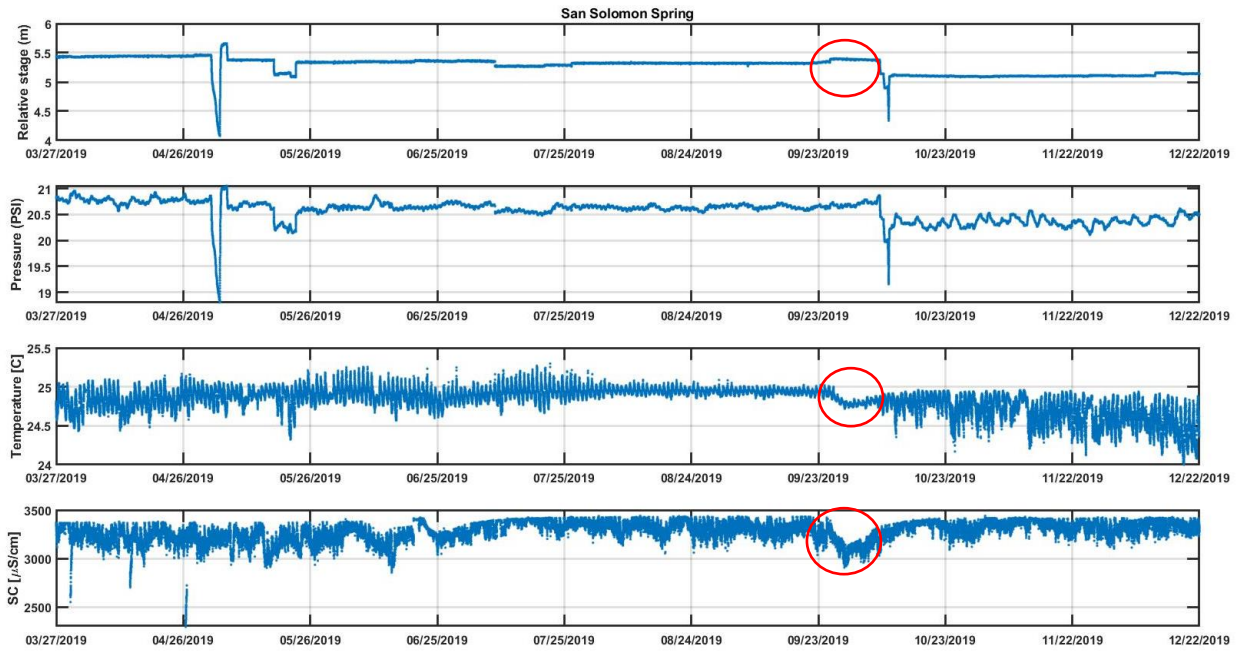
(h)

Watershed	Logger	Date	Start (hr)	Duration	Stage diff.	Comments
Cherry Creek	Cherry Upper Stream	---	---	---	---	Temperature response only
	Cherry Willow Spring	9/27/2019	1645	5 days	0.14 m	
	Cherry Willow Spring	10/2/2019	1315	4 hrs	0.63 m	
	Cherry Lower Stream	10/2/2019	1530	4 hrs	0.73 m	
	Cherry Lower Well	10/2/2019	1050	~2 months	0.81 m	WL in unused well remained elevated
		10/2/2019	Apparent travel time between Willow Spring and Cherry Lower = 2 hr, 15 min			
Limpia Creek	Limpia Upper Stream	10/2/2019	1625	4 hrs	0.57 m	
	Limpia Lower Stream	10/2/2019	---	---	---	No logger response
Madera Canyon	Madera Upper Stream	10/3/2019	---	---	---	Logger malfunctioning
	Madera Lower Stream	10/3/2019	0711	12 hrs	0.09 m	Water ponded after earlier rainfall.
(i)						

Figure 64. Logger data from June 25 to December 22, 2019: (a) Little Aguja; (b) Limpia Upper; (c) Limpia Lower; (d) Madera Upper; (e) Madera Lower; (f) Cherry Willow Spring; (g) Cherry Lower Stream; (h) Cherry Lower Well; and (i) Summary of logger responses to early Fall 2019 rainfall event.

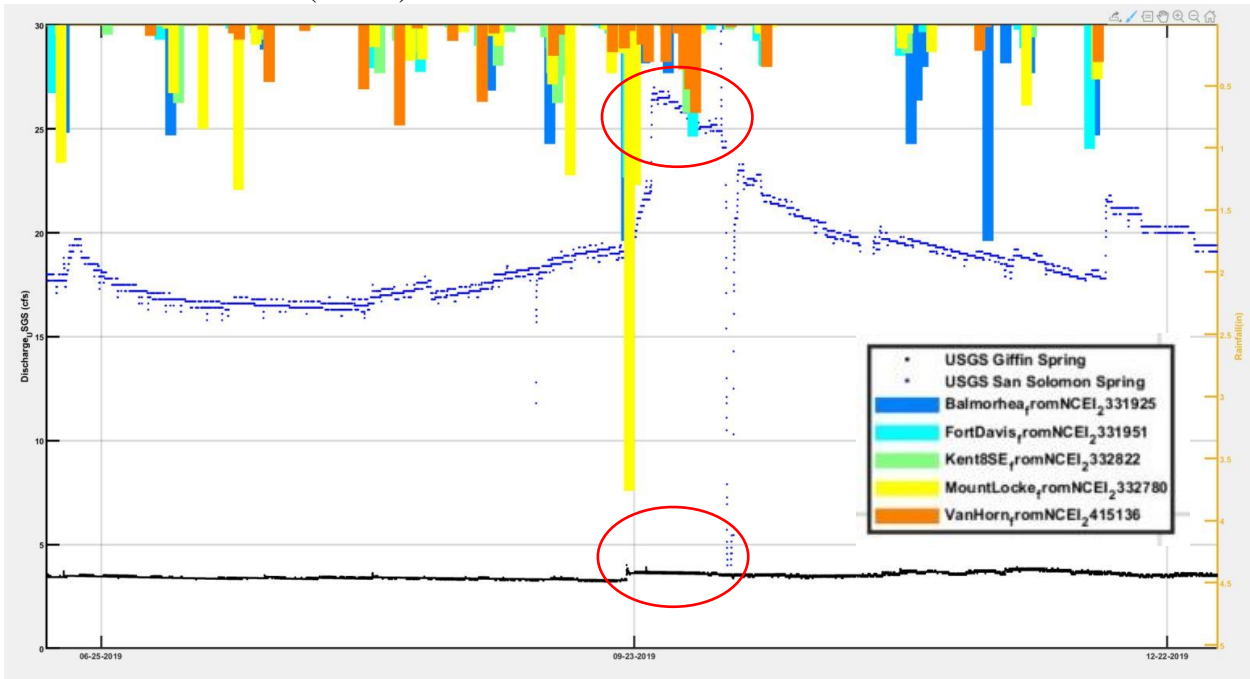
Figure 65 Balmorhea loggers

San Solomon Spring (AT) - March 27 to December 22, 2019



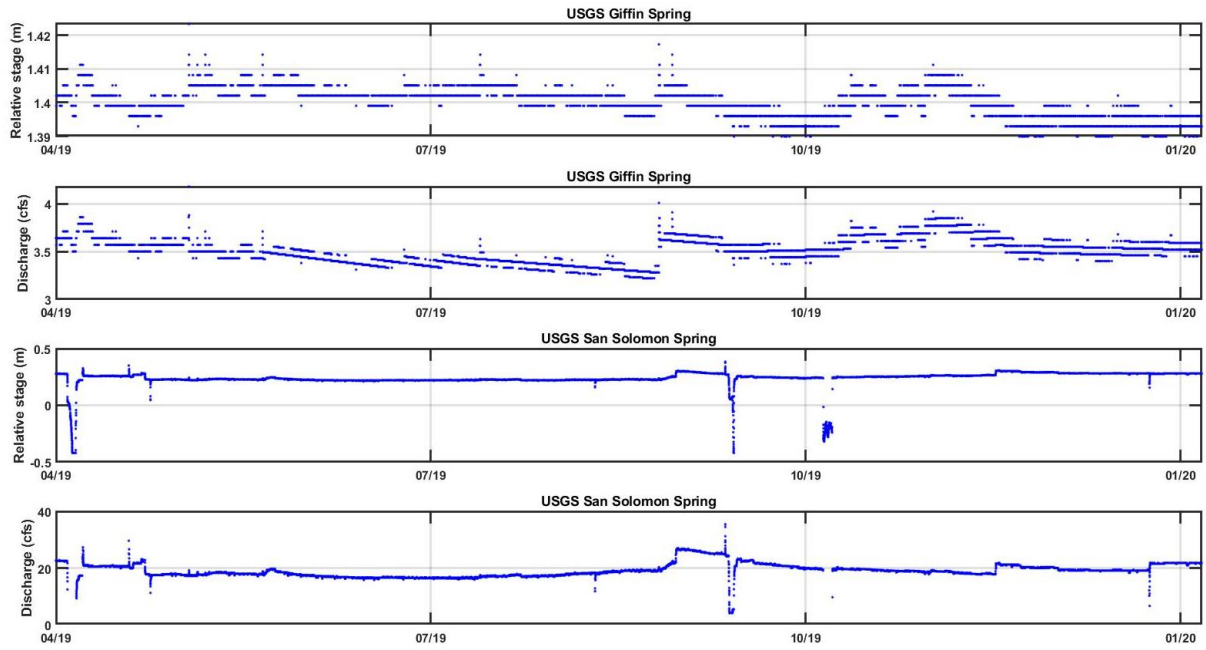
(a)

San Solomon flow rate (USGS)



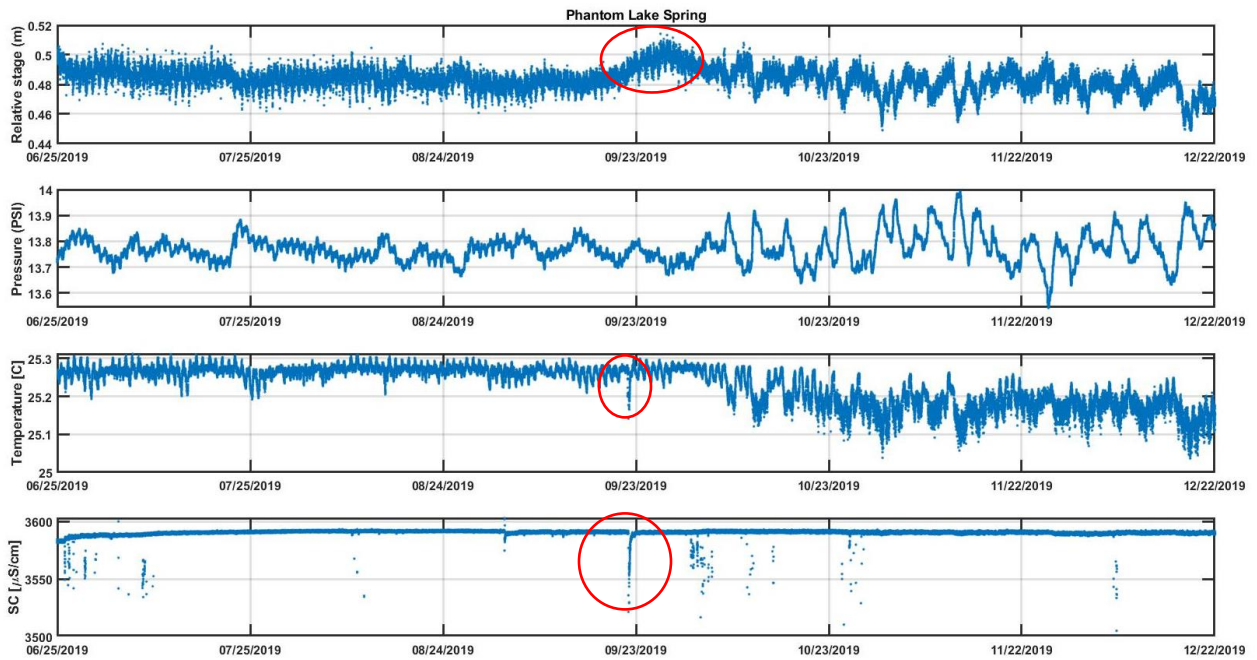
(b)

Giffin and San Solomon springs - April 2019 to January 2020



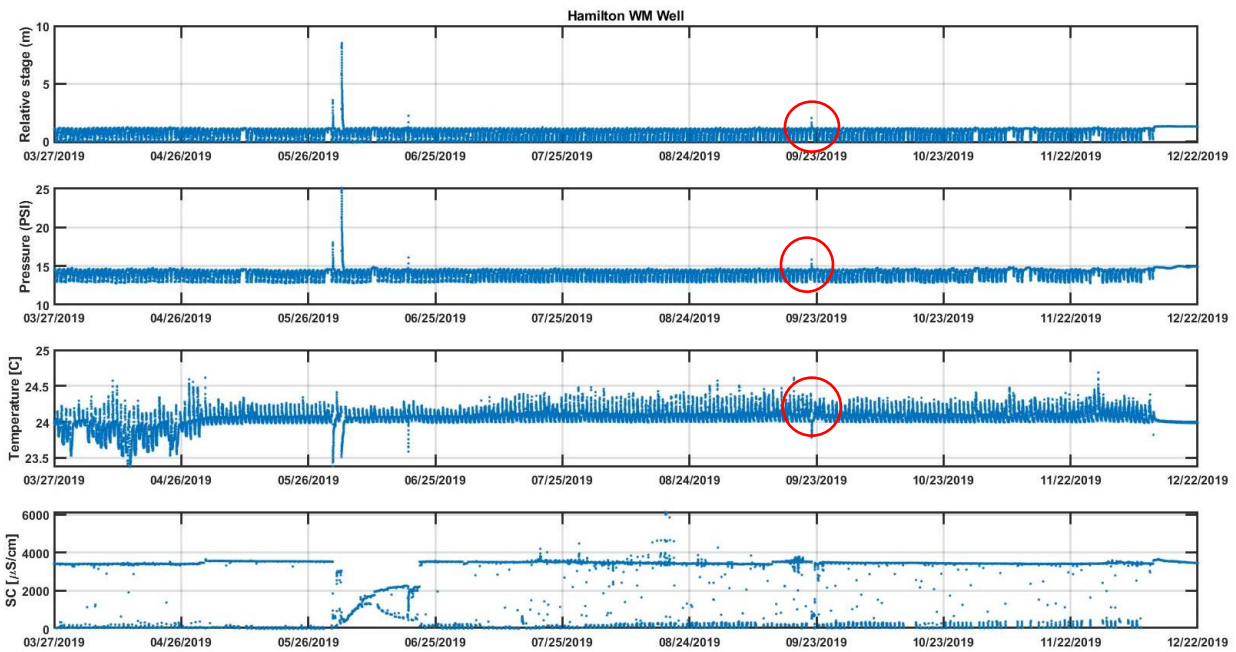
(c)

Phantom Lake Spring - June 25 to December 22, 2019



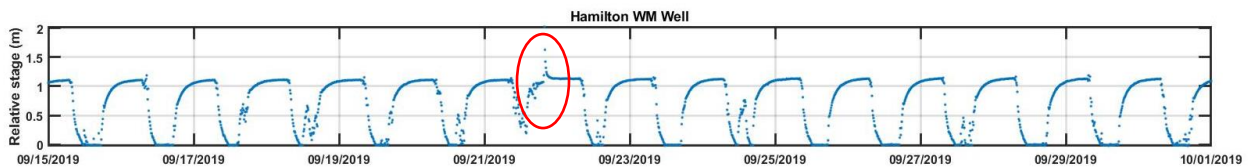
(d)

Hamilton Well - March 27 to December 22, 2019



(e)

Hamilton Well - September 17 to October 10, 2019



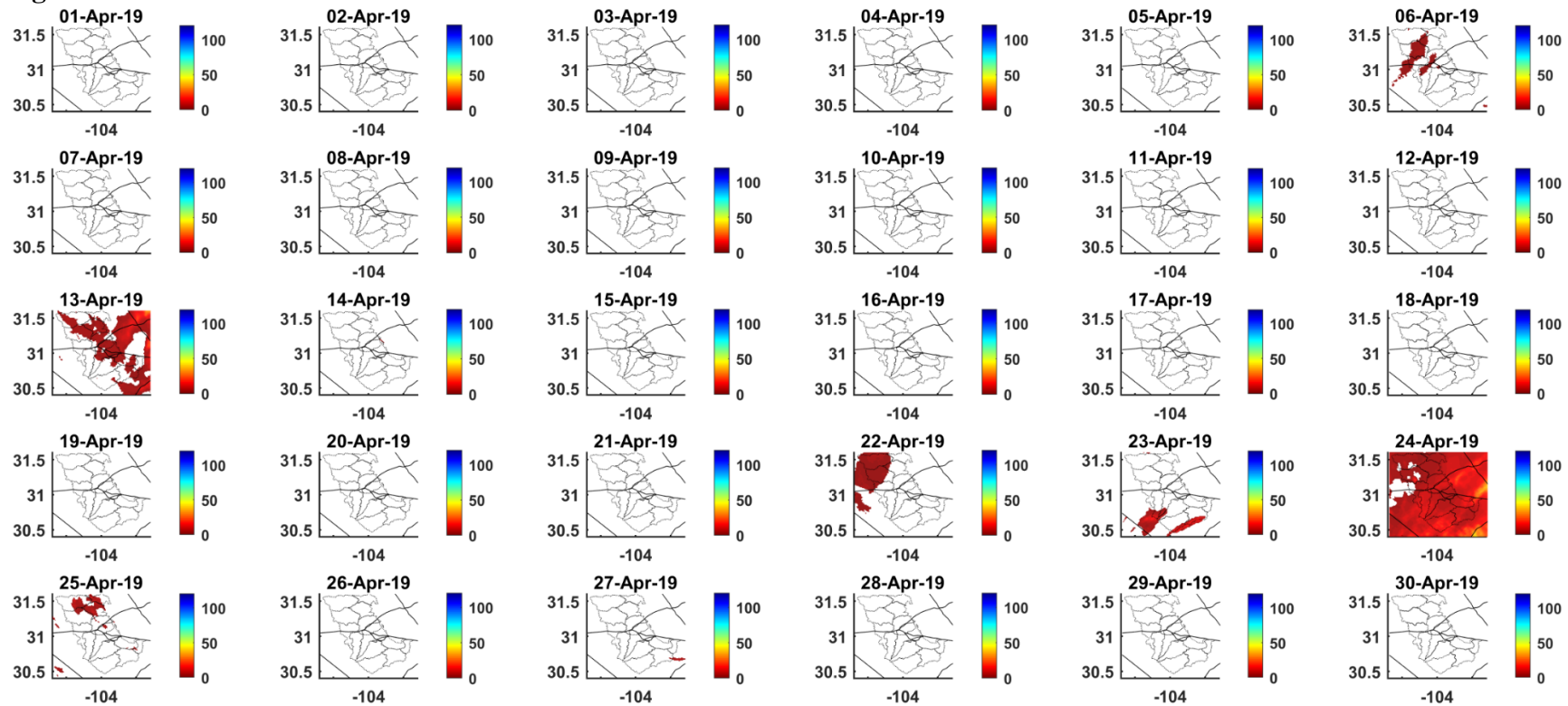
(f)

BEG Logger	Date	Start (hr)	Duration	Difference	Comments
Phantom Lake	9/20/2019	08:25	7 days	0.03 m rise	
	9/27/2019	18:55	---	---	Peak of pressure pulse in pool
	9/21/2019	19:35	40 min	0.13 C fall	
	9/21/2019	19:55	10 min	69 uS/cm fall	
	10/1-10/25	---	---	28-75 uS/cm	~4 sharp drops in SpC over 4 days
Hamilton WM	9/21/2019	19:30	20 min	0.90 m	
	9/24/2019	11:40	2+ hr	0.76 m	
	9/24-10/9	daytime			Up to nine small pressure pulses during pumping cycles.
Giffin Spring	9/21/2019	15:05	35 min	0.03 m	
East Sandia Spring	9/21/2019	15:30	40 min	0.04 m	
San Solomon Springs	9/25/2019	18:25	70 min	0.04 m	
Apparent travel time between 9/22 start of pressure response in Limpia Lower Stream to San Solomon Springs on 9/25 = 3 days, 3 hours					
Apparent travel time between 9/22 start of pressure response in Madera Lower Stream to San Solomon Springs on 9/25 = 4 days, 4 hours					

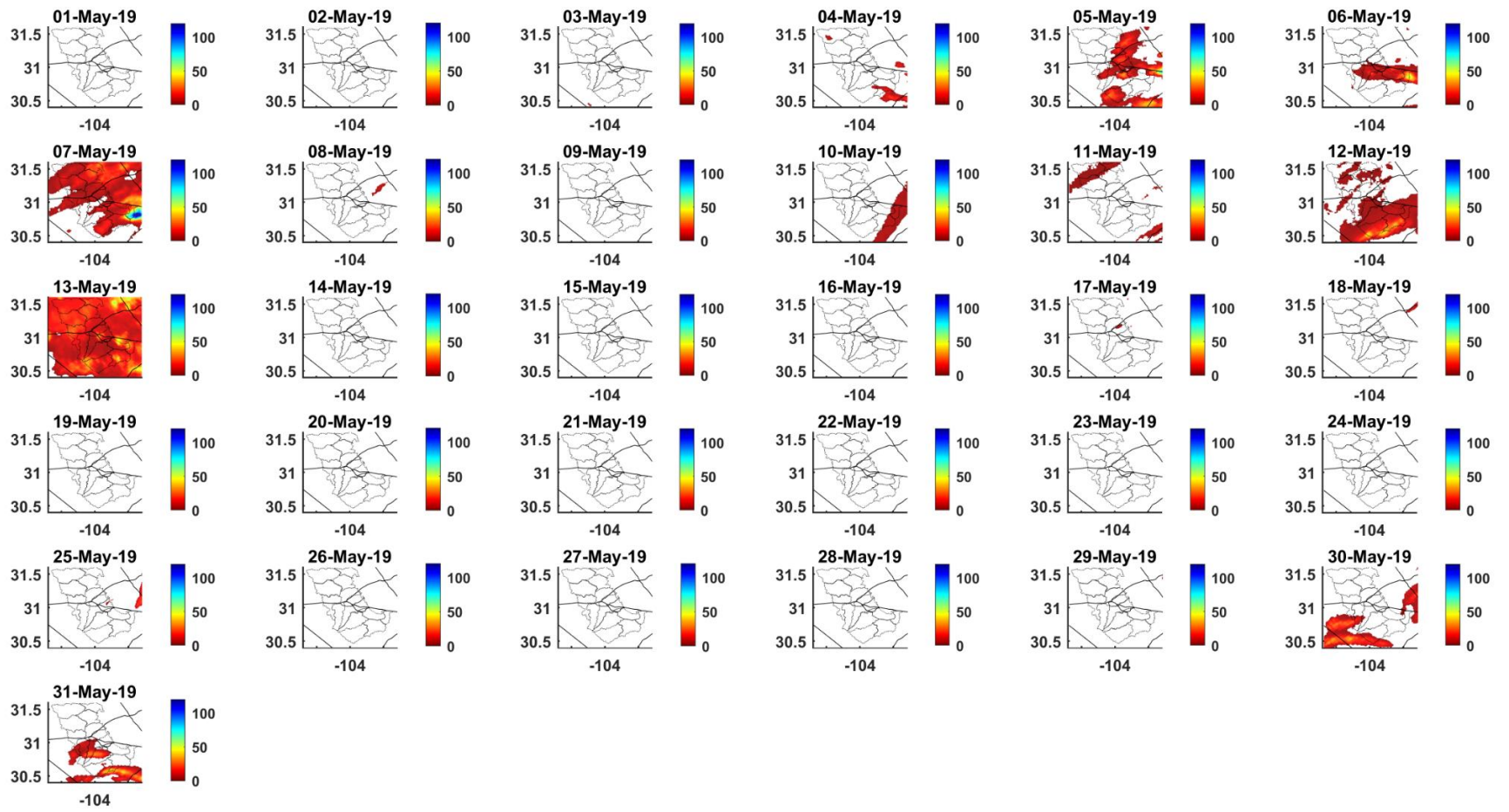
(g)

Figure 65. Logger data from Spring to December 2019: (a) San Solomon BEG logger; (b) USGS gauge data for San Solomon and Giffin springs plus regional rainfall; (c) USGS gauge data from Giffin and San Solomon springs; (d) Phantom Lake logger data; (e) and (f) Hamilton well logger data; (g) Summary of logger responses to September 17 – 26, 2019 rainfall.

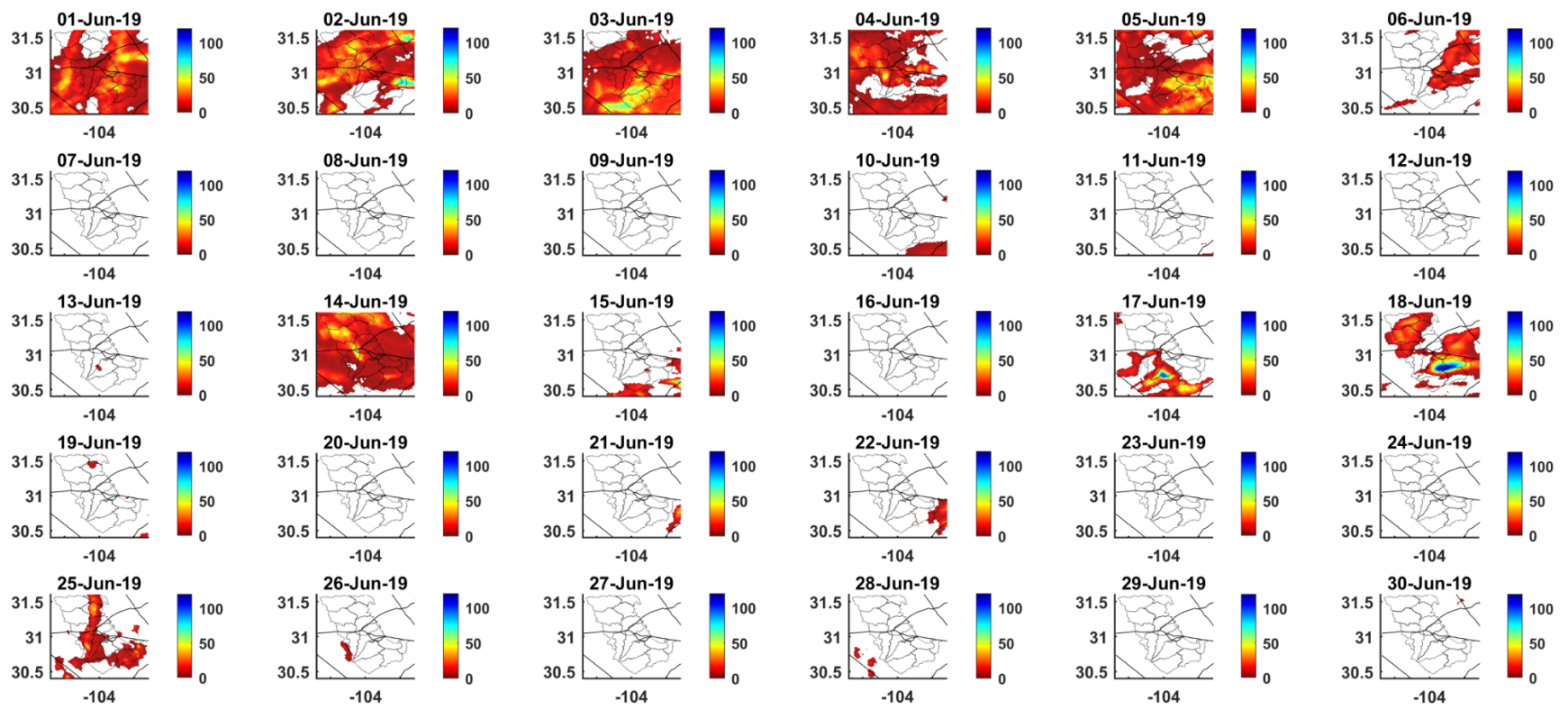
Figure 66 Radar rain data



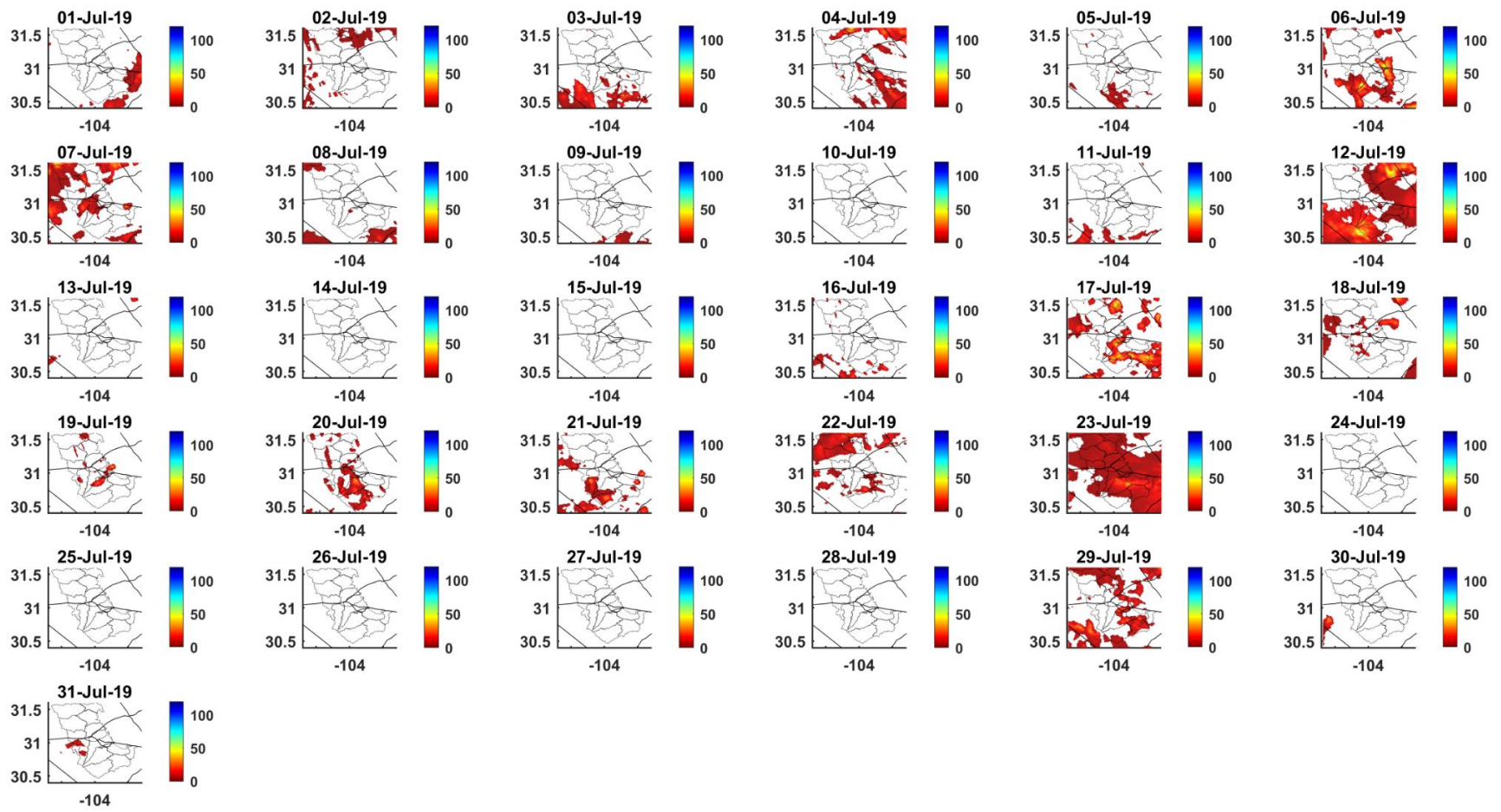
(a)



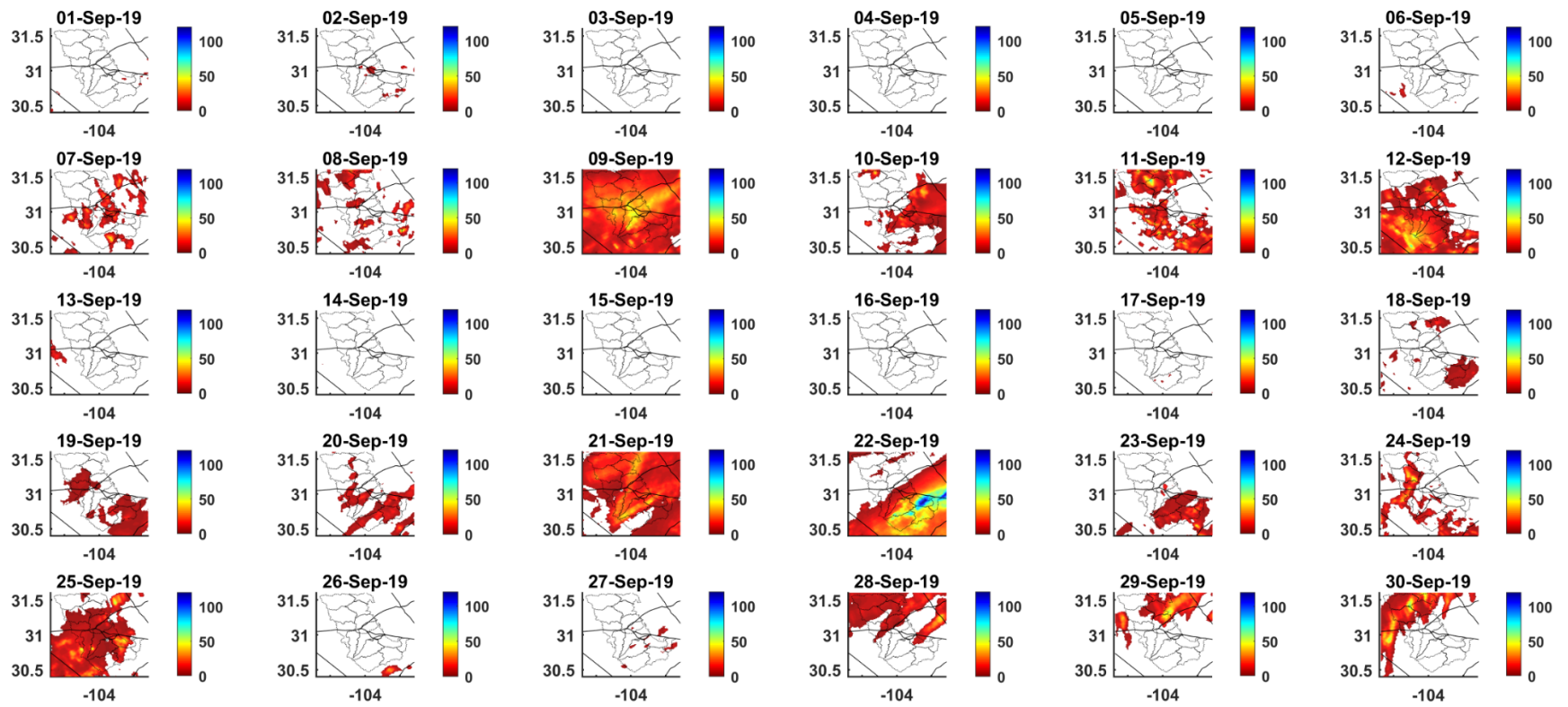
(b)

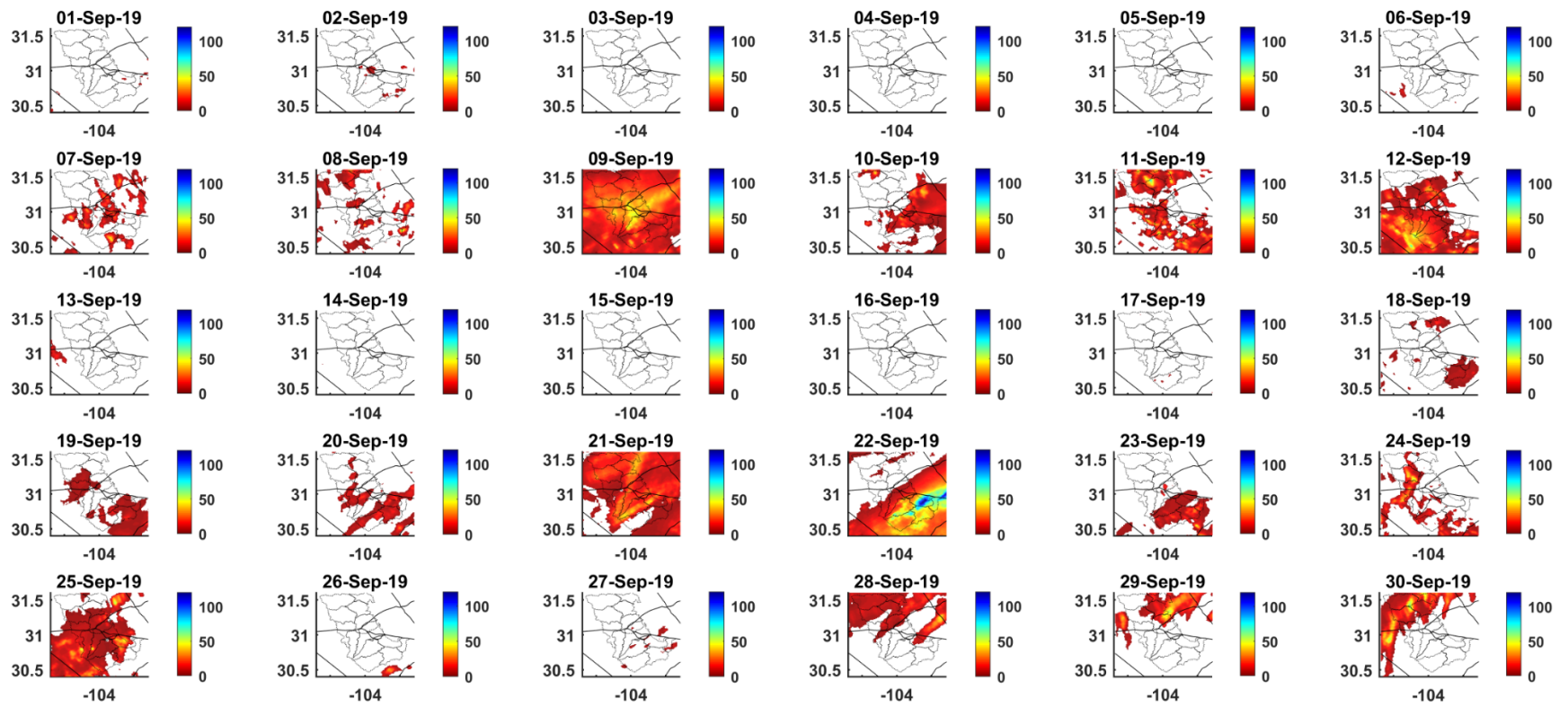


(c)

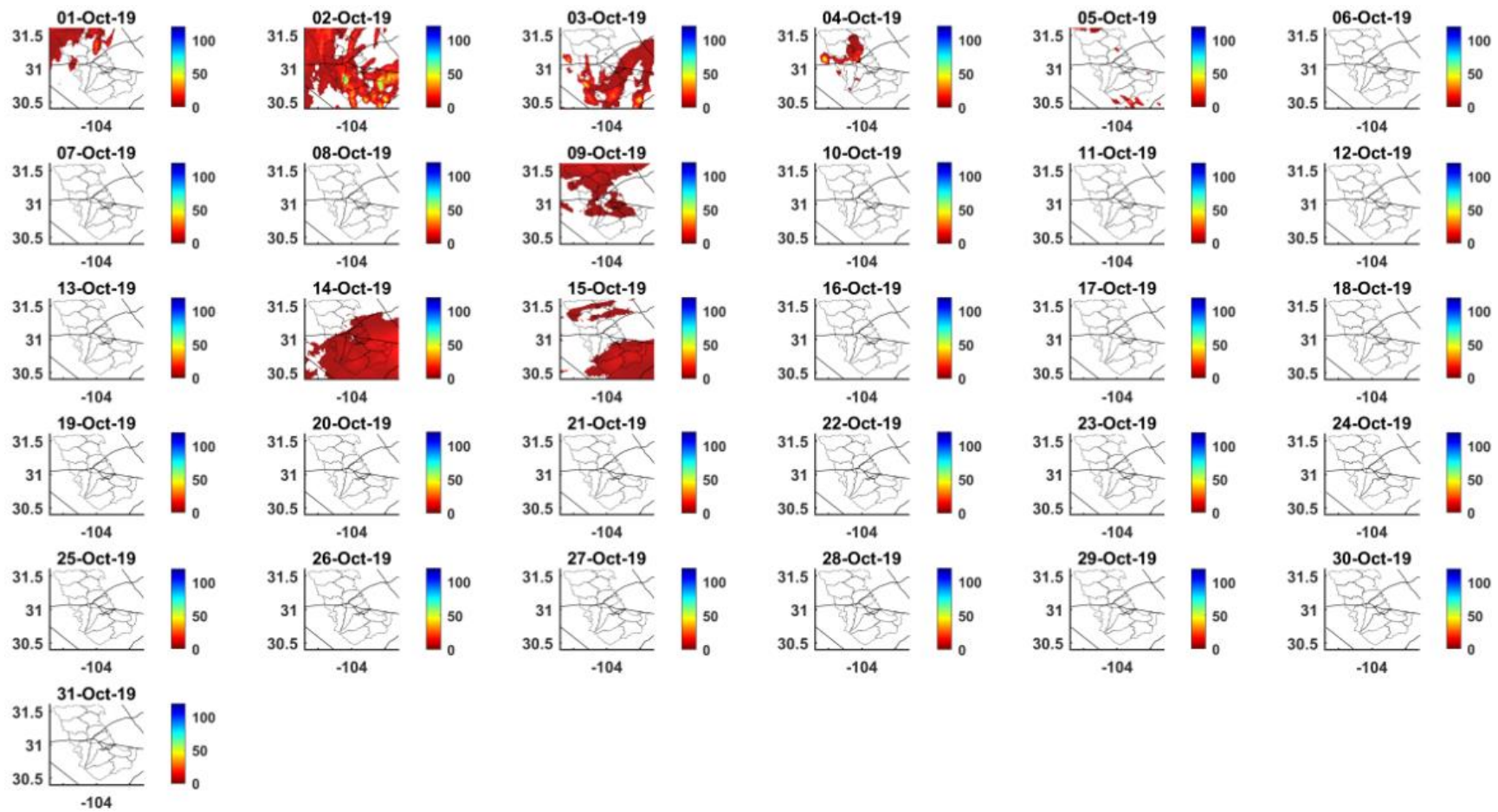


(d)

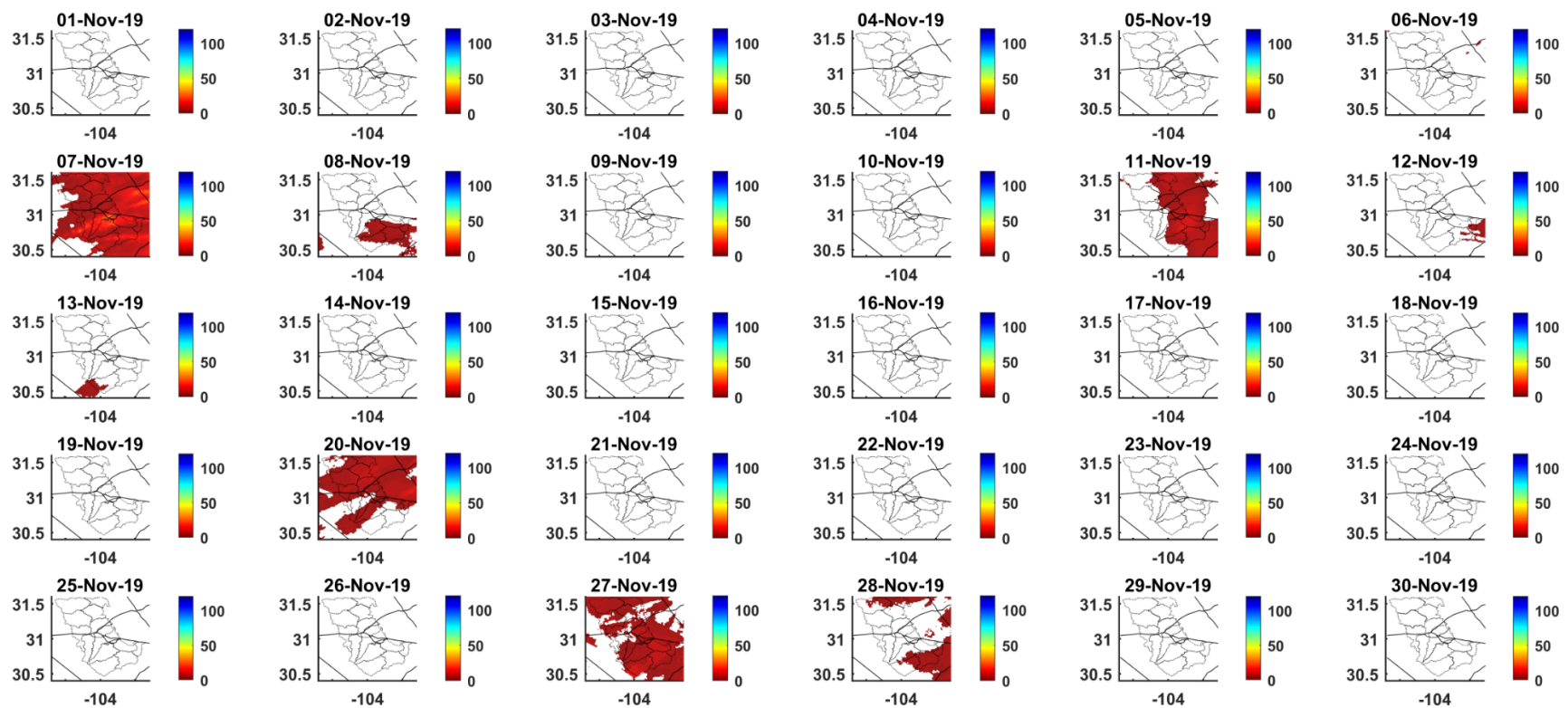




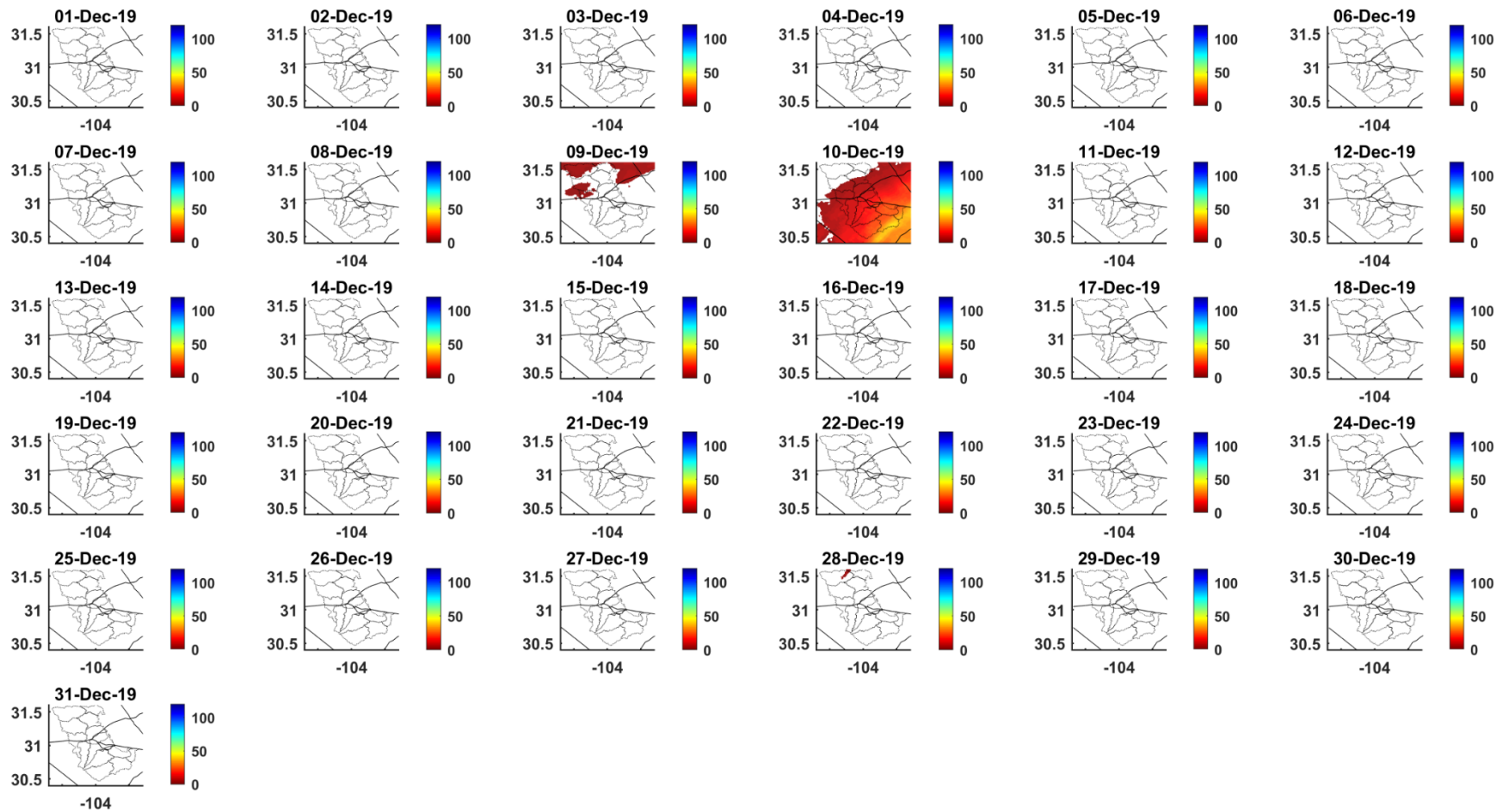
(e)



(f)



(g)



(h)

Figure 66. Precipitation (NOAA MRMS) for April 2019 (a), May 2019 (b), June 2019 (c), July 2019 (d), September 2019 (e), October 2019 (f), November 2019 (g), and December 2019 (h). The maps show the larger study with the I-20–I-10 split at the center of the map. Color scale of rain amount in mm/day.

Figure 67 Rain station and radar

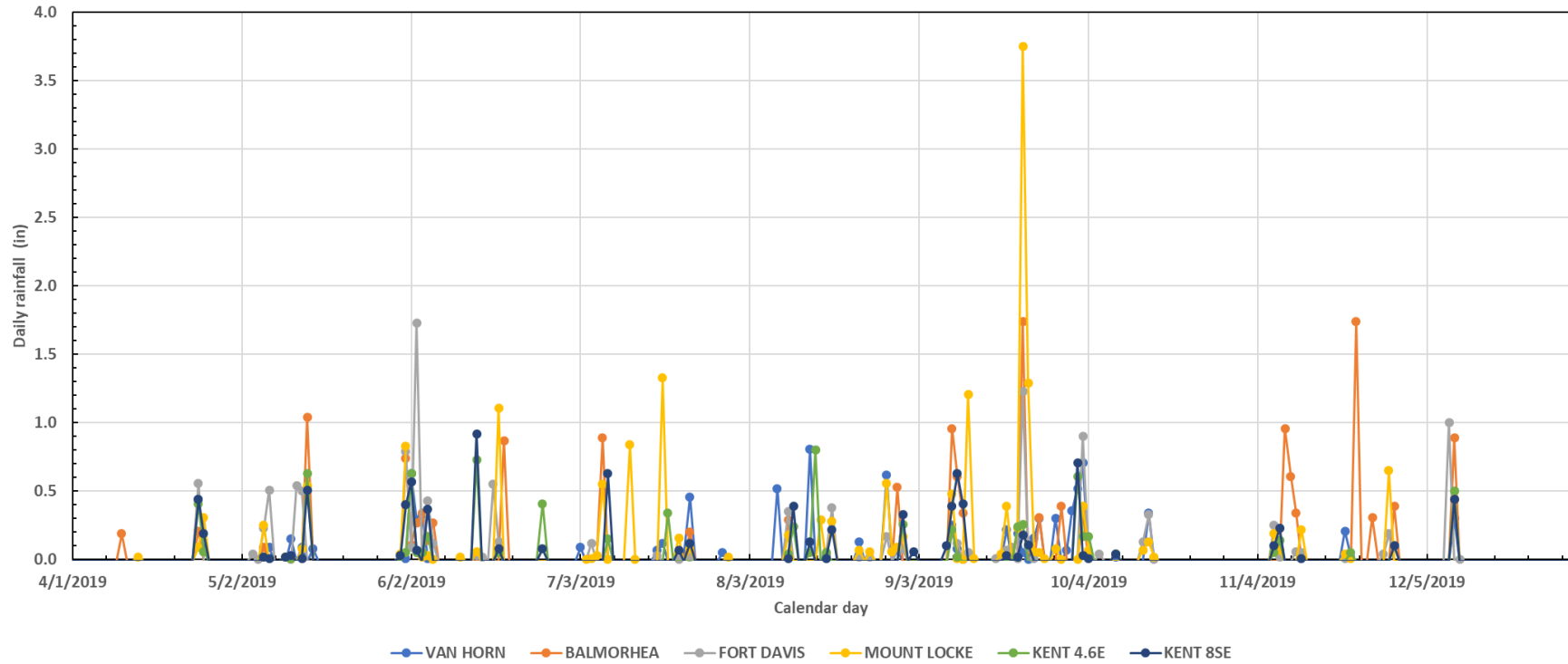


Figure 67. Daily rainfall as recorded in several weather stations for comparison to radar precipitation data (April to December 2021).

Figure 68 SSS and radar data

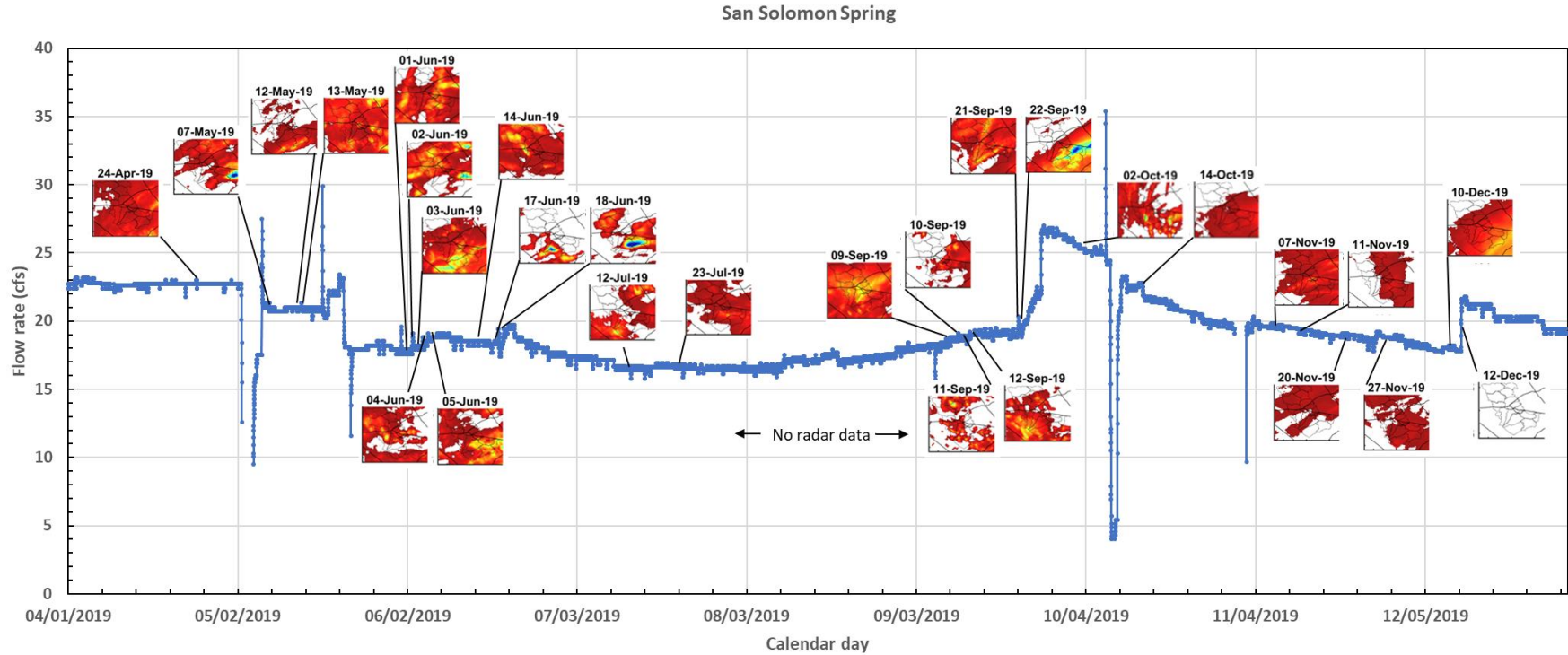


Figure 68. San Solomon Spring flow rate at the USGS gauge (April to December 2019) and daily spatial intensity of precipitation events estimated from radar data. Daily precipitation color-coded red are too low to generate a response at the springs.

Figure 69 Wells below bottom of igneous

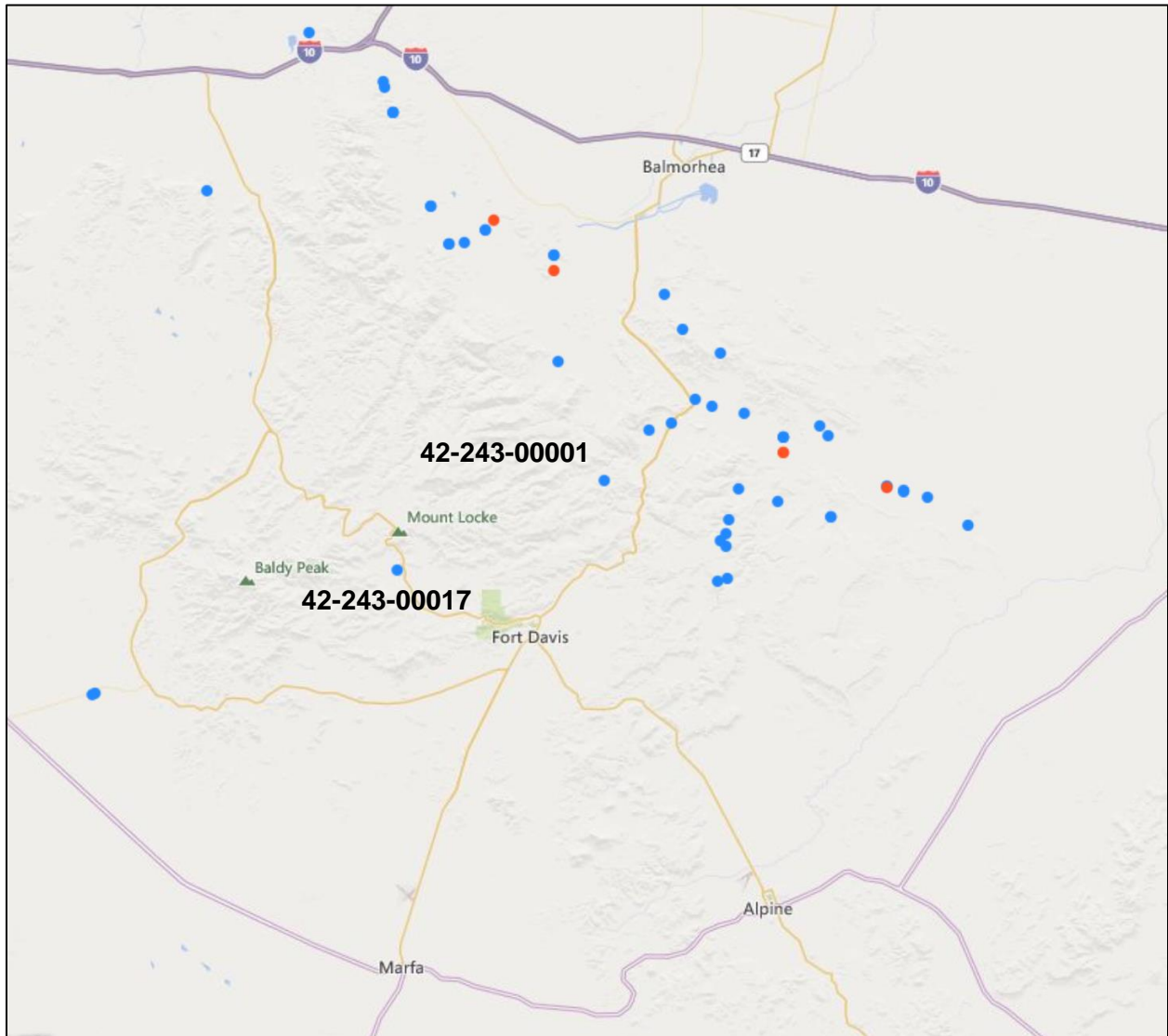
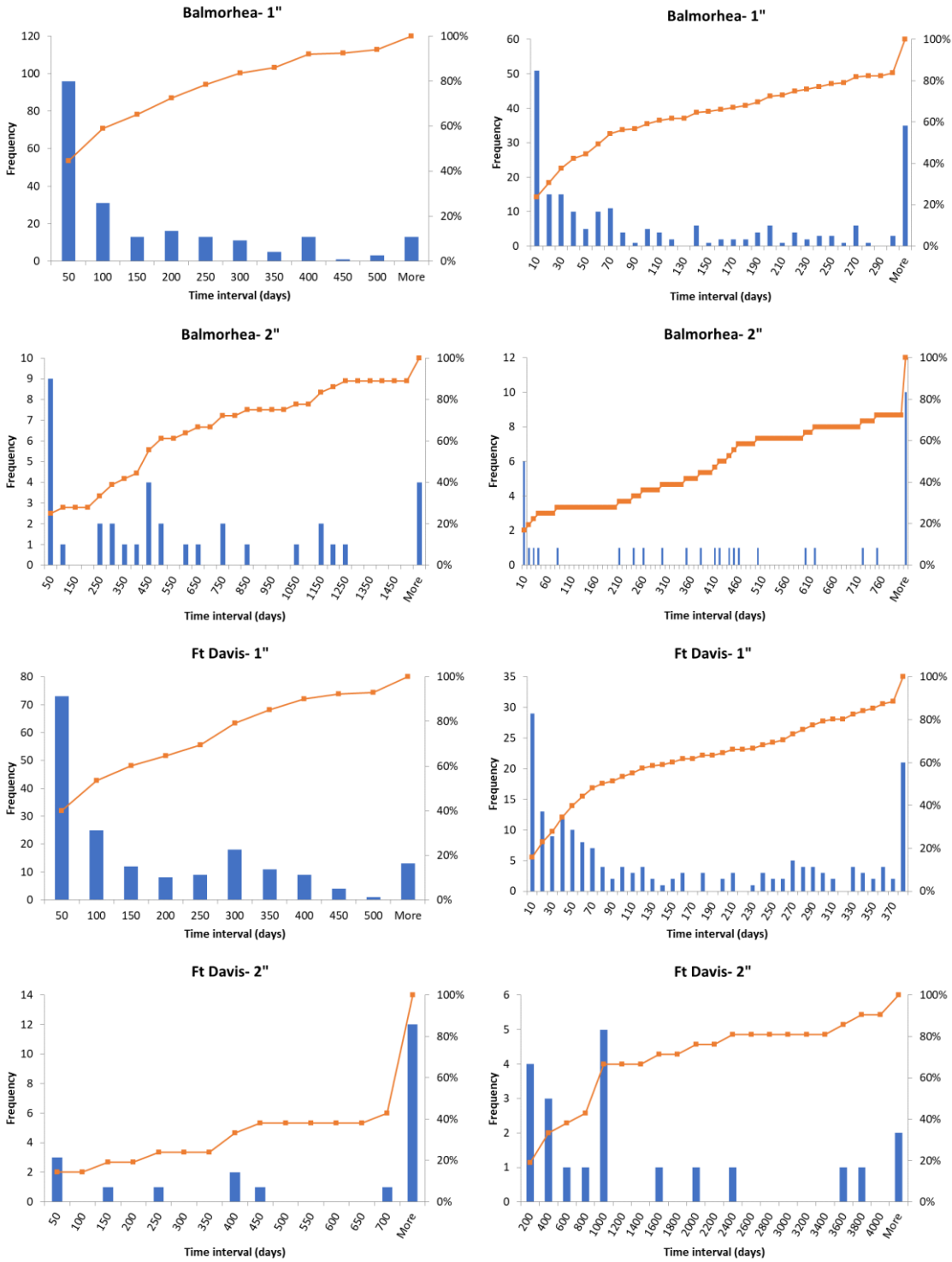


Figure 69. Oil and Gas exploratory wells in Jeff Davis County; all dry holes (blue) and wells with very limited production (red). All these wells penetrate Permian strata underneath Cretaceous layers and Cenozoic volcanic deposits of the Davis Mountains and vicinity. Courtesy of IHS Enerdeq.

Figure 70 Rain statistics



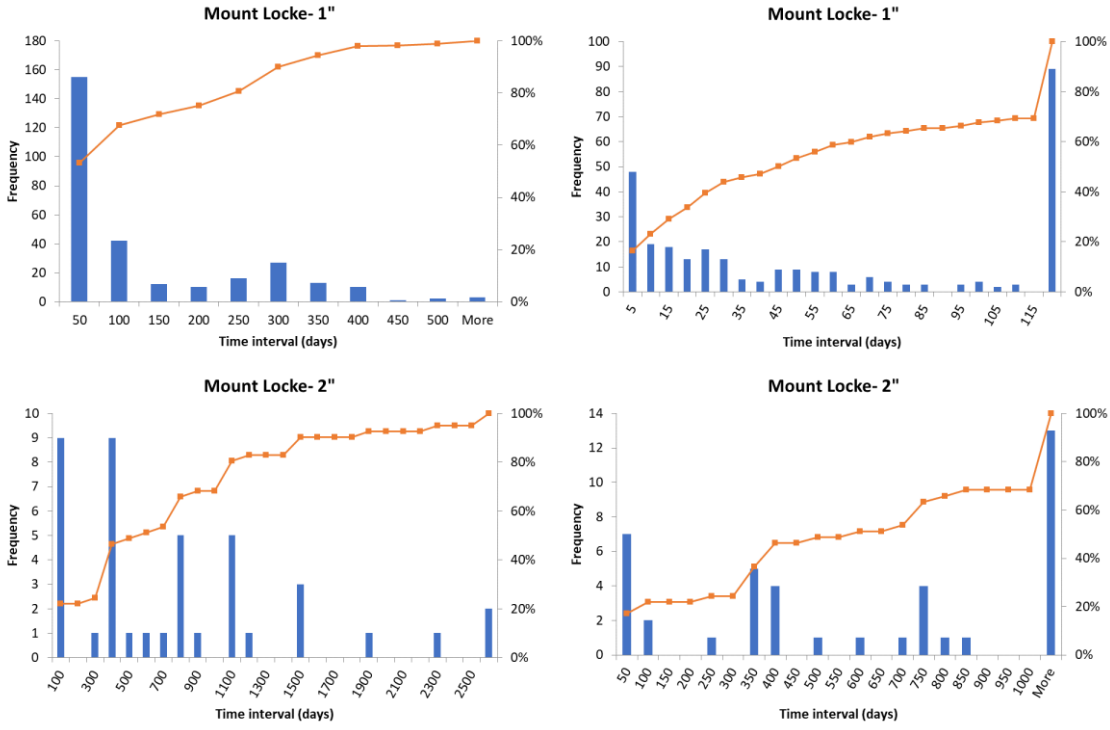
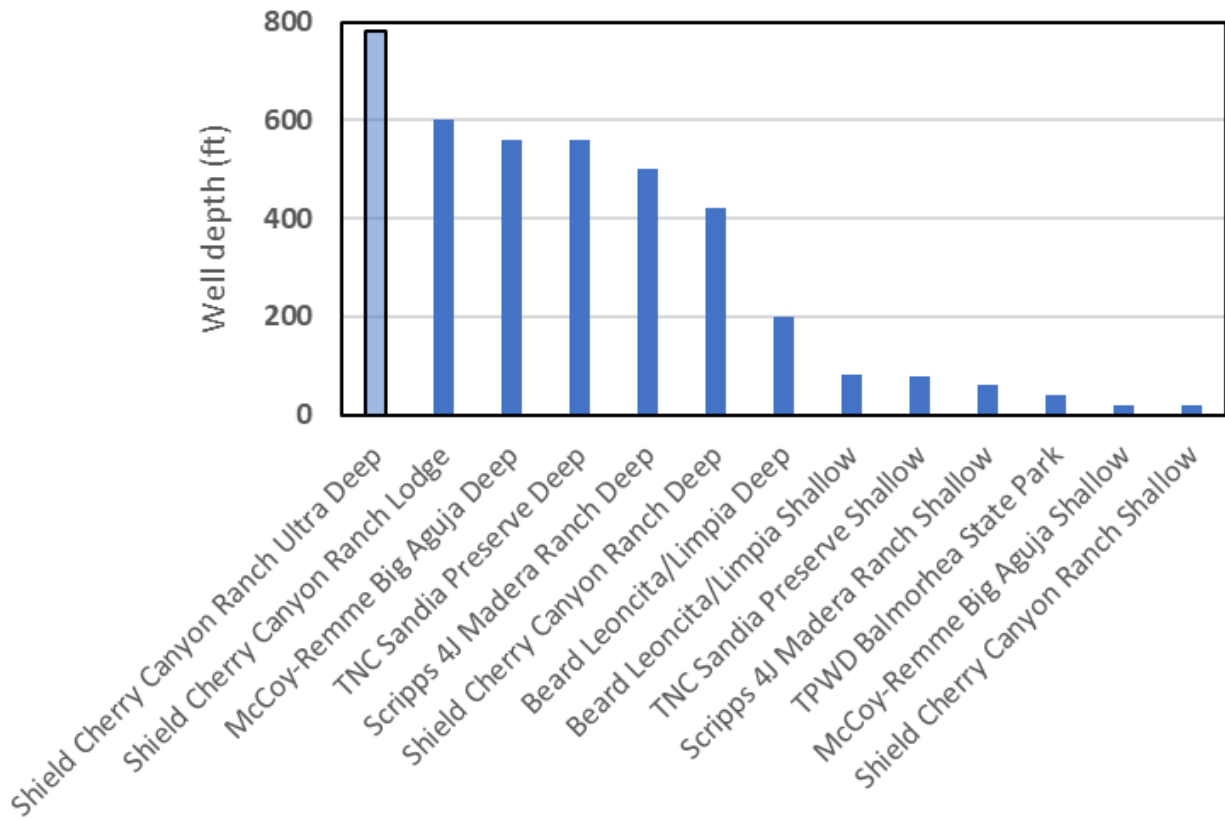


Figure 70. Time interval between successive precipitation events of at least 1” or 2” in a day for selected stations (Balmorhea, Fort Davis, Mount Locke). Plots on the right-hand side show higher-resolution distribution of small time intervals.

Appendix A: Well diagrams

This appendix show diagrams of the BEG-drilled wells sorted in the following order:

- Leoncita/Limpia deep well
- Leoncita/Limpia shallow well
- Balmorhea State Park shallow well
- McCoy-Remme Big Aguja deep well
- McCoy-Remme Big Aguja shallow well
- 4J Madera deep well
- 4J Madera shallow well
- Cherry Canyon deep well
- Cherry Canyon shallow well
- Cherry Canyon Lodge well
- TNC Sandia Preserve shallow well
- TNC Sandia Preserve deep well



WTX-LLMWD (RS)

Leoncita/Limpia Deep Well
drilled October 31st, 2019
(Becky Smyth)

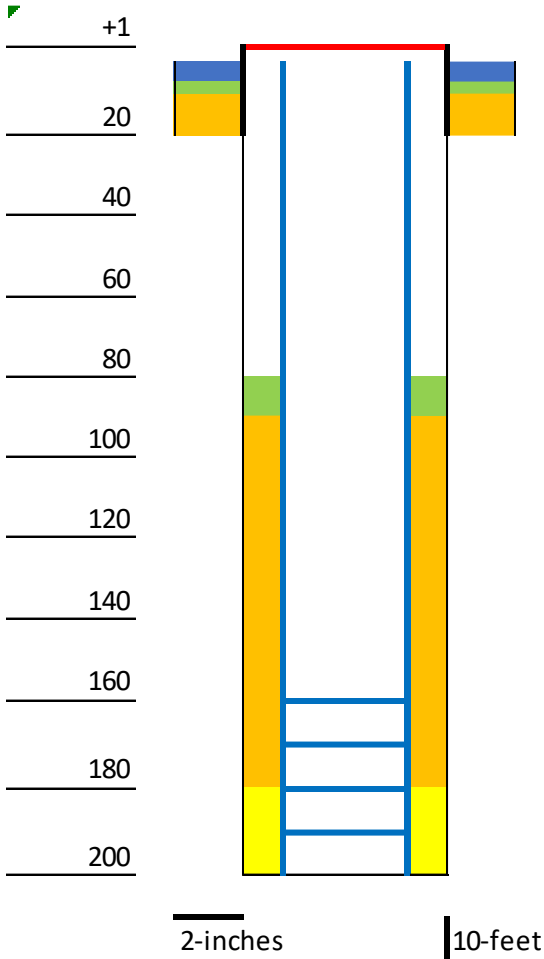
AquaTroll at 185'

Drilling Details:

7/20 WL = 161.5' btoc

12" hole sfc-20'

6"(?) hole 20'-200'



4 bags of cement for surface completion

1 to 1.5 bags of bentonite for annular seal
(depth of annular seal uncertain)

Casing Details:

8" steel casing sfc-20'

4.5" PVC casing sfc-200'

(blank sfc-160'; screened 160'-200', end cap?)

8 to 8.5 bags of bentonite

native material

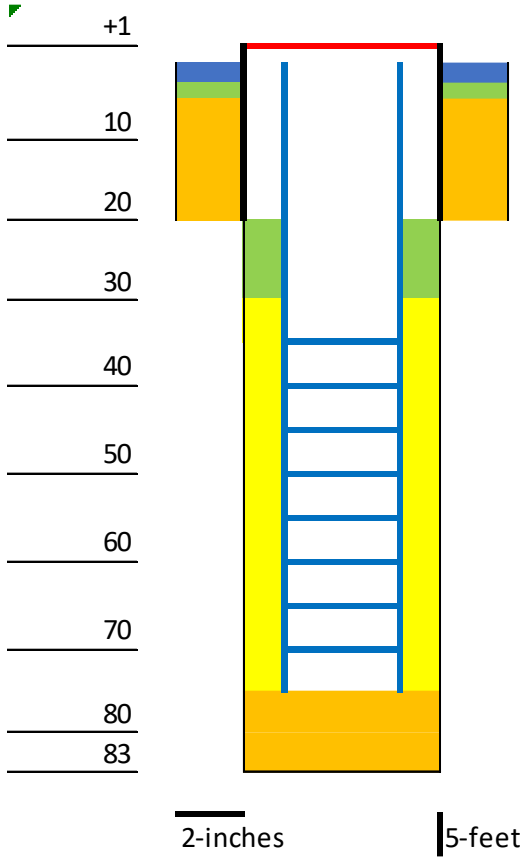
Broad Lithologic Overview:	
0'-60'	Alluvium
60'-110'	Clay w/ Sand
110'-200'	Gravel/Volcanics(?)

14 bags of sand (175'-200')

WTX-LLMWS (BW)

Leoncita/Limpia Shallow Well
drilled January 13th, 2020
(Brad Wolaver)

AquaTroll at 60' btoc
7/20 WL = 29.1' btoc



Drilling Details:

12" hole sfc-20'
8" hole 20'-83' TD

***NEED TO GET NUMBERS FOR SURFACE BENTONITE AND CEMENT PLUGS**

6 bags of bentonite/hole plug (20.5'-29')

Casing Details:

8" steel casing sfc-20'
4.5" PVC blank sfc-35'
screened 35'-75' (*no end cap)

Broad Lithologic Overview:	
0'-80'	Alluvium
80'-83'	Alluvium w/ Clay

25 bags of sand (29'-75')
native material (75'-83')

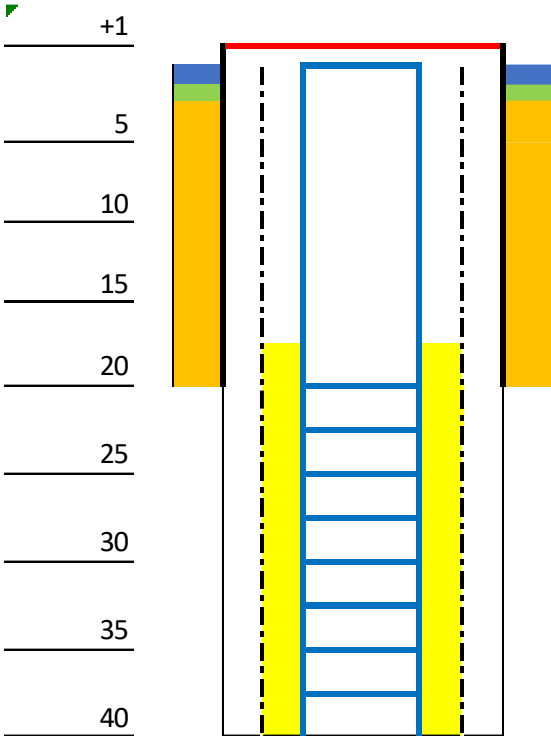
WTX-BSPMWS (BW)

Balmorhea SP Shallow Well drilled
January 14th & 15th, 2020
(Brad Wolaver)

AquaTroll at 35' btoc
7/20 WL = 16.7' btoc

Drilling Details:

12" hole sfc-20'
8" hole 20'-40' TD



4 bags of 94-lb cement for surface completion
4 50-lb bags of bentonite/hole plug
(depth of annular seal: 2'?)
native fill

Casing Details:

8" steel casing sfc-20'
6" slotted steel casing sfc-40' (to keep hole open)
4.5" PVC blank sfc-20', screened 20'-40' (*no end cap)

Broad Lithologic Overview:	
0'-40'	Alluvium

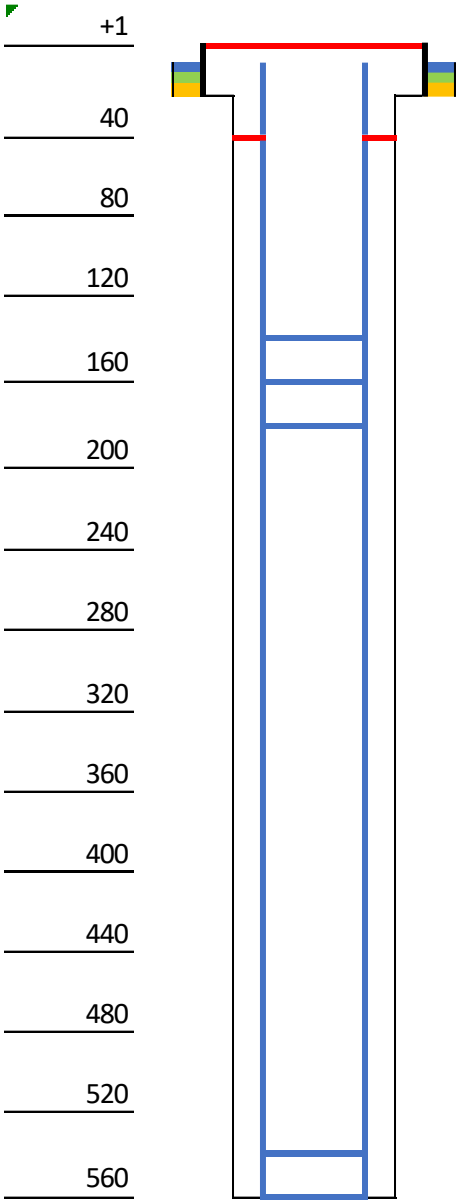
11 bags of sand (???'-40')

2-inches

2.5-feet

WTX-McRBAD (BW)

McCoy-Remme Big Aguja Deep Well drilled
January 20th-22nd, 2020 (Brad Wolaver)



6 bags of cement (sfc-3')
12 bags of bentonite/hole plug (around 8" sfc casing, 3'-8')
native fill
shale trap @ 40'

AquaTroll at 500' btoc
7/20 WL = 295.8' btoc

Drilling Details:
8" casing advance sfc-20'
6" hole 20'-560' TD

Casing Details:
8" steel casing sfc-20'
4.5" PVC casing sfc-563' (blank sfc-140' & 180'-540';
screened 140'-180' & 540'-560'; w/ end cap)

Broad Lithologic Overview:	
0'-18'	Alluvium
18'-45'	Yellow Clay
45'-560'	Gray Carbonaceous Shale

1-inch | 20-feet

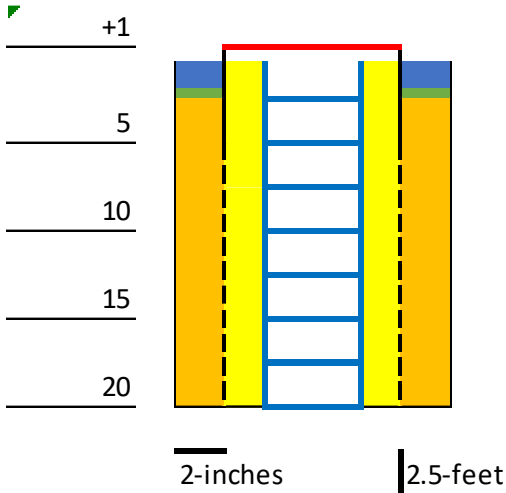
WTX-McRBAS (BW)

McCoy-Remme Big Aguja
Shallow Well drilled January
22nd & 23rd, 2020 (Brad
Wolaver)

AquaTroll at 19.5' btoc
7/20 WL = 18.1' btoc

Drilling Details:

12" hole sfc-6'
8" casing advance 6'-20'



Casing Details:

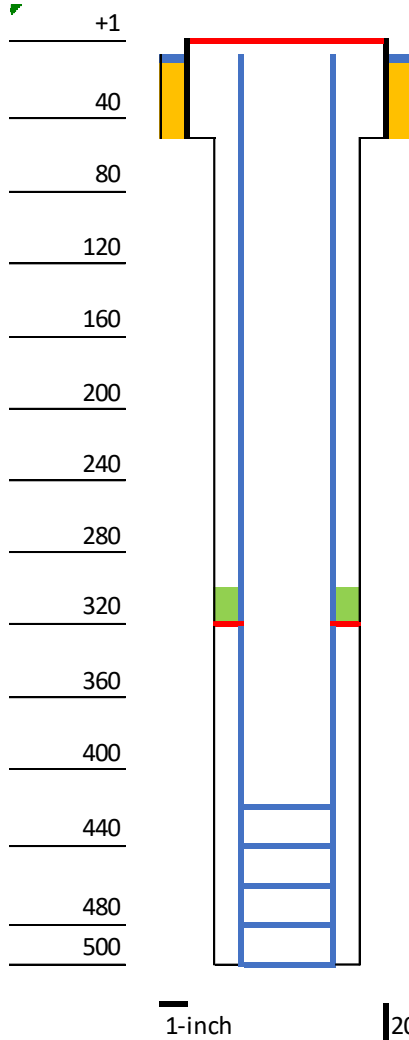
8" steel casing sfc-20' (perforated, 3 sets at 120° from 5'-18')
4.5" PVC screened sfc-20' (w/ end cap)

Broad Lithologic Overview:	
0'-18'	Alluvium
18'-20'	Yellow Clay

WTX-4JMMWD (KH)

4J Madera Deep Well drilled
January 23rd-28th, 2020
(Kelly Hattori)

Drilling Details: AquaTroll at 485' btoc
8" casing advance sfc-52' 7/20 WL = 379.2' btoc
6" hole 52'-500' TD



1 bag of cement (sfc-1')

native fill

Casing Details:

8" steel casing sfc-52'
4.5" PVC casing sfc-500' (blank sfc-420', screened 420'-500', w/ end cap)

Broad Lithologic Overview:

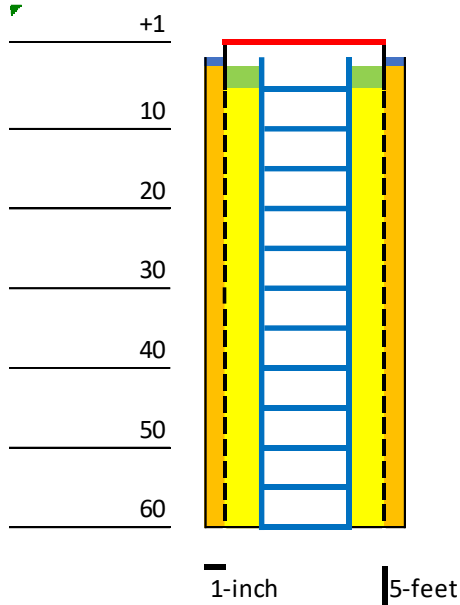
0'-60'	Alluvium
60'-140'	Yellow/Pale Brown Clay
140'-220'	Volcanics/Cobbles/Pebbles
220'-345'	Yellow/Gray Shale
345'-370'	Cave(?)
370'-420'	Pale Brown Limestone (minimal cuttings)
420'-500'	Gray Shale(?) (minimal cuttings)

5 bags of bentonite/hole plug (around 4.5" PVC casing, 305'-320')
shale trap @ 320'

WTX-4JMMWS (KH)

4J Madera Shallow Well drilled
January 29th, 2020 (Kelly Hattori)

RuggedTroll at 60' btoc
7/20 WL = dry



Drilling Details:

8" casing advance sfc-60'

- 1 bag of cement from sfc-1' (surface seal around 8" casing)
- 2 bags of bentonite/hole plug from 2'-8' (around 4.5" PVC)
- 28 bags of sand from 8'-60'
- native fill

Casing Details:

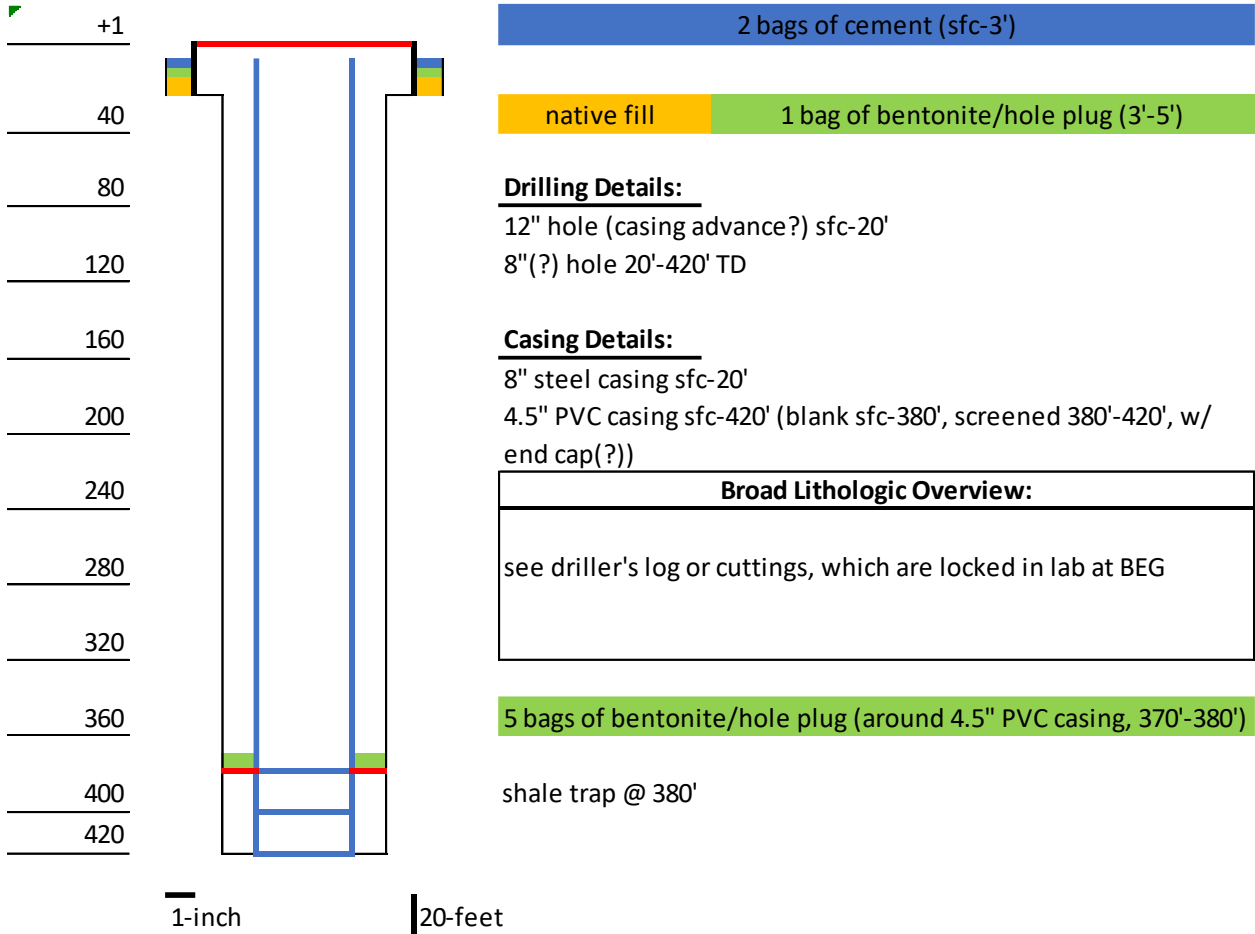
8" steel casing sfc-60' (perforated, 3 sets at 120° from 10'-58')
4.5" PVC screened sfc-60' (w/ end cap)

Broad Lithologic Overview:	
0'-56'	Alluvium
56'-60'	Yellow Clay
DTW = N/A (dry hole)	

WTX-SRMWD (RG)

Cherry Canyon/Shield Ranch Deep Well drilled
February 4th & 5th, 2020 (Ramon Gil)

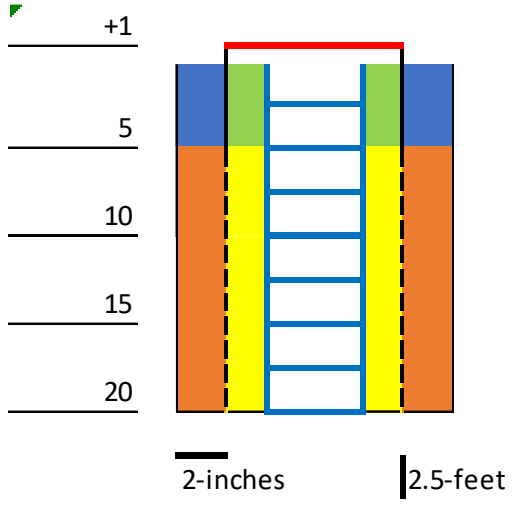
AquaTroll at 370' btoc
7/20 WL = 317.7' btoc



WTX-SRMWS (STM)

Cherry Canyon/Shield Ranch
 Shallow Well drilled February 17th,
 2020 (Tyson McKinney)

RuggedTroll at 18' btoc
 7/20 WL = dry



Drilling Details:

12" hole sfc-20'

- 2 bags of cement from sfc-5'
- 8 bags of pea gravel from 5'-20'
- 2 bags of bentonite/hole plug from 2'-5'
- 7 bags of sand from 5'-20'

Casing Details:

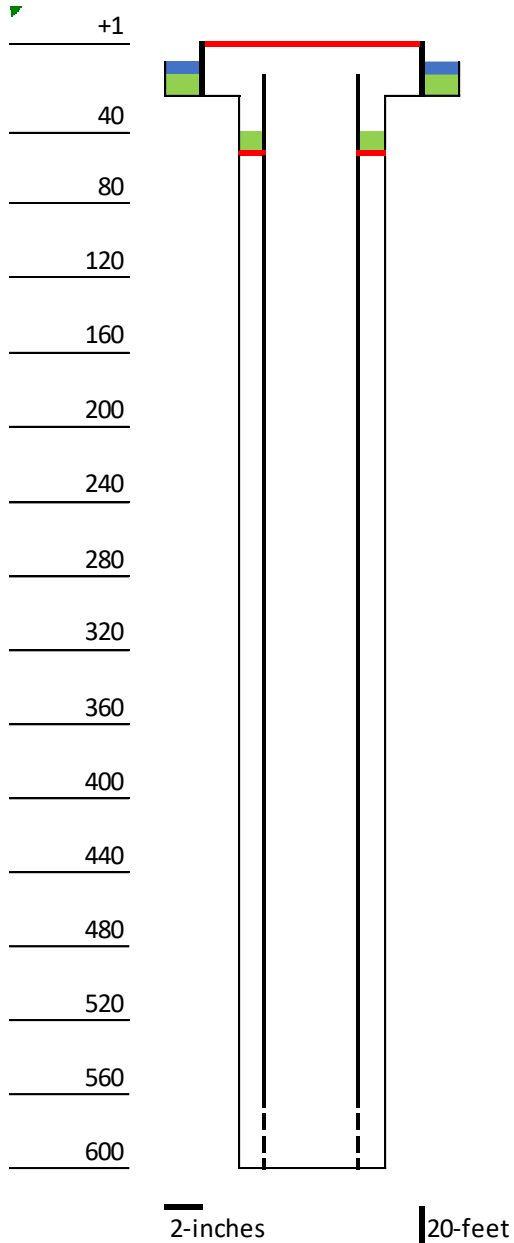
8" steel casing sfc-20' (perforated, 3 sets at 120° from 5'-18')
 4.5" PVC screened sfc-20' (w/ end cap)

Broad Lithologic Overview:	
0'-20'	Alluvium
DTW = N/A (dry hole)	

WTX-SRMWL (STM)

Cherry Canyon/Shield Ranch Lodge
Well drilled March 5th & 6th
(Tyson McKinney)

RuggedTroll at 550' btoc
7/20 WL = 471.0' btoc



3 bags of cement (sfc-???)

5 bags of bentonite/hole plug (around 8" sfc casing, depths unknown)

5 bags of bentonite/hole plug on top of shale traps (around 4" steel casing)

2 shale traps from 48'-50'

Drilling Details:

12" hole sfc-20'
6" hole 20'-600' TD

Casing Details:

8" surface casing sfc-20'
4" steel casing 10'-600' (1/8" torch-slotted from 560'-600')

Broad Lithologic Overview:	
0'-10'	Alluvium
10'-600'	Volcanics (rhyolite/trachyte)

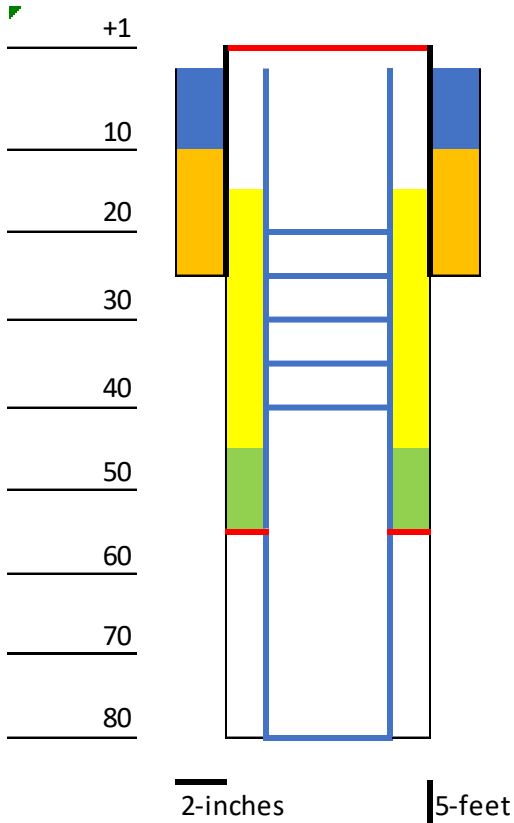
WTX-SPMWS (STM)

TNC Sandia Preserve Shallow Well drilled March 17th & 18th, 2020 (Tyson McKinney)

AquaTroll at 52' btoc
7/20 WL = 20.8' btoc

Drilling Details:

12" hole sfc-26'
8" hole 26'-80' TD



5 bags of cement (sfc-???)
native fill

Broad Lithologic Overview:	
0'-15'	Alluvium
15'-48'	Caliche/Freshwater Limestone
48'-80'	Gray Clay

11 bags of sand (tagged at 17')
3 bags of bentonite/hole plug (tagged at 45')

shale trap @ 55'

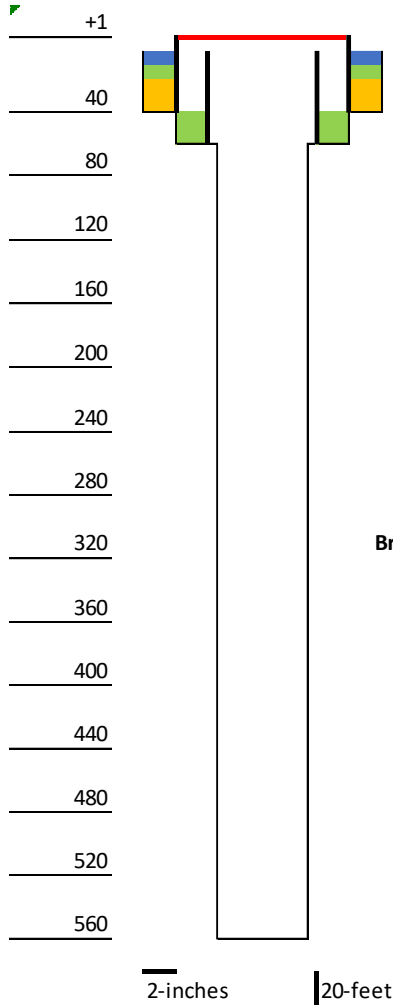
Casing Details:

8" steel casing sfc-26'
4.5" PVC blank sfc-20' & 40'-80'; screened 20'-40' (w/ end cap)

WTX-SPMWD (STM)

TNC Sandia Preserve Deep Well
drilled March 18th-20th, 2020
(Tyson McKinney)

AquaTroll at 251' btoc
7/20 WL (in open borehole) = 51.5' btoc



3 bags of cement (sfc-???)

2 bags of bentonite/hole plug (around 8" sfc casing)
6 bags of bentonite/hole plug (around 6" steel casing)
native fill

Drilling Details:

12" hole sfc-20'
9" hole 20'-60'
6" hole 60'-562' TD

Casing Details:

8" steel casing sfc-40'
6" steel casing sfc-60' (to seal off shallow water zone)
6" open hole 60'-560'

Broad Lithologic Overview:

0'-15'	Alluvium	
15'-48'	Caliche	
48'-280'	Gray Clay	
280'-560'	Interbedded limestone and clay/shale	
20-40 ft - water encountered during drilling		

Stratigraphic control comes from GAT sheet, USGS and TWDB publications
Surface Elevation = 3301 ft amsl

Possible Stratigraphic units (based on field notes; cuttings are locked in the lab) - rcs

0-15	alluvium	Pecos
15-48	freshwater limestone?	Huelster Fm.
48-150	high plasticity gray clay	Huelster Fm.
150-280	greenish-gray clay with trace H/C odor	Boquillas*
280-410	limestone	Boquillas/Buda*
410-470	powdery CaCO3	Boquillas/Buda*
470-500	gray shale	Del Rio*
500-540	black shale and CaCO3	Del Rio*
540-560	dark gray limestone	Edwards ?

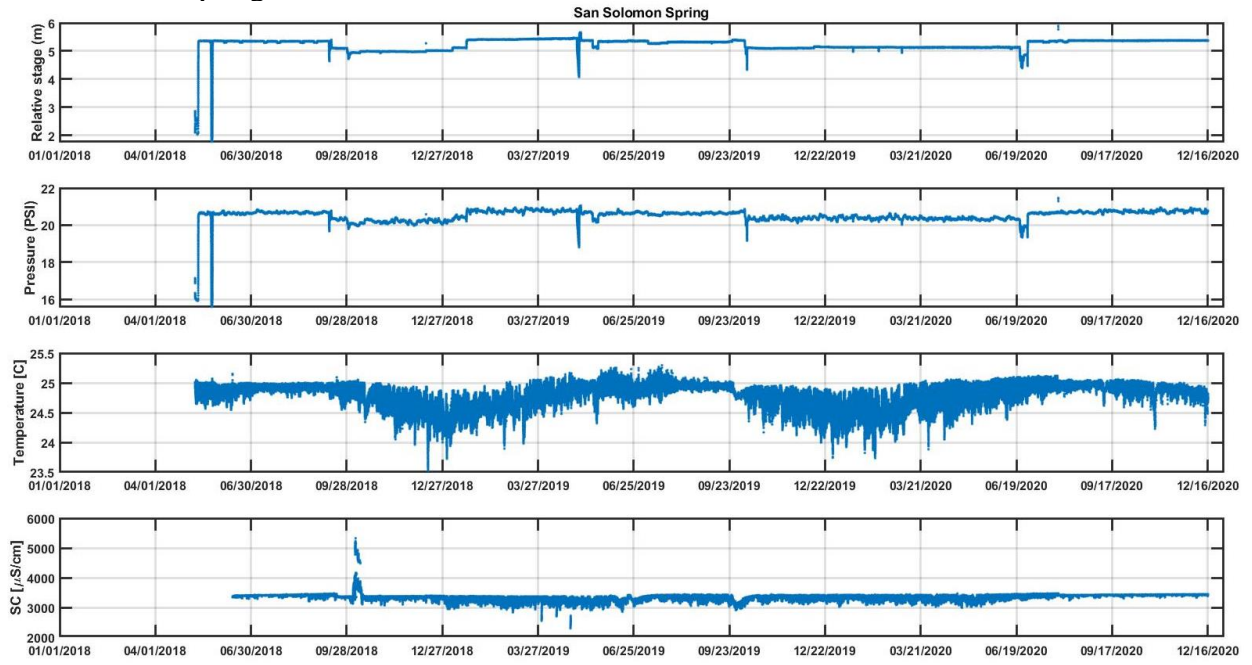
*These units are reported to be ~350 ft total thickness
540-150 = 410 ft - top Boquillas to top Edwards

Appendix B: Logger outputs

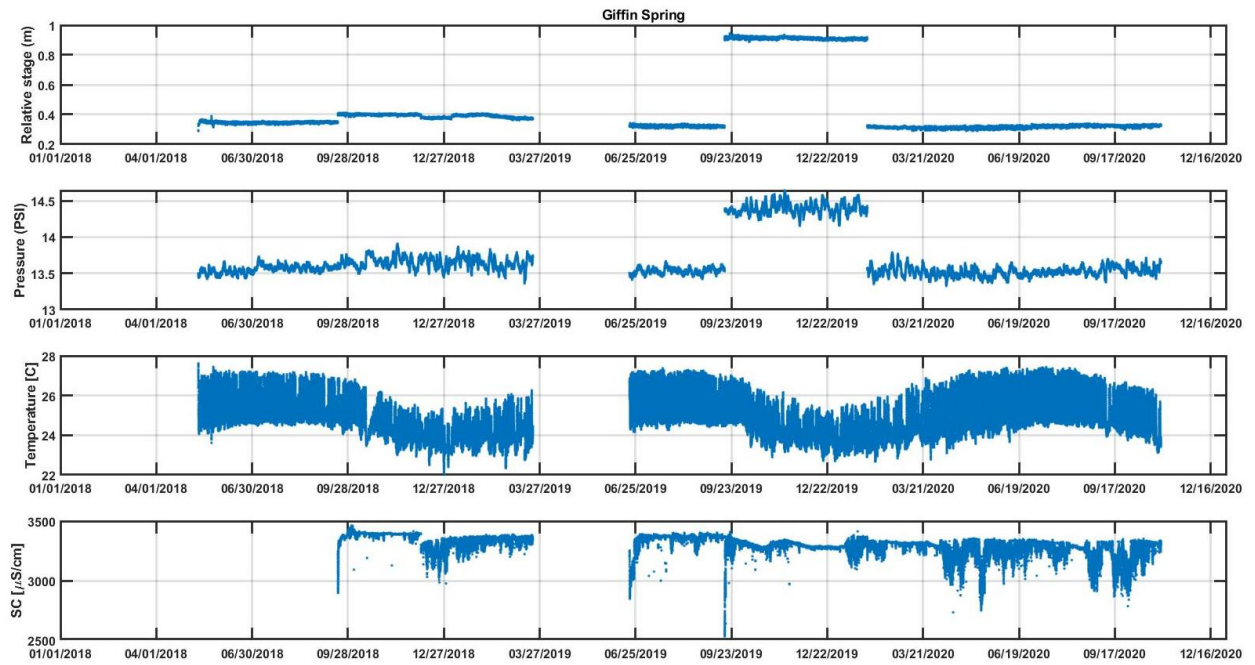
This appendix show full AT and RT logger outputs sorted in the following order:

- San Solomon Spring
- Giffin Spring
- Phantom Lake Spring
- East Sandia Spring
- Seven Springs
- Willow Spring
- Big Aguja Stream
- Cherry Upper Stream
- Cherry Lower Stream
- Limpia Lower Stream
- Limpia Upper Stream
- Madera Upper Stream
- Madera Lower Stream
- BSP Drain Canal
- Little Aguja Stream
- Hamilton WM Well
- BEG 4J Deep MW
- BEG BigA Deep MW
- BEG BigA Shallow MW
- BEG BSP MW
- BEG Cherry Deep MW
- BEG Limpia Shallow MW
- BEG Limpia Deep MW
- BEG Sandia Deep MW
- BEG Sandia Shallow MW
- Huelster #3 Well
- Cherry Lower Well
- BEG 4J Shallow MW
- BEG Lodge MW

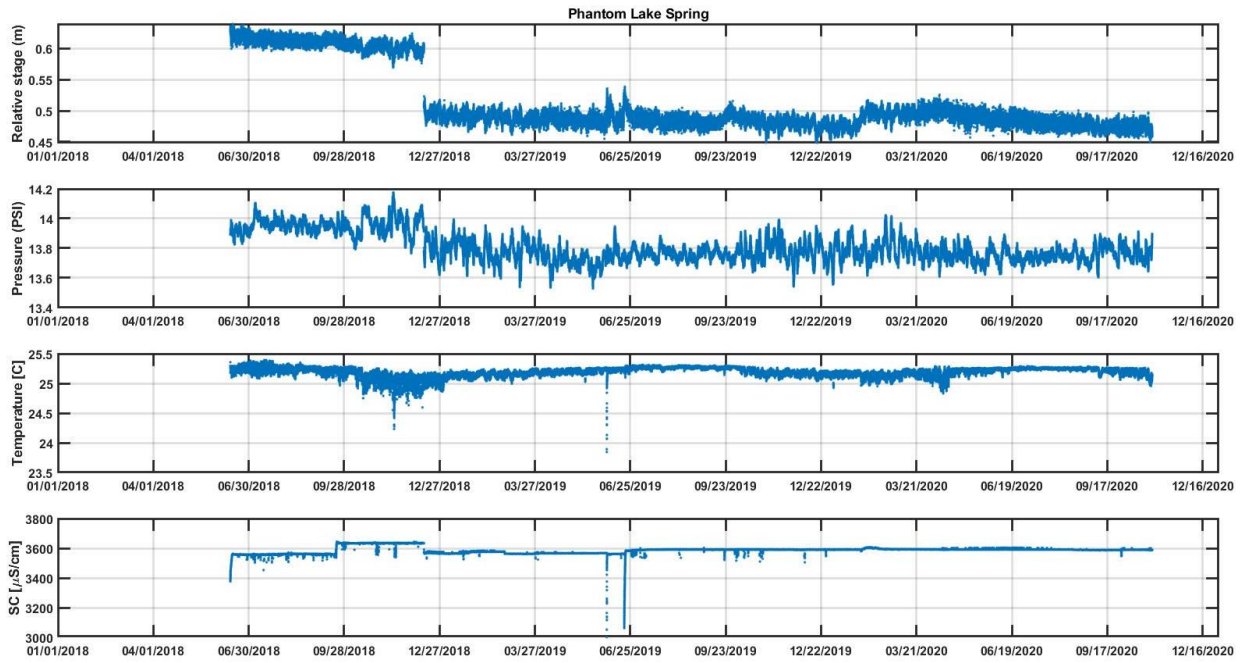
San Solomon Spring



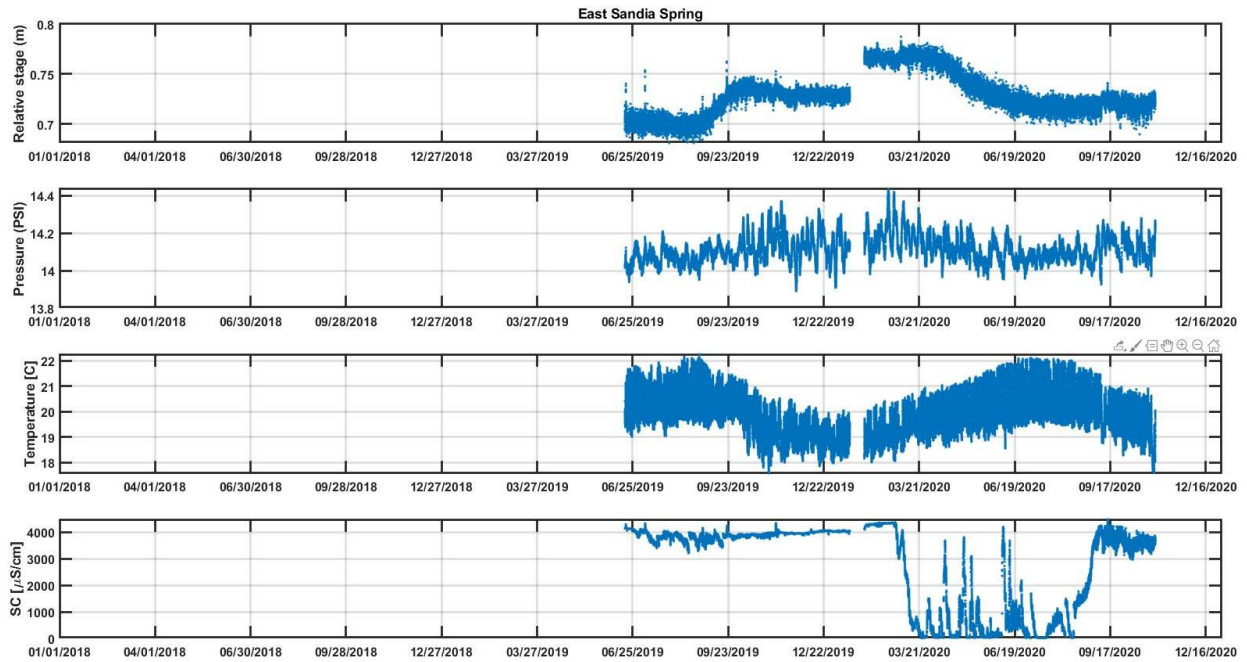
Giffin Spring



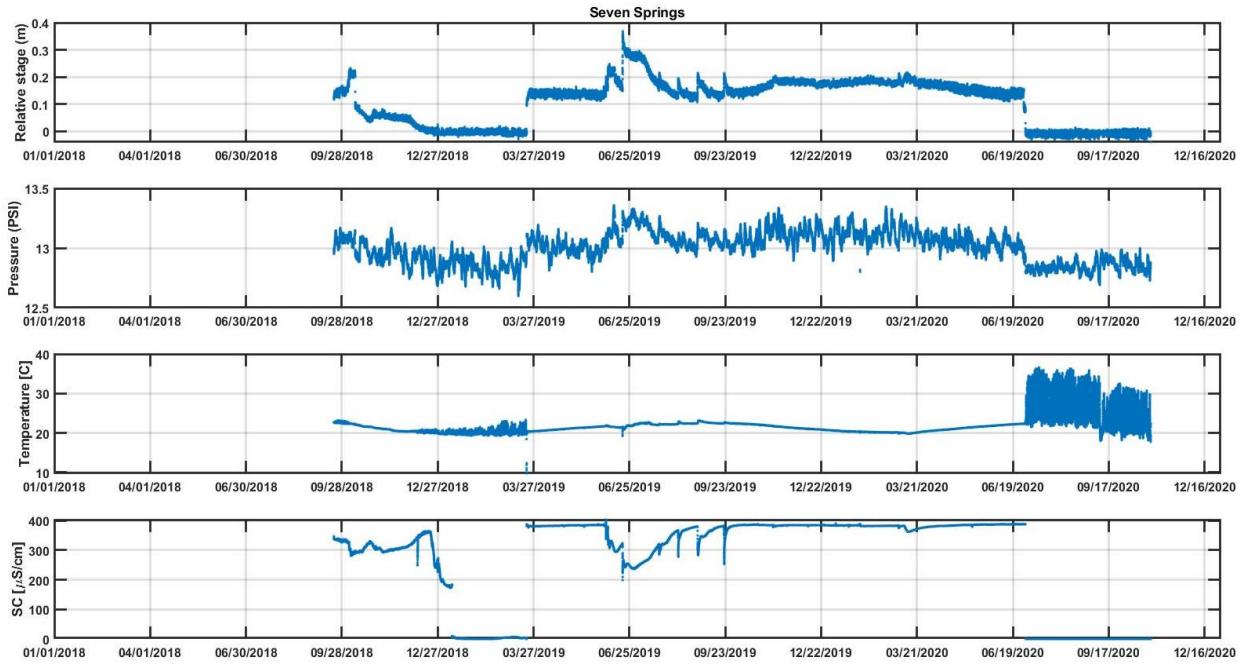
Phantom Lake Spring



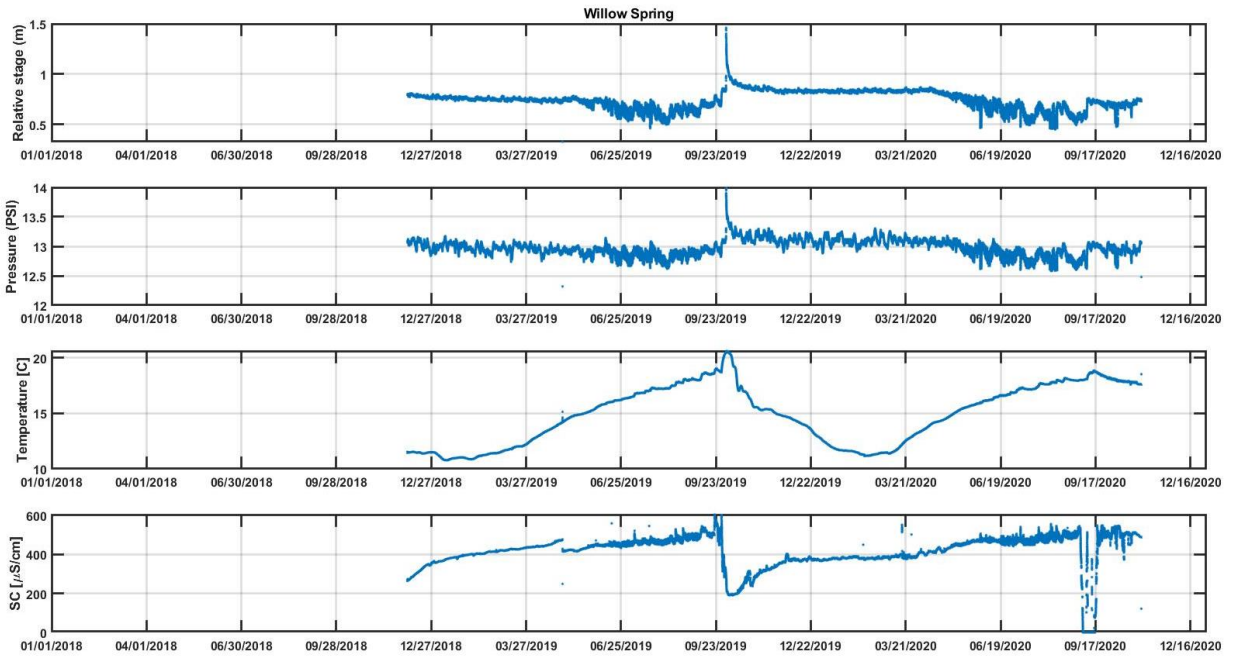
East Sandia Spring



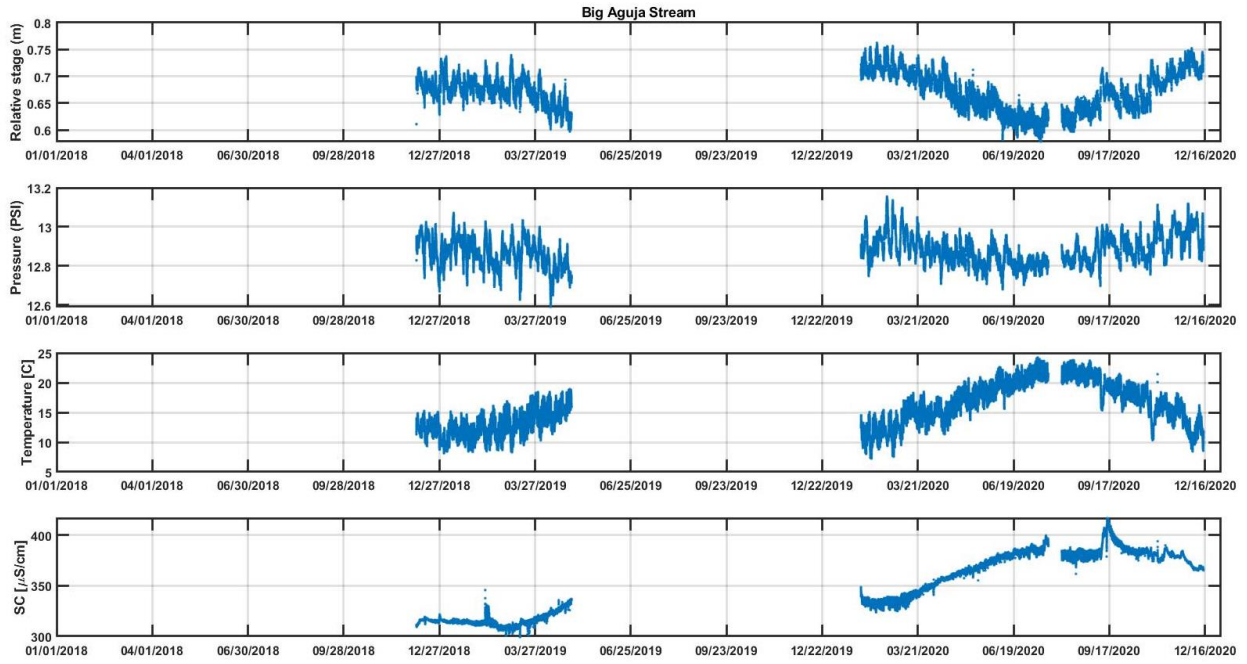
Seven Springs



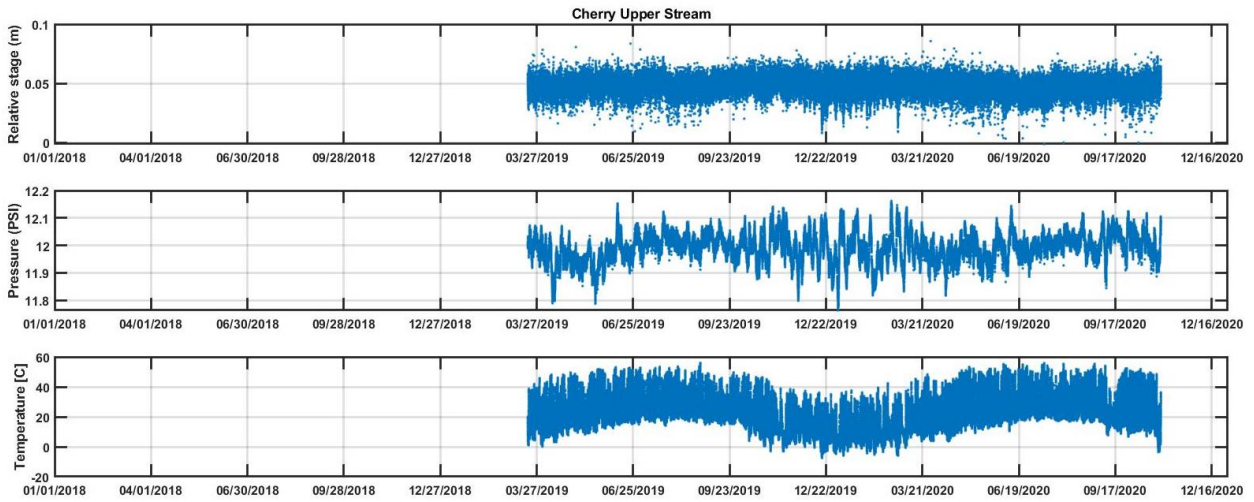
Willow Spring



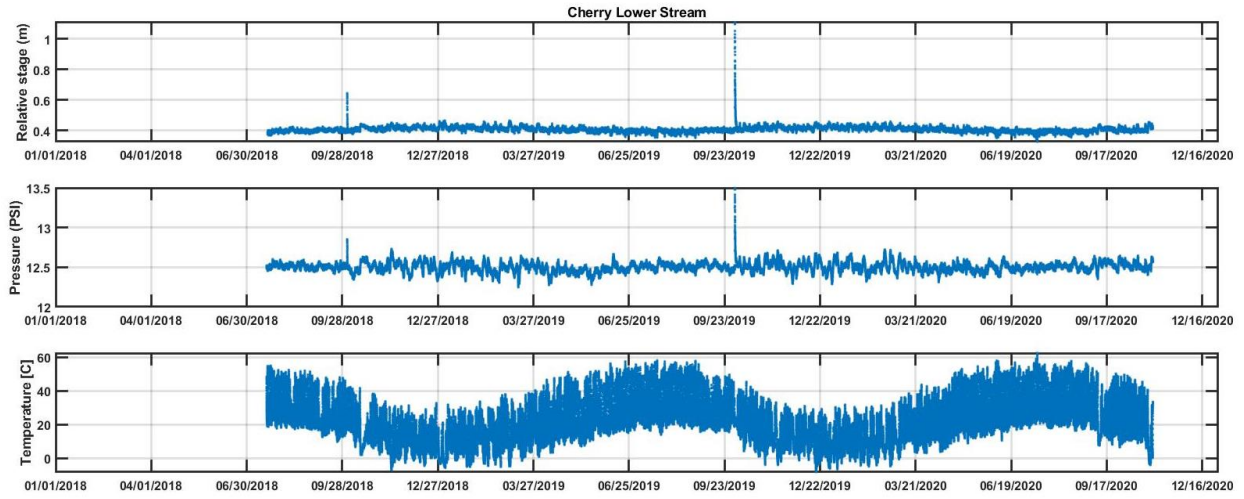
Big Aguja Stream



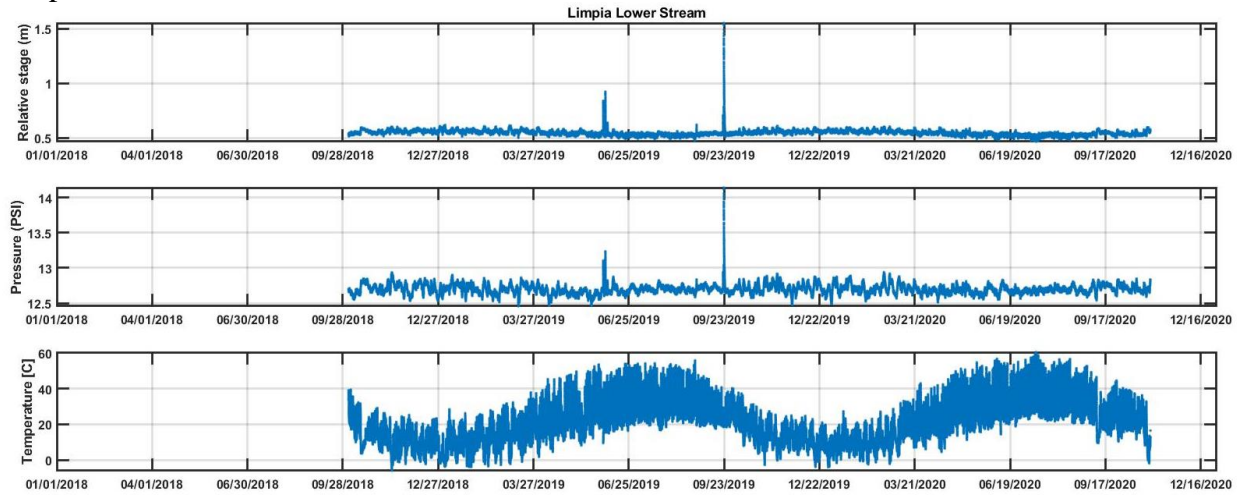
Cherry Upper Stream



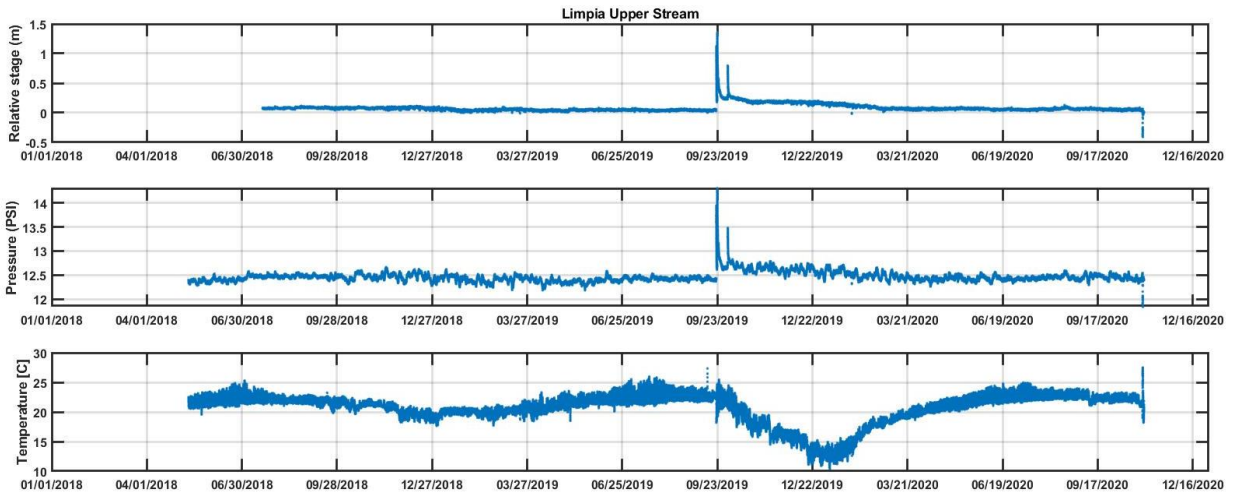
Cherry Lower Stream



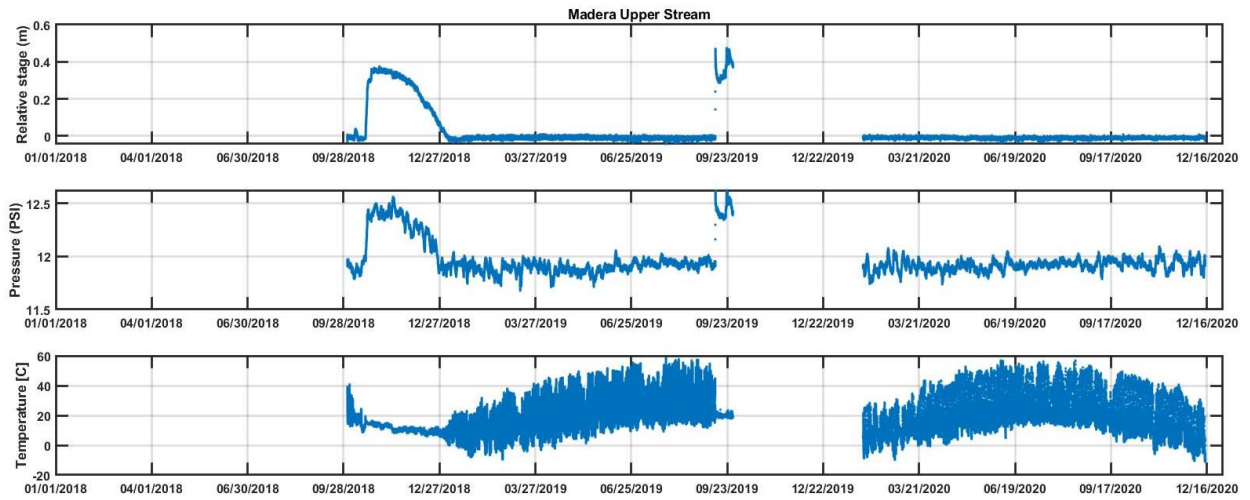
Limpia Lower Stream



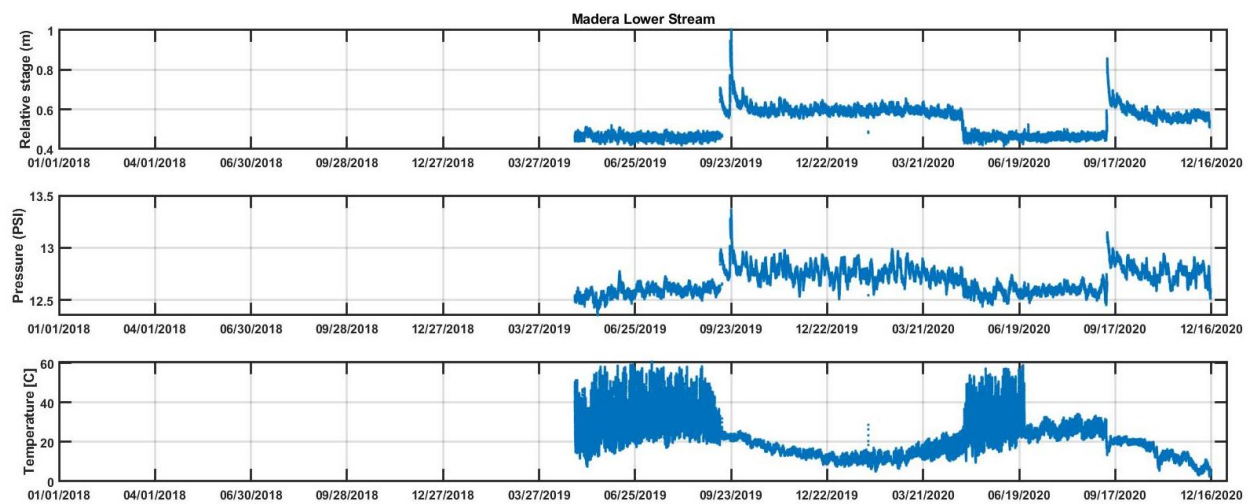
Limpia Upper Stream



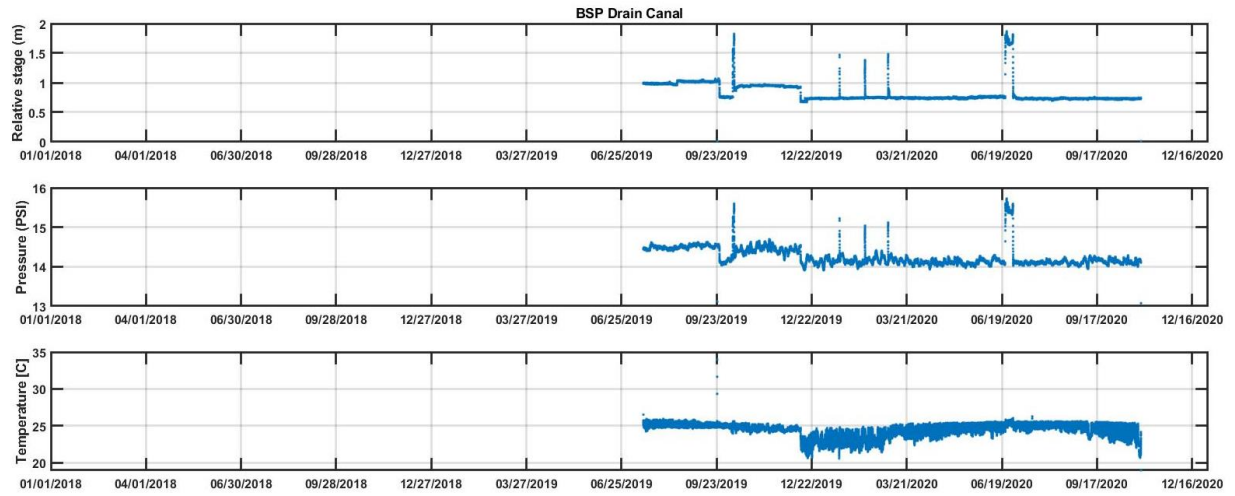
Madera Upper Stream



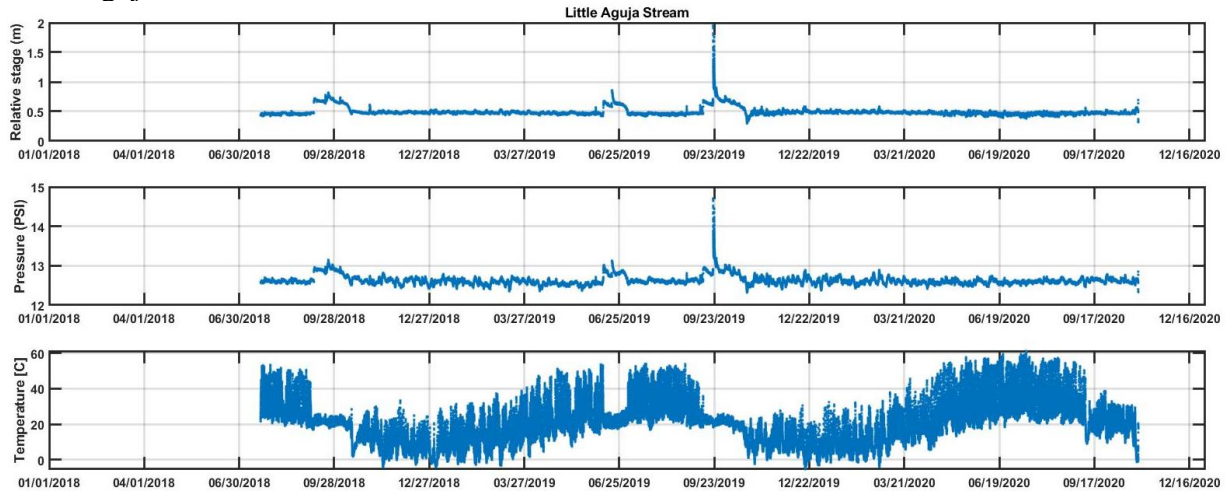
Madera Lower Stream



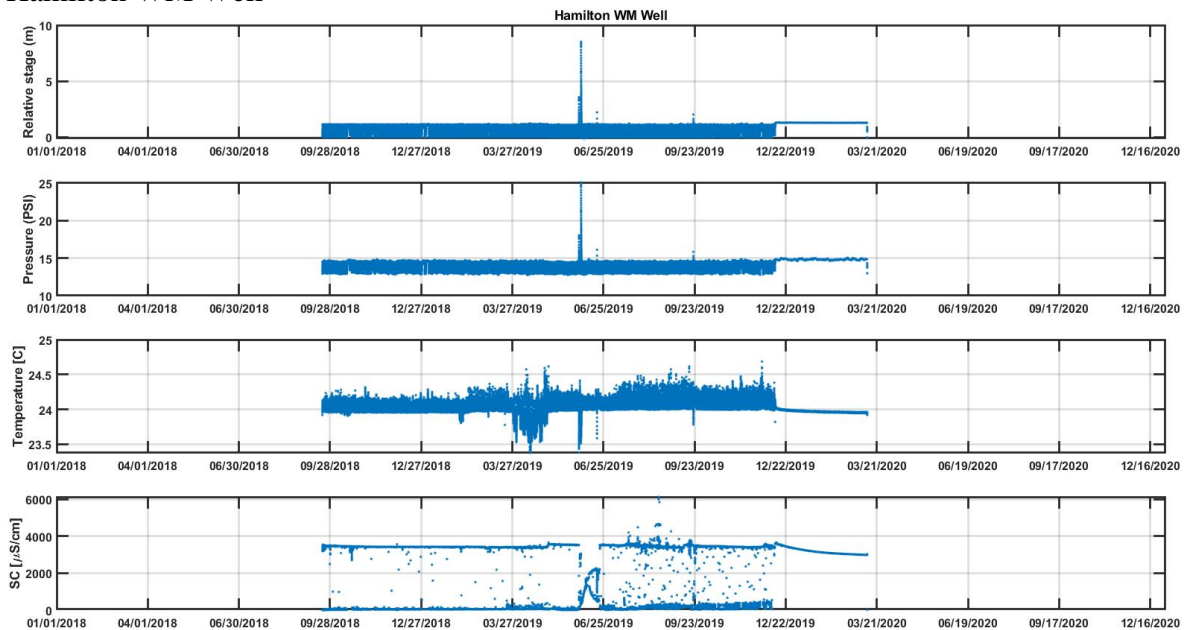
BSP Drain Canal



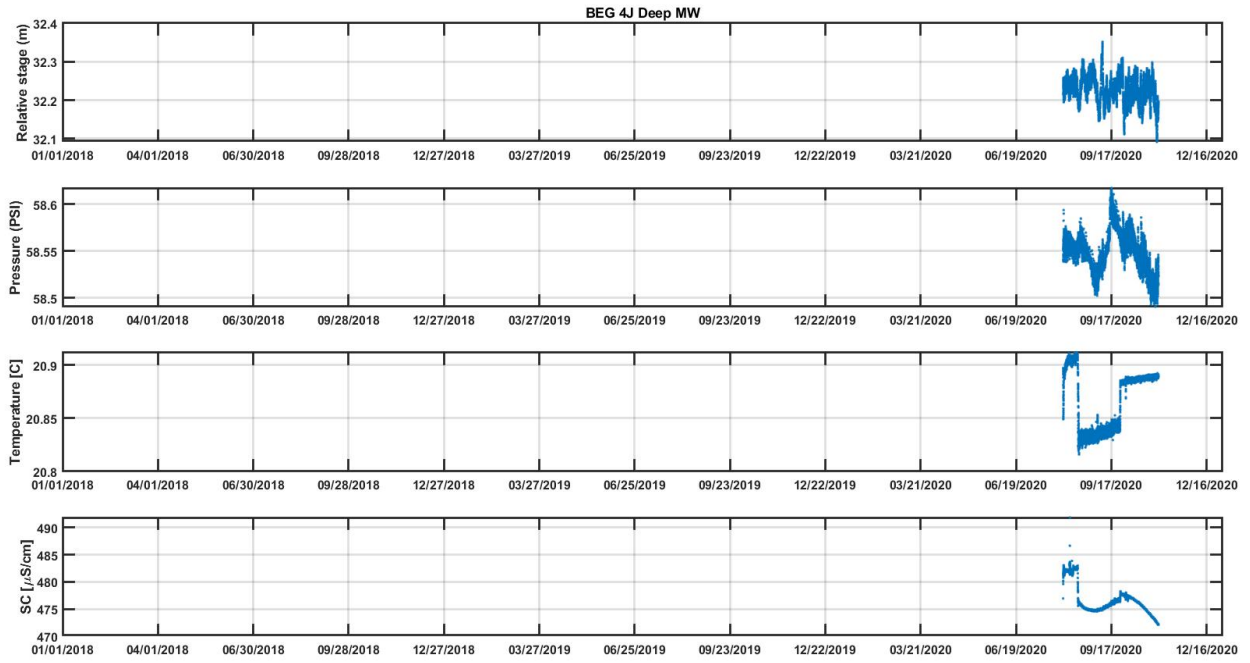
Little Aguja Stream



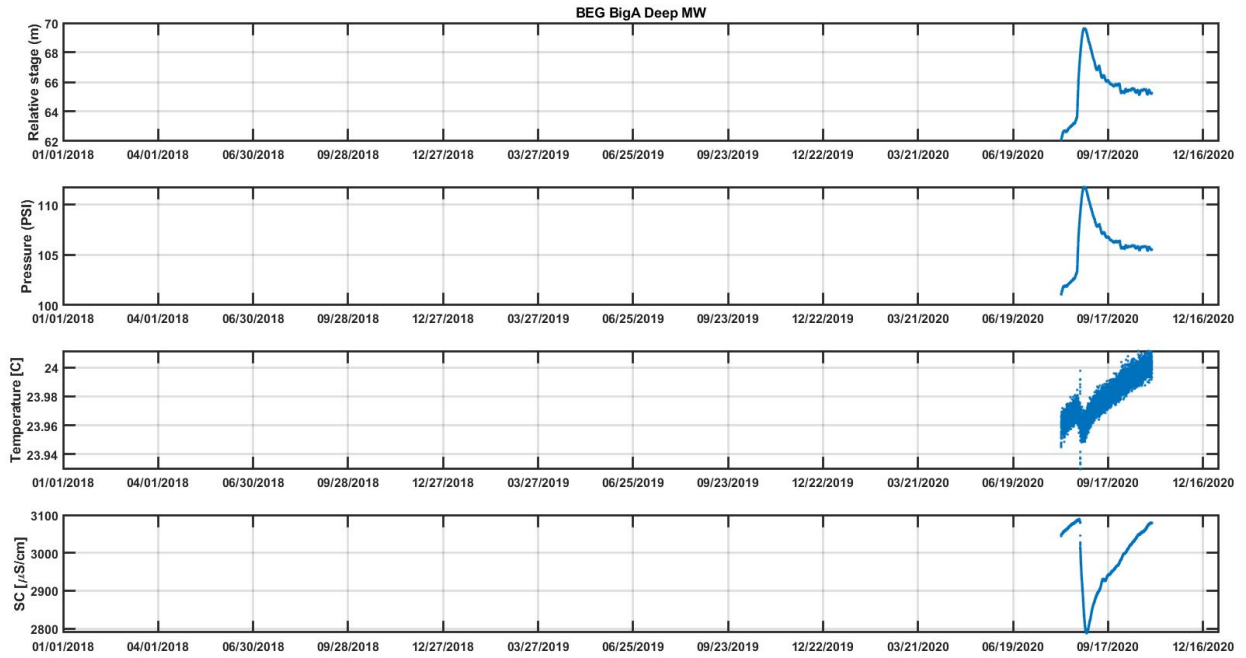
Hamilton WM Well



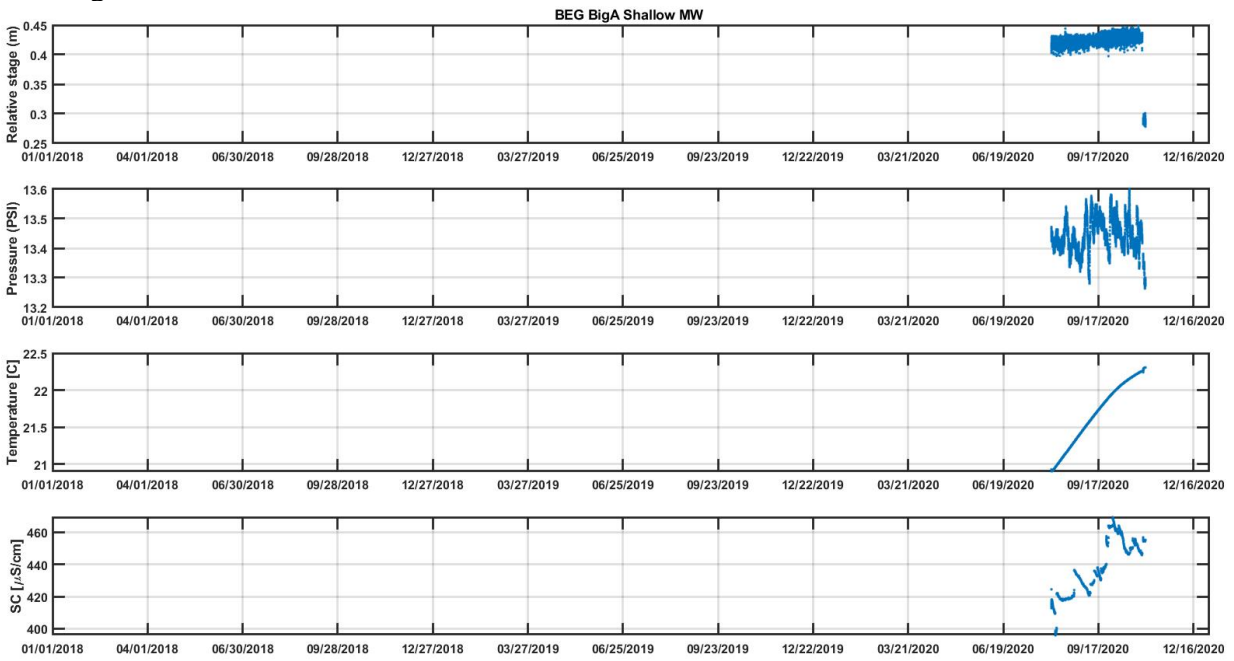
BEG 4J Deep MW



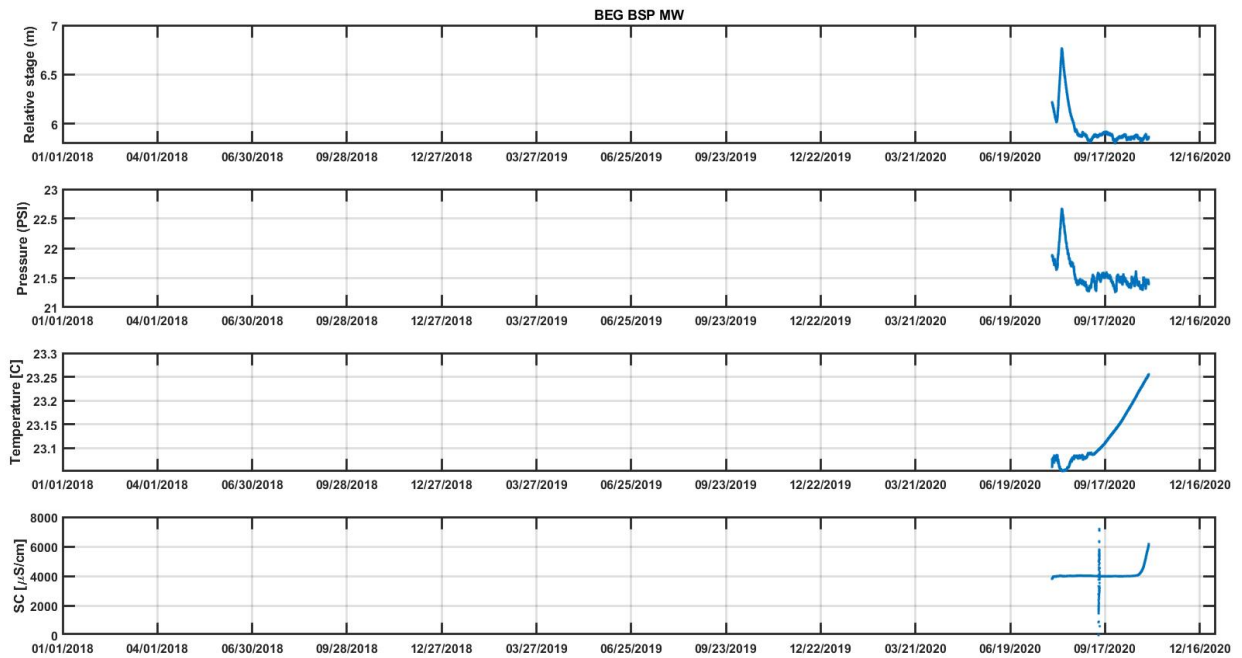
BEG BigA Deep MW



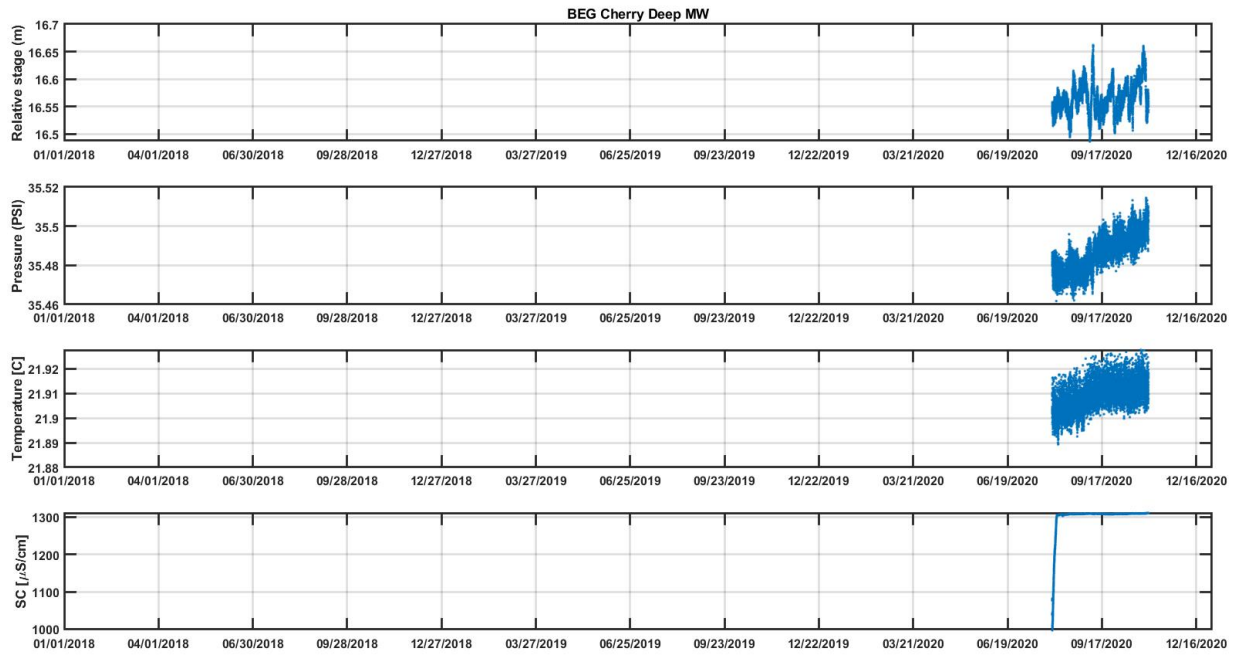
BEG BigA Shallow MW



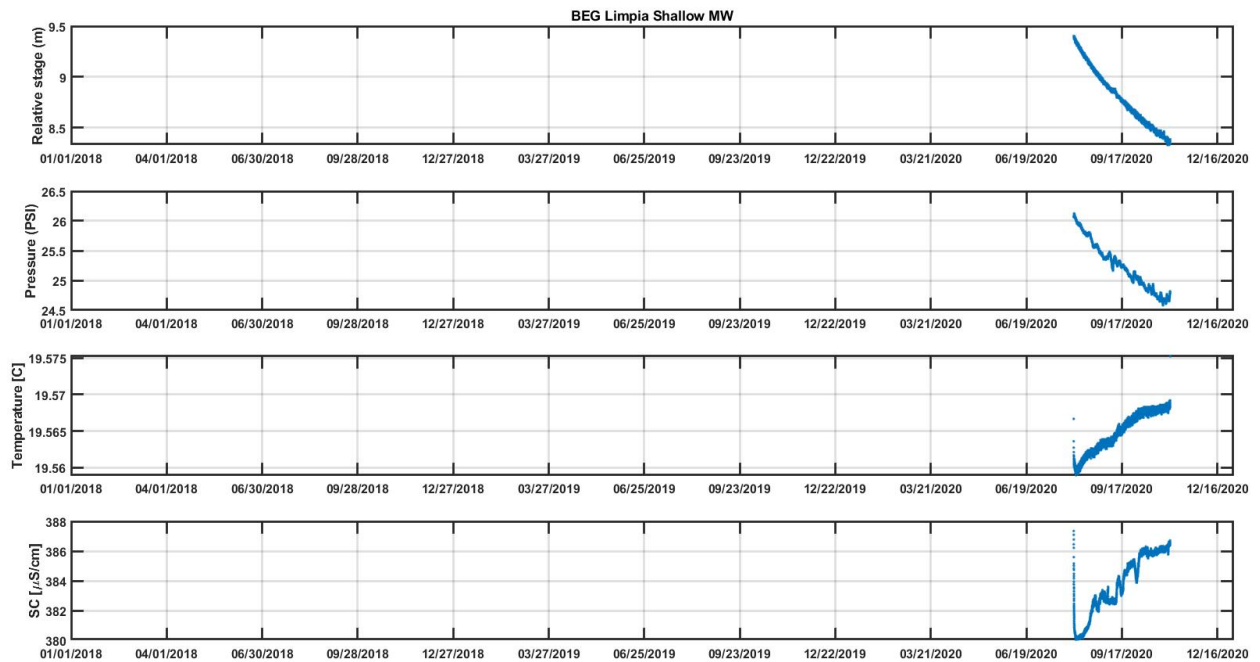
BEG BSP MW



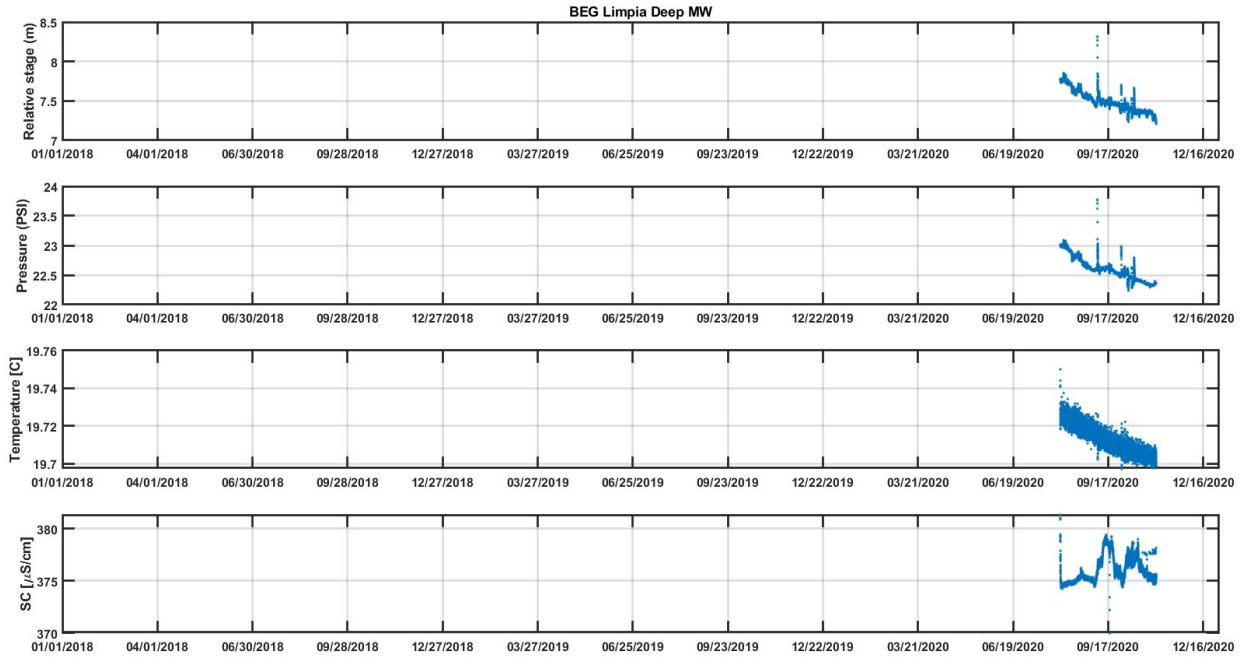
BEG Cherry Deep MW



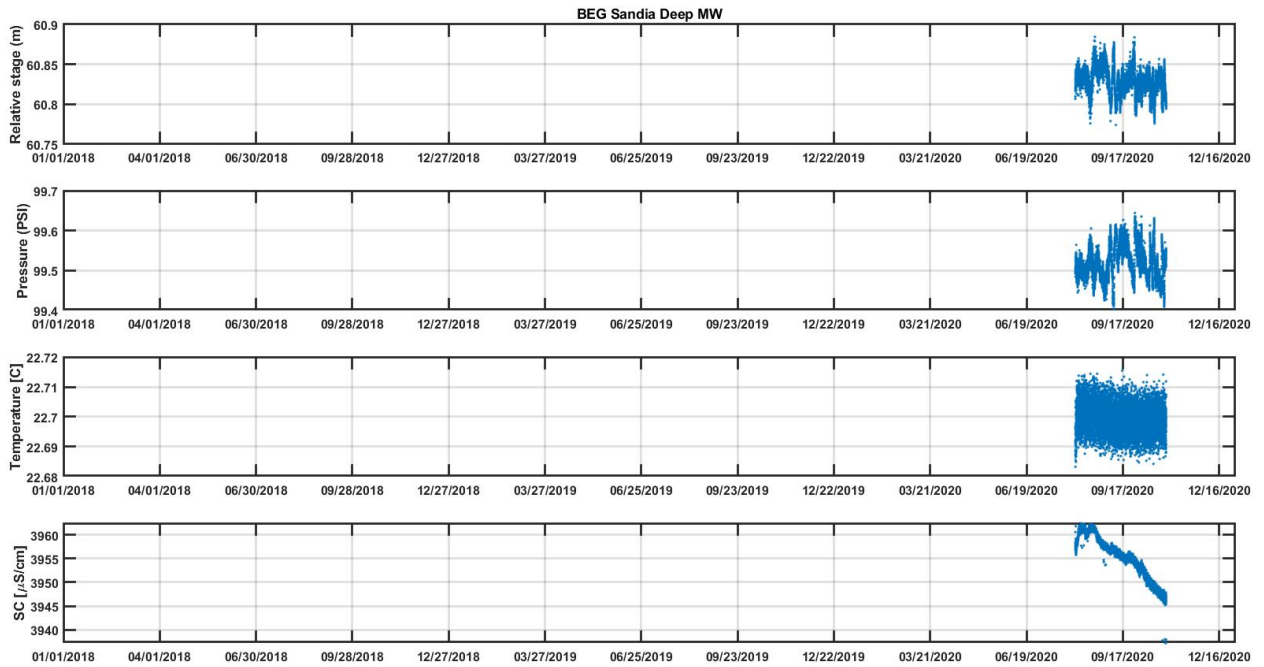
BEG Limpia Shallow MW



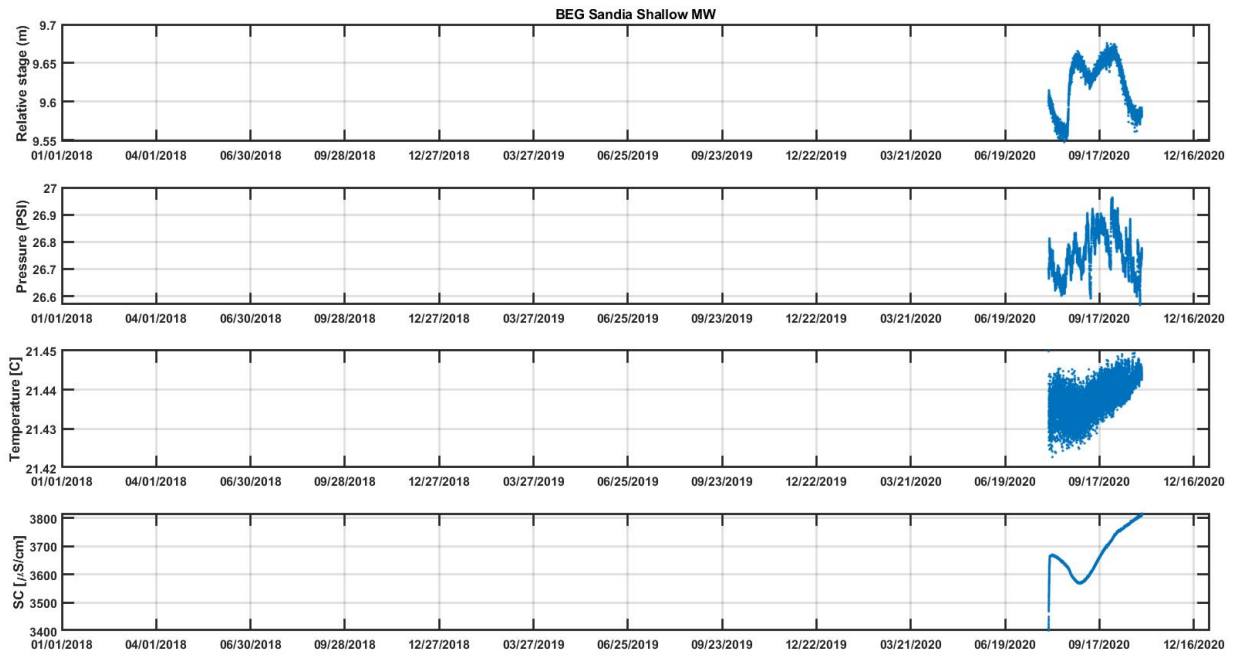
BEG Limpia Deep MW



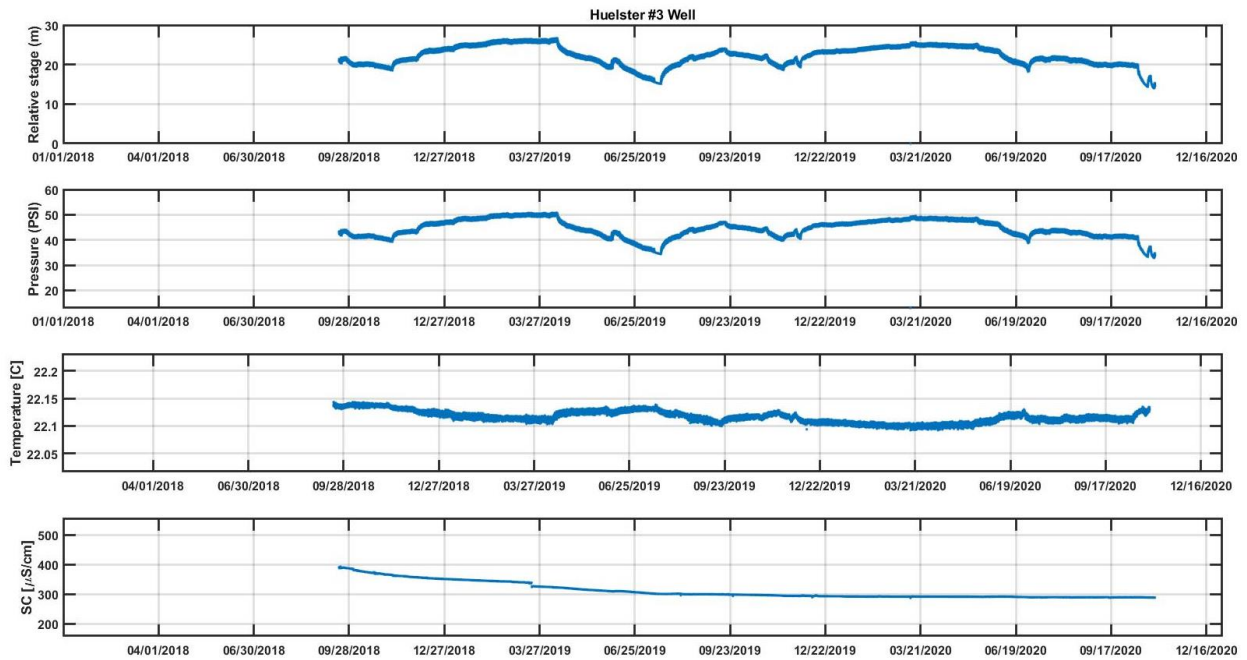
BEG Sandia Deep MW



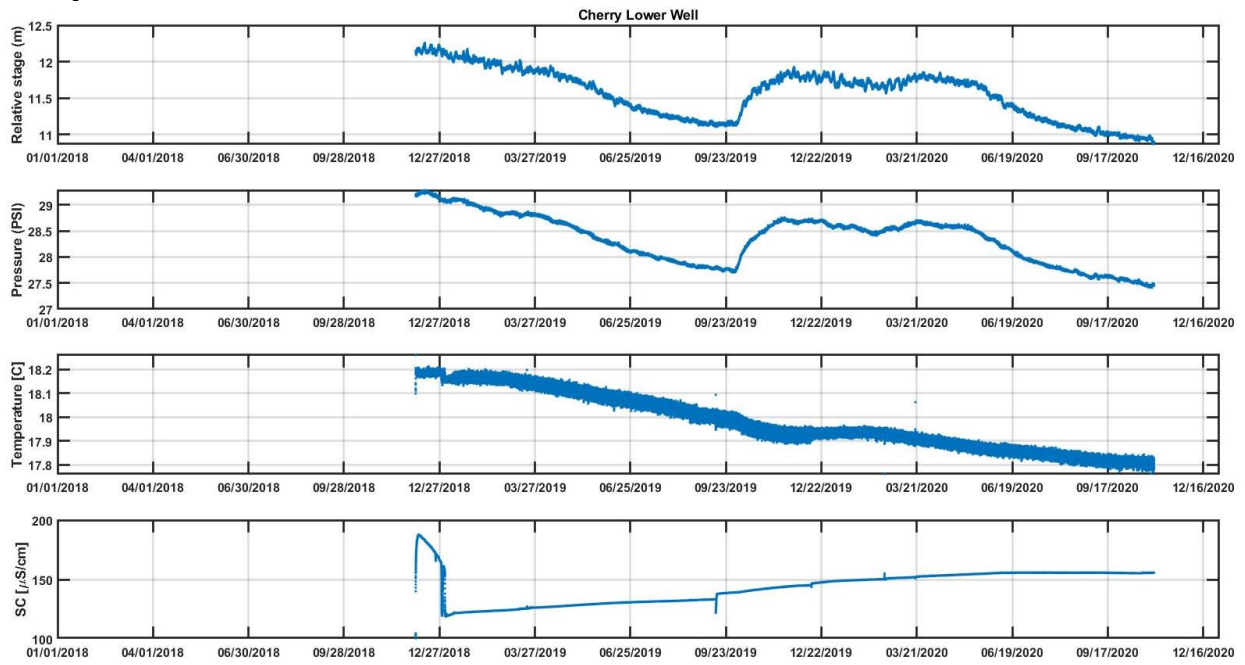
BEG Sandia Shallow MW



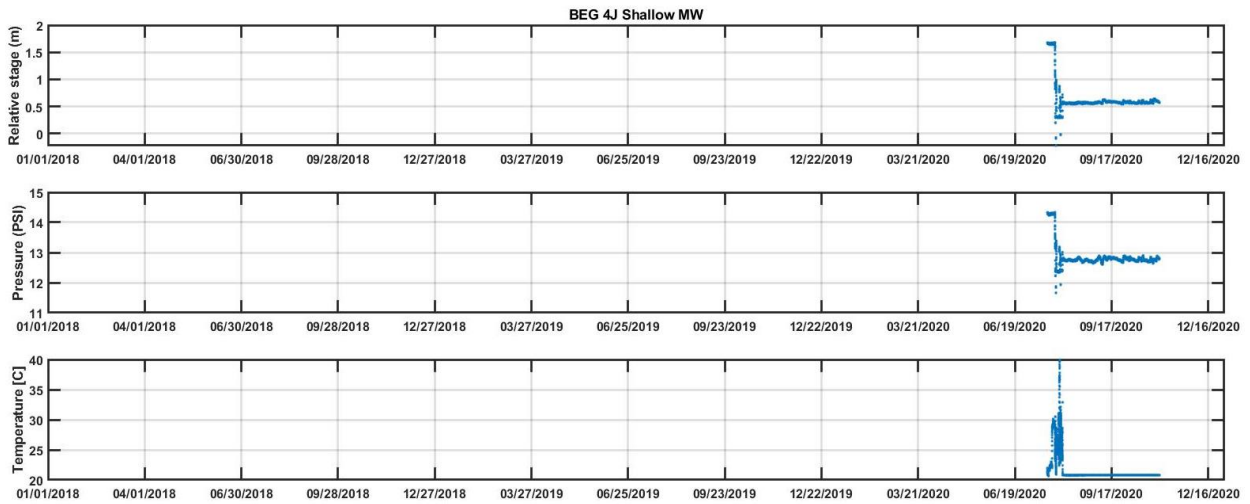
Huelster #3 Well



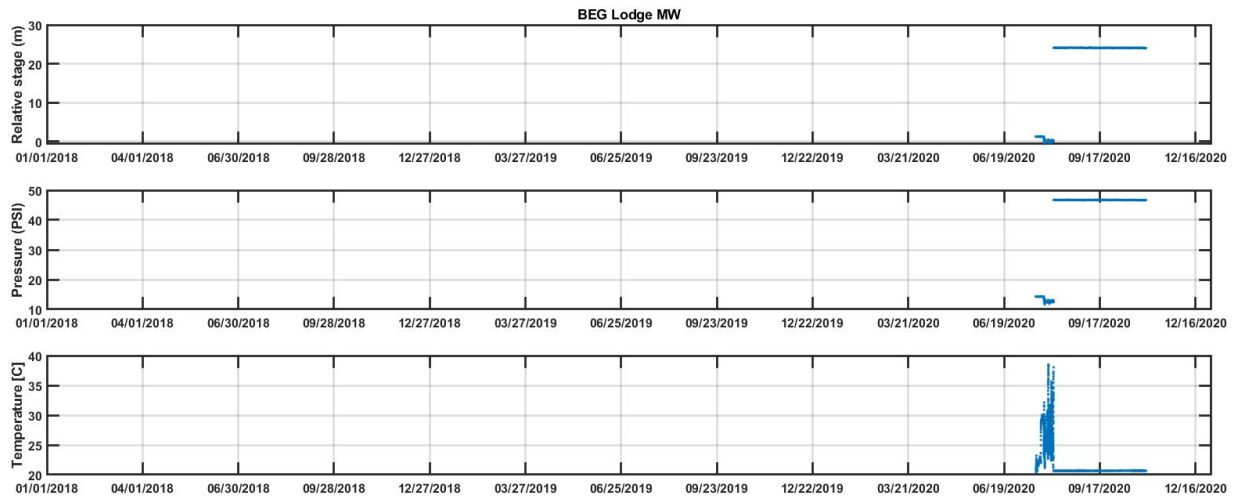
Cherry Lower Well



BEG 4J Shallow MW



BEG Lodge MW

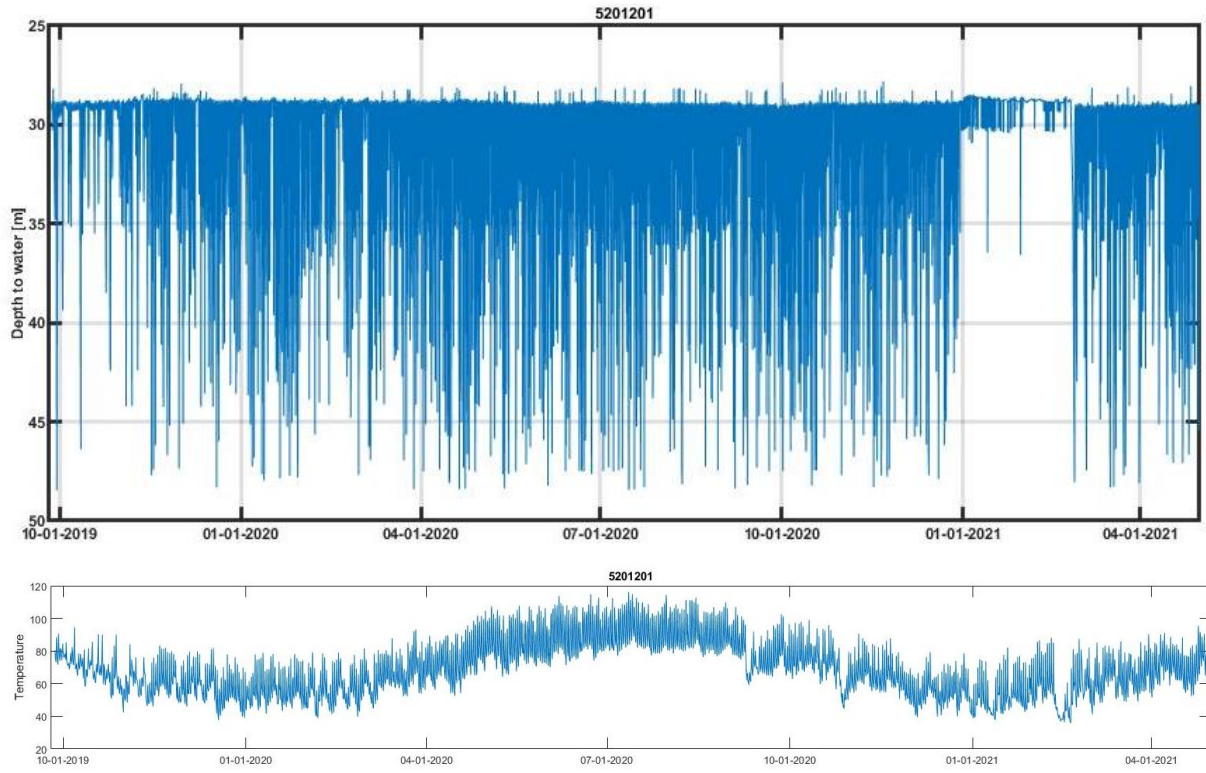


Appendix C: Sounder outputs

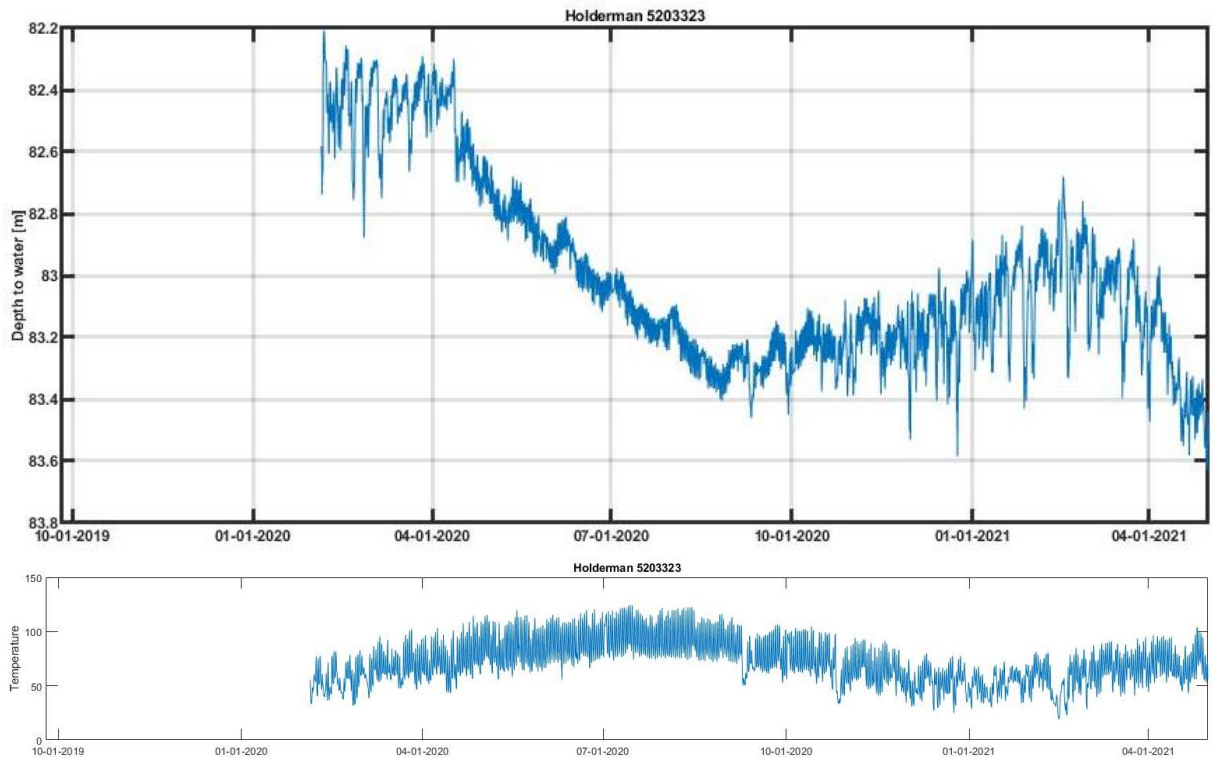
The unprocessed WellIntel[®] measurements (depth to water and temperature) from the sounders installed on the following water wells are presented below:

- Well 52-02-201
- Well 52-03-323 (Holderman)
- Huelster well
- MVWSC McIntire #1
- Pole Pen
- Timber Mountain Ranch
- Weinacht stock well
- Wildcat Draw

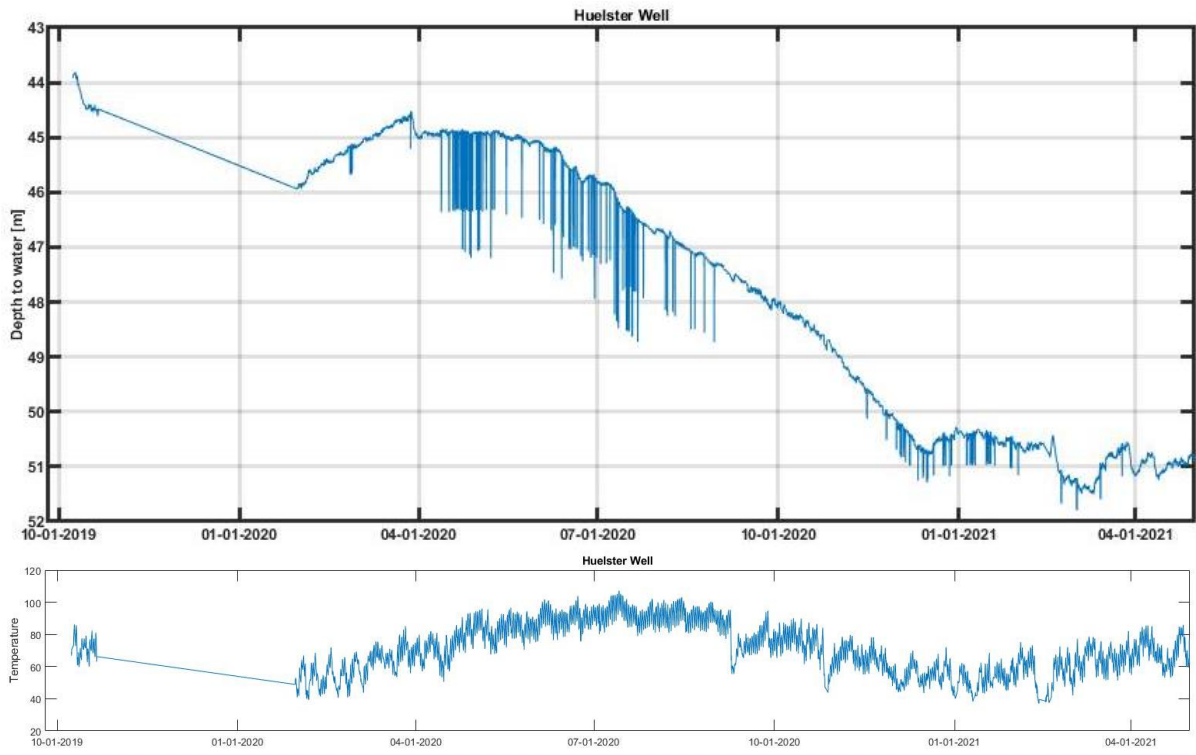
Well 52-02-201



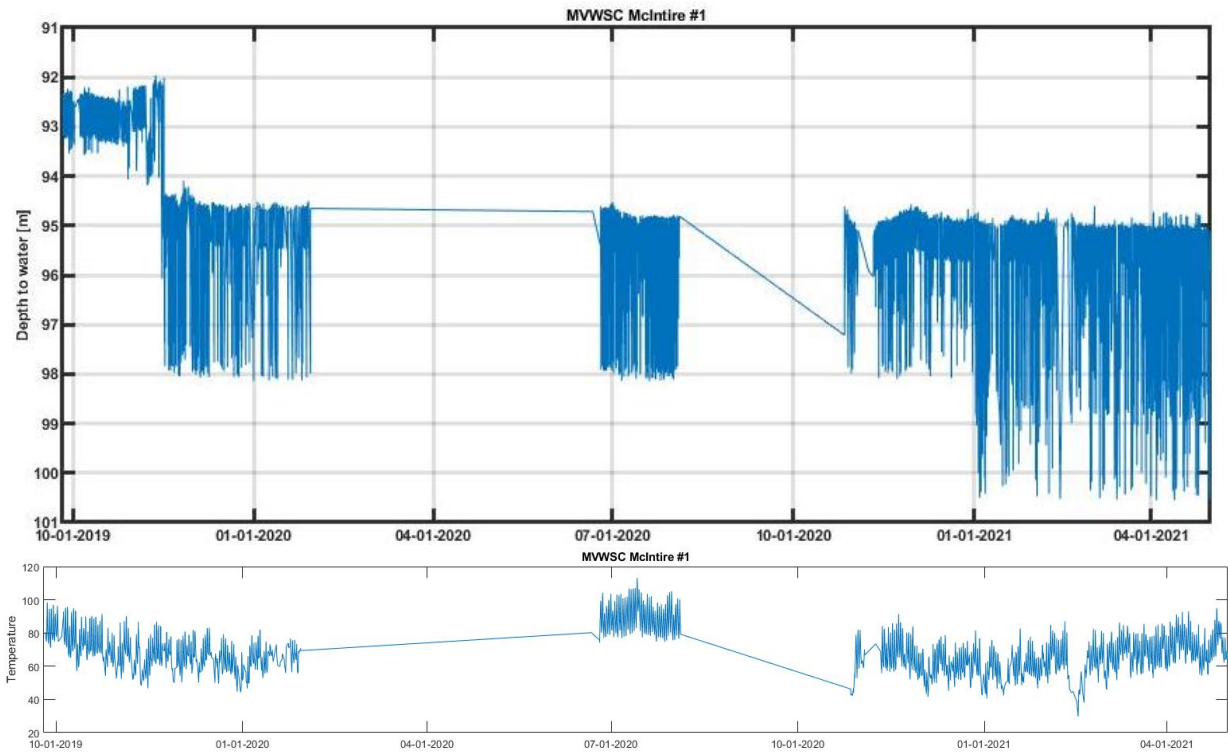
Well 52-03-323 (Holderman)



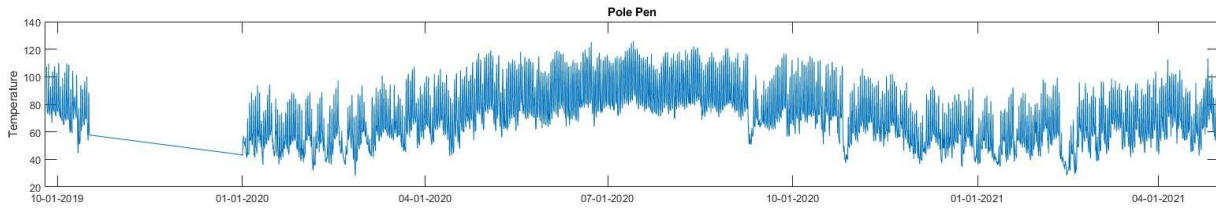
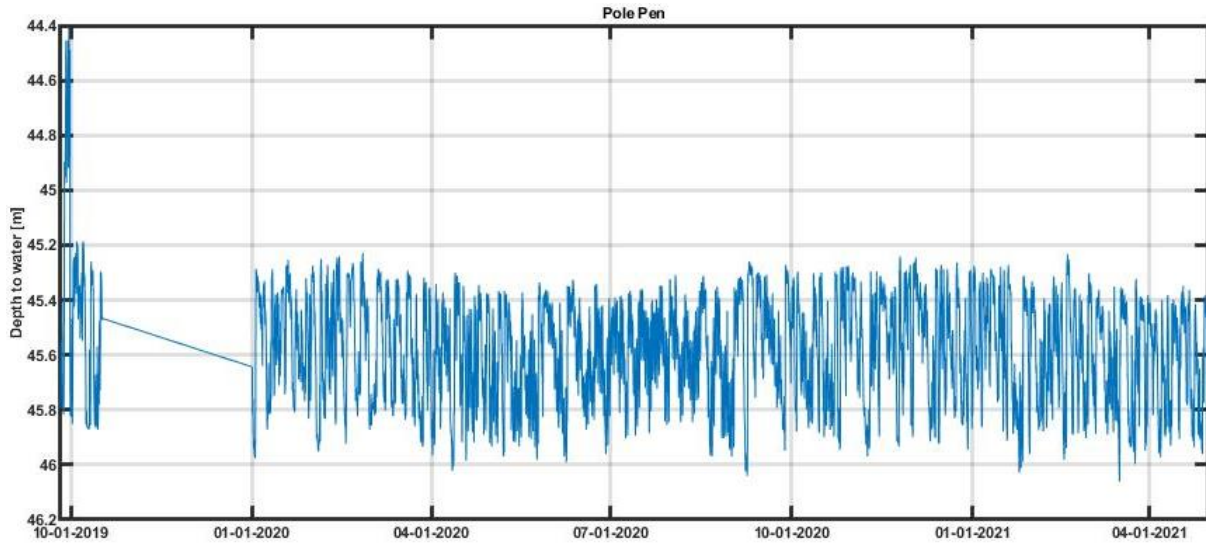
Huelster well



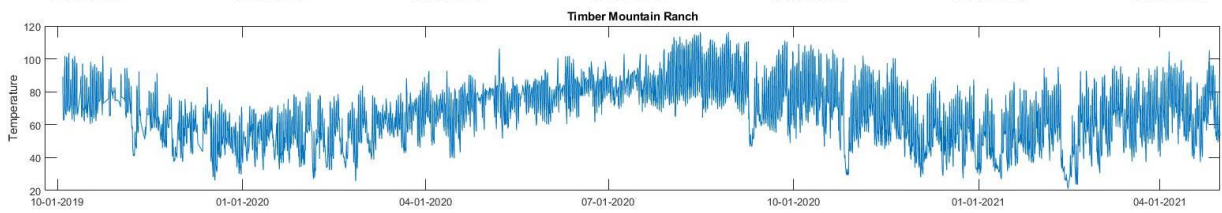
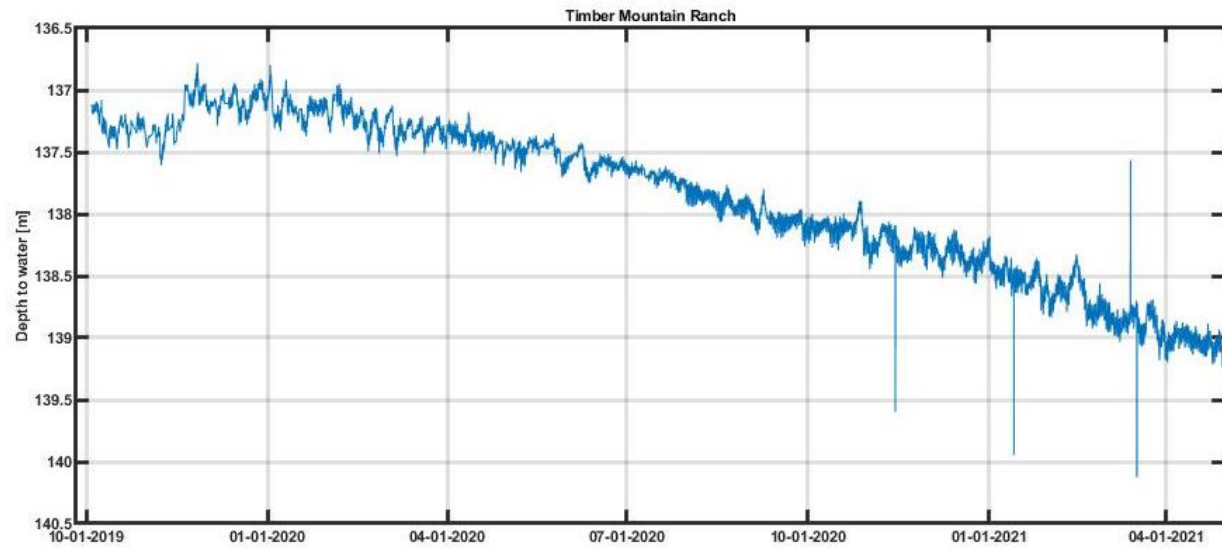
MVWSC McIntire #1



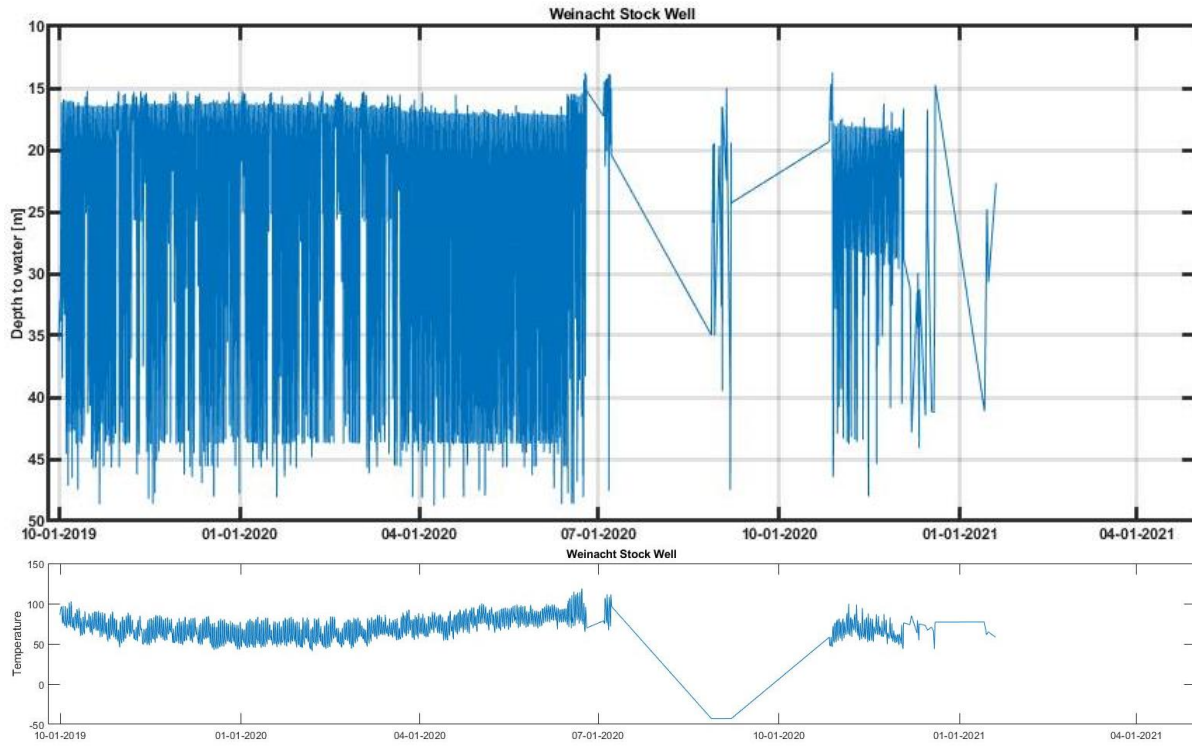
Pole Pen



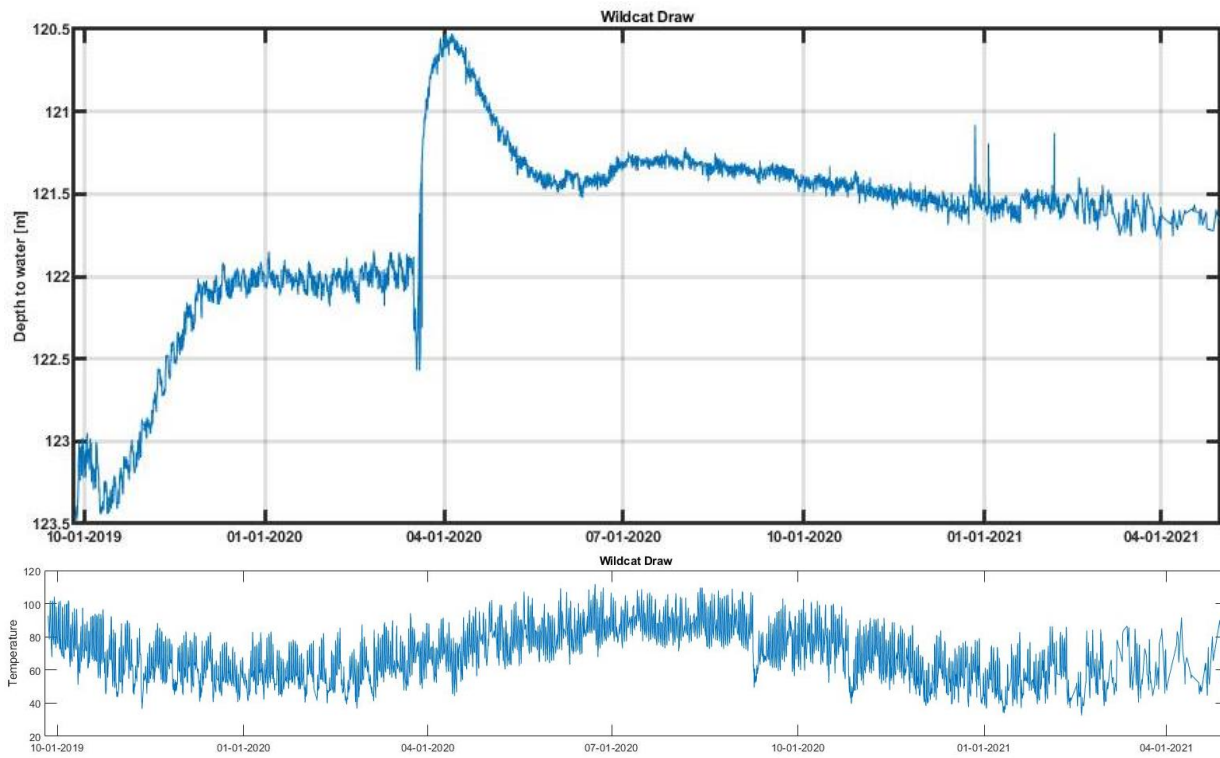
Timber Mountain Ranch



Weinacht stock well



Wildcat Draw



Appendix D: Methods for Chemical Analyses

Major elements

Major and minor cations and anions (lithium, sodium, ammonium, potassium, magnesium, calcium, fluoride, chloride, nitrite, bromide, nitrate, phosphate and sulfate) were analyzed on two Dionex ICS-1100 Ion Chromatography systems, one for anions and one for cations, equipped with an ASAP auto-sampler at the University of Texas at Austin, Bureau of Economic Geology. Samples were initially collected in 30 ml polyethylene bottles in the field. Samples were later diluted with de-ionized water so no component was over 100 ppm. Final elemental concentrations were determined by comparing the chromatograph of the unknown to a 5 -7 point calibration curve produced from dilutions of standard solutions. Correlation coefficients for all elements of the calibration curve are 99.99%. IC calibrations were periodically accessed by running standard solutions and new calibration standards were run when the error associated with standards fell outside 15%.

Trace elements

Trace and other elements (B, Mg, Al, Si, P, K, Ca, Ti, V, Cr, Mn, Fe, Co, Ni, Cu, Zn, As, Se, Rb, Sr, Zr, Mo, Ag, Cd, Sn, Sb, Cs, Ba, Tl, Pb, Bi, Th, and U) were analyzed on an Agilent 7500ce Quadropole inductively-coupled-plasma-mass-spectrometer (ICP-MS) at the University of Texas at Austin Department of Geological Sciences. Samples for trace metals were acidified to 2% HNO₃ immediately after collection and diluted so that the total dissolved solid content was close to 500 ppm.

DIC and C isotopes

Samples for $\delta^{13}\text{C}$ of dissolved inorganic carbon were collected in a 20 ml amber VOA vial with no head space. Samples were refrigerated at 4°C until analysis. Samples of dissolved inorganic carbonate (DIC) are measured for carbon isotope ratios ($\delta^{13}\text{C}$ values) and concentration (mg HCO₃/L) using a Thermo Electron Gas Bench II coupled to a Thermo Electron MAT 253 Isotope Ratio Mass Spectrometer (IRMS). Depending on the concentration of DIC in the sample, approximately 1ml of water is syringed into a Helium-purged 12ml septum capped vial (Exetainer, Labco). Samples are heated to 40°C in a heated sample block and approximately 0.25 ml of 100% phosphoric acid is syringed into each vial and the samples are heated for 20 hours. The headspace gas is sampled using CombiPAL autosampler with a two-hole needle. A continuous flow of 60ml/min helium is used to purge the CO₂ from the headspace through a Naphion dryer to remove water and a sample loop cooled with liquid nitrogen (LN) is used to collect and cryofocus the CO₂ gas. After 5 minutes of collection time the CO₂ gas is heated to room temperature and eluted through a gas chromatograph column (15m x 0.53mm ID, 25°C, 2.5 mL/min). The purified CO₂ gas is analyzed for carbon isotope ratios ($\delta^{13}\text{C}$ values) with the IRMS. Samples are calibrated against an internal sodium bicarbonate laboratory standard that is dissolved in deionized water at five separate concentrations to address potential peak area and concentration linearity effects. This laboratory standard is calibrated against NBS-19 and NBS-18 calcite standards and has a measured $\delta^{13}\text{C}$ value of -19.44‰.

Concentration of DIC is simultaneous measured with the $\delta^{13}\text{C}$ values using total peak area of CO₂ measured in the IRMS. A series of five different DIC concentration standards are made the day before analysis by dissolving measured masses of the sodium bicarbonate standard into measured volumes of deionized water. A CO₂ peak area vs. mmol CO₂ calibration curve is used calculate the mmol of CO₂ produced by each sample. Calculated mmol CO₂ is converted to mg HCO₃⁻ and divided by the volume of water added to calculate DIC concentration in terms of mg

HCO₃/L. The calculated DIC is a total DIC that may include dissolved CO₂(aq), HCO₃⁻ and H₂CO₃, depending on the pH or nature of the samples.

Water isotopes

Water-isotopic analyses were performed at the UT Austin Department of Geological Sciences. δ¹⁸O values of water were measured from water samples using continuous flow CO₂ equilibration techniques with a Thermo Electron Gas Bench II peripheral coupled to a Thermo Electron MAT 253 Isotope Ratio Mass spectrometer (IRMS). Briefly, 1ml of water is pipetted into a 12ml septum capped vial (Exetainer, Labco) that is then purged with a 5% CO₂ helium balance gas. Samples are equilibrated at 40°C for 12 hours. Equilibrated headspace gas is sampled in a continuous flow of helium and CO₂ is purified with a Nafion water drier and a Q plot gas chromatograph column (15m x 0.53mm ID, 25°C, 2.5 mL/min). Oxygen isotope ratios for CO₂ are collected with the IRMS. All values are reported in standard d notation with respect to SMOW oxygen isotope standard. Average precision (1s) of analysis is 0.05‰ for δ¹⁸O.

δD values were measured using a ThermoScientific temperature conversion elemental analyzer (TCEA) or a Picarro L2140-i Isotope and Gas Concentration Analyzer. Aliquots (1-microL) of water were injected into a heated septum injection port and reduced to hydrogen gas at 1440°C in the presence of glassy carbon. Measured δD values of H₂ gas from IAEA-SMOW, IAEA-GISP, and internally calibrated standards were used to generate a δD calibration curve. All analyses are reported in standard “permille” notation with respect to δDVSMOW=0‰. It should be noted that the method for δ¹⁸O is straightforward and rarely affected by contaminants but that the method for δD is easily affected by organics.

Sr isotopes

Sr isotope analyses were performed at the UT Austin Department of Geological Sciences. Water samples, field-filtered and acidified to 2% HNO₃, are stored in a 60 ml acid cleaned HDPE bottles. In a clean lab, an aliquot of each sample that contains 2-6 micrograms Sr was dried in a high purity Teflon beaker. The dried salt was dissolved in a few drops of concentrated (15N) HNO₃ to eliminate insoluble precipitates. The sample was dried down again. Sr was isolated using Eichrom Sr-specific resin in ion exchange columns. Samples were loaded onto the resin dissolved in 3N HNO₃ and Sr was eluted from the column in 0.05N HNO₃. Sr separates were dried down with ~20 µl dilute (~0.03M) H₃PO₄, dissolved in ~30 µl concentrated (15N) HNO₃ to break down organics, and dried again. Approximately 1-3 µg of Sr from each sample was loaded onto a Re filament with an additional 1 µl 0.4 M H₃PO₄ on top of a Ta-oxide activator slurry. Samples were run using a Thermo Fisher Scientific Triton TI thermal-ionization mass spectrometer, operated in static multi-collection mode. For each sample, 160 measurements were made (8 blocks of 20 cycles each) with an integration time 8 seconds. The laboratory analytical blank determined with these samples was 7 pg Sr. Typical laboratory analytical blanks are between 2 and 15 pg Sr. The mean ⁸⁷Sr/⁸⁶Sr value of 27 analyses of NBS987 measured in this lab over the past 6 months is 0.710276 with a two-standard deviation of 0.000013. Ratios were corrected for fractionation using ⁸⁸Sr/⁸⁶Sr = 8.375209 and an exponential fractionation law and ⁸⁷Sr was corrected for ⁸⁷Rb based on simultaneous measurement of ⁸⁵Rb and ⁸⁷Rb/⁸⁵Rb = 0.38600.

Some samples were sent to the University of Georgia (<https://cais.uga.edu/service/strontium-isotope-analysis/>) when the University of Texas laboratories were shut down during the pandemics.

Sulfur and oxygen isotopes of sulfate ($\delta^{34}\text{S}$ and $\delta^{18}\text{O}$)

Sulfate isotope analyses were performed by Isotech (<http://www.isotechlabs.com>; <http://www.isotechlabs.com/analytical/sampletype/water/sulfates.html>) on acidified samples. Sulfate is precipitated into BaSO_4 by adding a Ba salt. The analysis is then performed using an elemental analyzer (EA) coupled to an isotope ratio mass spectrometer (IRMS).

Chlorine isotope ($\delta^{37}\text{Cl}$)

Chlorine isotope analyses were performed at the UT Austin Department of Geological Sciences.

Dissolved gas concentrations and methane C and H isotopes

Dissolved gas samples were collected by two methods: the isoflask® designed by Isotech (<http://www.isotechlabs.com/>; <http://www.isotechlabs.com/products/isoflask>) and a custom made sampling process in which the water sample is held in a small vial with a tight cap as described below.

Samples analyzed for dissolved methane were collected by diverting a small portion of the outflow of the pump tapping the well through tubing ending in a syringe needle. A BD 1 inch, 23 gauge hypodermic needle (Fisher # 14-836-A) was pushed through a Bellco Glass Inc. 20 mm rubber septa (cat # 2048-11800A) of a sealed 60 ml serum vial. A second needle was also inserted through the serum vial that acted as a vent so the vial could be completely filled with groundwater. Water was allowed to flow through the serum vial for approximately 15 minutes, allowing for multiple volumes of water to cycle through the serum vial. The outflow needle was then removed followed immediately by the inflow needle leaving the vial filled with groundwater that had no contact with the atmosphere during sampling.

Samples in Isoflask® were sent to Isotech for dissolved methane (<http://www.isotechlabs.com>; http://www.isotechlabs.com/analytical/sampletype/water/dissolved_gases.html) and $\delta^{13}\text{C}$ and δD analyses. Samples in serum vials were analyzed at the UT Austin Department of Geological Sciences as per the following procedure. Prior to analysis, by using two separate syringes, 5 ml of helium gas was injected into the serum vial as 5 ml of fluid was simultaneously withdrawn resulting in a serum vial with 5 ml of head space and an internal pressure of 1 atmosphere. This sample was shaken for 25 to 30 minutes at 23.5°C to allow the headspace gas to equilibrate with the aqueous solution. Approximately 0.2 ml of the headspace gas was removed from the vial for analysis. and injected into an Agilent 7890A gas chromatograph equipped with a 30 meter 5Å mol sieve GC column and a thermal conductivity detector (TCD). Ar, O_2 , N_2 , and CH_4 concentrations in the headspace gas were measured using the TCD. Dissolved gas concentrations in the sample were calculated using the Henry's Law EPA method where the important model input values are the concentration of the gas component in the headspace, Henry's law constant for the gas, the temperature of the sample, the volume of the sample bottle, the headspace volume, and the molecular weight of the gaseous analyte.

The Agilent 7890A gas chromatograph is coupled to a combustion interface Isotope Ratio mass Spectrometer (IRMS) for carbon isotope ratio ($\delta^{13}\text{C}$) measurement in methane. Briefly, the eluent gas from the TCD is passed through a copper oxide-packed reactor heated to 700°C . This reactor quantitatively combusts the methane to CO_2 for $\delta^{13}\text{C}$ measurement. The stream of gas with the CO_2 is then passed through a methanol cold trap (-20°C) to remove water vapor from the gas. The dry CO_2 gas is then analyzed for $\delta^{13}\text{C}$ using a ThermoElectron Delta V plus continuous flow mass spectrometer. $\delta^{13}\text{C}$ values are reported in standard per mill (‰) notation relative to VPDB with NBS-19 = $+1.95\text{‰}$.

Hydrogen isotope ratios were measured using a Thermal Conversion Elemental Analyzer (TCEA) coupled to a ThermoElectron MAT 253 Isotope Ratio Mass Spectrometer. This method is similar to the previously described method, with the critical difference being the reduction of methane to H₂ gas through a ceramic reactor packed with glassy carbon at 1450°C. The evolved hydrogen gas is separated from N₂, O₂, and Ar using a 5Å mol sieve GC column. Hydrogen isotope ratios (δD values) are measured on the purified hydrogen gas and are reported in standard per mill (‰) notation relative to VSMOW water = 0‰ normalized such that the δΔ of SLAP water = -428‰.

Appendix E: Field photos

Photo 1 rain samplers



Photo 1. (a) TexNet Station at Balmorhea State Park: installing rain sample buckets near Balmorhea State Park TexNet station (Foreground) and rain sample jug inside bucket; (b) McDonald Observatory Affixing funnel to top of rain-sample bucket.

Photo 2 BaroTroll



(a)



(b)

Photo 2. (a) Madera Creek Rugged BaroTroll at Davis Mountain Preserve: logger hung in tree next to cistern behind the McIvor Center and close up; (b) BSP-TexNet Rugged BaroTroll at Balmorhea State Park: logger inside TexNet instrument box inside of fencing; rain sample buckets in foreground.

Photo 3 SSS pool logger



Photo 3. Installation of logger at the main orifice of San Solomon Spring in BSP pool.

Photo 4 Phantom Lake logger



Photo 4. Logger installation in Phantom Lake Cave (left) and view of cave entrance (right).

Photo 5 Giffin logger



Photo 5. Logger installed at USGS gauge downstream from Giffin Spring; upstream view

Photo 6 East Sandia logger



Photo 6. Logger installed at East Sandia Spring pool with hiking pole for scale

Photo 7 Seven Springs



Photo 7. Igneous Seven Springs AquaTroll on McCoy-Remme ranch property: view of logger housing mounted in spring box and downstream view from the spring box.

Photo 8 Willow Spring



Photo 8. Igneous Willow Spring AquaTroll on Cherry Canyon Ranch, logger is mounted inside on bottom of spring box.

Photo 9 Madera Upper



Photo 9. Madera Upper Stream RuggedTroll at Davis Mountain Preserve (downstream view): retrieving logger from dry streambed (April 2019) and from pooled water (September 2019).

Photo 10 Madera Lower



Photo 10. Madera Lower Stream RuggedTroll on 4J Madera Ranch: Installing logger (April 2019 - upstream view) and cutting fallen tree from logger site (downstream view).

Photo 11 Cherry Upper and Lower

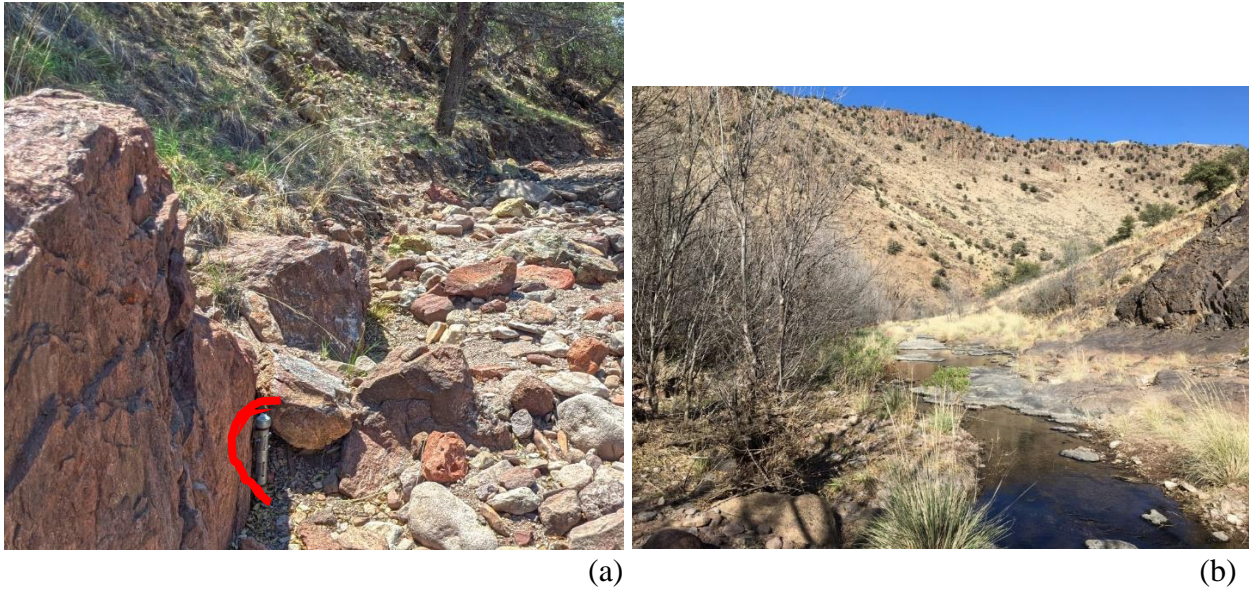


Photo 11. (a) Cherry Upper Stream RuggedTroll on Caldwell Ranch: logger in dry streambed (upstream view); (b) Cherry Lower Stream RuggedTroll on Cherry Canyon Ranch: downstream view of streambed logger site

Photo 12 Little Aguja and Big Aguja



Photo 12. (a) Little Aguja Stream RuggedTroll on Buffalo Trail Scout Camp: logger in dry streambed (downstream view); (b) Big Aguja Stream AquaTroll on McCoy-Remme ranch property: installation of logger downstream from perennial springs (December 2018).

Photo 13 Limpia Upper



Photo 13. Limpia Upper Stream RuggedTroll in Davis Mountains State Park: logger downstream from perennial spring (left) and spring orifice (right)

Photo 14 Limpia Lower



Photo 14. Limpia Lower Stream RuggedTroll on Leoncita Ranch, Limpia Pasture: upstream view of logger in pipe-housing

Photo 15 BEG Cherry deep



Photo 15. BEG Cherry Deep monitoring well AquaTroll on Cherry Canyon Ranch in the Davis Mountains: wellsite located behind truck (northwestern view).

Photo 16 Cherry Lower



Photo 16. Cherry Lower monitoring well AquaTroll on Cherry Canyon Ranch in the Davis Mountains: recently installed (November 2020) solar pump.

Photo 17 . BEG 4J Deep and Shallow Madera



Photo 17. BEG 4J Deep (AquaTroll) and Shallow (RuggedTroll) monitoring wells on 4J Madera Ranch: adjacent deep and shallow wells (southern view).

Photo 18 Huelster #3 and Hamilton WM



(a)



(b)

Photo 18. (a) Huelster Well #3 AquaTroll on Madera Valley Water Supply Corporation property: innovative logger installation; (b) Hamilton windmill well AquaTroll on Hamilton Ranch: wellhead with logger line secured at surface.

Photo 19 BEG Sandia deep and shallow



Photo 19. BEG Sandia Deep and Shallow MW AquaTroll sites BSP. Adjacent well sites – northeastern view

Photo 20 BEG BSP and BEG Big A. deep and shallow



(a)



(b)

Photo 20. (a) BEG BSP monitoring well AquaTroll at Balmorhea State Park: retrieving logger from well for downloading; (b) BEG BigA Deep (AquaTroll) and Shallow (RuggedTroll) monitoring wells at Big Aguja on McCoy-Remme ranch property.

Photo 21 BEG Limpia deep and shallow



Photo 21. BEG Limpia Deep (right) and Shallow (left) monitoring well AquaTrolls at lower Limpia Creek on Leoncita Ranch, Limpia Pasture.

Photo 22 WellIntel[®] sounders

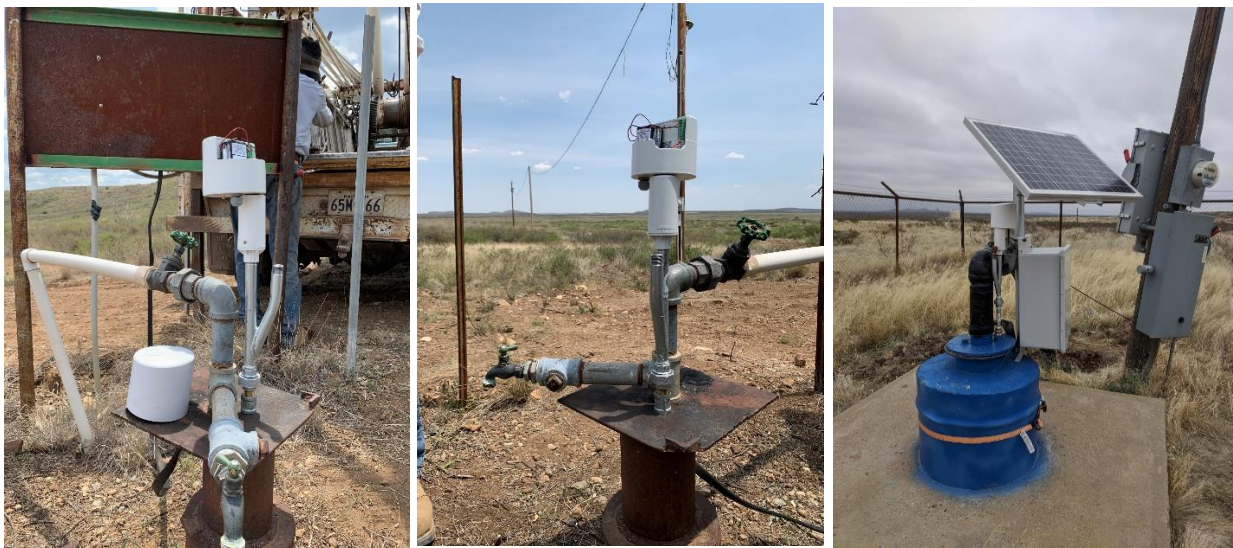


Photo 22. Examples of WellIntel[®] sounders (Balmorhea area)

